Tracing the cell fate of cardiomyocytes undergoing dedifferentiation upon myocardial ischemia via Runx1

(English)

Die dynamische Charakterisierung von dedifferenzierten Herzmuskelzellen nach myokardialer Ischämie über Runx1

(Deutsch)

Inauguraldissertation
zur Erlangung des Grades eines Doktors der Humanbiologie
des Fachbereichs Medizin
der Justus-Liebig-Universität Gießen

vorgelegt von Kulhei, Jennifer, geb. Götz

aus Lich

Gießen 2020

Max Planck Institute
for Heart and Lung Research
W.G. Kerckhoff Institute

JUSTUS-LIEBIG-
UNIVERSITÄT
GIESSEN

Aus dem Campus Kerkhoff der Justus-Liebig-Universität Gießen
und ihres Fachbereiches Medizin

Gutachter: PD Dr. Jochen Pöling

Gutachter: Prof. Dr. Tilman Borggrefe

Tag der Disputation: 10. November 2020

“Knowing is not enough; we must apply.

Willing is not enough; we must do.”

J.W. v. Goethe

I dedicate this work to my beloved mother

Table of contents

1. Introduction 1

1.1. The ischemic heart - the disease and cardioprotective therapeutic targets 1

1.2. Myocardial plasticity during CM dedifferentiation 4

1.3. Morphological characteristics of CM dedifferentiation 6

1.4. Runx1 - part of the RUNX gene family 9

1.5. Runx1 - isoforms and expression patterns 11

1.6. Cell tracing and fate mapping during myocardial renewal 12

1.7. High-throughput techniques linked to pathophysiology of the ischemic heart 14

2. Objectives of the work 15

3. Materials and Methods 16

3.1. Materials 16

3.1.3. Primary and secondary antibodies 17

3.1.4. Oligonucleotides 18

3.1.5. Equipment and software 19

3.1.6. Consumables 20

3.2. Buffers and solutions 20

3.2.1. Cell culture reagents, buffers, solutions and medium 20

3.2.2. Electrophoresis reagents, buffers and recipes 21

3.2.3. Western blotting reagents, buffers and recipes 22

3.2.4. Buffers for isolation of genomic DNA 22

3.2.5. Buffers for staining and special reagents for microscopy 22

3.3. Methods 23

3.3.1. Animal experimentations - approvals and guidelines 23

3.3.2. Mouse lines - origin, nomenclature and housing of animals 24

3.3.3. Different mouse lines and genetic background 24

3.3.3.1. $Runx1^{fl2}/\alpha MHC^{Cre}$ (heart specific knock-out) 24

3.3.3.2. Runx1-t2A-tTA-t2A ($Runx1^{tTA}$) 24

3.3.3.3. Runx1 Tracer: permanent labeling of once Runx1 expressing cells 25

3.3.3.4. Runx1 Viewer: labeling of current Runx1 expressing cells 27

3.3.4. Harvesting and preparation of mouse hearts for morphological analyses 27

3.3.5. Induction of myocardial infarction 28

3.3.6. Isolation of adult mouse cardiomyocytes (mACMs) 28

3.3.6.1. Strategy 1 (healthy heart) 29

3.3.6.2. Strategy 2 (injured heart) 31

3.3.7. Molecular biological methods 31

3.3.7.1. Isolation of genomic DNA from mouse tail biopsies 31

3.3.7.2. Polymerase chain reaction (PCR) 32

3.3.7.3. DNA agarose gel electrophoresis 32

3.3.7.4. Extraction of RNA from isolated and sorted mACMs 33

3.3.7.5. Procedure and analysis of next-generation-sequencing (NGS) 33

3.3.8. Biochemical methods 34

3.3.8.1. Extraction of proteins, quantification and electrophoresis 34

3.3.8.2. Western blotting and protein detection 35

3.3.9. Histological methods 36

3.3.9.1. Cryosectioning of mouse hearts 36

3.3.9.2. Conventional histological staining - H&E and trichrome 36

3.3.9.3. LacZ staining 37

3.3.9.4. Immunofluorescent and -histochemical staining 37

3.3.10. Biophysical methods 38

3.3.10.1. Compound and confocal microscopy 38

3.3.10.2. Transmission electron microscopy (TEM) 39

3.3.11. Live-cell sorting 40

3.3.12. Imaging analysis 41

3.3.12.1. Quantitative measurement of the infarct size in conventional trichrome and H&E staining 41

3.3.12.2. Colocalization image analysis of confocal microscopy 42

3.4. Statistical evaluation 43

4. Results 45

4.1. In vitro imaging analysis of Runx1 expression in adult mouse cardiomyocytes (mACMs) displayed phenotypical adaptions linked to dedifferentiation upon Oncostatin M (OSM) stimulation 45

4.2. Western Blot analysis of OSM-stimulated mACMs revealed a significant Runx1 expression on protein level in vitro already at 1 day post stimulation (dps) 47

4.3. Runx1 deficient mACMs displayed no altered morphology due to OSM stimulation in vitro as well as no significant expression of fetal marker proteins assigned to dedifferentiation 48

4.4. Successfully $Runx1_{traced}$ mACMs delivered equal phenotypical adaptions and responses on protein level upon OSM stimulation, when compared to wildtype cardiomyocytes 52

4.5. MI hearts revealed an increased Runx1 expression in the ischemic region of the left ventricular myocardium in vivo 55

4.6. Runx1 expression peaked in the ischemic region of the heart in vivo at 4 days post MI 56

4.7. Functionality of Runx1 deficient mice was validated via an absent expression of Runx1 in mACMs in the infarcted heart at 7 days post MI 58

4.8. Runx1 expressing cells were able to survive in the infarcted heart, which was demonstrated in Runx1 Viewer and Tracer mice at 4, 7 and 90 days post MI 59

4.9. The model of I/R turned out to increase the amount of surviving mACMs within the ischemic area and was therefore preferred to study processes of dedifferentiation in the infarcted myocardium 62

4.10. The amount of Runx1^{+} mACMs were increased by 3.75 fold due to switching from the permanent (I) to the temporary (I/R) LAD ligation model 64

4.11. Morphological characteristics and expression of dedifferentiation markers were observed on a microscopic and nanoscopic level in Runx1 Tracer mice at 7dpI/R 66

4.12. Isolation and sorting of living Runx1^{+} mACMs post I/R enabled down-stream next-generation sequencing (NGS) analysis 69

4.13. NGS analysis revealed 2081 differentially expressed genes and clusters of 2 subpopulations with a distinct genetic profile of Runx1$_{traced}$ mACMs post I/R 72

5. Discussion 80

5.1. Serum conditions effected the OSM-induced Runx1 expression, which triggered signs of dedifferentiation in adult mouse cardiomyocytes in vitro 80

5.2. Runx1 deficient mACMs responded to mOSM-activated signaling in vitro, but were masked by fibroblast contamination-mediated signaling and therefore lacked the re-expression of fetal genes as well as the capability to trigger processes of dedifferentiation 81

5.3. Successful tracing of mACMs confirmed the capability to follow processes of dedifferentiation via Runx1 expression 83

5.4. Myocardial ischemia model impacted the amount of Runx1^{+} CMs in vivo 83

5.5. Loss of sarcomeres and other signs of dedifferentiation were detectable in Runx1 transgenic animals on a microscopic and nanoscopic scale post I/R 84

5.6. Isolation and a successful live-cell sorting for downstream analysis was possible due to a stable endogenous tracing of RFP in Runx1$_{traced}$ mACMs 85

5.7. Dedifferentiated CMs might act as active modulators of the innate immune response after myocardial injury 87

5.8. Highly upregulated genes indicate cell transformation processes and might implicate a regeneration potential of Runx1$_{traced}$ ACMs 88

5.9. A temporally and spatially limited expression of Runx1 ensures the survival of adult cardiomyocytes post MI 90

5.10. Conclusions and outlook 91

6. Summary 95

7. Zusammenfassung 96

8. List of abbreviations 98

9. List of figures 101

10. Bibliography 104

11. Attachments 128

12. List of publications 146

13. Erklärung zur Dissertation 147

14. Acknowledgment 148

15. Curriculum Vitae 150

1. Introduction

1.1. The ischemic heart - the disease and cardioprotective therapeutic targets

According to investigations of the "organization for economic co-operation and development" (OECD), ischemic heart diseases remain as number 1 cause of death globally (Figure 1) in the last 15 years (OECD 2019).

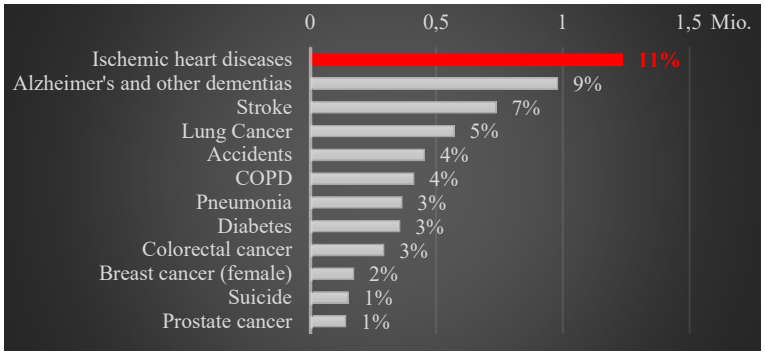

Figure 1: Main causes of mortality across OECD countries in 2017, adapted from OECD (2019). Note: Other causes of death not shown in the figure represent 15% of all deaths (OECD 2019).

Mainly initiated by an atherogenic or atherothrombotic occlusion of coronary vessels, myocardial infarction (MI) is characterized by the abrogation of nutrients and inadequate oxygen supply to a local area of the downstream heart muscle (myocardium) (Mann 2016). Since the 20th century, this restriction of blood supply is called myocardial ischemia, which frequently results in substantial loss of contracting cardiomyocytes (CMs) (Institute of Medicine 2010, Taqueti 2018). As a consequence, a plethora of structural changes, known as cardiac remodeling (Figure 2), adversely impairs physiological heart functions, particularly systolic pumping and/or diastolic filling capacity, which often lead to death or heart failure (Szibor 2014, Awada 2016).

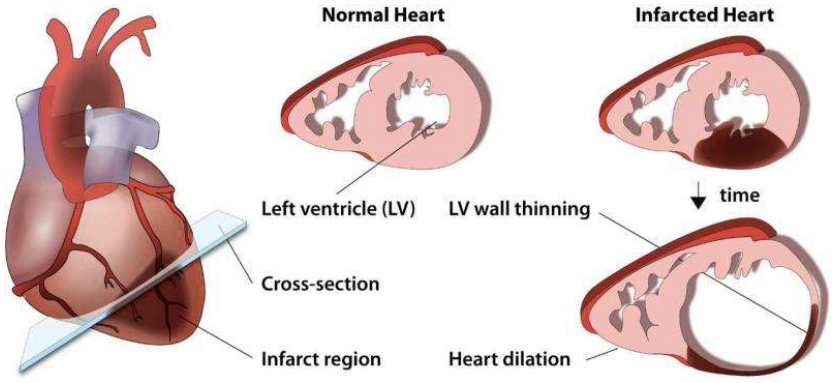

Figure 2: Cross-sectional view post myocardial infarction (MI), adapted from Awada et al. (Awada 2016). MI frequently causes severe damage and adverse remodeling in the left ventricular myocardium, leading over time to left ventricle (LV) wall thinning and dilation and ultimately progressing to contractile dysfunction and heart failure (Awada 2016).

An extraordinary amount of research has been carried out to understand the mechanisms by which the myocardium is damaged during ischemic injury (Piper 1998, Yellon 2007, Murphy 2008, Pell 2016). Thus, rodent models of myocardial ischemia either by a permanent or transient occlusion of the left anterior descending coronary artery (LAD), have been used to elucidate the pathophysiological and molecular mechanisms of cardiac remodeling (Yang 2002, Takagawa 2007). These dynamic and time-dependent processes are initially characterized by complex changes, occurring in both the necrotic region and the residual non-infarcted myocardium (Olivetti 1990, Yang 2002, Mann 2016). The associated morphological adaptions (Figure 3) are often illustrated via histological sections followed by hematoxylin-eosin (H&E) or Masson's trichrome (trichrome) staining and highlight 3 distinct regions: (A) the infarct zone with infiltrating inflammatory cells, fibrosis and little viable cardiomyocytes, (B) the border zone, which is defined as the demarcation area between inflammation and ischemia-spared tissue as well as (C) the remote zone with few to no inflammatory cells present and a preserved myocardial cell structure (Spata 2013).

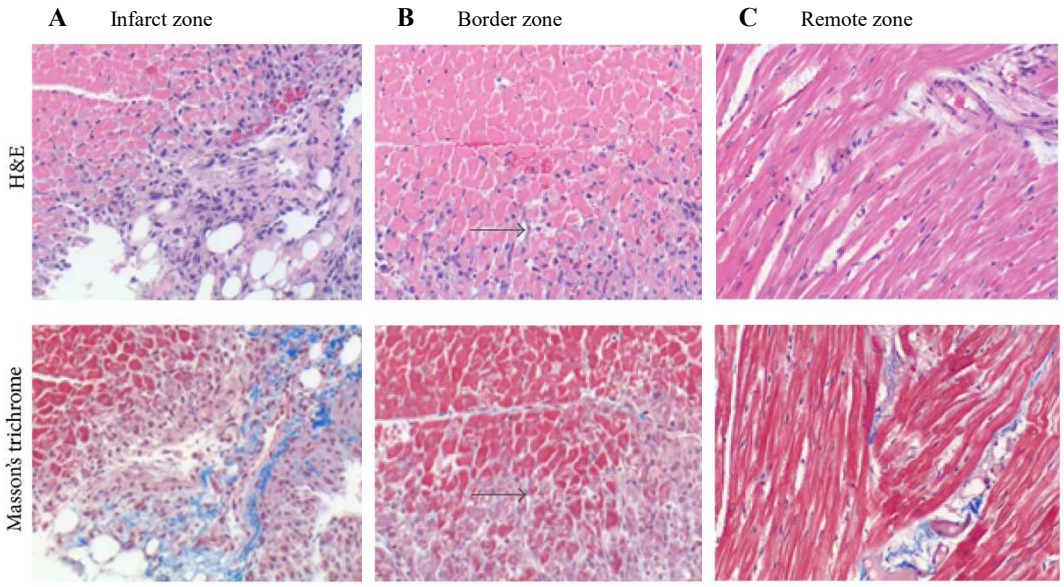

Figure 3: Histological analysis of 3 distinct morphological zones within the infarcted myocardium, adapted from Sparta et al. (Spata 2013). (A-C) Illustrated is the representative regional myocardial histology in a 20x magnification, with (A) infarct zone showing the area of cardiomyocyte death, inflammation (H&E) and fibrosis (Masson's trichrome), (B) border zone demonstrating the transition (delineated by blocked arrows) between normal cardiomyocytes (top) and ischemic tissue (bottom) and (C) remote zone consisting of a preserved myocardial cell structure (Spata 2013).

At a cellular level, loss of CMs occurs focally during MI, which leads to increased blood pressure and shear stress (hemodynamic load) on the surviving myocardium (Mann 2016). Simultaneously, molecular changes are triggered in various cardiac cell types

within the border zone and adjacent to the ischemic area as illustrated in Figure 3 (Nahrendorf 2010, Frangogiannis 2012, Spata 2013, Prabhu 2016). As a consequence, multiple pathophysiological factors converge to remodel the heart after MI either primary or secondary as a result of the increased hemodynamic load, culminating in ventricular dilation, altered cardiac relaxation and stiffness, fibrosis, and vascular rarefaction (Perrino 2006, Mann 2016, Prabhu 2016). Irreversible myocardial injury, extending from subendocardium to subepicardium, is displayed in a time-dependent scar formation, which progresses with increasing duration of ischemia (Myers 1974, Murry 1986, Kloner 1989, Zhang 2018). Reperfusion itself, however, can also paradoxically induce CM death independent of the ischemic episode by a process known as reperfusion injury (Takemura 2009, Hausenloy 2013). So far, many treatments have been identified that conveyed robust cardioprotection in experimental animal models of myocardial ischemia and reperfusion injury (Davidson 2019). But translation of these cardioprotective approaches into the clinical setting of MI for patient benefit has been disappointing (Davidson 2019). One important reason might be that MI is multifactorial, causing CM death via multiple mechanisms as well as affecting other cell types, including platelets, immune cells, fibroblasts, endothelial and smooth muscle cells (Awada 2016, Davidson 2019). In addition, several pharmacological cardioprotective strategies (visualized in Figure 4), during or after MI, act through common end-effectors (e.g. Phosphoinositid-3-Kinase (PI3K)-mediated Akt activation), but often fail due to the differences between preclinical models of experimental myocardial ischemia and the complex clinical scenario in patients, including age, comorbidities and co-treatments (Tsang 2005, Awada 2016, Xue 2016, Davidson 2019). In order to effectively translate cardioprotection to MI patients, a multitarget therapy is necessary (Davidson 2019). In this regards, MI treatments need to combine drug targeting of vascular injury/inflammation with targeted drug delivery for CM loss as well as pharmacological agents that activate endogenous mechanisms of cardioprotection while inhibiting cell death cascades (Ruiz-Meana 2003, Ibanez 2013, Ferdinandy 2014, Hausenloy 2017, Heusch 2017, Davidson 2019). Furthermore, the identification of a key factor that addresses all common signaling pathways in the context of myocardial ischemia could rule out possible pharmacological interactions that have been observed particularly for cardiac drugs (Nolan 2000, Mateti 2011, Dumbreck 2015).

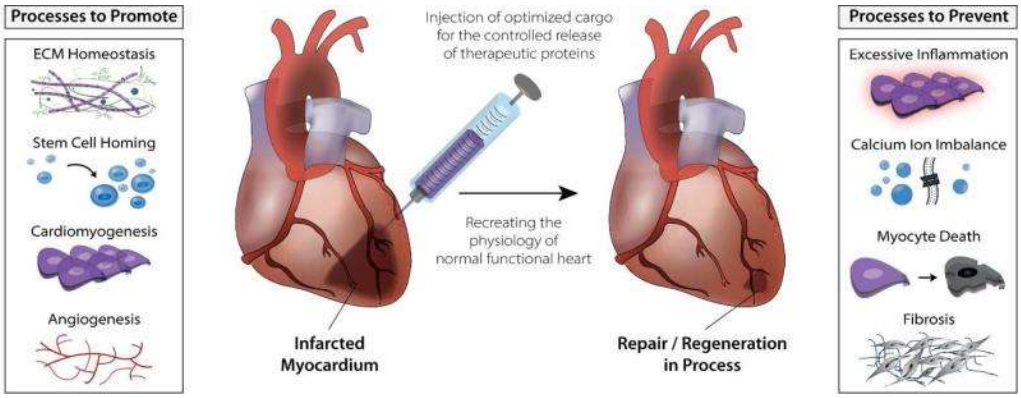

Figure 4: Repair and regeneration mechanisms of the infarcted myocardium driven by delivery of proteins that address distinctive MI pathologies, adapted from Awada et al. (Awada 2016). To treat MI, a therapy needs to promote extracellular matrix (ECM) homeostasis, stem cell homing, cardiomyogenesis, angiogenesis as well as to prevent excessive inflammation, calcium ion imbalance, CM death and fibrosis (Awada 2016). Thus, some processes like ECM homeostasis and calcium ion balance need to happen as early as possible and therefore need to be promoted, whereas others such as fibrosis have to be prevented after MI (Awada 2016). Injecting a protein delivery system, which carries for instance a specific protein of interest and delivers it in a physiological way, offers the potential to trigger repair and regeneration signaling cascades in order to restore a functional myocardium (Awada 2016).

1.2. Myocardial plasticity during CM dedifferentiation

For decades it has been thought that once mammalian cells committed to a specific lineage, their cell fate becomes totally restricted (Cai 2007, Cherry 2012, Puri 2015). This process of differentiation gradually reduces the potential of so-called terminally differentiated cells to stop dividing permanently (Cai 2007). Thus, cell transformation processes like reprogramming, transdifferentiation and dedifferentiation have been controversially discussed as alternative regeneration mechanisms within the scientific research community, as displayed in Figure 5 (Slack 2001, Slack 2008, Slack 2009, Jopling 2011). These subsets of metaplasia are characterized by the conversion of one differentiated cell into another and hereby crossing tissue boundaries committed to different cell lineages (Tosh 2002, Jopling 2011, Mann 2016).

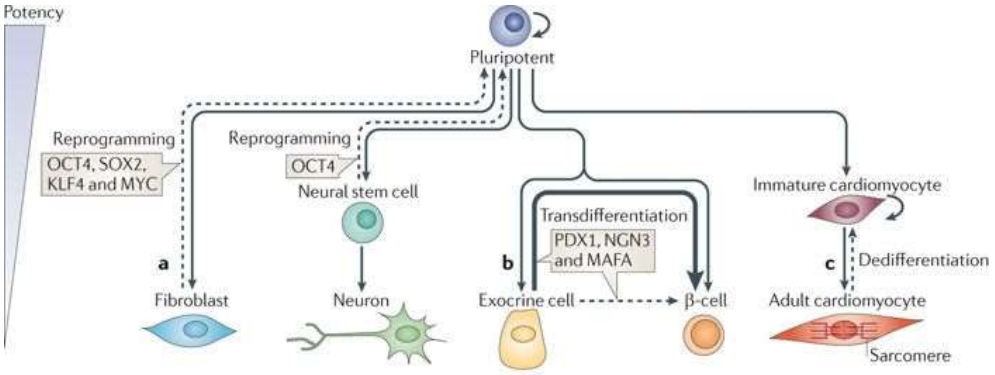

Figure 5: Reprogramming, transdifferentiation and dedifferentiation, adapted from Jopling et al. (Jopling 2011). Pluripotent cells inherit the capability of differentiating down any given lineage to give rise to a range of different cell types (indicated with solid arrows) (Jopling 2011). Reprogramming (**a**, indicated with dashed arrow) neuronal stem cells and fibroblasts as well as transdifferentiated cells (**b**, i.e. pancreatic exocrine cells) requires the expression of different transcription factors (Octamer-binding transcription factor 4 (OCT4), sex determining region Y (SOX2), Krüppel-like factor 4 (KLF4), MYC, duodenum homeobox 1 (PDX1), neurogenin 3 (NGN3) or MafA (MAFA)) (Jopling 2011). Dedifferentiation (**c**, indicated with curved arrow) refers to regression of a mature cell within its own lineage, which allows it to proliferate: Heart regeneration is facilitated by this means, what involves a dedifferentiation step (dashed arrow) of terminally differentiated CMs beforehand (Jopling 2011).

Dedifferentiation is a process by which cells develop in reverse, i.e. from a more differentiated to a less differentiated state, rendering a specialized phenotype closer to their ancestor with enhanced plasticity, as illustrated in Figure 5-7 (Cai 2007, Zhang 2010, Jopling 2011, Bloomekatz 2016). The phenomenon can be observed at the levels of genes, proteins, morphology and function in different tissues and organs of plants, invertebrates, amphibians and animals including humans (Zhao 2001, Cai 2007, Pöling 2012). It has been strengthened in an augmented number of studies that certain mammalian cell types, exposed to appropriate signals, can be dedifferentiated to cells with a progenitor-like cell phenotype, generating different types of functional cells for the repair of damaged tissue (Cai 2007, Grafi 2009, Puri 2015). Accumulating evidence suggests that heart regeneration, which is no longer limited to non-mammalian vertebrates, involves dedifferentiation processes for the restoration of cardiac contractility as well as concomitant proliferation for the replacement of lost CMs (Driesen 2007, Poss 2010, Turan 2016).

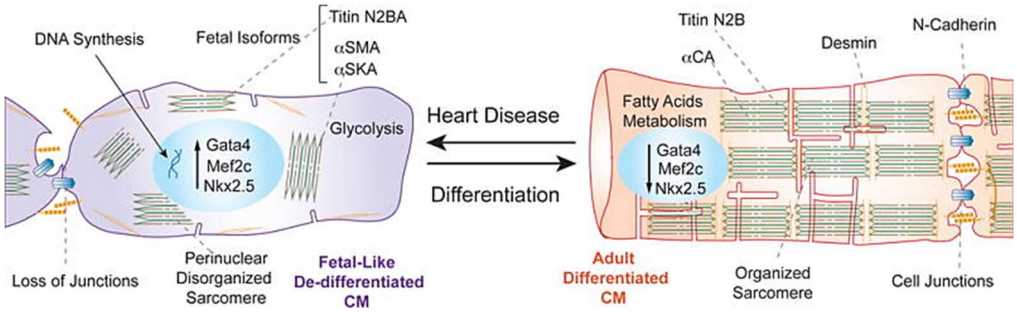

Figure 6: The different properties of dedifferentiated (left) and mature (right) CMs, adapted from Bloomekatz et al. (Bloomekatz 2016). CMs associated with heart disease (left) display dedifferentiated/fetal-like characteristics compared to mature adult CMs (right) (Bloomekatz 2016). These fetal-like characteristics include a metabolic change from fatty acid metabolism to glycolysis, activation of early cardiac transcription factors such as Gata4, Mef2c, Nkx2.5 and increased alpha-smooth-muscle actin (αSMA) expression (Bloomekatz 2016). Additionally, loss of T-tubules, sarcomere (αSKA) re-arrangements, including the re-localization of Desmin (orange) and the re-distribution of gap junctions away from cell-cell contacts, have been observed in diseased hearts (Bloomekatz 2016).

1.3. Morphological characteristics of CM dedifferentiation

The study of dedifferentiation in animals has been limited for a long time due to a lack of appropriate tools that uncouples the stage of dedifferentiation from the cell cycle (Grafi 2009, Kretzschmar 2018). But mainly in non-purified cell cultures of adult CMs, dedifferentiation has been investigated extensively at the phenotypical level (Zhang 2010). Many studies have demonstrated that compared to mature cells, dedifferentiated cells experience characteristically morphological changes: Fewer organelles and a higher karyoplasmic ratio, loss of structural integrity paralleled by the re-arrangement of the cytoskeleton, flatness and sprouting (Figure 7) as well as the ability to proliferate (Cai 2007, Zhang 2010, Wang 2017). Such results indicate substantial cellular plasticity of postnatal mammalian CMs accompanied with the potential to generate new CMs from proliferating, dedifferentiated CMs, but without complete reversion to a cardiac progenitor state (Bersell 2009, Zhang 2010).

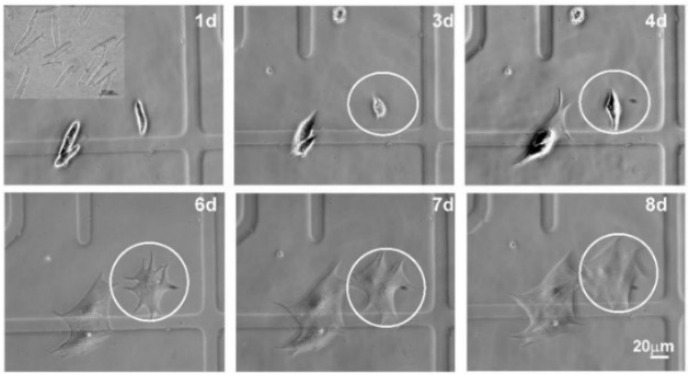

Figure 7: Morphological characteristics of purified CMs, adapted from Zhang et al. (Zhang 2010). Isolated CMs dedifferentiate, round up, start sprouting, become flat and tend to divide (Zhang 2010).

Leri et al. postulated in 2015 that phenotypical adaptions activate cell cycle genes in correlation to cardiogenesis like αSMA (Figure 8, displayed as α SM actinin) and progenitor markers like atrial natriuretic peptide (ANP) (Leri 2015). Therefore, CMs are consequently not postmitotic terminally differentiated, but rather are able to multiply (Anversa 1998, Soonpaa 1998, Wohlschlaeger 2010, Leri 2015). Further studies suggested that dedifferentiated ventricular CMs in vivo re-acquire a primitive cell phenotype, re-enter the cell cycle and synthesize DNA (Anversa 1998, Soonpaa 1998, Wohlschlaeger 2010, Leri 2015, Sukhacheva 2016, Wang 2017). However, difficulties exist in regard to the evaluation of CM proliferation, e.g. in case of the absence of cell death, in which the measurement of the number of ventricular CMs would seem to be the only approach that can demonstrate unequivocally the degree of CM hyperplasia (Leri 2015). Furthermore, the concomitant presence of a widespread (necro-) apoptotic CM loss, together with multiple foci of myocardial injury and tissue scarring, complicates this type of analysis, resulting in an underestimation of the extent of cell replacement in the injured heart (Leri 2015).

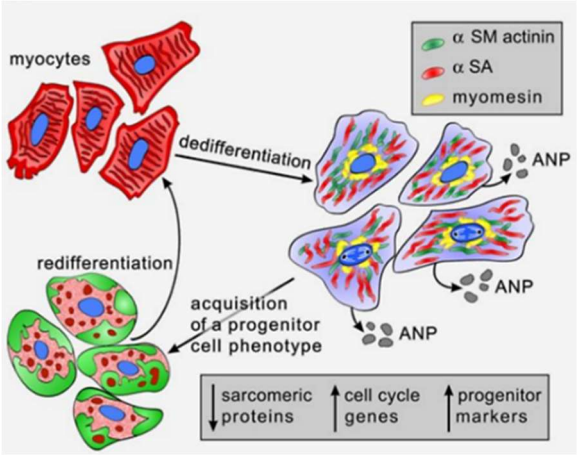

Figure 8: Dedifferentiation of pre-existing CMs, adapted from Leri et al. (Leri 2015). Dedifferentiated CMs downregulate sarcomeric proteins (e.g. sarcomeric alpha-actinin, here: α SA), whereas cell cycle genes correlated to cardiogenesis (e.g. αSMA, here: α SM actinin) and progenitor markers (e.g. myomesin and atrial natriuretic peptide (ANP)) are upregulated (Ruzicka 1988, Boettger 2009, Szibor 2014). The findings, as illustrated by Leri et al., indicate a potential source of newly formed CMs post ischemic injury (Leri 2015). In addition, Leri et al. and others postulated that CMs dedifferentiation in vivo may trigger the re-acquisition of a primitive cell phenotype, assuming a re-gained ability to multiply (Kubin 2011, Leri 2015).

Promising findings regarding the molecular mechanisms of dedifferentiation have been described by Kubin et al. (Kubin 2011). Here, Oncostatin M (OSM), an inflammatory cytokine of the interleukin-6 (IL-6) superfamily, is reported to play a major

pathophysiological role for acute MI and for chronic dilated cardiomyopathy (Kubin 2011). Other studies have also demonstrated that OSM induces CM dedifferentiation in form of morphological changes, activation of fetal genes, expression of progenitor cell markers and enables cell cycle progression (Song 2007, Hohensinner 2008, Kubin 2011, Lörchner 2015, Hashmi 2019). At the protein level, OSM-dependent CM dedifferentiation can be observed as evidenced by the upregulation of progenitor cell-related proteins like ANP, αSMA, α-actinin (ACTN1) or myomesin and by the down-regulation of differentiated cell-related proteins like sarcomeric alpha-actinin (Sarc actinin/ACTN2) or alpha-myosin heavy chain (αMHC) (Cai 2007, Driesen 2009, Zhang 2010, Kubin 2011, Leri 2015). Surprisingly, Kubin et al. demonstrated in their affymetrix DNA microarray and corresponding quantitative RT-PCR analysis (Figure 9) a drastic upregulation of the Runt-related transcription factor 1 (Runx1) in OSM-treated adult rat CMs, which was inversely regulated in differentiated CMs (derived from embryonic stem cells) and absent in non OSM-treated controls (Kubin 2011, Tang 2018). Until then, Runx1 had only been investigated in case of hematopoiesis owing to the frequent involvement of this gene in leukemic translocations (Blyth 2005, Kubin 2011).

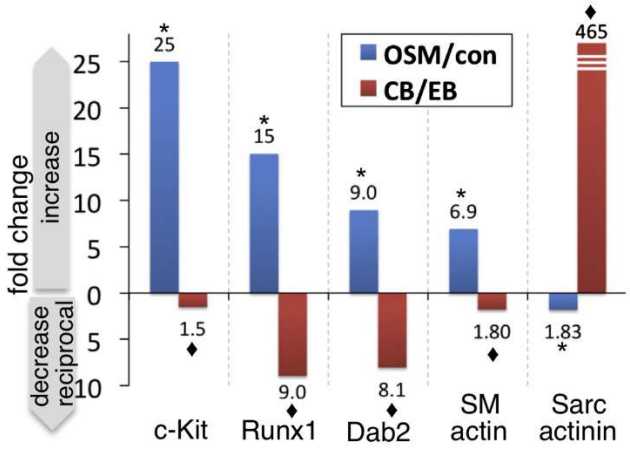

Figure 9: Affymetrix DNA microarray analysis from embryonic stem cells subjected to CM differentiation (CB/EB) in comparison to Oncostatin M (OSM)-treated CMs (OSM/con), adapted from Kubin et al. (Kubin 2011). Typical progenitor cell marker genes like c-Kit, Dab2 and the transcription factor Runx1 appeared significantly upregulated in OSM-treated CMs but were inversely regulated in differentiated cardiac muscle cells. The results were validated via quantitative RT-PCR analyses, whereby αSMA (here: SM actin) served as positive control, displaying dedifferentiation. In addition, downregulation of sarcomeric proteins like sarcomeric alpha-actinin (here: Sarc actinin) was found (Kubin 2011, Leri 2015).

Besides that, OSM is involved in complex cellular processes such as modulation of the ECM, regulation of cell proliferation, cell survival, cell growth and gene activation

(Heinrich P.C. 1998, Kubin 2011, Pöling 2012, Nagahama 2013). Furthermore, it has been associated with airway remodeling or lung parenchymal fibrosis (Heinrich P.C. 1998, Nagahama 2013). In 2015, Lörchner et al. demonstrated an intercellular positive feedback loop of macrophage trafficking throughout OSM, which initiated a downstream cascade instrumental for the inflammatory homeostasis during myocardial healing (Lörchner 2015). Coherent with its appearance during inflammation, it became apparent in several in vitro studies that OSM activates a broad array of signaling pathways (i.e. Jak/STAT, MAPK, PI3K), thereby regulating genes such as IL-6, matrix metalloproteinase 1 (MMP-1) and tissue inhibitor of metalloproteinases 1 (Timp1), as visualized in Figure 10 (Fritz 2010, Richards 2013).

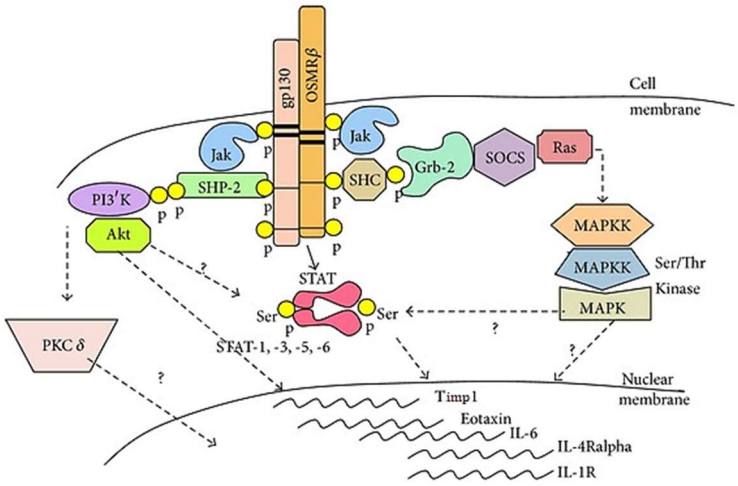

Figure 10: OSM receptor (OSMR) signaling, adapted from Richards and modified from Fritz (Fritz 2010, Richards 2013). A schematic representation of signal transduction initiated through the OSM binding is visualized(Richards 1993). Besides the activation of Jak/STAT and MAPK signaling pathways in connective tissue cells, OSM activates additional signaling intermediates in fibroblasts, including STAT5, STAT6, the PI3K/Akt pathway, the novel protein kinase C (PKC) isoform PKC delta (PKCδ) and results in increased transcriptional levels of Timp1 and IL-6 (Fritz 2010, Richards 2013).

1.4. Runx1 - part of the RUNX gene family

The RUNX family of genes, also known as acute myeloid leukemia (AML) and core-binding factor-alpha (CBFα), comprises a group of crucial transcription factors and orchestrators of diverse developmental processes with roles in proliferation, differentiation, apoptosis, cell lineage specification and their paradoxical effects in cancer (Blyth 2005, Wang 2010, Chuang 2013, Ito 2015, Mevel 2019). The RUNX protein family includes 3 RUNX genes: RUNX1, RUNX2 and RUNX3, each with distinct tissue-

specific expression patterns (Jones 1999, Blyth 2005, Ito 2015, Tang 2018). Although residing on different chromosomes, all 3 RUNX genes have a similar genomic organization with 2 promotors (P1 and P2) and an evolutionary conserved Runt domain (Figure 11A) (Levanon 2003, Levanon 2004, Wang 2010). The Runt domain enables the binding at the promotor of target genes as well as protein-protein interactions with its binding partner CBF-beta (CBFβ), which confers high-affinity DNA binding and stability of the complex (Figure 11B) (Levanon 2003, Levanon 2004, Blyth 2005). The RUNX gene products have well-defined biological functions orchestrated via a spatiotemporal expression and are tightly regulated through interacting proteins, what is reflected in different phenotypes of corresponding knock-out (KO) mice (Levanon 2004, Chuang 2013, De Bruijn 2017). The effects of Runx-CBFβ regulation are clearly lineage and stage specific and include the crucial choices between cell cycle exit and continued proliferation on the one hand and between differentiation and self-renewal on the other hand (Yan 2004, Blyth 2005, Wang 2010).

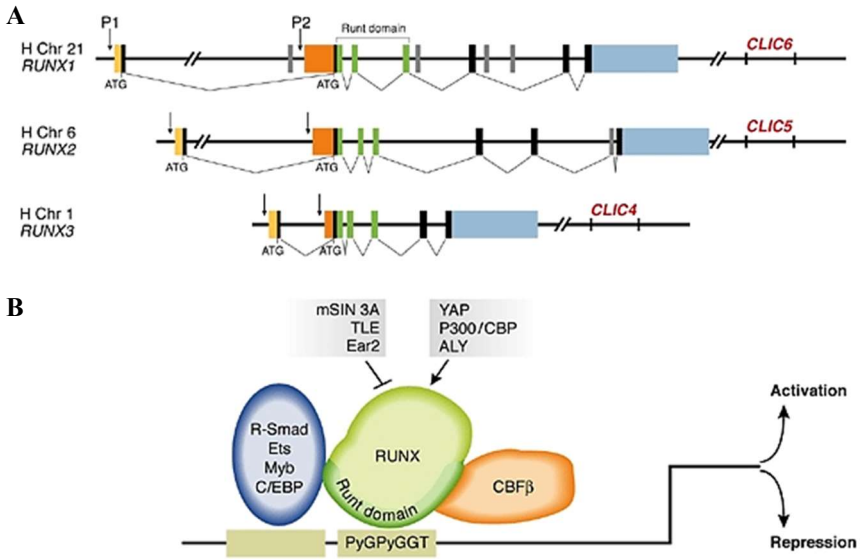

Figure 11: The mammalian RUNX genes: structure and mode of function, adapted from Levanon et al. (Levanon 2003, Levanon 2004). (A) The 3 mammalian RUNX genes have a similar genomic organization with 2 promoters (P1 and P2), which give rise to 2 biologically distinct 5´ untranslated regions (UTRs) (yellow and orange) (Levanon 2004). In humans and mice, each gene resides on different chromosomes (human 21, 6 and 1 and mouse 16, 17 and 4, respectively) (Levanon 2004). The highly conserved Runt domain is encoded by 3 exons, as marked in green. Exons comprising the transactivation domain are shown in black and grey and the 3´ UTR in blue (Levanon 2004). **(B)** The Runt domain directs binding to the RUNX DNA-motif (PyGPyGGT) at the promoter of target genes and protein-protein interactions with the core-binding factor-β (CBFβ) (Levanon 2003). The Runx proteins bind to the same DNA motif and either activate or repress transcription through interactions with other exemplarily listed transcription factors (blue ellipse) and co-activators (arrows) or co-repressors (blocked line) (Levanon 2003).

1.5. Runx1 - isoforms and expression patterns

First identified in 1991, the research community mainly focused on the effect of Runx1 in the context of acute leukemia and cancer (Okuda 1996, Okada 1998). The major physiological function of Runx1 was revealed by gene-targeting studies, showing that Runx1 is required for definitive hematopoiesis (Okuda 1996, Wang 1996, Okada 1998, Challen 2010). Although the absence of Runx1 does not affect primitive hematopoiesis or development of the yolk sac vasculature, $Runx1^{-/-}$ embryos die between embryonic day 11.5 (E11.5) and E12.5 due to extensive hemorrhaging and complete effacement of hematopoiesis (Okuda 1996, Wang 1996, Challen 2010). In addition, Runx1 acts heterogeneously in different cell lines, e.g. it is activating the transcription of a target gene in some cells, whereas it is suppressing it in others (Tang 2018). This agile functionality is achieved throughout differential splicing and utilization of 2 promoters, resulting in different isoforms with molecular sizes between 20-52kDa (Figure 12) (Challen 2010, Tang 2018).

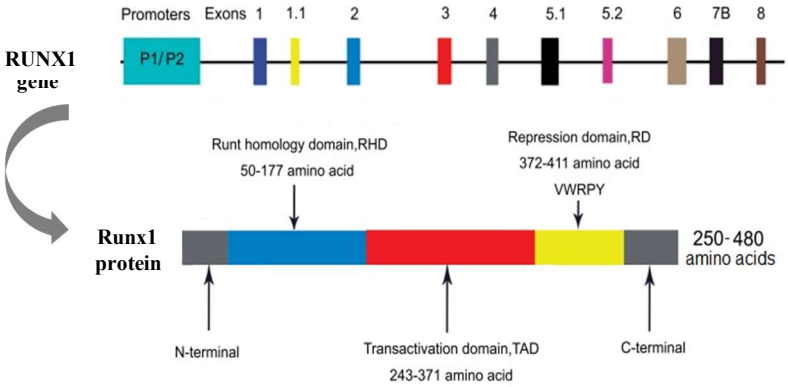

Figure 12: The structure of the RUNX1 gene and Runx1 protein, adapted from Tang et al. (Tang 2018). Expression of RUNX1 is initiated by 2 promoters (distal P1 and proximal P2), resulting in different mRNAs of RUNX1, and is translated by different exons (Challen 2010, Tang 2018). The promoters are separated from each other by >100 Kb within the genome (Challen 2010). These 4 subtypes of the Runx1 protein are composed of different combinations of domains that give rise to different features, enabling agile functionality either as a transcriptionally repressive or as an active factor (Tang 2018). All isoforms share the highly conserved Runt DNA-binding domain (RHD), whereas the transactivation domain (TAD), the repression domain (RD), containing the inhibitory VWRPY motif at the extreme carboxyl terminus (C-terminal, for interaction with the co-repressors), are expressed only in particular isoforms (Ito 2015).

A tissue-specific expression of RUNX1 genes is tightly regulated at transcriptional and post-transcriptional levels, but the molecular mechanisms that control the spatial and temporal patterns of RUNX1 expression are still not clear (Tang 2018). Furthermore, recent studies attributed Runx1 to act as a cytoplasmic attenuator of nuclear factor

"kappa-light-chain-enhancer" of activated B-cells (NF-κB) activity, indicating an active Runx1 translocation from the nucleus to the cytoplasm, which serves to modulate the innate immune response in the airway (Tang 2018). These findings highlight the importance of maintaining a precise intracellular level of RUNX1, as described for respiratory epithelial cells (Tang 2018). Even more, Li et al. reported the ability of Runx1 to regulate and modulate its own activity by homodimerization via C-terminus-C-terminus interactions (Li 2007). In its function as a molecular scaffold, Runx1 might be an interesting candidate for combinatorial transcription control, which is required for lineage commitment and tissue-specific gene expression (Lian 2004, Li 2007). Nevertheless, Runx1 expression is restricted to the epithelium of several glandular soft tissues including lung, trachea, thyroid and salivary glands and absent in the myocardium despite the left and right valvular region (V) of the heart at stage E16.5 (Figure 13) (Levanon 2001, Lian 2003).

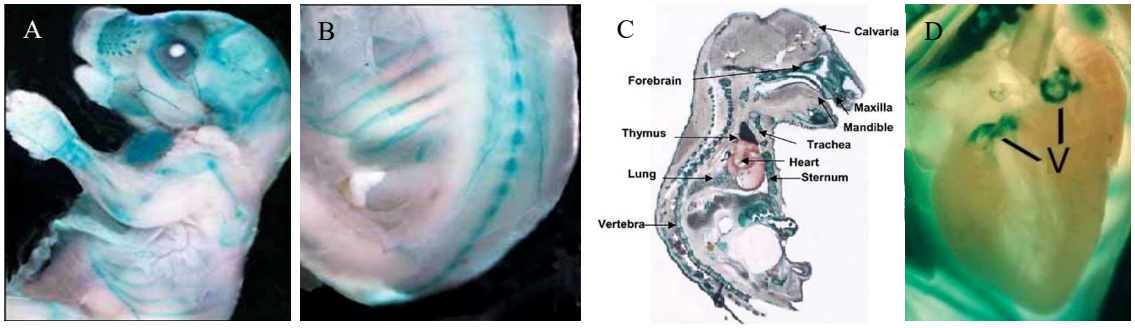

Figure 13: Runx1 activity in skeletal and soft tissues of neonatal mice, adapted from Lian et al. and Levanon et al. (Levanon 2001, Lian 2003). (A-D) X-gal staining of $Runx1^{lacZ/+}$ newborn (A-C) and embryonic (D) mice after removal of the skin from whole embryo (A+B), except at the snout and paws, displayed a Runx1 driven beta-galactosidase (βgal) activity in the indicated skeletal and soft tissues: (A) Sagittal view of upper body, (B) rotated view of lower body, and (C) cryosectional view of newborns (Lian 2003). A negative tissue (heart) is also shown despite a βgal/X-gal staining (D), showing an expression of Runx1 in the left and right valvular region (V) of the heart at stage E16.5 (Levanon 2001).

1.6. Cell tracing and fate mapping during myocardial renewal

Due to the high heterogeneity and complexity of the pathophysiology of ischemic heart disease, it is necessary to go other ways for the identification of novel therapeutic strategies (Perrino 2017). For such a purpose, successful lineage-tracing experiments have been evolved and continue to revolutionize stem cell biology in order to understand single cell dynamics, the fate of distinct cells during development and regeneration (Chong 2014, Hsu 2015). Lineage tracing strategies (illustrated in Figure 14) mark the cells of interest at a particular time point and their derived progeny at later time points

(Chong 2014, Hsu 2015). Cell fate determination requires (a) sufficiently stable and non-toxic markers, (b) a careful assessment of cells to be tracked and (c) markers, which remain exclusively in the original cell and progeny population (Hsu 2015). To especially investigate cardiac development and CM regeneration, lineage-tracing studies have been performed in zebrafish, chicks and mice (Foglia 2016, Sanchez-Iranzo 2018). To date, 2 major systems have been successfully used for lineage tracing in transgenic mice, i.e. the tetracycline-sensitive system (e.g. Tet-OFF) and the Cre/LoxP-recombinase system (either constitutive or inducible) (Gossen 1992, Jaisser 2000). In case of Tet-OFF (Figure 14), the tetracycline-sensitive transcriptional activator (tTA), under the control of an appropriate promoter sequence (e.g. gene of interest), remains always "on" and is able to activate the gene expression of transgenes via a regulatory tetracycline response element (TRE) positioned upstream of a transgenic cassette (Chong 2014). The Cre/LoxP-recombinase system allows a genetic labeling of cardiac and non-myocyte lineages by the usage of conditional gene recombination in a temporal and cell type specific manner (Figure 14) (Chong 2014, Zhang 2019).

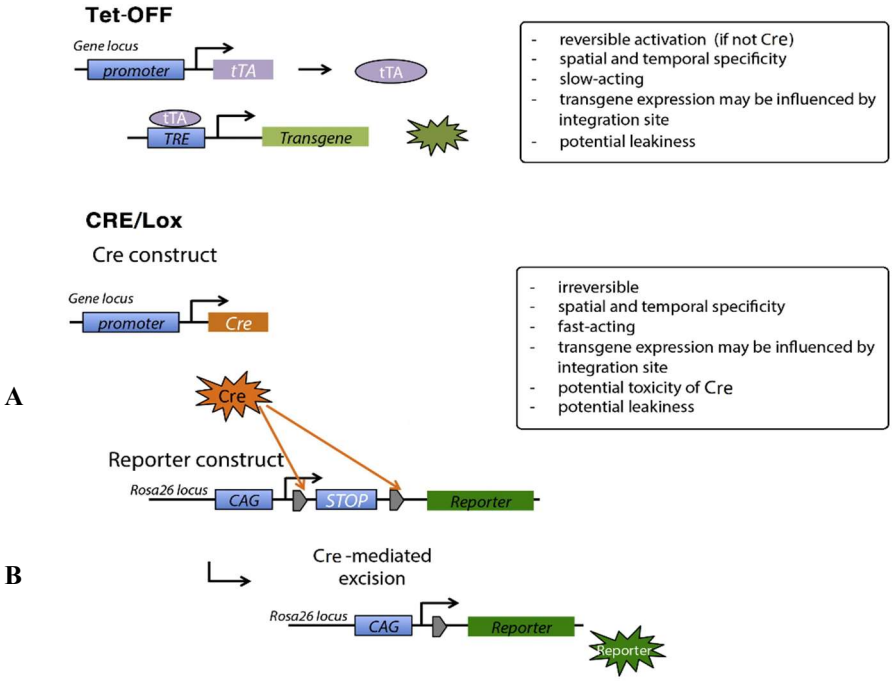

Figure 14: Genetic lineage tracing strategies, adapted from Chong et al. (Chong 2014). The Tet-OFF system is characterized by tetracycline-sensitive transcriptional activator (tTA) expression under the control of an appropriate promoter sequence (e.g. gene of interest), whereby the expression of a reporter transgene downstream of the tetracycline response element (TRE) gets activated (Chong 2014). The Cre/Lox system for genetic lineage tracing consists of 2 main elements: **(A)** The genetic construct, in which the gene for Cre is placed under control of an appropriate promoter to gain lineage specific expression, **(B)** the reporter construct, from which the expression of a marker protein occurs after Cre-mediated excision of a "STOP" cassette, flanked by 2 LoxP sites (Chong 2014). Without Cre, the STOP cassette inhibits the expression of the marker (Chong 2014).

1.7. High-throughput techniques linked to pathophysiology of the ischemic heart

Since modifications of cardiac gene expression have been consistently linked to pathophysiology of the ischemic heart, the integration of epigenomic and transcriptomic data seems to be a promising approach in order to identify crucial disease networks, which could ameliorate the outcome of these patients (Perrino 2017). High-throughput techniques like next-generation (NGS) or deep sequencing allow genome-wide investigation of genetic variants, identification of epigenetic modifications or profiling of associated gene expression patterns (Hausenloy 2017, Perrino 2017). In contrast to other approaches, which are primarily based on a pathophysiological model, following a putative, single molecular target, these unbiased strategies might be more helpful to identify full networks and multiple key targets, determining cardiac dysfunction in response to myocardial ischemia as well as to reperfusion (Figure 15) (Perrino 2017).

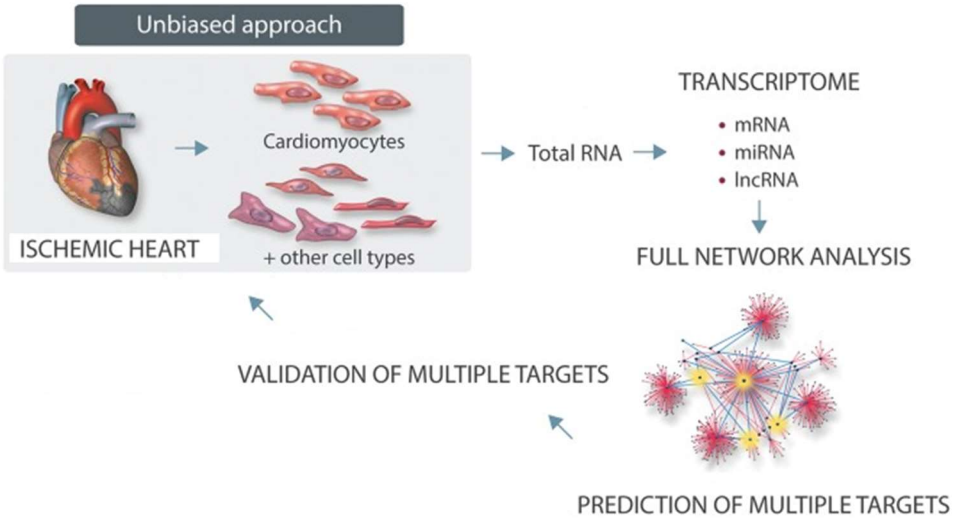

Figure 15: Illustration of an unbiased experimental omics approach by using transcriptomic profiling, adapted from Perrino et al. (Perrino 2017). Compared to a hypothesis-driven investigation, an unbiased research approach through omics methodologies has a strong potential to speed up the discovery process and to give broader insights into signaling hubs, which get activated by myocardial ischemia (Perrino 2017). Furthermore, transcriptomic profiling provides quantitative and qualitative analyses of gene expression and splicing variants and facilitates to assess alterations in the heart throughout disease progression and in response to environmental changes or treatments (Perrino 2017). Global approaches provide large data sets, which can be used for unbiased evaluations of pathophysiological processes without a priori assumption (Perrino 2017).

2. Objectives of the work

As a primary goal of this work, I wanted to assess in detail the dynamic pattern of CM dedifferentiation after the onset of experimental MI and to investigate the cell fate of dedifferentiated CMs as well as their molecular characteristics during cardiac remodeling. Based on the results of the studies by Kubin et al. (Kubin 2011), I assumed that the transcription factor Runx1 is the central inductor and regulator of CM dedifferentiation and therefore used it as the primary target gene for the validation of CM dedifferentiation. I clearly restricted the first part of the thesis to elucidate the Runx1 kinetics in vitro and in vivo. In parallel, I compared the dedifferentiation properties of Runx1 deficient with wildtype CMs in response to OSM. Furthermore, I performed an intensive micro- and nanoscopic analysis of morphological characteristics in 2 different models of myocardial ischemia (permanent vs. temporary LAD ligation) to evaluate the impact of the infarct size in relation to levels of Runx1 expression. Hence, I analyzed the amount of dedifferentiated heart muscle cells in vivo as a function of predominant $Runx1^{+}$ cells at different time points and degrees of damage. In the next step, I determined the contribution of $Runx1^{+}$ dedifferentiated CMs to myocardial regeneration and tissue plasticity after ischemic damage by a genetic cell tracing approach. The manipulation of the Runx1 gene locus therefore opened up the possibility of temporarily labeling (Runx1 Viewer) or permanently tracing (Runx1 Tracer) descendants of $Runx1^{+}$ CMs that have dedifferentiated in the heart upon myocardial injury. For this purpose, I established a genetic approach in mice, in which the transcriptional activator (tTA) was inserted at the end of the endogenous Runx1 locus. After mating with corresponding tTA-controlled Cre and reporter mice, my 2 genetic strategies (Runx1 Viewer/Tracer) enabled me, to determine the fate (survival, proliferation) of dedifferentiated CMs in the infarcted heart (Soriano 1999, Krestel 2001, Schönig 2002). Therefore, the Runx1 reporter mice were subjected to both models of experimental MI. In the following, I assessed the corresponding Runx1 expression by β-galactosidase activity (X-gal/lacZ staining) as well as the occurrence of other typical markers of dedifferentiated CMs via an immunohistochemical analyses. In the final part of the study, I combined the cell-lineage tracing approach with live-cell sorting, followed by next-generation sequencing (NGS) to deeply profile dedifferentiated CMs from the infarcted myocardium. With this experimental setting, I aimed to provide further insights into the transcriptome of dedifferentiated CMs such as proliferative activity or the ability for redifferentiation.

3. Materials and Methods

3.1. Materials

3.1.1. Chemicals and reagents

Chemicals	Company
2,4,6-Tris(dimethylaminomethyl)phenol (DMP)	SERVA Electrophoresis GmbH
2-Dodecenylsuccinic acid anhydride (DDSA)	SERVA Electrophoresis GmbH
2-Mercaptoethanol	Sigma-Aldrich®
Acetic acid	Carl Roth® GmbH + Co. KG
Adenosine	Sigma-Aldrich®
Agarose	Sigma-Aldrich®
Ampotericin B (fungizone)	Gibco™
Aprotinin	Sigma-Aldrich®
Aqua, endotoxin-free, Ecoainer®	B. Braun Melsungen AG
BenchMark™ protein ladder	Invitrogen™
Benzamidine	Sigma-Aldrich®
Bicine	Sigma-Aldrich®
Bis-Tris	AppliChem GmbH
Bovine serum albumin (BSA)	Pierce™/ Sigma-Aldrich®
Bromo phenol blue	Merck Millipore®
Calcium chloride ($CaCl_2$)	Carl Roth® GmbH + Co. KG
Cytosine β-D-arabinofuranoside (AraC)	Sigma-Aldrich®
Creatine-hydrate	Sigma-Aldrich®
Dimethylsulfoxide (DMSO)	Merck Millipore®
Disodium hydrogen phosphate (Na_2HPO_4)	Carl Roth® GmbH + Co. KG
Dithiothreitol (DTT)	Carl Roth® GmbH + Co. KG
DNA ladder (100kb)	Fermentas Life Sciences
Entelan®	Merck Millipore®
Ethanol	Carl Roth® GmbH + Co. KG
Ethanol, EM grade	SERVA Electrophoresis GmbH
Ethidium bromide	AppliChem GmbH
Ethylenediaminetetraacetic acid (EDTA)	Carl Roth® GmbH + Co. KG
Fetal calf serum (FCS)	Sigma-Aldrich®
Glycerol	Carl Roth® GmbH + Co. KG
Glycid ether 100	SERVA Electrophoresis GmbH
Glucose	Carl Roth® GmbH + Co. KG
Hanks balanced salt solution (HBSS)	Gibco™
HEPES	Sigma-Aldrich®
Hydrochloric acid (HCl)	Carl Roth® GmbH + Co. KG
IPG buffer 3-10NL	GE Healthcare
Iodoacetamide	Sigma-Aldrich®
Isopropanol	Sigma-Aldrich®
L-carnithine	Sigma-Aldrich®
Leupeptin	Sigma-Aldrich®
Magnesium chloride ($MgCl_2$)	Sigma-Aldrich®
Magnesium sulfate ($MgSO_4$)	Carl Roth® GmbH + Co. KG
Medium 199	Gibco™
MES SDS running buffer 20x	Invitrogen™
Methanol	Carl Roth® GmbH + Co. KG
Methylnadic anhydride (MNA)	SERVA Electrophoresis GmbH
Mowiol 4-88	Sigma-Aldrich®
Nitrocellulose transfer membrane	Protran
NuPAGE 4-12% bis-tris gel, 1mm x 17-well	Invitrogen™
Osmium tetroxide, 4% aqueous solution	PechineyScience Services

Parafilm	Pechiney
Paraformaldehyde	Merck Millipore®
PCR buffer mix	Eppendorf
Penicillin / streptomycin	Gibco™
Peptide calibration standard	Bruker™
Phenylmethylsulfonylfluoride (PMSF)	Sigma-Aldrich®
Polyanetholesulfonic acid (PAS)	Sigma-Aldrich®
Potassium chloride (KCl)	Carl Roth® GmbH + Co. KG
Potassium dihydrogen phosphate (KH_2PO_4)	Sigma-Aldrich®
Propylene oxide	SERVA Electrophoresis GmbH
Red Alert™ (Ponceau) 10x	Novagen
Rotiphorese gel 40 (19:1)	Carl Roth® GmbH + Co. KG
Skim milk powder	Sigma-Aldrich®
Sodium bicarbonate ($NaHCO_3$)	Sigma-Aldrich®
Sodium chloride (NaCl)	Carl Roth® GmbH + Co. KG
Sodium dodecylsulfate (SDS)	Carl Roth® GmbH + Co. KG
Sodium fluoride (NaF)	Sigma-Aldrich®
Sodium orthovanadate	Sigma-Aldrich®
Taurine	Sigma-Aldrich®
Tetramethylethylenediamine (TEMED)	Sigma-Aldrich®
Trifluoracetic acid (TFA)	Sigma-Aldrich®
Tris-HCl	Carl Roth® GmbH + Co. KG
Tween 20	Carl Roth® GmbH + Co. KG
Uranyl acetate*2H2O	SERVA Electrophoresis GmbH
Whatman® Filter paper	Sigma-Aldrich®
Xylol	Carl Roth® GmbH + Co. KG

3.1.2. Enzymes and recombinant proteins

Proteins and enzymes	**Company**
Collagenase type II	Worthington Industries
Nase I	Promega GmbH
Elastase	Sigma-Aldrich®
Oncostatin M (Mouse)	R&D Systems
Proteinase K	Carl Roth® GmbH + Co. KG
RNase A	Roche
RNasin®	Invitrogen™
RNA polymerases	Promega GmbH
Sequencing grade modified trypsin, porcine	Promega GmbH
Soybean trypsin inhibitor	Worthington Industries
SuperScriptTM II reverse transcriptase	Invitrogen™
Trypsin	Promega GmbH

3.1.3. Primary and secondary antibodies

Primary antibodies	**Coupling**	**Host**	**Dilution**	**Company**
α-actinin 1 (ACTN1)	-	Rabbit	1:100	Sigma-Aldrich®
α-sarcomeric actin (ACTN2)	-	Mouse	1:100	Sigma-Aldrich®
α-smooth muscle actin (αSMA)	-	Mouse	1:100	Sigma-Aldrich®
Pan-actin (Actin)	-	Rabbit	1:5000	Cell Signaling
Atrial natriuretic peptide (ANP)	-	Rabbit	1:50	Chemicon
F-actin	-	Mouse	1:100	Abcam

F-actin	Alexa 488	Mouse	1:100	Invitrogen™
F-actin	Alexa 633	Mouse	1:100	Dyomics
Lectin	FITC	Ulex europaeus	1:100	Merck KGaA
Moesin	-	Rabbit	1:100	Cell Signaling Technology
PCM1	-	Mouse	1:100	Santa Cruz Biotechnology
RFP-Booster	Atto647N	Alpaca	1:200	Chromotek
Runx1	-	Rabbit	1:100	abcam
Runx1	AF 568	Rabbit	1:100	abcam
Runx1	AF 647	Rabbit	1:100	abcam
Timp1	-	Rat	1:1000	R&D Systems
Secondary antibodies	**Coupling**	**Host**	**Dilution**	**Company**
Anti-goat	Alexa 488	Chicken	1:100	Invitrogen™
Anti-goat	Alexa 594	Chicken	1:100	Invitrogen™
Anti-goat IgG (H+L)	Biotin	Donkey	1:100	Dianova GmbH
Anti-goat	Cy3	Donky	1:300	Sigma-Aldrich®
Anti-goat	HRP	Rabbit	1:1000	Sigma-Aldrich®
Anti-mouse	Alexa 488	Donkey	1:100	Abcam
Anti-mouse	Alexa 594	Donkey	1:100	Invitrogen™
Anti-mouse IgG (H+L)	Biotin	Donkey	1:100	Dianova GmBH
Anti-mouse	Cy3	Donkey	1:300	Sigma-Aldrich®
Anti-mouse	FITC	Donkey	1:100	Merck Millipore®
Anti-mouse	HRP	Goat	1:1000	Pierce
Anti-rabbit	Alexa 594	Goat	1:100	Invitrogen™
Anti-rabbit IgG (H+L)	Biotin	Donkey	1:100	Dianova GmbH
Anti-rabbit	Cy3	Donkey	1:300	Sigma-Aldrich®
Anti-rabbit	FITC	Goat	1:100	Merck Millipore®
Anti-rabbit	HRP	Goat	1:1000	Pierce
Anti-rat	Alexa 488	Donkey	1:100	Invitrogen™
Anti-rat	Alexa 594	Donkey	1:100	Invitrogen™
Anti-rat IgG (H+L)	Biotin	Donkey	1:100	Dianova GmbH
Anti-rat	Cy3	Donkey	1:300	Sigma-Aldrich®
Anti-rat	HRP	Rabbit	1:1000	Amersham
Streptavidin	FITC	Streptomyces avidinii	1:100	Rockland
Streptavidin	Cy3	Streptomyces avidinii	1:300	Rockland
Streptavidin	HRP	Streptomyces avidinii	1:5000	Invitrogen™

3.1.4. Oligonucleotides

The oligonucleotides were obtained from Sigma-Aldrich® Chemie GmbH (Steinheim).

Gene	Primer name	Sequence (5'→3')	Annealing temperature
Runx1-YFP	mRUFP forB	CAT GGT GGG CGG AGA GAG AT	58°C
Runx1-YFP	mRUFP revB:	GCT GAA CTT GTG GCC GTT TA	58°C
YFP-tTA	mYFPtTA-forC	CGGGATCACTCTCGGCAT	56°C
YFP-tTA	mYFPtTA-revC	AGGGTAGGCTGCTCAACTCC	56°C
FLP	flp gt_s	GTC CAC TCC CAG GTC CAA CTG CAG CCC AAG	61°C
FLP	flp gt_as	CGC TAA AGA AGT ATA TGT GCC TAC TAA CGC	61°C
LC1Cre	MH61-Cre	GACCAGGTTCGTTCACTCATGG	55°C
LC1Cre	MH63-Cre	AGGCTAAGTGCCTTCTCTACAC	55°C

Rosa26	RosaFA	AAA GTC GCT CTG AGT TGT TAT	57°C
Rosa26	RosaRF	GGA GCG GGA GAA ATG GAT ATG	57°C
Rosa26	Rosa-SpliAC	CAT CAA GGA AAC CCT GGA CTA CTG	57°C
GFPlacZ	Lac Z s	GTTGCAGTGCACGGCAGATACACTTGCTGA	55°C
GFPlacZ	Lac Zas	GCCACTGGTGTGGGCCATAATTCAATTCGC	55°C

3.1.5. Equipment and software

Equipment	Company
Axioplan 2 imaging	Carl Zeiss
Biofuge	Heraeus Instruments
Bio-plex system	Bio-Rad®
BioSorter	Union Biometrica Inc.
Casting chamber	Hoefer
Cell culture incubator	Heraeus Instruments
Cell scrapers	Greiner Bio-One®
ChemiDoc™ MP system	Bio-Rad®
Deep freezer (-80° C)	Liebherr
Electrophoresis unit (Agarose)	Peqlab
Ettan IPGphor II isoelectric focusing	System Pharmacia Biotech
FLUOstar® galaxy microplate reader	BMG
Freezer (-20° C)	Liebherr
Gel documentation unit	Bio-Rad®
Glasses (20 x 20cm and 20 x 22.5cm)	Bio-Rad®
Gyrotory water bath shaker	New Brunswick Scientific Co.
Humidity chambers (autoclavable)	LabArt UG & Co. KG
Laminar flow hood	Nuair
Ice machine	Eurfriger
iCycler (RT-PCR)	BioRad
JEM-1400Plus electron microscope	JEOL GmbH
LabChip Gx Touch 24	Perkin Elmer
Leica CM3050 S kryostat	Leica Biosystems
Leica TCS SP5 (confocal microscope)	Leica Microsystems
Leica TCS SP8 (confocal microscope)	Leica Microsystems
Light microscope DM IL	Leica Microsystems
Master cycle gradient PCR	Eppendorf
Microwave oven	Sharp
Microplate (96-wells)	Greiner Bio-One®
NextSeq500 instrument	Illumina
Nikon DS-Ri2 16.25 megapixels CMOS camera	Nikon Cooperation
Nikon Eclipse N*i*-E	Nikon Cooperation
Nylon mesh	Greiner
PELCO R2 rotary mixer	Ted Pella, Inc.
Perfusion systems for cell isolation (PSCI-M)	Hugo Sachs Elektronik Harvard Apparatus GmbH
pH meter	VWR
Plastic boxes (20 x 20 cm)	Nalgene
PCR machines: Thermocycler SensoQuest Eppendorf Mastercycler EP Gradient S DNA Engine Tetrad 2 iCycler iQ Multicolor Real Time	 Biomedizinische Elektronik GmbH Eppendorf AG Bio-Rad® Bio-Rad®
Power supply	Bio-Rad®
Power supply (Consort EV261)	Sigma-Aldrich®
Sonopuls® HD 2070 ultrasonic homogenizer	Bandelin
SlideExpress 2	Märzhäuser WETZLAR GMBH

Tissue culture dishes	Greiner Bio-One®
Trockenofen UM 500	Memmert
Ultramicrotome Ultracut E	Reichert-Jung / Leica Microsystems
Ultra-diamond knife, 45° knife angle	Diatome
Vacuum pump unit	RFA
VersaDocTM 3000	Bio-Rad®
Vortexer	VWR
XCell II™ Blot module	Invitrogen™
Software	**Company**
Fiji/ImageJ	National Institutes of Health
FlowPilot	Union Biometrica
Image Lab	Bio-Rad®
Imaris (x64, 8.4.0)	Bitplane AG
LASX	Leica Microsystems
NIS-Elements	Nikon Cooperation
Quantity One	Bio-Rad®
TEM Center, Ver. 1.6.11.4714	JEOL GmbH

3.1.6. Consumables

Dishes and plates	**Company**
96-well flat bottom microplates	Greiner Bio-One®
6-well and 96-well Cellstar® cell culture plates	Greiner Bio-One®
10cm Cellstar® cell culture dishes	Greiner Bio-One®
10cm Petri dishes	Greiner Bio-One®
Nunc™ Lab-Tek™ II CC2™ chamber slide system	ThermoFisher Scientific™
Pipetting	**Company**
Cellstar® serological pipettes	Greiner Bio-One®
Combitips® Plus electronic pipette tips	Eppendorf
Disposable pipette tips	Greiner Bio-One®
Fisherbrand™ SureOne™ filter tips	ThermoFisher Scientific™
Tubes and filters	**Company**
1mL CryoTube™ vials	Nunc™
1.5 and 2mL Polypropylene tubes	Eppendorf
12mL Polypropylene two-position cap tubes	Greiner Bio-One®
15 and 50mL Cellstar® polypropylene tubes	Greiner Bio-One®
PCR 8er SoftStrips 0.2mL	Biozym®
Sectioning and staining	**Company**
Anti-rolling glass plate 70mm	Leica Biosystems
Cu/Rh, 200 mesh, grids	Plano
FSC 22 clear frozen section compound	Leica Biosystems
Microtome blades S35	FEATHER® Safety Razor Co. Ltd.
SuperFrost™ ultra plus adhesion slides	Thermo Scientific™
Tissue-Tek® OCT™	Labtech International Ltd
Sequencing (NGS)	**Company**
miRNeasy micro kit	QIAGEN©
SMARTer® stranded total RNA-seq kit	Takara Clontech

3.2. Buffers and solutions

3.2.1. Cell culture reagents, buffers, solutions and medium

Perfusion buffer (calcium free), pH 7.4	**Concentration**	**Company**
NaCl	113mM	Sigma-Aldrich®
KCL	4.7mM	Sigma-Aldrich®
KH_2PO_4	0.6mM	Sigma-Aldrich®

Na_2HPO_4	0.6mM	Sigma-Aldrich®
$MgSO_4$ x $7H_2O$	1.2mM	Sigma-Aldrich®
$NaHCO_3$	12mM	Sigma-Aldrich®
$KHCO_3$	10mM	Sigma-Aldrich®
HEPES	10mM	Sigma-Aldrich®
Taurin	30mM	Sigma-Aldrich®
2.3-Butanedionemonoxime (BDM)	10mM	Sigma-Aldrich®
D(+)-glucose	5.5mM	Carl Roth® GmbH + Co. KG
Remark: Perfusion buffer was titrated to pH 7.4 with HCl and sterile filtered before BDM was added. 10mM BDM was always freshly prepared on the day of perfusion. Therefore, 2.5g of BDM was diluted in 50mL Aqua Braun (B. Braun®) and sterile filtered and directly added to the 2L of Perfusion buffer (1x).		
Digestion buffer	**Concentration**	**Company**
Liberase DH	0.25mg/mL	Roche
Trypsin	0.14mg/mL	Sigma-Aldrich®
$CaCl_2$	12.5µM	Merck Millipore®
Remark: Prepared in perfusion buffer (calcium free)		
Stop buffer	**Concentration**	**Company**
FCS	5% or 10% (see methods)	Sigma-Aldrich®
$CaCl_2$	12.5µM	Sigma-Aldrich®
Remark: Prepared in digestion buffer		
Cell culture medium, pH 7.3	**Concentration**	**Company**
Medium 199 (M199)	-	Gibco
Creatine x H_2O	5mM	Sigma-Aldrich®
L-carnithin x HCl	2mM	Sigma-Aldrich®
Taurin	5mM	Sigma-Aldrich®
HEPES	25mM	Sigma-Aldrich®
Pen-Strep	1%	Sigma-Aldrich®
FCS	2, 5 or 10% (see methods)	Sigma-Aldrich®
ITs supplement	1%	Sigma-Aldrich®

3.2.2. Electrophoresis reagents, buffers and recipes

Reagents and consumables	**Volume**	**Company**
Protein Marker VI (10 - 245) prestained	5µL/lane	AppliChem®
Nunc™ Tris-Acetate Mini Gels with multi-shells	10µL/lane	Thermo Scientific™
Phosphate-buffered saline (PBS)	**Concentration**	**Company**
Na_2HPO_4	10mM	Roth®
KH_2PO_4	1.5mM	Merck Millipore®
NaCl	137mM	Merck Millipore®
KCl	2.7mM	Merck Millipore®
Remark: pH was adjusted to 7.4 with HCl.		
Protease/phosphatase inhibitor mix	**Concentration**	**Company**
Benzamidin	250mg/mL	Sigma-Aldrich®
Aprotinin	2mg/mL	Sigma-Aldrich®
Leupeptin	2mg/mL	Sigma-Aldrich®
PMSF	0.2M	Sigma-Aldrich®
$NaVO_4$	1M	Sigma-Aldrich®
NaF	1M	Sigma-Aldrich®
Protein extraction buffer	**Concentration**	**Company**
Tris-HCl, pH 8.8	100mM	Roth®
EDTA	10mM	Bio-Rad®
1.4-Dithiothreitol (DTT)	40mM	Carl Roth® GmbH + Co. KG
Sodium dodecyl sulfate (SDS) ultra-pure ≥ 99.5%	10%	Carl Roth® GmbH + Co. KG
Remark: pH was adjusted to 8.0 with HCl.		

Protein loading buffer (5x)	Concentration	Company
Tris-HCl, pH 6.8	66.7mM	Carl Roth® GmbH + Co. KG
Sodium dodecyl sulfate (SDS) ultra-pure ≥ 99.5%	2%	Carl Roth® GmbH + Co. KG
Glycerol	27%	Carl Roth® GmbH + Co. KG

3.2.3. Western blotting reagents, buffers and recipes

Protein transfer buffer	Concentration	Company
Bis Tris	25mM	Applichem®
Bicine	25mM	Sigma-Aldrich®
EDTA	1mM	Bio-Rad®
Methanol	20%	Carl Roth® GmbH + Co. KG
1x Tris-EDTA (TE) buffer	**Concentration**	**Company**
Tris-HCl, pH 7.4	10mM	Carl Roth® GmbH + Co. KG
EDTA	1mM	Bio-Rad®
1x Tris-Acetat-EDTA (TAE)	**Concentration**	**Company**
Tris-HCl, pH 7.8	40mM	Carl Roth® GmbH + Co. KG
Acetic acid	40mM	Carl Roth® GmbH + Co. KG
EDTA	2mM	Carl Roth® GmbH + Co. KG
1x MES SDS Running buffer, pH 7.3	**Concentration**	**Company**
MES	50mM	Carl Roth® GmbH + Co. KG
Tris-HCl	50mM	Carl Roth® GmbH + Co. KG
SDS	0.1%	Carl Roth® GmbH + Co. KG
EDTA	1mM	Bio-Rad®
10x TBS buffer (5L)	**Concentration**	**Company**
NaCl	50mM	Carl Roth® GmbH + Co. KG
Tris-HCl	50mM	Carl Roth® GmbH + Co. KG
Remark: pH was adjusted to 7.6 and volume was filled up with distilled water.		
1x TBS-T buffer (5L)	**Volume**	**Company**
10x TBS buffer	250mL	Carl Roth® GmbH + Co. KG
Tween 20	5mL	Carl Roth® GmbH + Co. KG
Remark: Volume was filled up with distilled water.		
20x Transfer buffer (2L)	**Weight**	**Company**
Bicine	163.2g	Carl Roth® GmbH + Co. KG
Bis Tris	209.3g	Applichem®
EDTA	12g	Bio-Rad®
Remark: Volume was filled up with distilled water.		
1x Transfer buffer (5L)	**Volume**	**Company**
20x Transfer buffer	250mL	Carl Roth® GmbH + Co. KG
Methanol	1000mL	Carl Roth® GmbH + Co. KG
Remark: Volume was filled up with distilled water.		

3.2.4. Buffers for isolation of genomic DNA

Tail lysis buffer (TENS)	Concentration	Company
Tris-HCl, pH 8.0	40mM	Carl Roth® GmbH + Co. KG
EDTA, pH 8.0	100mM	Bio-Rad®
NaCl	100mM	Carl Roth® GmbH + Co. KG
Sodium dodecyl sulfate (SDS) ultra-pure ≥ 99.5%	1%	Carl Roth® GmbH + Co. KG

3.2.5. Buffers for staining and special reagents for microscopy

EGTA, 0.5M (pH 7.5)	Concentration	Company
EGTA	19.02g/100mL	Carl Roth® GmbH + Co. KG
Remark: pH was adjusted to 7.5 using 10N NaOH.		

Epon	**Weight**	**Company**
Glycid ether	47.04g	SERVA Electrophoresis GmbH
DDSA	24.7g	SERVA Electrophoresis GmbH
MNA	28.26g	SERVA Electrophoresis GmbH
DMP	1.3g	SERVA Electrophoresis GmbH
Remark: Glycid ether, DDSA and MNA were measured under the fume hood and gently mixed for 20 minutes. Afterwards, DMP was added and mixed again for 30 minutes.		
Sodium phosphate buffer (SPP), pH 7.4 (1L)	**Concentration**	**Company**
Na_2HPO_4 (141.96g/L)	1M	Carl Roth® GmbH + Co. KG
NaH_2PO_4 (137.99g/L)	1M	Carl Roth® GmbH + Co. KG
Remark: Volume was filled up with distilled water and pH adjusted to 7.4.		
lacZ fixation solution	**Volume**	**Company**
SPP	50mL	-
GDA-Solution, 25% in H2O	800µL	Carl Roth® GmbH + Co. KG
$MgCl_2$, 1M	100µL	Carl Roth® GmbH + Co. KG
EGTA, 0.5M, pH 7.5	500µL	Carl Roth® GmbH + Co. KG
lacZ staining solution	**Volume**	**Company**
lacZ wash solution	48mL	-
$K_3(FeCN_6)$ (Stock: 16.463g/100mL)	500µL	Carl Roth® GmbH + Co. KG
$K_4(FeCN_6)$ (Stock: 21.12g/100mL)	500µL	Carl Roth® GmbH + Co. KG
X-gal, 5%	1mL	Carl Roth® GmbH + Co. KG
Remark: Stock solutions and prepared staining solution were stored light protected at 4°C.		
lacZ wash solution	**Volume**	**Company**
$MgCl_2$, 1M	2mL	Carl Roth® GmbH + Co. KG
Na-desoxycholat (1% in H2O)	10mL	Carl Roth® GmbH + Co. KG
NP-40 (2% in H2O)	10mL	Carl Roth® GmbH + Co. KG
Remark: Volume was filled up to 1L with SPP.		
PFA solution, 4%	**Quantity**	**Company**
Paraformaldehyde	4g	Merck Millipore®
NaOH	1N	Carl Roth® GmbH + Co. KG
PBS	0.2M	-
Remark: 4.0g paraformaldehyde were dissolved at 60°C in 40mL distilled water. The solution was then clarified with 1N NaOH and cooled down. Afterwards, the solution was diluted 1:1 with 0.2M PBS and the mixture was filtered and finally filled up to 100mL with distilled water. The finished 4% PFA solution was frozen in aliquots of about 50mL in falcons at -20°C and stored until use. Early before use an aliquot had to be thawed and stored at +4°C for 2 weeks.		
X-gal stock solution	**Concentration**	**Company**
X-gal (408.6g/mol)	50mg/mL	Carl Roth® GmbH + Co. KG
Remark: X-gal was dissolved in Dimethylformamide and stored light protected at -20°C.		

3.3. Methods

3.3.1. Animal experimentations - approvals and guidelines

All experimental work with animals followed the legal requirements of the German animal welfare act and the European direction for animal welfare and protection (Verbraucherschutz 1972, Union 2010). The experiments were approved by the local authority (Regierungspräsidium Darmstadt) and performed in line with the corresponding animal protocols.

3.3.2. Mouse lines - origin, nomenclature and housing of animals

The mouse lines used for my thesis, listed below, were kept in plastic cages on litter, while dry food and water were given as they wished. A strict day and night cycle of 12 hours each was followed. The mice were ear punched at the age of 2 to 3 weeks for distinctive identification. In addition, tail biopsies were taken at the same time to obtain genomic DNA for determination of the corresponding genotype.

Abbreviation	Mouse line	Origin
Wildtype	C57Bl6/J	Jackson Lab/MPI-HLR
$Runx1^{fl2}$	Runx1-flox-flox	Jackson Lab
$Runx1^{fl2}/\alpha MHC^{Cre}$	Runx1-flox-flox/alpha-Myosin-Heavy-Chain-Cre	Jackson Lab/MPI-HLR
$Runx1^{tTA}$	Runx1-t2A-tTA-t2A	MPI-HLR
Runx1 Tracer	$Runx1^{tTA}/LC1^{Cre}/Rosa26^{stopfloxlacZ}$ $Runx1^{tTA}/LC1^{Cre}/Rosa26^{stopfloxRFP}$	MPI-HLR
Runx1 Viewer	$Runx1^{tTA}/Tg^{GFPtetO7lacZ}$	MPI-HLR

3.3.3. Different mouse lines and genetic background

3.3.3.1. $Runx1^{fl2}/\alpha MHC^{Cre}$ (heart specific knock-out)

The conditional Runx1 mouse strain, Runx1-flox-flox ($Runx1^{fl2}$), was purchased from The Jackson Laboratory (ID: B6;129-Runx1tm3.1Spe/J; JAX stock no #010673) and has been initially generated by Growney et al. (Li 2004, Growney 2005). These mice possessed LoxP sites on each side of exon 4 of the targeted gene, as described by the Jackson Laboratory and originated from Li et al (https://www.jax.org/strain/010673 , Li 2004). Those animals that were homozygous for this allele, were viable, fertile, of normal in size and did not display any gross physical or behavioral abnormalities, according to the Jackson Laboratory and proven by own observation and testing. (https://www.jax.org/strain/010673). The $Runx^{fl2}$ mouse line was used to generate a mutant strain, particularly deficient for Runx1 in CMs. For this purpose, the alpha-Myosin-Heavy-Chain-Cre mouse line (αMHC^{Cre}) was used (Agah 1997). By mating the $Runx1^{fl2}$ with the αMHC^{Cre} mice, the resulting offspring exhibited Runx1 exon 4 deletion in αMHC-expressing CMs ($Runx1^{fl2}/\alpha MHC^{Cre}$).

3.3.3.2. Runx1-t2A-tTA-t2A ($Runx1^{tTA}$)

The Runx1-t2A-tTA-t2A strain constituted a genetic knock-in mouse model, based on a self-cleaving t2A approach, as applied before in my department and described by Salwig

et al. (Salwig 2019). Therefore, a 2A-sfYFP-2A-tTA-cassette was inserted downstream of the Runx1-promotor**,** right after exon 8**,** and ended with the tetracycline-controlled transactivator (tTA) gene before the stop-codon of the whole gene sequence. This gene construct, displayed in Figure 16, was cloned as part of a scientific in-house cooperation indenting to generate the basis for Runx1 labeling and tracing. Chimeric animals, resulted from embryonic-stem cell injection, were mated with an in-house FLP deleter mouse strain in order to lose the FRT-flanked neomycin cassette (Rodriguez 2000, Growney 2005). Afterwards, Runx1^{tTA} mice were crossed back with C57Bl6/J mice for 5 generations to receive a relatively pure genetic background.

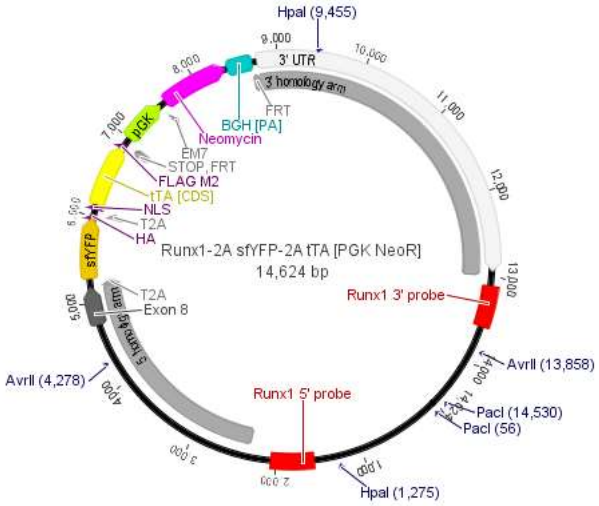

Figure 16: Genetic Runx1-t2A-tTA-t2A construct of the Runx1^{tTA} knock-in model. The cloning of the genetic construct shown was achieved by an in-house scientific cooperation and represented the basis for further generation of a Runx1-mediated labeling and tracing.

3.3.3.3. Runx1 Tracer: permanent labeling of once Runx1 expressing cells

The starting point for the genetic Runx1 tracing was the mating of Runx1^{tTA} with a transgenic LC1^{Cre} mouse line, which was initially described by Schönig et al. (Schönig 2002). By using this approach, the Runx1 initiated tTA expression (Tet-OFF) enabled the activation of Cre expression by binding of the tTA protein to the promoter region of LC1^{Cre}. In order to mark cells with Runx1 permanently, the Runx1^{tTA}/LC1^{Cre} line was then crossed with a Rosa26^{stopfloxlacZ} mouse line. This line, established by Soriano et al., inherited a LoxP-flanked DNA STOP sequence, which prevented the expression of the downstream β-galactosidase (βgal) (Soriano 1999). The LC1^{Cre}-initiated homologous recombination of LoxP sites enabled a permanent βgal expression in the cell offspring.

By this means, an efficient recombination occurred in all tissues, where Runx1 induced tTA expression was once present, what enabled in the following a permanent Runx1 tracing by lacZ expression and is visualized in Figure 17. This specific mouse line (Runx1 Tracer) was used to follow the cell fate of once Runx1 expressing cells, whereas Runx1 tracing was visualized by lacZ staining.

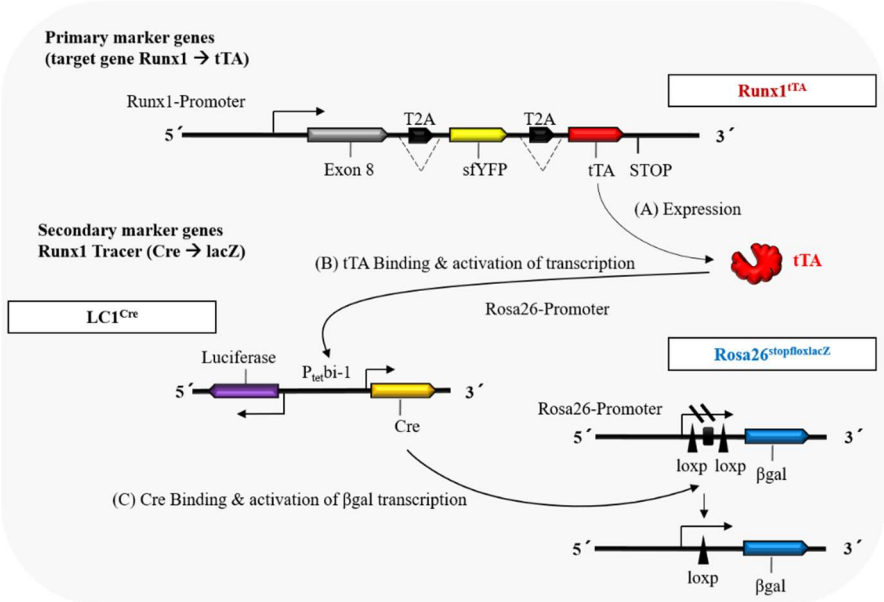

Figure 17: Schematic illustration of the genetic lineage tracing approach. (A) The activation of Runx1 transcription triggered the tetracycline-controlled transactivator (tTA) protein expression in cells of the Runx1^{tTA} strain. **(B)** The expressed tTA was then able to bind to the bidirectional promotor of the LC1^{Cre}, which led to an activated Cre expression. **(C)** The Cre-recombinase operated as a transcriptional activator of β-galactosidase (βgal) expression. Therefore, once Runx1 expressing cells could be made visible by lacZ staining.

To achieve a suitable mouse line for live-cell sorting of Runx1-traced CMs, the Runx1^{tTA}/LC1^{Cre} mice were mated with the Rosa26^{stopfloxRFP} mouse line, which was initially established by Luche et al. (Luche 2007). Here, a LoxP-flanked DNA STOP sequence prevented the expression of the downstream RFP gene. This specific mouse line was used to follow the cell fate of once Runx1 expressing cells by RFP fluorescence. Then, the expressed tTA activated, under the control of the Runx1 promotor, the LC1^{Cre}, which further excised the floxed stop codon in the Rosa26^{stopfloxRFP} to enable the RFP expression.

3.3.3.4. Runx1 Viewer: labeling of current Runx1 expressing cells

To monitor current expression of Runx1 post MI, the Runx1^{tTA} strain was mated with the transgenic mouse line Tg^{GFPtetO7lacZ}, which was purchased from The Jackson Laboratory (ID: B6N.Cg-Tg(tetO-GFP,-lacZ)G3Rsp/J; JAX stock no # 018913) and was initially established by Krestel et al. and (https://www.jax.org/strain/018913 , Krestel 2001). In this transgenic mouse line, animals expressed both, a humanized green fluorescent protein (GFP) and βgal (lacZ), under the control of a bi-directional Tet-responsive element (TRE or tetO7), whereas no GFP or lacZ expression was reported in the absence of tTA (https://www.jax.org/strain/018913 , Krestel 2001). When mated them with Runx1^{tTA} mice in my study, especially lacZ expression was used to discriminate the current Runx1 expression (Figure 18).

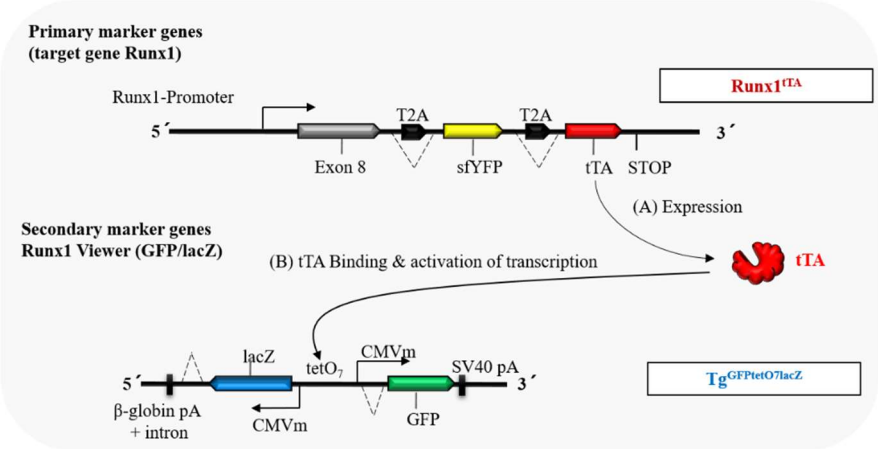

Figure 18: Schematic illustration of the genetic labeling approach. (A) The activation of Runx1 transcription-triggered tTA expression in cells of the Runx1^{tTA} strain. **(B)** The expressed tTA was then able to bind to the bidirectional promotor of the Tg^{GFPtetO7lacZ}, which led to activated lacZ expression. This approach made it possible to label currently Runx1 expressing cells via lacZ staining.

3.3.4. Harvesting and preparation of mouse hearts for morphological analyses

For conventionally histological and immunohistochemical analysis, the experimental animals were sacrificed by cervical dislocation with subsequent cutting of the diaphragm, according to the approved animal protocol, and the entire hearts were withdrawn. After washing the heart in ice-cold PBS, the atria and the aortic arch were removed. The embedding was done according to the reports of Peters et al., but with slight adaptions (Peters 2003, Peters 2003). Here, the ventricular heart tissue, including base and apex, was embedded in either FSC 22® or Tissue-Tek® OCT™ freezing medium for frozen

sections without prior fixation. The embedded parts were frozen in isopentane**,** cooled with liquid nitrogen and stored at -80°C until further use, as similarly described in Coirault et al.(Coirault 2007).

To obtain isolated CMs for in vitro analyses, the mouse was first anaesthetized with 0.1mL/10g KM ketamine/xylazine, according to the approved animal protocol. A sufficient depth of anesthesia was achieved, when inter-toe and lid reflexes were absent. Next, the abdomen was opened via a cross-section and a cut through the ribs parallel to the sternum up to the neck was performed. Last, the heart was withdrawn from the anaesthetized animal together with the lungs followed by an ex vivo perfusion of the isolated organ (without lungs).

3.3.5. Induction of myocardial infarction

Experimental myocardial infarction was induced in mice by ligating the left anterior descending coronary artery (LAD). Here, 2 different models (permanent (I) and temporary (I/R) LAD ligation) were applied by authorized scientists, according to the approved animal protocols (3.3.1) and in line with previously described in vivo experimentations from my laboratory and those of other groups (Lutgens 1999, Lörchner 2015, Xu 2018).

3.3.6. Isolation of adult mouse cardiomyocytes (mACMs)

The isolation of adult mouse cardiomyocytes (mACMs) was performed for in vitro analyses or for my established live-cell sorting approach, what was in line with the protocols of O'Connell et al., Eppenberger-Eberhardt et al., Li et al. and Mbogo et al. with individual, slight adaptions and as described below (Eppenberger-Eberhardt 1990, Li 1993, O'Connell 2007, Mbogo 2016). Depending on whether CMs were isolated from an intact or a diseased heart, strategy 1 (healthy heart) or strategy 2 (injured heart) was followed. The hearts were removed, according to descriptions above (3.3.4) and in line with the corresponding animal approvals.

3.3.6.1. Strategy 1 (healthy heart)

This strategy was used for my in vitro analyses of cultured CMs according to the protocol of Louch et al. and others with slight adaptions (Xu 2009, Louch 2011). After harvesting the heart, as described in 3.3.4, the isolated organ was mounted onto the perfusion systems for cell isolation (PSCI-M). In the initial phase, the heart was filled with a calcium-free perfusion buffer (3.2.1) to flush out the blood cells from the organ. In the second step, the myocardium was dissociated by perfusing the heart for 30 minutes with a flow rate of 70±5mL/minute and at a constant pressure of 70±5mmHg, using a collagenase-based (60 mg collagenase plus 60µL 100mM Ca^{2+} in 60 mL HBSS) enzymatic digestion buffer (3.2.1). In the meantime, cell culture plates were pre-coated with 10µg/mL of laminin. After digestion, the heart was chopped in the same collagenase-added digestion buffer followed by a filtering through a mesh with large pores into a 50mL falcon tube. Further on, the CM suspension was centrifuged at 25*g for 2 minutes and the supernatant was discarded. After CMs were washed by gently re-suspending the cell pellet in 10mL 5% FCS stop buffer**,** a next centrifugation step at 25*g for 2 minutes followed. Then, the cell pellet was gently taken up in 5mL 10% FCS stop buffer and placed on a Ca^{2+} gradient in order to obtain isolated, resting, rod-shaped CMs. When the final Ca^{2+} concentration was reached, the suspension was centrifugated at 25*g for 2 minutes and the supernatant was discarded. Next, CMs were gently taken up in 25mL culture medium**,** containing 10% FCS. After laminin-coated plates were washed with HBSS, the CM suspension was added to the plates and kept at 37°C and at 5% CO_2 for 2 hours. Then, the medium was gently exchanged and cells were kept in 5% serum for another day. On day 2, culturing of CMs was shifted to 2% serum and OSM or BSA (CON) treatment was started. For this purpose, the respective substance was added to the CM culture medium for a specified period and the incubation of the CMs was continued at 37°C and at 5% CO_2. Medium exchange was performed every second day and in any case 1 day before harvesting the cells for protein analyses. The cytokine stimulation scheme is visualized in tabular form (see next page). If the CMs were used for protein analyses, cells were lysed with protein extraction buffer**,** including proteinase/phosphatase inhibitors**,** and protein isolation was continued (3.2.2).

Group A (Isolation date)	Topic:	Dedifferentiation of OSM-treated cardiomyocytes triggered by Runx1 expression						
	Metrics:	No. of animals, (Genetic background), Project name						
Animal 1		**Approach (test)**	**Isolation**	**Media exchange**	**Stimulation 1 day**	**Media exchange**	**Media exchange**	**Stimulation 4 days**
ID, Age (weeks), ear-tag			**Monday**	**Tuesday**	**Wednesday**	**Thursday**	**Friday**	**Saturday**
Sample	**Well description**		**Day 1**	**Day 2**	**Day 3**	**Day 4**	**Day 5**	**Day 6**
Control	1.1	Slide 1 (IHC)	5 % FCS	2% Serum + BSA	Harvest			
24h OSM	1.2		5 % FCS	2% Serum + OSM	Harvest			
Control	2.1	ø3cm dish (protein)	5 % FCS	2% Serum + BSA	Harvest			
24h OSM	2.2		5 % FCS	2% Serum + OSM	Harvest			
Control	3.1	Slide 2 (IHC)	5 % FCS	2% Serum + BSA	-	2% Serum + BSA	2% Serum + BSA	Harvest
96h OSM	3.2		5 % FCS	2% Serum + OSM	-	2% Serum + OSM	2% Serum + OSM	Harvest
Control	4.1	ø3cm dish (protein)	5 % FCS	2% Serum + BSA	-	2% Serum + BSA	2% Serum + BSA	Harvest
96h OSM	4.2		5 % FCS	2% Serum + OSM	-	2% Serum + OSM	2% Serum + OSM	Harvest
Animal 2		**Approach (test)**	**Isolation**	**Media exchange**	**Stimulation 1 day**	**Media exchange**	**Media exchange**	**Stimulation 4 days**
ID, Age (weeks), ear-tag			**Monday**	**Tuesday**	**Wednesday**	**Thursday**	**Friday**	**Saturday**
Sample	**Well description**		**Day 1**	**Day 2**	**Day 3**	**Day 4**	**Day 5**	**Day 6**
Control	5.1	Slide 1 (IHC)	5 % FCS	2% Serum + BSA	Harvest			
96h OSM	5.2		5 % FCS	2% Serum + OSM	Harvest			
Control	6.1	ø3cm dish (protein)	5 % FCS	2% Serum + BSA	Harvest			
96h OSM	6.2		5 % FCS	2% Serum + OSM	Harvest			
Control	7.1	Slide 2 (IHC)	5 % FCS	2% Serum + BSA	-	2% Serum + BSA	2% Serum + BSA	Harvest
96h OSM	7.2		5 % FCS	2% Serum + OSM	-	2% Serum + OSM	2% Serum + OSM	Harvest
Control	8.1	ø3cm dish (protein)	5 % FCS	2% Serum + BSA	-	2% Serum + BSA	2% Serum + BSA	Harvest
96h OSM	8.2		5 % FCS	2% Serum + OSM	-	2% Serum + OSM	2% Serum + OSM	Harvest

3.3.6.2. Strategy 2 (injured heart)

This strategy was used to gain CMs for my live-cell sorting approach. The first 2 steps corresponded to the initial steps already described in strategy 1. But here, the dissociation of CMs was done for 60 instead of 30 minutes. After the enzymatic digestion, the atria and aorta were removed. The ventricles were divided into ischemic (IZ^{**}) and remote zone (RZ^{*}) fractions and further CM separation was achieved by in solution digestion in cell culture dishes. After the tissue was completely dissociated, the cell suspension was transferred into 50mL falcon tubes. After the CMs had settled to the bottom of the falcon tube, a centrifugation of the cell suspension followed at 300rpm for 1 minute. Next, the supernatant was then removed and the CMs were gently resuspended in perfusion buffer. Each cell solution was pre-plated onto an uncoated cell culture dish at 37°C and at 5% CO_2 for 1 hour. According to Mbogo et al., through this approach only the remaining fibroblast attached on the plates, whereas CMs stayed detached in solution (Mbogo 2016). Because of that, my procedure delivered a pure CM suspension for the sorting procedure. Further on, the cell suspension was transferred into a 50mL falcon tubes and kept on ice until the sorting took place. By this means, CMs were prevented to attach onto the plastic walls of the tube.

3.3.7. Molecular biological methods

3.3.7.1. Isolation of genomic DNA from mouse tail biopsies

The isolation of genomic DNA from murine tail biopsies was done in line with the corresponding experimental animal approval and performed, according to the descriptions of Hofstetter et al. and others, but with slight adaptions (Thomas 1989, Couse 1994, Hofstetter 1997). First, about 3-5mm large murine tail biopsies were lysed in 500µL TENS buffer**,** including 10µL Proteinase K while shaking at 55°C overnight. Then, the dissolved tails were briefly vortexed and centrifuged at full speed and at RT for 10 minutes. Next, the supernatant was transferred into a fresh 1.5mL tube and 500µL ice cold isopropanol was added to precipitate the genomic DNA. Again, tubes were centrifuged at full speed and at RT for 10 minutes. Here, the supernatant was discarded and the resulting pellet was washed with 70% ethanol followed by a full speed centrifugation step at RT for 10 minutes. Afterwards, the ethanol was discarded and the DNA was dried at RT. Last, the obtained DNA pellet was dissolved in 100µL TE buffer

(pH 7.5) while shaking at 55°C. For subsequent genotyping by PCR, 1µL of each DNA solution was used.

3.3.7.2. Polymerase chain reaction (PCR)

For genotyping, the isolated DNA fragments (3.3.7.1) were exponentially amplified by a polymerase chain reaction (PCR). In all PCRs, a heat-stable Taq DNA polymerase was used (Saiki 1988). Furthermore, the following standard PCR mix was prepared:

Component	Concentration
Taq DNA polymerase	0.07U/µL
Taq buffer (10x)	2.5µL/25µL (1x)
$MgCl_2$	50mM
dNTPs	10µM
Forward primer	10µM
Reverse primer	10µM
Genomic DNA	5ng/µL
Remark: Volume was filled up to 25µL with sterile distilled water.	

The above reagents were mixed thoroughly and subjected to PCR. The reaction mixture was pipetted on ice and the PCR reactions were performed in PCR machines. Depending on the length of the desired DNA fragment and the melting temperature of the oligonucleotides, the following procedure was used: initial denaturation at 95°C for 3 minutes, followed by 35 cycles of A) denaturation at 94°C for 30 seconds, B) hybridization at the required annealing temperature for 30 seconds, C) elongation at 72°C for 1 minute and D) final extension at 72°C for 10 minutes. The oligonucleotides and corresponding annealing temperatures used for my genotyping procedure are listed at paragraph 3.1.4.

3.3.7.3. DNA agarose gel electrophoresis

The separation of DNA fragments was done by agarose gel electrophoresis, as described by Lee et al., but with minor adaptions (Lee 2012). Here, agarose was mixed with electrophoresis buffer (1x TAE) and heated in the microwave oven until the agarose was completely dissolved. After the solution was cooled down to 55°C, ethidium bromide was added (1µL/100mL) and poured into a casting tray inside a gel box together with a well comb. Then, the comb was removed after solidification and the gel tray was placed in an electrophoresis unit filled with 1x TAE buffer. Hence, the electrophoresis was performed

at 100V and at RT for 1 hour. Finally, the PCR products were visualized by UV illumination and recorded with a gel documentation system.

3.3.7.4. Extraction of RNA from isolated and sorted mACMs

For the isolation of total RNA, including small RNAs, each fraction of CMs (IZ^{**}/RZ^{*}) was directly sorted into 6-well plates. Here**,** Nunc™ Polycarbonate membrane inserts with a pore size of 3µm were placed in wells of the carrier plate and perfusion buffer was added. After cells were collected, the culture plate was transferred to the clean bench to avoid contamination with foreign RNA. To gain a high pure RNA preparation for the further sensitive downstream application, I used the miRNeasy micro kit and the corresponding protocol for animal-derived cells (QIAGEN 2012), but with the following additional steps. First, the perfusion buffer was gently removed below the filter and 700µL QIAzol lysis reagent was added on top of the filter at RT for 5 minutes. After this incubation step, the filter grid was carefully torn off the holder, gently swayed in the lysis solution and then placed at the edge of the dish to allow the residual solution to drip off. Last, the lysate was transferred to tubes contained in the kit and the protocol was followed.

3.3.7.5. Procedure and analysis of next-generation sequencing (NGS)

The total RNA for sequencing was isolated from live-cell-sorted CMs**,** using the miRNeasy micro kit, as described in 3.3.7.4, and was combined with on-column DNase digestion (DNase-free DNase set) to avoid contamination by genomic DNA, in line with other studies (QIAGEN 2012, Gauvrit 2018, Salwig 2019). Hereafter, next-generation sequencing (NGS) was done in-house by the bioinformatics department, using the deep sequencing platform, as described by Salwig et al., but with individual aspects according to my samples (Salwig 2019). The RNA and library preparation integrity were verified with LabChip Gx Touch 24. Then, the RNA amount was adjusted to the number of isolated cells acquired by the live-cell sorting procedure (200-1000 cells/sample), as similarly reported by Hübner et al. (Hübner 2018) . Next, approximately 4ng of the total RNA was used as input for the SMARTer® stranded total RNA-seq kit - pico input mammalian, analogically to Gauvrit et al. (Gauvrit 2018). The sequencing procedure itself was performed on the NextSeq500 instrument**,** using v2 chemistry but resulting in an average of 39 million reads per library with 1x75bp single end setup (Gauvrit 2018).

In the following, bioinformatic analyses were done along the descriptions of Salwig et al. and in line with Davis et al., Liao et al. and Künne et al. (Davis 2013, Liao 2014, Kuenne 2015, Salwig 2019). Further on, I used the established NGS gene set in order to cluster specific deregulated genes, as described in 3.4.

3.3.8. Biochemical methods

3.3.8.1. Extraction of proteins, quantification and electrophoresis

To analyze protein expression levels, lysates of CMs, stimulated in 3cm cell culture dishes under different conditions, were obtained (3.3.6). For this purpose, the medium was gently removed and the dishes were washed 3 times with ice cold PBS. Next, a total volume of 100µL protein extraction and protein loading buffer, in a ratio of 3:2 and supplemented with protease/phosphatase inhibitors, was added. The cells were then scratched and the lysate was taken up in Eppendorf™ tubes. After a brief sonication procedure**,** using a Sonopuls® HD 2070 ultrasonic homogenizer at 20% power and with 10 pulses for 5 milliseconds each, 2µL of the sample was used to measure the corresponding protein concentration with an established colorimetric assay on a FLUOstar® Galaxy microplate reader**,** following the manufacturer's instructions (Lowry 1951).

In addition, to prepare the remaining sample for protein electrophoresis, DTT was added to a final concentration of 0.04M. Next, samples were boiled at 99ºC for 2 minutes, cooled down to RT and then diluted to a final concentration of 1µg/µL. SDS-polyacrylamide gel electrophoresis (SDS-PAGE) was performed, according to the initially described protocol by Schägger and Jagow, but with some adaptions (Schägger 1987). Hence, pre-cast NuPAGE™ 4-12% bis-tris protein gels (17-well-sized) were used and 5µL of protein marker VI or 10µg of the sample protein was loaded per well. The SDS-PAGE was carried out in XCell SureLock™ mini-cells containing MES buffer. The mini-cells were placed on ice and connected to an electrophoresis power supply. Protein electrophoresis was performed at 75V for the first 15 minutes and increased up to 175V for in the following 75 minutes to achieve the desired separation. After completion of protein electrophoresis, the cassette surrounding the SDS-PAGE gel was removed and protein detection was performed by Western blotting.

3.3.8.2. Western blotting and protein detection

For the detection of protein expression levels, an electrophoretic protein transfer from SDS-PAGE gels to an unmodified nitrocellulose membrane was performed, as described for Western blotting by Burnette, but with slight adaptions (Burnette 1981). The SDS-PAGE gel was placed in direct contact to the Protran™ 0.45µm NC nitrocellulose blotting membrane, whereas the nitrocellulose membrane was allowed to get pre-soaked in protein transfer buffer. The gel and membrane were sandwiched by a pre-soaked filter paper and blotting sponges inside the blotting module. Next, the module was inserted into a XCell SureLock™ mini-cell and protein transfer buffer was added to the mini-cell's inside chamber as well as cold tap water to the outer chamber. Furthermore, the mini-cell was connected to an electrophoresis power supply and protein transfer was carried out at 30V for 2 hours. Afterwards, the successful protein transfer was checked with a RedAlert™ Western Blot stain.

For multiplexing, the membrane was cut into different sections in accordance to the expected molecular weight of the proteins to be detected. Then, RedAlert™ stain was removed by incubating distilled water followed by TBS-T buffer, whereas all steps were subsequently performed under gentle shaking. Next, membranes were transferred to a solution of 5% skim milk powder in TBS-T buffer and incubated at RT for 1 hour in order to block unspecific protein binding to the membrane. After membranes were washed 5 times with TBS-T buffer, the desired primary antibody was diluted, following the manufacturer's instructions into a solution of either 3% skim milk powder or 3% BSA in TBS-T buffer, and added to the membrane for an incubation at 4ºC overnight. The following day, the first antibody solution was taken away and the membrane was washed 5 times with TBS-T buffer for 5 minutes to remove unbound remains of the first antibody. Next, the membrane was incubated with the corresponding second antibody in a solution of 3% skim milk powder (in TBS-T buffer) in the respective dilution at RT for 1 hour. After another 3 washing steps with TBS-T buffer to remove the secondary antibody remains, the membrane was then incubated with SuperSignal™ West Femto substrate. The emitted chemiluminescence was detected by either VersaDocTM 3000 and evaluated with the software Quantity One or by the ChemiDoc™ MP system and assessed with the Image Lab 6.0.1 software.

3.3.9. Histological methods

3.3.9.1. Cryosectioning of mouse hearts

Serial cryosectioning of mouse hearts, stored at -80°C, was performed in a Leica CM3050 S cryostat at -22°C to -21°C, as described by Fischer et al. (Fischer 2008). After insertion of a microtome blade, FEATHER® S35, the tissue block was fixed with compound (Tissue-Tek® OCT™/FSC 22®) on a specimen holder, which was locked in the cryostat slider. Next, the protruding compound was carefully removed with a razor blade and the specimen holder was correctly aligned with the blade. Then, a cut thickness of 30µm was used to reach the starting point for cryosectioning the heart tissue, what was visually checked with test cuts made on SuperFrost™ ultra plus adhesion microscopic glass slides. As soon as the myocardium was reached, the cut thickness was adjusted to 7µm in order to acquire the final cuts, which were transferred again onto SuperFrost™ ultra plus adhesion microscopic glass slides. Further fixation and staining procedures were followed, as described below (3.3.9.2-3.3.9.4).

3.3.9.2. Conventional histological staining - H&E and trichrome

Hematoxylin-eosin (H&E) staining was performed according to the descriptions of Feldman et al., but with minor adaptions (Feldman 2014). First, the cardiac sections were directly fixed in ice-cold acetone at RT for 5 minutes followed by drying at RT for 30 minutes. Next, the cell nuclei were stained with hematoxylin solution gill no. 3 at RT for 10 minutes. Then, tissue slides were washed with distilled water 3 times at RT for 5 minutes**.** Afterwards, the cytoplasm was stained in red by eosin incubation at RT for 10 minutes. To fix the eosin staining, sections were dehydrated by running through an ethanol gradient of 70%, 95% and 100%, whereby the slides were incubated at each concentration and at RT for 1 minute. This was followed by a 1 minute clarification step in xylene. Last, the H&E-stained heart sections were capped with Entelan®. Image acquisition was performed by using the microscope Nikon Eclipse Ti-E with the 16.25 megapixels Nikon DS-Ri2 CMOS camera in combination with the SlideExpress 2 system.

For trichrome staining, frozen heart sections were thawed without fixation at RT for 30 minutes. The dried slides were then rinsed in distilled water at RT for maximal 2 minutes. Next, the trichrome staining was performed in line with the protocol of N.C. Foot, but with minor adaptions (Foot 1933). Here, the cell nuclei were displayed in black due to

hematoxylin staining, whereas the CMs were stained in red by Biebrich scarlet acid fox. Subsequently, the collagen fibers were stained in blue by the usage of aniline blue. Finally, the stained heart sections were covered with Entelan® and imaged, as described for H&E-stained slides.

3.3.9.3. LacZ staining

In my studies, lacZ staining was performed to detect the β-galactosidase (β-gal) activity in lacZ transgenic tissues, as described by Salwig et al. (Salwig 2019), but with slight adaptions. First, the sections were fixed with lacZ fixation solution at RT for 5 minutes. Next, the sections were rinsed 3 times in lacZ wash solution for 10 minutes. Then, slides were incubated in pre-warmed, freshly filtered lacZ staining solution in the dark at 37°C overnight. After repeated washing steps with PBS, the frozen sections were covered with Mowiol and imaged with the Axioplan 2 imaging system.

3.3.9.4. Immunofluorescent and -histochemical staining

The immunofluorescent staining of isolated mACMs was performed in Nunc™ Lab-Tek™ II CC2™ 2 or 4-well chamber slides. The staining protocol was based on the descriptions of Staudt et al., but was slightly modified (Staudt 2007). Here, the culture medium was gently removed and CMs were directly fixed with 4% PFA in PBS at RT for 15 minutes. Next, cells were carefully washed 3 times each with PBS for 5 minutes and permeabilized with 0.05% Triton-X in PBS at RT for 15 minutes followed again by 3 PBS washing steps. Further on, primary and secondary antibodies were diluted and applied in 0.005% Triton-X in PBS working solutions during incubation, which took place in an autoclavable humidity chamber. Uncoupled primary antibodies were used in 1:100 dilutions and incubated at 4°C overnight. Deviations of the corresponding dilutions used for some antibodies are listed (3.1.3). After repetitive PBS washing steps, the respective secondary antibody was applied and incubated according to the manufacturer's instructions (3.1.3). Without any additional washing, the cellular nuclei were stained with DAPI by adding 1µg/mL in PBS at RT for 2 minutes. Again, cells were carefully washed 3 times each with PBS for 5 minutes and finally covered with Mowiol. Immunofluorescent stained mACMs cultures were imaged with the confocal microscope Leica TCS SP8.

For immunohistochemical staining of cryosections, the frozen heart sections were thawed at RT for 30 minutes prior fixation and afterwards handled in accordance with the protocol of Toma et al., but with slight variations (Toma 2002). Here, fixation and all washing steps were carried out in glass dye troughs from different manufacturers. Fixation was performed with 4% PFA in PBS at RT for 5 minutes. Then, the sections were washed 3 times each with PBS at RT for 10 minutes. Next, the incubation of antibodies followed, which took place in autoclavable humidity chambers. Primary antibodies were incubated at 4°C overnight and washed 3 times with PBS for 10 minutes each at RT. The respective secondary antibodies were applied and incubated according to the manufacturer's instructions (3.1.3). Subsequently, 2µL DAPI (1µg/mL in PBS) was added directly into the droplets of the last antibody dilution and incubated at RT for 10 minutes. Finally, slides were washed 3 times for 5 minutes with PBS at RT and covered with Mowiol. Immunohistochemical stained heart sections were imaged with the confocal microscopes Leica TCS SP5 or SP8.

3.3.10. Biophysical methods

3.3.10.1. Compound and confocal microscopy

Cell cultures were examined with the Leica DM IL LED microscope. There, phase contrast as well as brightfield images were acquired with software-automated illumination settings. In contrast, immunofluorescent-stained cell cultures were examined with the Leica TCS SP8. Here, the 405nm, 488nm and 555nm emission spectra were detected by photomultiplier tubes and a respective smart gain of maximal 600V, whereas the 647nm emission spectrum was acquired with a hybrid detector and a respective smart offset of 1.5-2.5%. Conventionally histological staining of cryosections were assessed with the Nikon Eclipse Ni-E microscope, whereas images were taken with the 16.25 megapixels DS-Ri2 CMOS camera. The lacZ-stained sections were examined via the Axioplan 2 imaging system. The immunohistochemical-stained heart sections were acquired with the Leica confocal microscopes TCS SP5 or SP8.

3.3.10.2. Transmission electron microscopy (TEM)

According to the protocols of Sitte et al. (Sitte 1982) and Laue et al. (Laue 2010), ultramicrotomy followed by transmission electron microscopy (TEM) was used to characterize the processes of dedifferentiation in infarcted Runx1 Tracer animals on a structural level beyond the diffraction limit of fluorescent imaging. Therefore, single $1mm^2$ large heart tissue pieces were used and the preparation for TEM was done in accordance with the established and further on described protocol, which was in line with others (Reimer 1959, Girbardt 1974, Sitte 1982, Laue 2010):

(A) Fixation of samples: A chemical fixation of samples was performed (1% PFA, 2.5% glutaraldehyde in 0.05M HEPES buffer, pH 7.2) at RT for 2 hours and the samples were then kept at 4°C, until all of them were acquired.

(B) Embedding of samples: Every of the following steps was performed under agitation on a rotator and took place at RT, if not mentioned otherwise. Initially, samples were taken out of the fixation solution and rinsed 3 times each in 0.05M HEPES buffer for 10 minutes. Next, post-fixation for lipids was achieved by transferring the tissue pieces into 1% OsO_4 (in aqua bidest) solution for 1 hour, in which they had to stay light-protected during the whole incubation time. In the following, the samples were rinsed in aqua dest 3 times each for maximal 10 minutes. Next, they were stained en bloc by placing them in 2% uranyl acetate (in aqua bidest) under light protection for 1 hour, what was followed by a graded series of dehydration steps: 20 minutes in 30% ethanol, 20 minutes in 50% ethanol, 2 times each in 70% ethanol for 10 minutes, 2 times each in 95% ethanol for 10 minutes and 4 times each in 100 % ethanol for 15 minutes (EM grade). Then, the samples were situated in propylene oxide (PO) twice for 30 minutes each, what was followed by 1 hour incubation in PO and epon in a ratio of 2:1 and subsequently in a ratio of 1:1 for 30 minutes up to 1 hour. The next aim was to continuously increase the epon concentration by evaporation of the solvent. Therefore, the sample vials and the epon mixture were kept on the rotary mixer overnight. This was also necessary to prevent the formation of a superficial layer of pure epon, which would have impaired the evaporation of the solvent in the lower part of the vial. After overnight incubation, the samples were transferred into freshly prepared epon at RT for approximately 4 hours. For the final embedding, each tissue piece was positioned in a gelatin capsule, labeled, filled up with fresh epon and polymerized at 60°C for 48 hours.

(C) Ultrathin sectioning: Ultrathin sectioning was done at an ultramicrotome with diatome ultra diamonds at an angle of 45°. The tissue sections was sectioned with 70nm thickness and placed on HR24 Cu/Rh grids, as described by Sitte et al. (Sitte 1982).

(D) Transmission electron microscopy (TEM): TEM was performed at the Jeol JEM-1400Plus (120kV) electron microscope with a LaB6 cathode. Image acquisition was performed with the EM-14800 Ruby camera (resolution: 3296 x 2472-pixel, 1439 dpi).

3.3.11. Live-cell sorting

For live-cell sorting of mACMs, which were isolated from injured hearts (3.3.6.2), the BioSorter platform was used. This large particle flow cytometer, designed for the in-flow measurement of objects ranging from 1 – 1500µm in size, was equipped with a 500µm interchangeable fluidics and optics core assemblies (FOCA) to sort living CMs. The CM suspension was supplied via a standard 50mL conical falcon tube (40mL working volume) with the suspended stirrer. Instrumental control, defining the corresponding gating as well as data acquisition and post-acquisition analysis, was done with the FlowPilot software developed for BioSorter. First, automated cleaning procedures (auto-cleaning) were started, whereas a flushing cascade, containing detergents, 70% ethanol and distilled water, were used to prepare the instrument for the sorting process. Next, the obtained CM suspensions were diluted 1:20 with perfusion buffer and then divided into aliquots of 40mL running volume per falcon tube. Here, 4µL of DAPI solution was added and gently mixed. The suspensions were supplied one after each other under constant stirring. Runx1-traced ($Runx1_{traced}$) mACMs were sorted with a 3-step gating strategy, as displayed in Figure 19. The starting point of the sorting procedure was the exclusion of cell debris by setting TOF restrictions. Here, all events were recorded in a gate for optical density (EXT) and the corresponding sizes (TOF). Then, CM aggregates were excluded by setting EXT restrictions, where only single and long cells were taken into the next gating step. Furthermore, restrictive DAPI settings were used to exclude dead CMs, which then appeared with a high DAPI signal compared to intact CMs. In the following, $Runx1_{traced}$ mACMs were identified due to their fluorescent emission in the RFP channel, which was excited with the 561nm solid-state laser and detected with an emission filter of 615/24nm bandwidth. The individual CMs were captured and collected either in

laminin-coated 2 or 4-well chamber slides for imaging or in 6-well plates for RNA isolation (3.3.7.4).

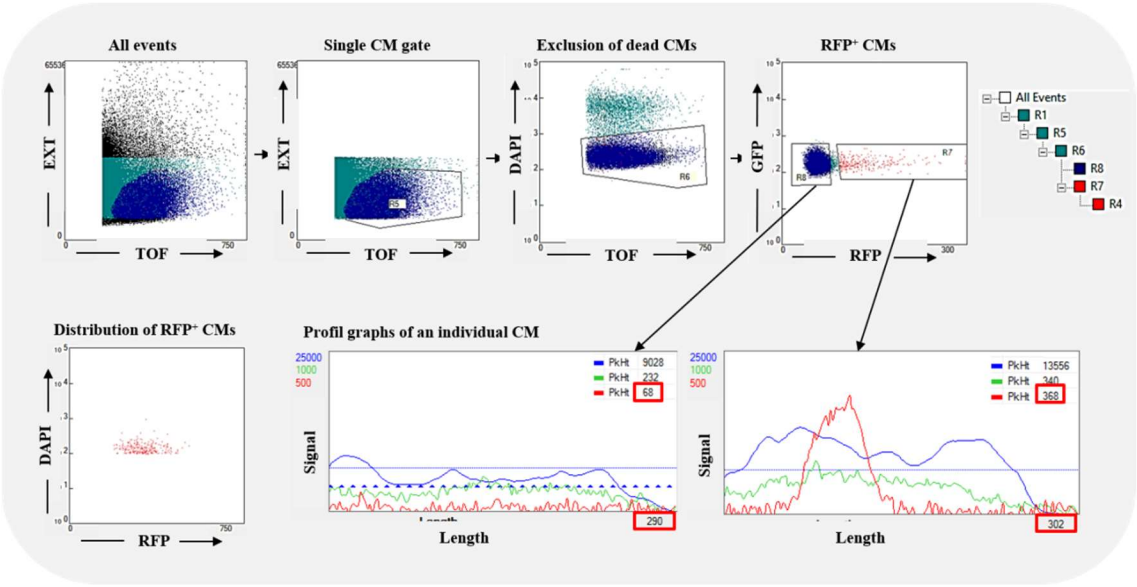

Figure 19: A 3-step gating strategy for live-cell sorting of ischemic Runx1$_{traced}$ mACMs. The exclusion of cell debris was done by setting TOF restrictions, whereas all events were recorded in a gate for optical density (EXT) and the corresponding sizes (TOF). Next, CM aggregates were excluded by setting EXT restrictions. Only single, long cells were taken into the next gating step to avoid doublets. Furthermore, dead cells were excluded by restrictive DAPI settings, in which dead CMs appeared with a higher DAPI signal compared to intact cells. Then, Runx1$_{traced}$ mACMs were identified due to their endogenous RFP emission and separated in 2 subgroups (RFP$^-$ and RFP$^+$). The profile plot identified individual CMs and was used to analyze and monitor each single sorted CM, their RFP intensity signal as well as the corresponding length.

3.3.12. Imaging analysis

3.3.12.1. Quantitative measurement of the infarct size in conventional trichrome and H&E staining

The ImageJ 1.34 software was used to measure areas of infarct and the corresponding LV**,** what was in line with Takagawa et al. (Takagawa 2007). Here, the area of infarction was determined as percentage of the total LV section, which resembled the infarct size (IS). First, I converted the digital image to grey scale and to a fully screen view. Then, the scar was measured in each section**,** following the approach of area measurement by using the analyze/set measurement options in Fiji. Next, the infarcted scar area and the total area of the LV myocardium were traced manually in the digital images, using a polygon selection button on the tool bar in Fiji, and both parameters were then quantified automatically by the software. The units of area measurement as well as the whole cross-sectional region were indicated as pixels. The IS expressed as percentage was calculated

by dividing the sum of infarcted areas from all sections by the sum of LV areas from all sections (including those without infarct scar) and multiplied by 100 (Takagawa 2007).

3.3.12.2. Colocalization image analysis of confocal microscopy

Colocalization analysis were done by using confocal microscopy (Leica TCS SP8) and a 3-dimensional image analysis software (Imaris Version 8.4.0). Here, a 2-channel experiment (i.e. red for Runx1 vs. green for PCM1) was used to determine double-positive cells (i.e. $PCM^+/Runx1^+$), marking $Runx1^+$ mACMs. Furthermore, I took the accumulation of green signal within the nucleus as a positive indication for the CM nuclei marker PCM1 (Bergmann 2011, Bergmann 2015). My approach was therefore a 3-step method. In step 1, the segmentation of the cell nuclei in the green channel took place to identify CM ($PCM1^+$). In step 2, the segmentation of positive signals in the red channel was done to confirm $Runx1^+$ cells. Finally, filtering the nuclei for positive signals in the red channel was performed in step 3**,** which enabled the identification of $PCM1^+/Runx1^+$ cells and represented Runx1 expressing mACMs. The cell nuclei were segmented by a user interface element of the software, which guided through a sequence of dialogs (wizard) displayed as colocalized volumes. Furthermore, it was necessary to selectively determine the voxels within these volumes for quantification. Here, the surface creation wizard in Imaris (Version 8.4.0) was used with the following settings:

Step 1: Segmentation of the cores in the green channel	
Algorithm	Enable region of interest = false Enable region growing = false Enable tracking = false
Source channel	Source channel index = 2 (green channel) Enable smooth = true Surface grain size = 0.500µm Enable eliminate background = true Diameter of largest sphere = 5.00µm (size of nucleus)
Threshold	Enable automatic threshold = false Manual threshold value = 31.3865 Active threshold = true Enable automatic threshold B = true Manual threshold value B = 212.207 Active threshold B = false
Classify surfaces	Number of voxels above 304

The red channel identified those regions, where areas of stronger coloration (nuclei of $Runx1^+$ cells) stood out from the background. Again, surface segmentation was used,

applying local contrast to identify regions that were approximately the size of nuclei (>5µm). Therefore, the following settings were used in the wizard:

Step 2: Segmentation of the positive regions in the red channel	
Algorithm	Enable region of interest = false Enable region growing = false Enable tracking = false
Source channel	Source channel index = 3 (red channel) Enable smooth = true Surface grain size = 0.500µm Enable eliminate background = true Diameter of largest sphere = 5.00µm (size of nucleus)
Threshold	Enable automatic threshold = false Manual threshold value = 23.5003 Active threshold = true Enable automatic threshold B = true Manual threshold value B = 135.695 Active threshold B = false
Classify surfaces	Number of voxels above 10.0

The last step (step 3) of the colocalization analysis enabled the quantification of green nuclei, which also inherited a red signal, representing Runx1^{+} CMs. Here, the nuclei identified in step 1 were filtered, if they contained positive red regions. For this purpose, a binary channel was created, which was used as the operational basis for the filter. There, the red surfaces enclosed the positive red voxels. Next, a filter mask was applied, which ensured that all voxels within the red surface were set to the value 1, whereas all voxels outside the surface were set to the value 0. A threshold value of 0.5 was selected. As soon as a voxel with an intensity above 0.5 was identified (i.e. a voxel with a value of 1), the nucleus was counted as positive. To get the negative nuclei in a separate surface object, the same filter was used, but with a threshold range of 0 to 0.5. The number of cores in each case was read out in the “statistic tabs” of the surface objects. The analysis with equal settings was performed with images of both experimental MI models.

3.4. Statistical evaluation

Statistical analyses were carried out and graphic representations created by using Microsoft® Excel® 2016. The graphical data presentation based on the mean value of each group with error bars corresponding to the standard error of the mean (SEM). The existence of statistically significant differences between groups was assessed through the parametric Student's t-test, one of the most commonly used statistical tests for comparing samples (Gauthier 2007). Here, a 2-tailed unpaired Student’s t-test was applied, if 2

independent groups were compared and obtained as biological replicates with different treatments (e.g. OSM/Con) and at different time points (Horne 1998, Cherry 2012, DeVries 2020). Correspondingly, p-values below 0.05 were considered as statistically significant. To evaluate the acquired live-cell sorting data set and to quantify the TOF and fluorescent intensities, I used the FlowPilot software developed for BioSorter. Here, it was possible to export the collected data set to Microsoft® Excel® 2016 for further post-processing, as described above. To cluster specific deregulated genes, which were identified to be significantly up- or downregulated in $Runx1_{traced}$ ischemic mACMs, I used the established NGS gene set. Here, I calculated the means of cardiomyocyte subgroups from the ventricular fractions (n=4), IZ^{**} and RZ^{*}, and their corresponding fold changes (IZ^{**}/RZ^{*}). The data set was sorted on the first level according to the height of the fold change (FC) and followed by the significance. Next, the genes with a FC above 2.5 in combination with a p-value below 0.05 were carefully reviewed. In addition, the gene expression of key factors regarding dedifferentiation (i.e. Runx1, αSMA, ACTN1, Moesin) as well as of structural markers to identify the CM profile (i.e. PCM1, αMHC, cardiac Troponin, ACTN2) was checked. Of those, interesting candidates were pulled out by choosing FCs above 10 and p-values below 0.05.

4. Results

4.1. In vitro imaging analysis of Runx1 expression in adult mouse cardiomyocytes (mACMs) displayed phenotypical adaptions linked to dedifferentiation upon Oncostatin M (OSM) stimulation

First, I wanted to know if a mouse Oncostatin M (OSM)-initiated Runx1 expression could be demonstrated in vitro and was creating the same phenotypical changes as in case of rat adult cardiomyocytes (rACMs), which was described by Kubin et al. (Kubin). Therefore, adult mouse cardiomyocytes (mACMs) were isolated, seeded into a cell culture system and stimulated with recombinant OSM to enable the expression of Runx1. Upon OSM stimulation, mACMs started sprouting, elongation and flattening, which correlated with a dismantled and condensed contractile apparatus (Figure 20). Phase contrast imaging revealed initial signs of sprouting at 1 day post stimulation (dps), whereas first elongated cells were observed at 4dps. After 7 days of stimulation with OSM, mACMs appeared totally flattened with a dismantled contractile apparatus. In comparison, control mACMs (BSA-stimulated and listed as "CON") stayed rod shaped at 4dps, but started sprouting without dismantling after 7 days of stimulation. The morphological characteristics of OSM-induced dedifferentiation increased over the time of observation, from seeding to 7dps, in accordance with the findings of OSM-stimulated rACMs (Kubin 2011, Pöling 2012, Szibor 2014).

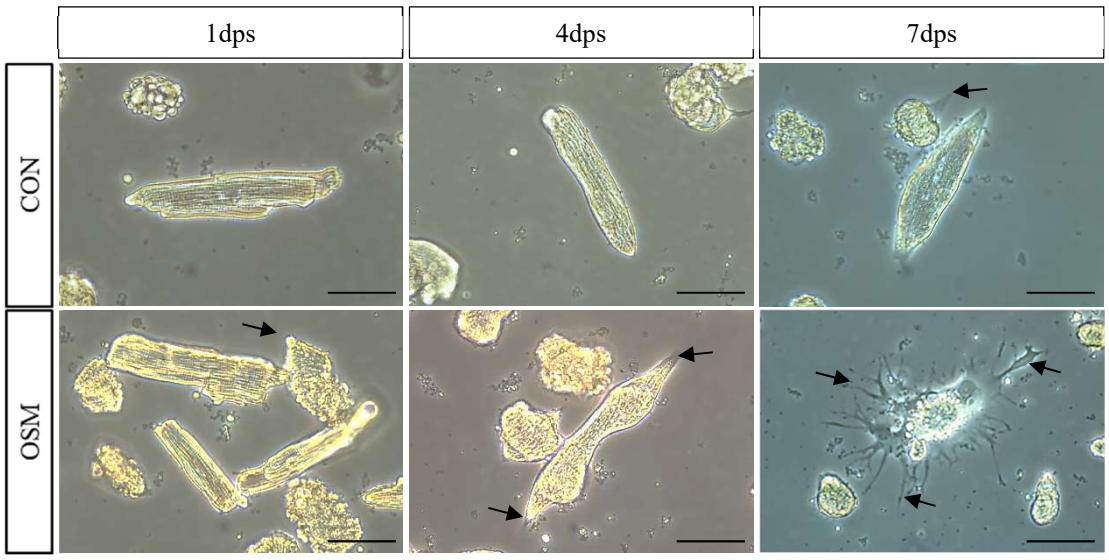

Figure 20: Phenotypical changes of mouse Oncostatin M (OSM)-stimulated cultures of mouse adult cardiomyocytes (mACMs). Representative phase contrast images at 1, 4 and 7 days post stimulation (dps) with OSM or BSA (CON) are shown. OSM treatment induced typical morphological characteristics of CM dedifferentiation, i.e. anterior/posterior elongation (black arrows) and flattening at 4 and 7dps. Cardiac cells appeared dismantled with a condensed contractile apparatus. Scale bars = 50µm.

Additionally, I used confocal microscopy imaging to visualize the Runx1 kinetics in dedifferentiating mACMs. Here, fluorescent-labeled Runx1 could be detected in OSM-treated mACMs already at 1dps, along with initial signs of sprouting (Figure 21). Runx1 expression was only visible in 1 of 2 nuclei. But at 7dps, Runx1 labeling was detectable in both nuclei of binucleated CMs, besides a specific Runx1 expression, which remained in the nucleus. To visualize the structural adjustments during dedifferentiation, the CM marker sarcomeric α-actinin (ACTN2) was used (Kubin 2011, Pöling 2012, Szibor 2014). A complete loss of sarcomeric structures could be observed in OSM-stimulated mACMs at 7dps, whereas CMs treated with BSA (CON) stayed Runx1 negative and showed an intact contractile apparatus over the same time. The confocal microscopy analysis (Figure 21) revealed the same morphological changes of OSM-stimulated mACMs, as demonstrated by phase contrast imaging (Figure 20). To visualize the cell surface in those cells via confocal imaging, F-actin was stained additionally at 7dps. This marked a dismantled contractile apparatus with a repression/degradation of sarcomeres in OSM-treated Runx1^{+} mACMs. As described above, the microscopic analyses revealed that the morphological changes in dedifferentiated mouse CMs correlated with a lacking fluorescent staining for sarcomeres and a positive staining for Runx1.

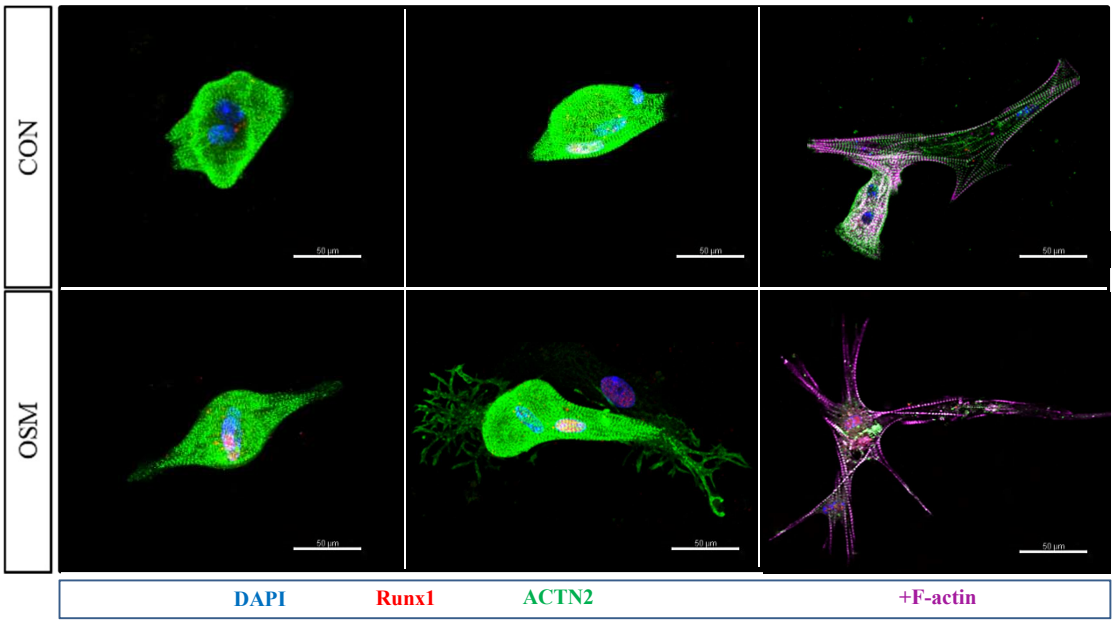

Figure 21: Visualized Runx1 expression in OSM-stimulated cultures of mACMs. Representative immunofluorescence images of fixed mACMs indicated Runx1 expression detectable at 1, 4 and 7dps in case of OSM stimulation. mACMs revealed a condensed and degraded CM marker sarcomeric α-actinin (ACTN2) at 7dps. Scale bars = 50µm.

4.2. Western Blot analysis of OSM-stimulated mACMs revealed a significant Runx1 expression on protein level in vitro already at 1 day post stimulation (dps)

In order to demonstrate that the Runx1 expression in CMs undergoing dedifferentiation is a consequence of increased OSM signaling, I analyzed the expression of the tissue inhibitor of metalloproteinase 1 (Timp1), which is a well-known downstream target of OSM-stimulated CMs (Weiss 2005, Kubin 2011). Here, repetitive Western Blot analyses of OSM-stimulated mACMs indicated a positive stimulation of the OSM receptor (OSMR), as validated via Timp1 (Figure 22A). Representative time points of OSM stimulation demonstrated a significant Timp1 expression at 1 and 7dps (C+E). Correspondingly, protein levels of Runx1 in OSM-treated mACMs were significantly increased at 1dps compared to control-stimulated CMs, whereas Runx1 was just slightly but not significantly upregulated 7dps (Figure 22B+D).

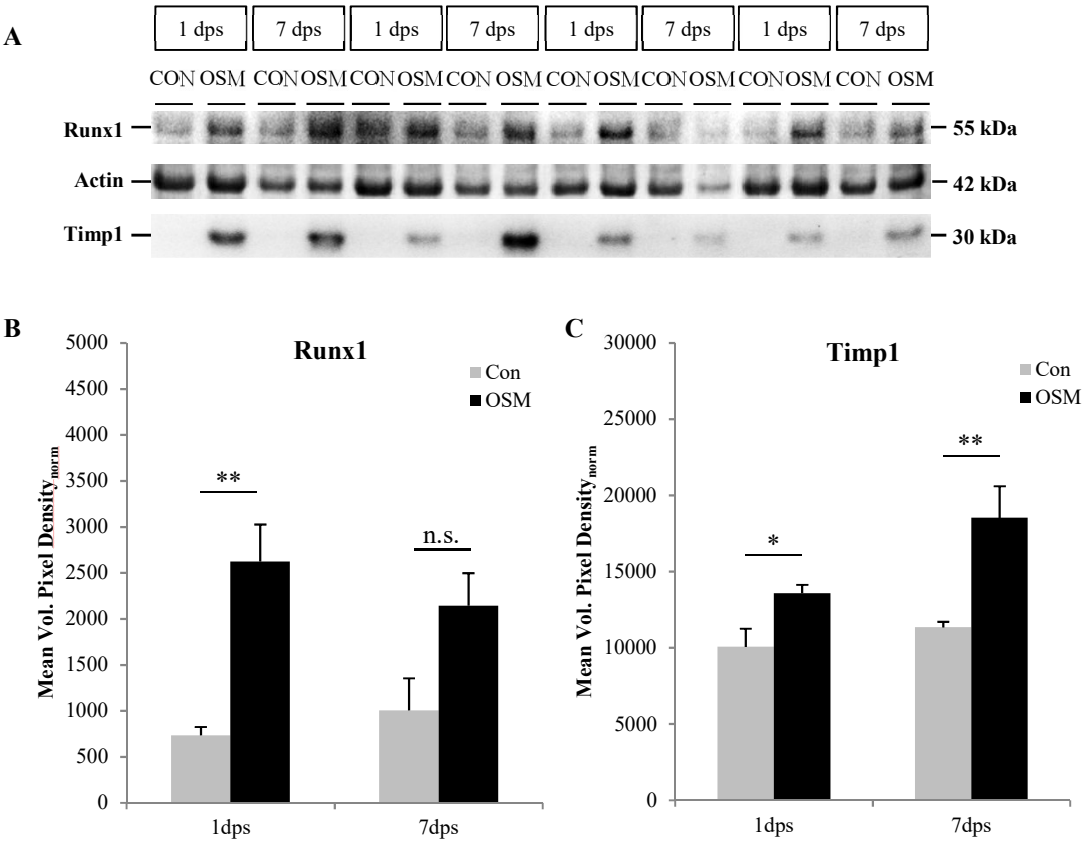

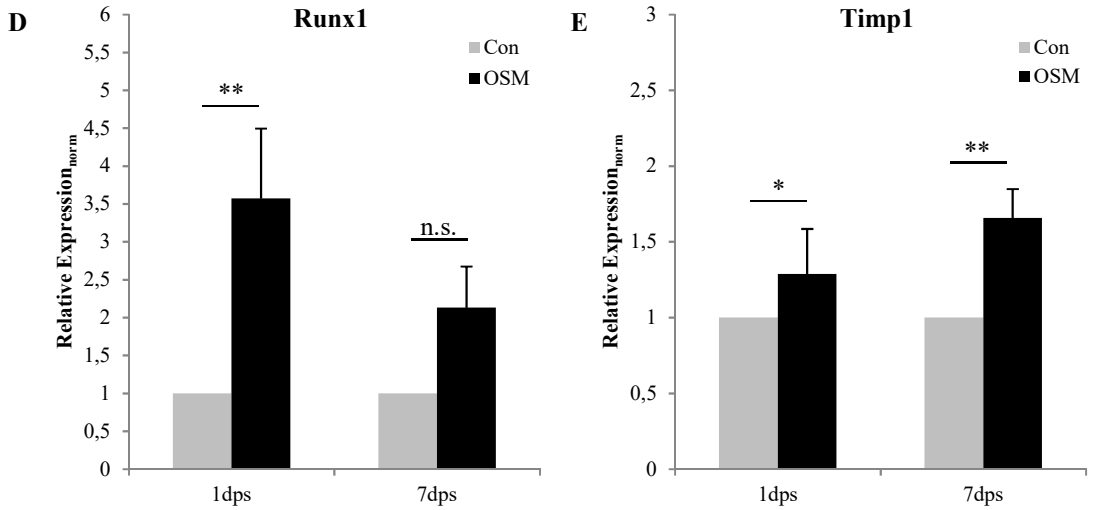

Figure 22: Expression patterns of Runx1 and Timp1 in OSM-treated mACMs. (A) Western Blot analysis of Runx1 and TIMP1 expression in lysates of OSM or CON-stimulated mACMs, while Pan-actin (Actin) served as a loading control. **(B+C)** Quantitative, densitometric analysis of samples described in (A) based on mean volume pixel density of bands (n=4 for each time point) for Runx1 (B) and Timp1 (C). **(D+E)** Relative expression of Runx1 and Timp1 in OSM-related to CON-treated mACMs at indicated time points (n=4 for each time point). Data were normalized to Actin levels and are presented as mean ± SEM. Statistical significance was determined with a 2-tailed unpaired t-test. **P<0.01; *P<0.05; n.s. = P>0.05.

4.3. Runx1 deficient mACMs displayed no altered morphology due to OSM stimulation in vitro as well as no significant expression of fetal marker proteins assigned to dedifferentiation

In view of having found an OSM-induced Runx1 expression, which was associated with dedifferentiation in mACMs, the question raised, if signs of dedifferentiation could also be detected in case of missing Runx1 expression. To address this inquiry, I used Runx1 deficient CMs from heart specific Runx1 knock-out animals ($Runx1^{fl2}/\alpha MHC^{Cre}$) in the following in vitro studies. Here, $Runx1^{fl2}$ mACMs were defined as control experiments, since the Runx1 gene expression has been described not to be altered just by insertion of 2 LoxP sites (Hall 2009, Michel 2010, Oh-McGinnis 2010). Upon OSM treatment, $Runx1^{fl2}$ mACMs revealed the same morphological changes as observed before, i.e. OSM-stimulated $Runx1^{fl2}$ mACMs showed phenotypical characteristics of dedifferentiation (elongation, sprouting) at 7dps and emerged as a total network formation at 14dps (Figure 23). In contrast, Runx1 deficient mACMs kept either their rod shape pattern or simply started to round up and died. Surprisingly, $Runx1^{fl2}/\alpha MHC^{Cre}$ mACM cultures revealed contaminations with fibroblasts (white arrows), which have been described as responsive to OSM stimulation in form of growth, collagen deposition and chemotaxis (Scaffidi 2002, Nagahama 2013).

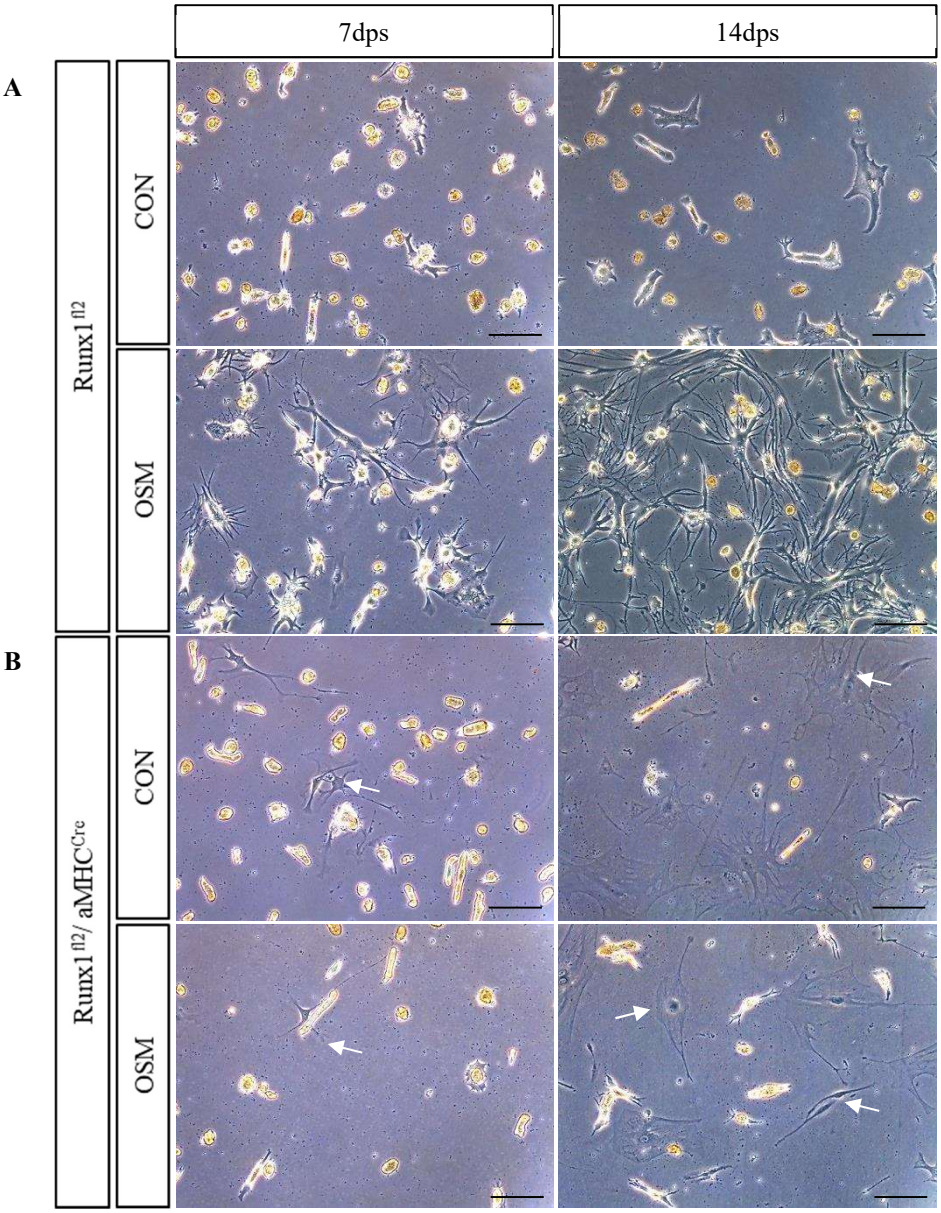

Figure 23: In vitro study of mACMs from Runx1^{fl2} and Runx1 deficient (Runx1^{fl2}/αMHC^{Cre}) mice upon OSM treatment. Representative phase contrast images were taken at 7 and 14dps, which demonstrated the incapability of Runx1 deficient mACMs to dedifferentiate **(B)** in comparison to Runx^{fl2} mACMs **(A)**. Runx1^{fl2} mACMs responded to OSM stimulation with elongation and total loss of structural markers (less phase contrast, right panel), whereas Runx^{fl2}/αMHC^{Cre} mACMs indicated a high contrast of contracting material and no altered cell length. In contrast to control mACMs, Runx1 deficient mACMs showed signs of fibroblast contamination (white arrows) upon OSM treatment (C.G. 1999, Scaffidi 2002, Nagahama 2013). Scale bars = 100µm.

The absence of dedifferentiation in Runx1 deficient and OSM-stimulated mACMs was validated by immunofluorescent staining of specific markers for dedifferentiation combined with confocal microscopy. Here, the imaging analysis proved absent Runx1 signals 14dps in Runx1 deficient mACMs (Figure 24). In contrast to Runx1^{fl2} CMs, OSM-stimulated mACMs lacking Runx1 showed no expression of fetal stem-cell like markers (ACTN1, ANP), indicating a disability to undergo dedifferentiation in Runx1 deficient

CMs. In addition, the sarcomeric structures were not dismantled in Runx1 absent mACMs, but rather appeared rod shaped with a condensed contractile apparatus, denoting the incapability to dedifferentiate and to decline sarcomeric proteins (e.g. ACNT2).

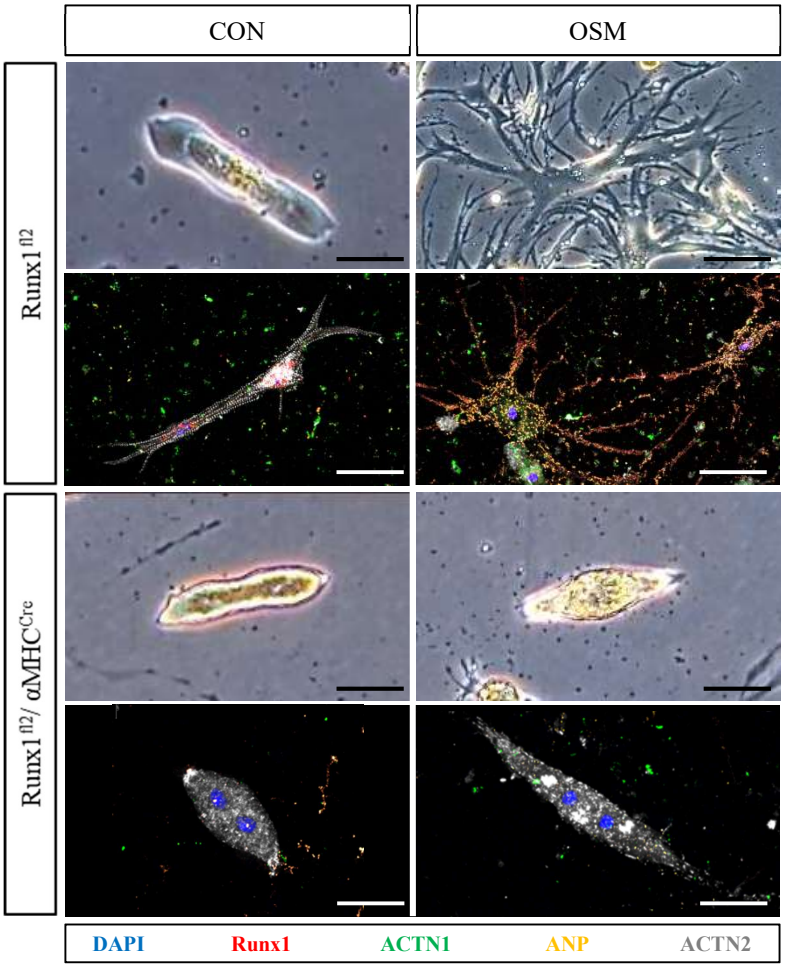

Figure 24: Immunofluorescence and phase contrast imaging of isolated CMs from Runx1^{fl2} and Runx1^{fl2}/αMHC^{Cre} mice (heart specific knock out) subjected to OSM treatment. Immunohistochemical staining of mACMs demonstrated the incapability of Runx1 deficient mACMs to dedifferentiate in comparison to control CMs at 14dps. Runx1^{fl2} mACMs responded to OSM stimulation with elongation and total loss of ACTN2, expression of ACTN1, release of ANP and were marked as Runx1 positive. In contrast, Runx1^{fl2}/ αMHC^{Cre} mACMs showed no evidence of ACTN2 loss and increased ACTN1, ANP or Runx1 expression. Scale bars = 50µm.

Beyond the previous imaging analysis (Figure 24), I wanted to demonstrate the incapability of dedifferentiation in Runx1 deficient CMs on protein level. Besides this, my aim was to show a lack of Runx1 expression in case of OSM stimulation. For this reason, a sufficient OSM signaling induction in CMs lacking Runx1 expression via Western Blot analysis was tested. Here, OSM-treated control CMs (Runx1^{fl2}) showed a slight increase of Runx1, whereas Runx1 deficient mACMs had no altered Runx1 expression levels. In addition, a positive stimulation of OSM has been validated via

Timp1 as a consequence of increased OSM signaling (Richards 1993, Drechsler 2012, Adrian-Segarra 2018). Therefore, representative time points of OSM stimulation revealed a significant Timp1 expression at 1 and 7dps in Runx1^{fl2} and Runx1 deficient mACMs. Furthermore, I checked protein expression levels of representative fetal marker genes (ACTN1, αSMA) to elucidate the dependency of dedifferentiation indicators on Runx1 expression. Here, repetitive Western Blot analyses revealed a slight but not significant increase of fetal markers like ACTN1 (1.75 fold) and αSMA (2 fold) in Runx1 expressing mACMs at 7dps, whereas ACTN1 and αSMA slightly decreased in Runx1 deficient CMs, though with a high statistical dispersion (Figure 25).

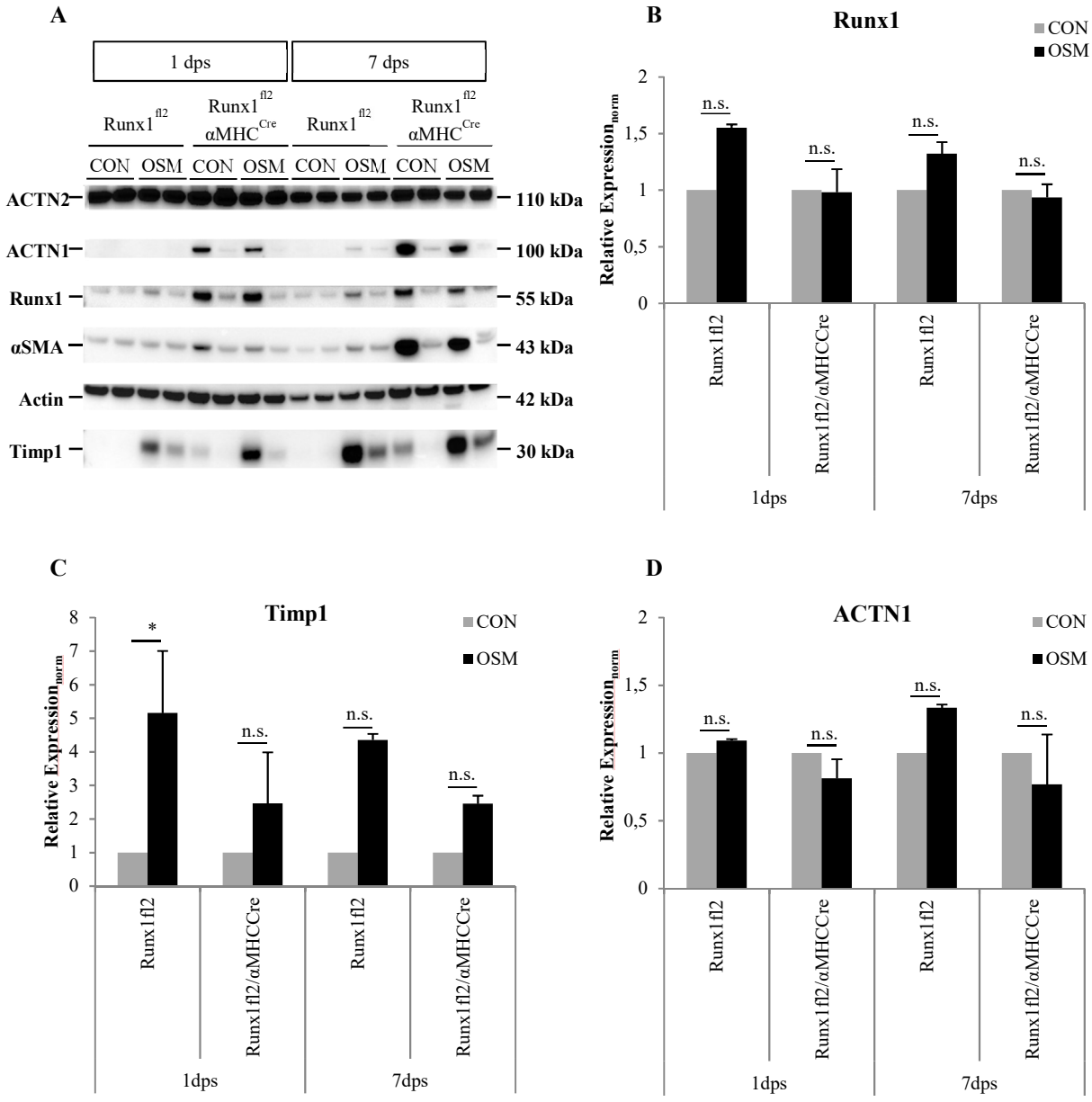

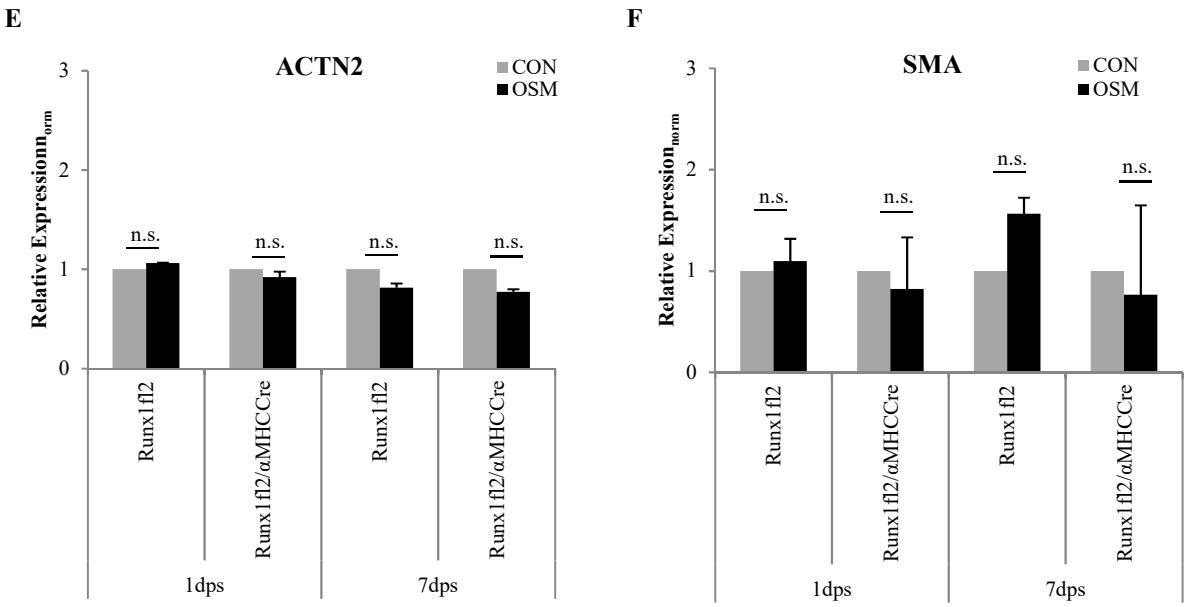

Figure 25: Dynamic expression pattern of different dedifferentiation and ACM markers of isolated CMs from adult Runx1^{fl2} and Runx1^{fl2}/αMHC^{Cre} mice (heart specific knock out) subjected to OSM application to induce dedifferentiation in vitro. (A) WB analysis confirmed the disability of Runx1 deficient mACMs to degrade ACTN2 (A+E) and to express Runx1 (A+B), ACTN1 (A+D) and αSMA (A+F) as dedifferentiation characteristics in comparison to Runx1^{fl2} CMs, which showed a significant difference of Runx1 (A+B) and ACTN1 (A+D) protein levels upon OSM treatment already at 1dps. TIMP1 (A+C) levels were significantly upregulated in OSM-treated mACMs as signs of increased OSM signaling. Pan-actin (Actin) served as loading control. **(B-F)** Data are displayed as relative expression levels of tested proteins in OSM-related to CON-treated mACMs at indicated time points (n=2 for each time point). Data were normalized to Pan-actin (Actin) levels and are presented as mean ± SEM. Statistical significance was determined with a 2-tailed unpaired t-test. *P<0.05, n.s.=P>0.05.

Overall, Runx1 deficient mACMs displayed no altered morphology due to OSM stimulation as well as no significant expression of fetal marker proteins. Additionally, OSM-stimulated Runx1 deficient mACMs revealed an activated OSM signaling, but lacked the capability to express Runx1 in order to trigger processes associated with dedifferentiation.

4.4. Successfully Runx1$_{traced}$ mACMs delivered equal phenotypical adaptions and responses on protein level upon OSM stimulation, when compared to wildtype cardiomyocytes

So far, I have shown a positive relation between signs of CM dedifferentiation and the Runx1 expression (Figure 20-22) as well as the incapability of Runx1 deficient mACMs to induce phenotypical adaptions due to OSM stimulation in my in vitro studies (Figure 23-25). Despite these findings, the purpose of dedifferentiation and the fate of dedifferentiated CMs remained still unclear (Kubin 2011, Pöling 2012, Szibor 2014). For addressing both issues in vivo, a reporter mouse strain, harboring a tTA under the control

of the Runx1 promotor, was used to generate a transgenic tracing approach. Via additional breeding with the tTA responsive $LC1^{Cre}$ and $Rosa26^{stopfloxlacZ}$ mouse line, cell labeling of once Runx1 expressing ACMs was established (Soriano 1999, Schönig 2002). This Runx1 tracing approach allowed the labeling of CMs as well as several different Runx1 expressing cell lineages, which were described to be involved in hematopoiesis and myeloid cell differentiation (Abe 2005, Kilbey 2010, Zhou 2018). Those cells, which had once switched on the Runx1 expression, appeared with a positive lacZ staining (hereinafter referred to as "Runx1 Tracer"). To elucidate, if phenotypical characteristics of dedifferentiation occurred in transgenic mACMs in the same manner as observed before, CMs from Runx1 Tracer mice were isolated, stimulated with OSM, lacZ stained and examined via light microscopy. In contrast to the findings shown in Figure 20, OSM-treated mACMs turned $lacZ^+$ at 4dps, whereas Runx1 expression was observable already at 1dps (Figure 26). Additionally, Runx1-traced $lacZ^+$ ($Runx1_{traced}lacZ^+$) displayed characteristical signs of dedifferentiation. Hence, CMs appeared elongated at 4dps and totally flattened with no contractile apparatus at 7dps. These findings demonstrated the functionality of my transgenic approach, but revealed a temporal offset of Runx1 expression as well as the evidence of visible tracing.

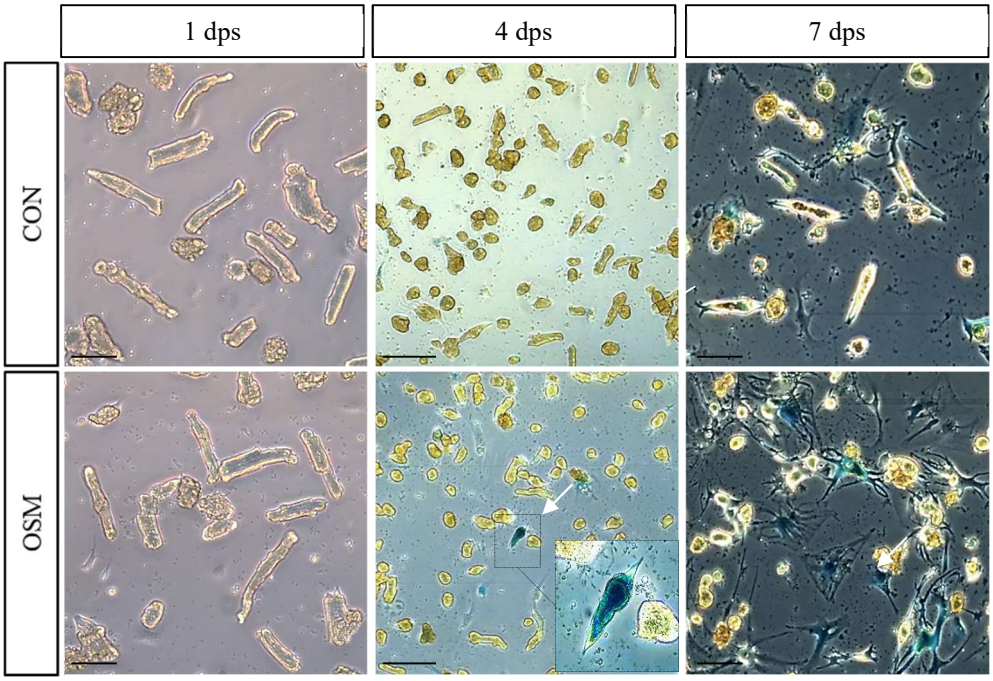

Figure 26: OSM stimulation of transgenic mACMs revealed the same Runx1 responsivity as wildtype mACMs. ACMs of transgenic animals were isolated and stimulated (OSM vs. CON) for at least 7 days. CMs became $lacZ^+$ already after 4 days upon OSM treatment, indicating a successful tracing of Runx1 expression via lacZ staining. First signs of dedifferentiation (flatting, sprouting, formation of protrusions) could be observed. Almost all OSM stimulated ACMs were marked as $lacZ^+$ at 7dps, when compared to controls. Scale bars = 50µm (1 and 7dps), = 100µm (4dps).

Aiming to verify a functional tracing, I elucidated protein levels of Runx1 in OSM-stimulated mACMs from Runx1 Tracer animals. To underline a direct association of lacZ staining and Runx1 expression, I used the time point post stimulation (4dps), on which I examined $lacZ^{+}$ cells in the preliminary trial during my light microscopy analysis (Figure 26). Moreover, due to the shortage of samples for sufficient repetitive studies, I chose only 4dps to proof the association of positive lacZ staining with increased Runx1 expression. Here, repetitive Western Blot analyses of mACMs were done. Measurements of cell lysates delivered a significant increase of Runx1 on protein levels and of Timp1, which served as an experimental control (Figure 27A). Densitometric quantification of Western Blot bands revealed a significant increase of Runx1 levels in OSM-treated mACMs at 4dps, in comparison to CON-stimulated samples (Figure 27B). Timp1 was only and significantly expressed in OSM-stimulated mACMs, as expected, and validated the involvement of the OSM signaling cascade. Taken together, my in vitro data substantiated an OSM-induced Runx1 expression in wildtype and Runx1 Tracer mACMs, associated with morphological and phenotypical adaptions of dedifferentiation. Beyond that, transgenic mACMs responded with the same emergence upon OSM treatment as non-transgenic (wildtype) CMs, reflecting their capability for further in vivo studies.

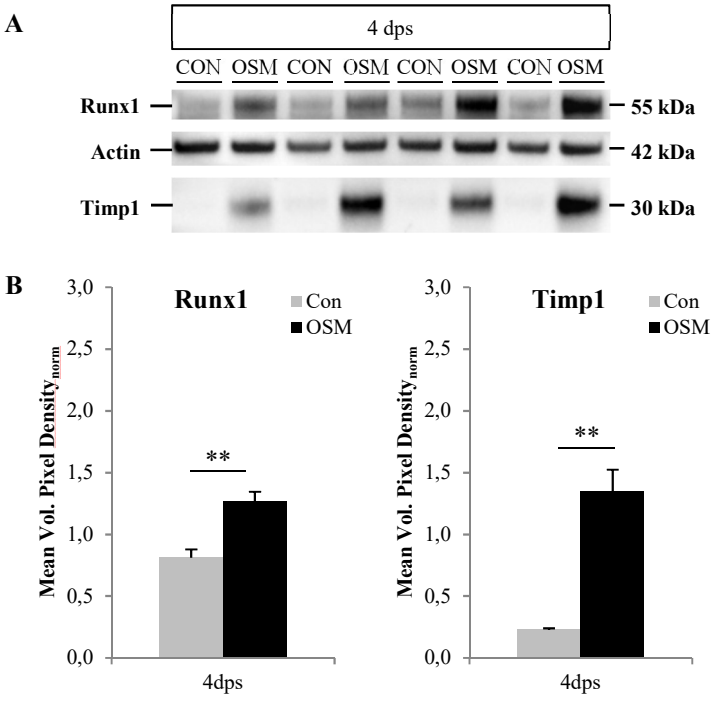

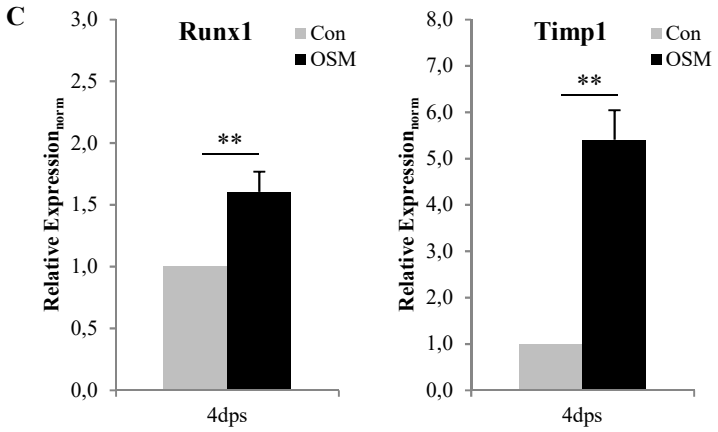

Figure 27: Runx1 and Timp1 expression of cultivated and stimulated Runx1 Tracer mACMs. (A) Western Blot analysis of OSM stimulation confirmed a similar expression peak of Runx1 and TIMP1 and proved a successful as well as correlative expression profile upon OSM treatment. Cells were harvested and lysed to compare Runx1 expression levels with the lacZ staining at 4dps, as shown in Figure 7. Pan-actin (Actin) served as a loading control for quantitative evaluation and normalization. **(B)** Quantitative, densitometric analysis of samples described in (A) based on mean volume pixel density of bands (n=4 for each time point) for Runx1 and Timp1. **(C)** Relative expression of Runx1 and Timp1 in OSM-stimulated related to CON-treated mACMs at indicated time points (n=4 for each time point). Data are presented as mean ± SEM. Statistical significance was determined by a 2-tailed unpaired t-test. **P<0.01; *P<0.05.

4.5. MI hearts revealed an increased Runx1 expression in the ischemic region of the left ventricular myocardium in vivo

Starting point of this part-study was to disclose potential differences of Runx1 expression in heart sections of sham-operated, i.e. non-infarcted, mice in comparison to experimental myocardial ischemia as well as to elucidate the kinetic Runx1 expression pattern in the infarcted heart. In a first approach, wildtype (C57Bl6/J) mice were subjected to a permanent ligation of the left anterior descending coronary artery (LAD) and sacrificed 1 week post MI. To visualize the degree of harm, I used a conventional staining procedure (trichrome), which marked fibrotic areas in blue and intact tissue in red. In comparison to morphological observations, fluorescent labeling of Runx1 was applied for confocal microscopy analyses in order to investigate the presence of the transcription factor post MI. Runx1 was absent in the sham mouse heart, as indicated by a completely reddish tissue color and missing fluorescent labeling in the confocal image (Figure 28, sham). However, I was able to show that murine hearts, which have been subjected to MI, showed a dilated left ventricular phenotype along with a fibrotic scar formation (Figure 28, I), in accordance with the literature (Gao 2012, Prabhu 2016). Fluorescent staining of Runx1 was especially observed in the border zone (BZ) between the antero-septal scar (bluish stained) and the adjacent normal myocardium (red stained). This observation was

accompanied by a loss of the myocardial network marked via a diminished F-actin staining, when compared to sham controls (Figure 28). This observation validated the evidence of increased Runx1 expression in the posterior border zone (BZ) of the myocardium after the induction of myocardial injury.

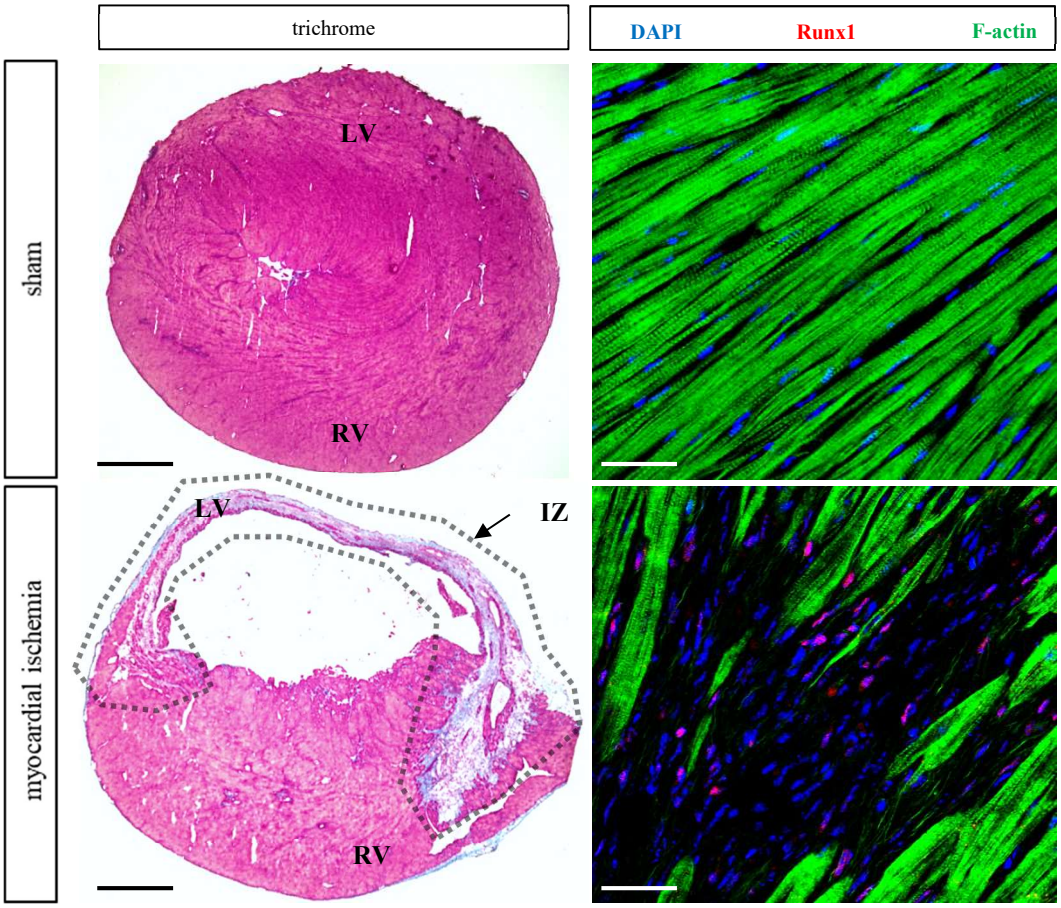

Figure 28: Runx1 expression upon experimental myocardial ischemia. Wildtype (C57Bl6/J) mice were subjected to permanent ligation of the LAD (I) and compared to sham controls (sham). Trichrome staining of cryosections revealed an obvious destruction of the left ventricle (LV), indicated by a loss of myocardium along with a fibrotic scar formation. Fluorescent staining displayed Runx1^{+} cells within the infarct zone (IZ), whereas Runx1 was completely absent in the intact myocardium of sham hearts. Scale bars (black) = 50µm, (white) = 200µm.

4.6. Runx1 expression peaked in the ischemic region of the heart in vivo at 4 days post MI

To gain deeper insights, which kind of role dedifferentiation might play, I started to acquire a kinetic profile of Runx1^{+} cells after the onset of experimental myocardial infarction. Therefore, wildtype mice were subjected to permanent LAD ligation (I) and sacrificed along different states of cardiac remodeling, i.e. 1, 4, 7, 14, 21 and 90 days post myocardial infarction (dpI). To demonstrate the dynamics of Runx1 expression, Runx1

fluorescent labeling was quantified at different time points and compared to 1dpI, since Runx1 was absent in sham animals (Figure 28). Runx1 expression was detectable in almost all stages of remodeling in small cells (white arrows, Figure 29), but peaked at 4dpI, potentially representing infiltrating immune cells. As the majority of Runx1^{+} mACMs were detected at 7dpI (Figure 29, red arrows), I focused on that time point, addressing the purpose of dedifferentiation.

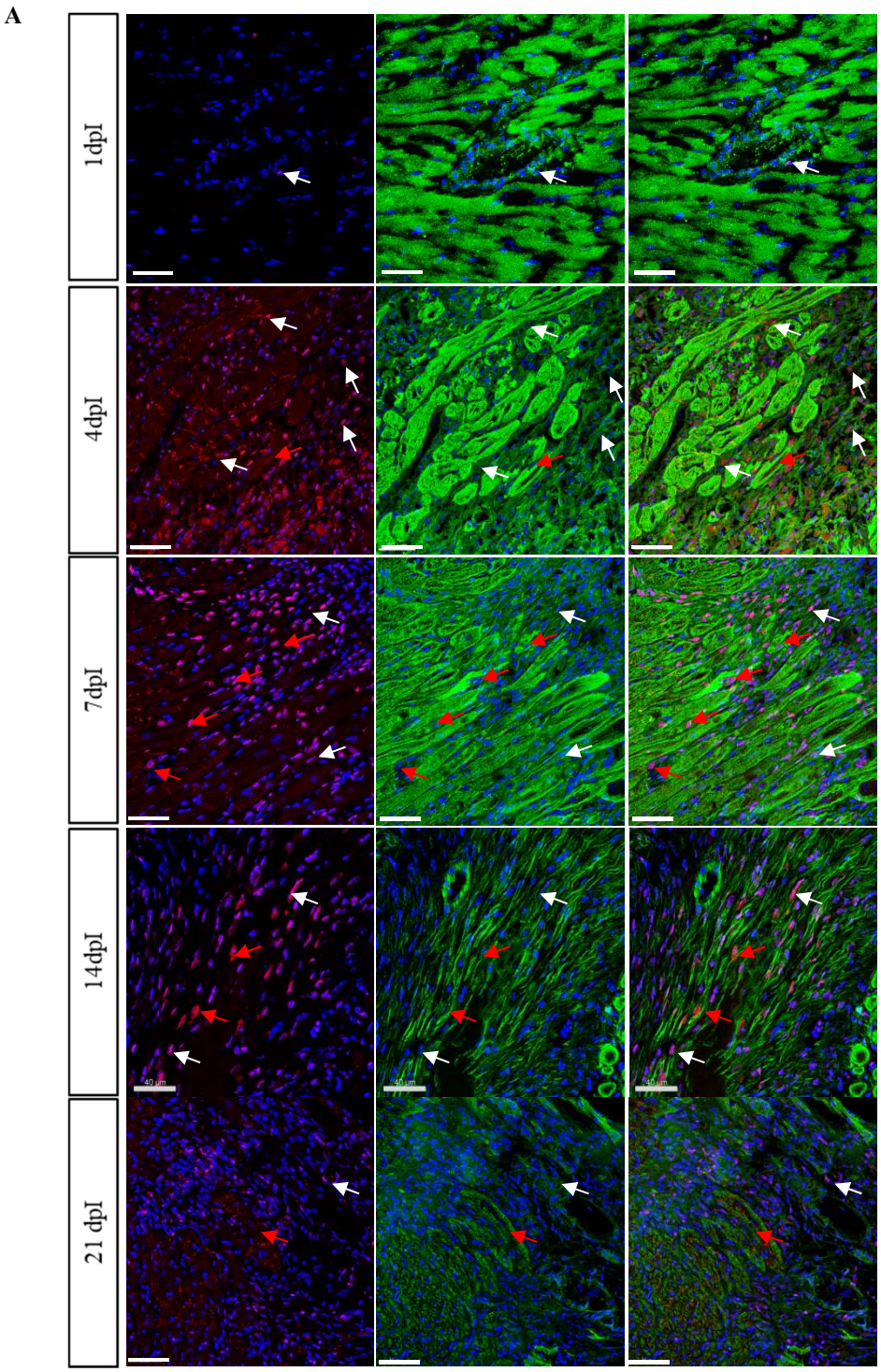

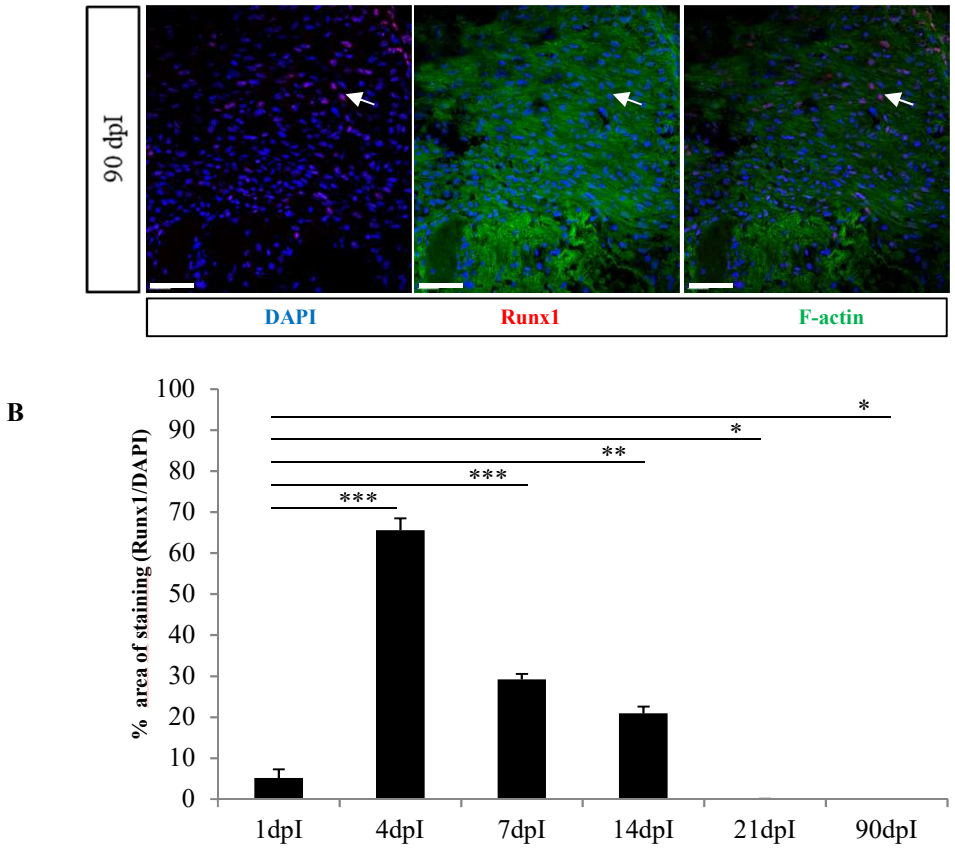

Figure 29: Kinetic pattern of Runx1 expression in wildtype animals after myocardial infarction. Mice were subjected to permanent LAD ligation in order to monitor the Runx1 expression profile and were sacrificed 1, 4, 7, 14, 21 and 90 days post infarction (dpI). Cryosectioning followed by IHC staining for Runx1, F-actin (structure) and DAPI (nuclei) was obtained. **(A)** Representative images of each time point are shown as overlays: DAPI/Runx1 (left panel), DAPI/F-actin (middle panel) and DAPI/Runx1/F-actin (right panel). The amount of $Runx1^{+}$ cells (white arrows) increased significantly up to 4dpI and declined thereafter. The majority of $Runx1^{+}$ staining within mACMs was detectable at 7dpI. Scale bars = 40µm. **(B)** Threshold-based quantitative analysis of images was determined with ImageJ. Quantified Runx1 fluorescent labeling was compared to 1dpI. Statistical significances were determined by a 2-tailed unpaired t-test. *P<0.05, **P<0.01, ***P<0.001.

4.7. Functionality of Runx1 deficient mice was validated via an absent expression of Runx1 in mACMs in the infarcted heart at 7 days post MI

Additionally, I longed to know, if the observed in vitro effects of the heart specific Runx1 deficiency could also be related to an absent Runx1 expression in the infarcted heart. For this purpose, I used the established $Runx1^{fl2}$/αMHC^{Cre} mice and subjected them to permanent LAD ligation. The infarcted hearts were harvested at the peak point of Runx1 expression in CMs, based on my previous findings (Figure 29). The fluorescent intensity levels of Runx1 were compared to cross-sectional staining of $Runx1^{fl2}$ mice with no altered Runx1 expression. Runx1 deficient heart sections revealed no co-localization of Runx1 with the CM specific marker ACTN2, whereas overlays of both markers were

detectable in Runx1^{fl2} mice (Figure 30). These findings indicated a reliable functionality of the heart-specific knock-out model. Furthermore, it strengthened my in vitro observation and pretended Runx1 as a positive and secure marker of CM dedifferentiation.

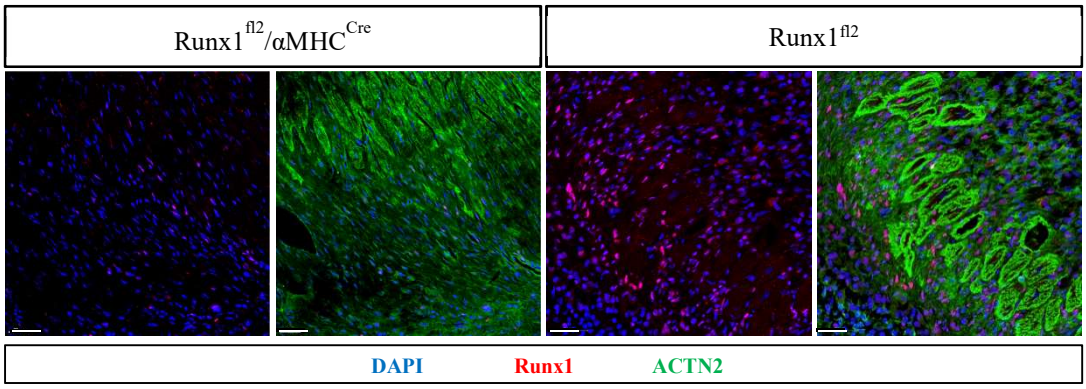

Figure 30: Runx1 expression of heart specific deficient mice, which were subjected to permanent LAD ligation. Runx1^{fl2}/αMHC^{Cre} mice were subjected to permanent occlusion of the LAD and compared to infarcted Runx1^{f2} animals. Mice were sacrificed at 7dpI at the peak point of Runx1 expression. Runx1 fluorescence was barely detectable in Runx1 deficient mice and no co-localization between Runx1 and ACTN2 could be observed. In comparison, Runx1^{fl2} mice showed the same Runx1 expression profile as wildtype mice, but with less Runx1^{+}/ACNT2^{-} and Runx1^{+}/ACTN2^{+} double positive cells. Scale bars = 50µm.

4.8. Runx1 expressing cells were able to survive in the infarcted heart, which was demonstrated in Runx1 Viewer and Tracer mice at 4, 7 and 90 days post MI

To validate the observations of the fluorescent staining and to follow the cell fate of Runx1 expressing cells, I used the previous described Runx1 labeling approach (the referring in vitro results are displayed in Figure 26) for my in vivo studies of myocardial damage. Initially, I designed my Runx1 Viewer mice with the identical genetic Runx1^{tTA} concept as for the Tracer mice, but switched to a LC1^{Cre}/Rosa^{stopfloxlacZ} construct, I worked with below. Monitoring of the current Runx1 expression was established by a tTA-responsive bidirectional promoter for GFP-lacZ (Krestel 2001). By this means, lacZ staining revealed an actual Runx1 expression and disappeared, if the Runx1 level declined (hereinafter referred to as Runx1 Viewer). Therefore, I was able to track the cell fate of Runx1^{+} cells by comparing both transgenic strains. Animals of both strains were subjected to permanent LAD ligation (I) and sacrificed at 4, 7 and 14dpI to map the dynamics of Runx1 expression as well as to mark the survival of once Runx1 expressing cells within the ischemic region of the injured heart. Runx1 Viewer mice revealed the same correlative dynamics as examined in wildtype animals (Figure 29). Here,

Runx1$_{traced}$lacZ^{+} expression (Figure 31, red arrows) was visible in all stages of myocardial remodeling, whereas the majority of Runx1$_{traced}$lacZ^{+} cells were detected at 7dpI. At this time point, lacZ staining turned up as laminar scattered over the whole cross-sectional area, but the highest contrast could be found within the IZ of the LV. Furthermore, only a few Runx1^{+} cells, which retained within the scar, could be noticed at later stages of cardiac remodeling (90dpI). LacZ staining of Runx1 Viewer heart cryosections appeared as not specific post MI and was difficult to correlate with the morphological structures of ACMs via widefield imaging.

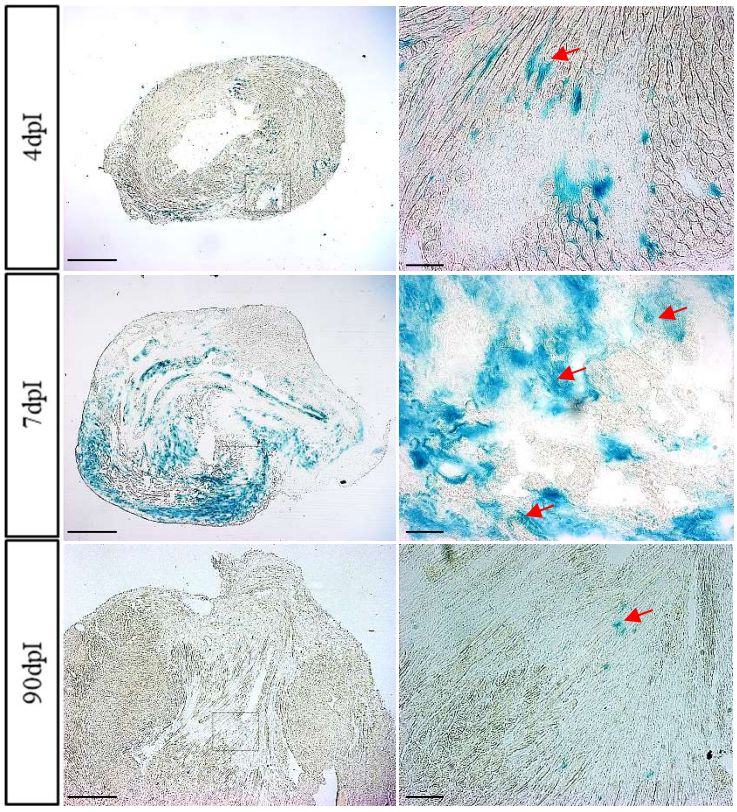

Figure 31: Monitoring of the current Runx1 expression in correlation with lacZ expression in Runx1 Viewer animals upon myocardial ischemia. Runx1 Viewer mice were subjected to permanent LAD ligation to monitor the dynamic pattern of Runx1 after myocardial ischemia via lacZ staining. Representative widefield images revealed a lacZ-associated Runx1 expression at 4, 7 and 90dpI, whereas most Runx1$_{traced}$lacZ^{+} ACMs (red arrows) were detectable at 7dpI. The lacZ staining appeared unspecific and therefore made the quantification impossible. Nevertheless, the dynamics of Runx1 expression corresponded to fluorescent Runx1 staining in cryosections of wildtype hearts after MI. Scale bars = 500µm (left), = 50µm (right).

In addition, Runx1 Tracer mice disclosed a different appearance of lacZ staining in MI hearts in comparison to Runx1 Viewer animals, as illustrated in Figure 32. Here, Runx1$_{traced}$lacZ^{+} cells could be detected in almost all cryosections of Tracer hearts post MI, whereas lacZ patches were distributed as laminar staining (grey arrows) over the

whole cross-sectional area at 4, 7 and 90dpI. Runx1$_{traced}$lacZ^{+} cells were marked as high contrast dots (black arrows) as well as laminar patches (grey arrows) at 7 and 90dpI and were mainly located within the scar and other areas of the ischemic region. The lacZ staining remained stable until the later stages of cardiac remodeling, indicating a proper survival of once Runx1^{+} cells upon ischemia. But the unspecific lacZ staining made it impossible to distinguish different cell types from each other within the infarcted area. Combinations of conventional and fluorescent staining did also not reach the expected results (data not shown). Furthermore, the identification of Runx1$_{traced}$lacZ^{+} ACMs was barely detectable, since only a few ACMs survived within the ischemic region. Because of a massive coagulative necrosis of CMs in association with a loss of cross striation and a disappearance of nuclei, a valid discrimination of mACMs was impeded. Consequently, it was necessary to drop the method of the permanent LAD ligation in order to increase the visibility of Runx1^{+} mACMs in vivo.

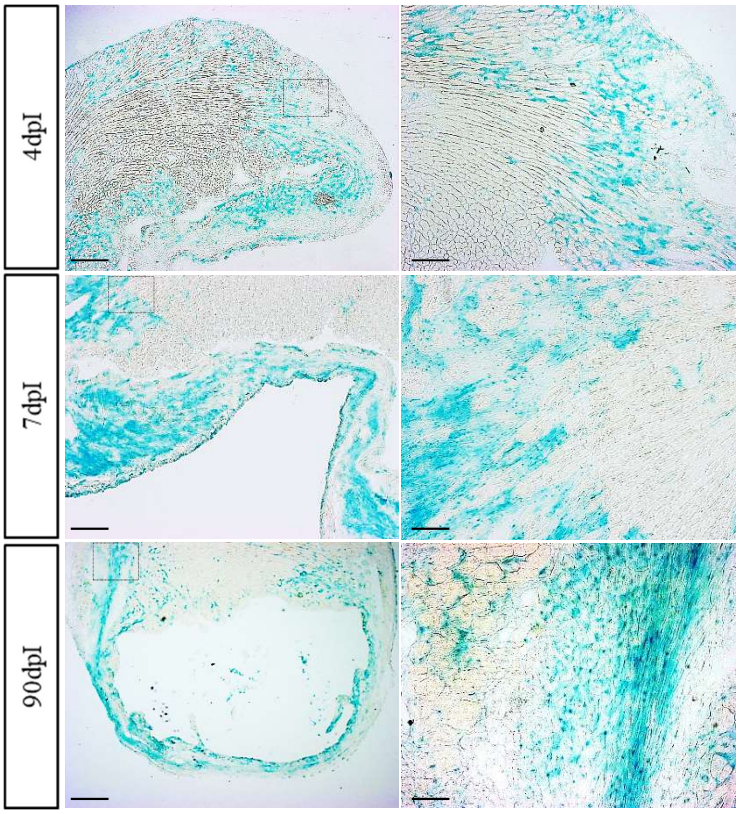

Figure 32: Tracking the cell fate of Runx1$_{traced}$lacZ expression in Runx1 Tracer animals upon myocardial ischemia. Runx1 Tracer mice were subjected to permanent LAD ligation to follow the cell fate of Runx1^{+} cells via lacZ staining during myocardial ischemia. Representative bright field images revealed a functional Runx1 tracing via lacZ staining. LacZ staining appeared as laminar patches (grey arrows) at 4dpI, whereas high contrast dots (black arrows) could be identified within the scar and other areas of the ischemic region at 7 and 90dpI. Runx1$_{traced}$lacZ staining was almost consistent during cardiac remodeling, indicating a survival of once Runx1^{+} cells. Scale bars = 200µm (left), = 50µm (right).

4.9. The model of I/R turned out to increase the amount of surviving mACMs within the ischemic area and was therefore preferred to study processes of dedifferentiation in the infarcted myocardium

To increase the number of surviving CMs for further analyses and to improve the Runx1 tracing approach for quantification, I switched to the ischemia/reperfusion (I/R) model. The I/R method is an alternative and well-established model of myocardial damage, in which animals are subjected to a temporary occlusion of the LAD, followed by a specific time of reperfusion (Hamacher-Brady 2007, Lukacs 2012). Hence, Runx1 Tracer mice were subjected to I/R and hearts were harvested at 1, 4, 7 and 14dpI/R. Myocardial injury characterized by a diminished ACTN2 staining (Figure 33) was apparently detectable at 4 and 7dpI/R. Damaged mACMs turned up with less sarcomeres (light grey), almost no clear cell surface, fragile and destructed. In contrast to hearts with permanent LAD ligation, a population of intact mACMs appeared within the ischemic region. Moreover, the surviving mACMs showed also less ACTN2 staining, especially in the adjacent areas, which were in contact with dying mACMs, adumbrating dedifferentiation processes. Furthermore, hearts revealed marginal myofibrillar deformation characterized by a lack of CM interconnection and myocardial composition (lacking ACTN2 staining, black holes) at 14dpI/R, suggesting either CM regeneration and/ or proliferation.

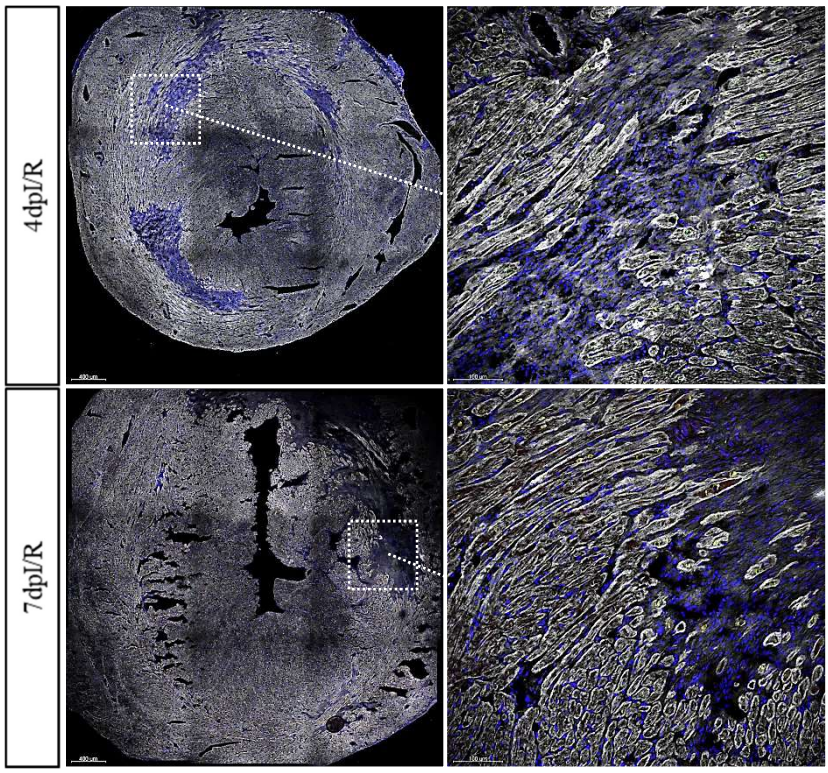

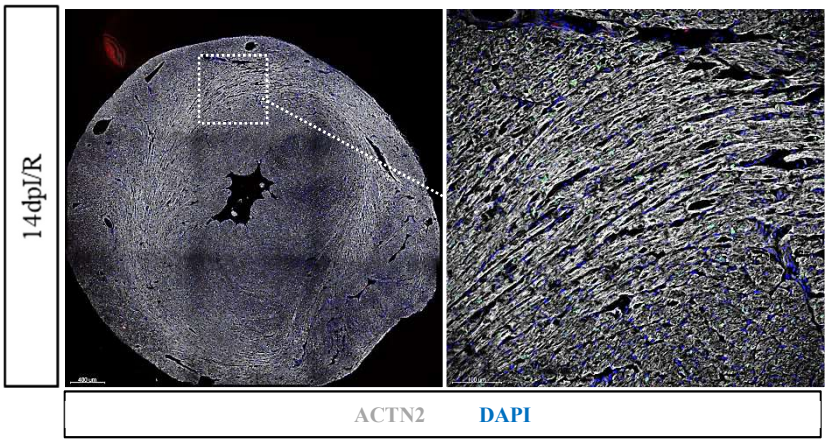

Figure 33: Myocardial damage and remodeling in Runx1 Tracer animals upon I/R injury. Representative confocal images of cryosections at 4, 7 and 14 days post I/R (dpI/R) stained for sarcomeres (ACTN2) and nuclei (DAPI) to observe myocardial damage. Apparently, the ischemic region was constituted by frayed mACMs within the restricted IZ at 4 and 7dpI/R. Damaged mACMs were recognized by a poor ACTN2 staining (light grey, less intense) and appeared fragile as well as destroyed with no clear cell surface. In contrast, myocardial structures were only slightly destructed at 14dpI/R, but the lack of ACTN2 staining indicated broken cardiac myofibrillar composition. Scale bars = 400µm (left), = 100µm (right).

Next, I wanted to know, if dedifferentiation was able to drive the survival of mACMs post MI, depending on the extent of myocardial damage. Therefore, I took hearts from both models of myocardial ischemia (permanent LAD ligation vs. I/R) at the peak point of Runx1 expression in mACMs (7dpI/+R) and quantified the percentage of the IZ in the hearts of both models, displaying the assessed ex vivo infarct size, as described by Redfors et al. and others (Califf 1985, Graham 2001, Redfors 2012). By the means of trichrome staining, I was able to show that the myocardial damage was more than twice as large in the permanent occlusion model of the LAD as in the model of temporary artery occlusion (Figure 34A-C). The fibrotic formation seemed also much more intense in case of permanent LAD ligation. Consequently, temporary coronary artery occlusion (I/R) of Runx1 Tracer hearts revealed a more pointwise lacZ staining in Runx1^{+} cells, but also failed to enable a reliable quantification of Runx1^{+} ACMs post MI without any additional staining. Especially, the mapping of lacZ dots, belonging to different or the same mACMs, was impossible and therefore further methods were required.

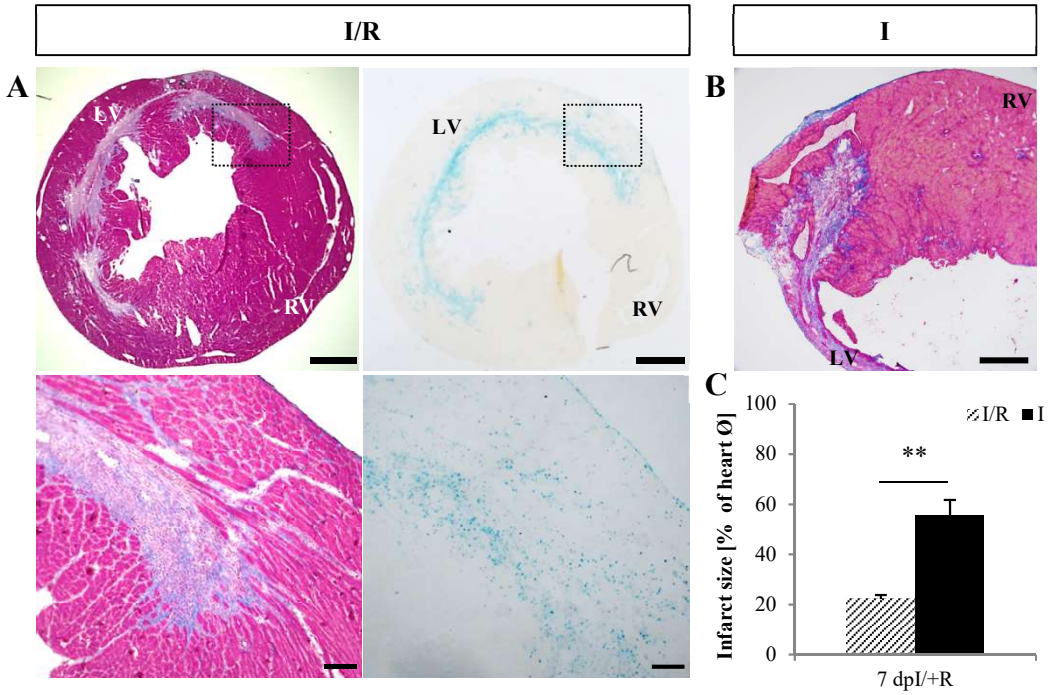

Figure 34: Comparative analysis of the infarct size in different experimental MI animal models. (A+B) Representative images of I/R (A) revealed a significant higher amount of intact myocardium compared to permanently LAD ligated hearts (B). Furthermore, the composition of the ischemic area contained fibrotic tissue (bluish color) to a higher content than in I/R hearts. In total, the ex vivo infarct size appeared as twice as large in the permanent LAD ligation compared to the I/R model. In addition, lacZ staining of Runx1 Tracer mice appeared dotlike and equally distributed across the whole ischemic area, including the border zone (BZ) 7dpI/R and indicating a larger amount of Runx1$^+$ surviving cells. **(C)** Quantification of the ex vivo infarct size (displaying the infarct zone = IZ) was done via trichrome staining of cryosections followed by image data analysis, which was obtained by assessing 10 tissue sections per method (I/R vs. I). Data are presented as mean ± SEM. Statistical significance was determined by a 2-tailed unpaired t-test. **P<0.01. (LV) = left ventricle, (RV) = right ventricle. Scale bars = 200µm (upper panel), = 50µm (lower panel).

4.10. The amount of Runx1$^+$ mACMs were increased by 3.75 fold due to switching from the permanent (I) to the temporary (I/R) LAD ligation model

Pursuing the question of the quantification of Runx1$^+$ mACMs post MI, I proceeded with immunohistochemical staining of cryosections. By the usage of PCM1 as a marker of ACM nuclei in combination with Runx1, indicating mACM dedifferentiation, the amount of Runx1$^+$ mACMs was detected in a co-localization analysis of confocal images. An additional Lectin staining allowed the detection of intact cells, in which Lectin binds to carbohydrates presented on the cell membrane surface (Gonatas 1973, Emde 2014). I still wanted to investigate, whether a temporary occlusion of the LAD followed by a prolonged reperfusion (I/R) led to an increase of Runx1$^+$ mACMs in contrast to the model of persistent vessel occlusion. A comparison of both methods via an immunohistological approach combined with serial sectioning answered this question to a certain extent. Thus,

it appeared that hearts upon I/R sustained a certain amount of intact (Lectin surrounded) mACMs ($PCM1^+/ACTN2^+$) within the infarcted region post ischemia, whereas hearts upon permanent LAD ligation completely lost their contractile network and cell-cell-contacts within the infarct zone (Figure 35A&B). These observations concurred with the infarct size analyses (Figure 34). Quantification of the overall $Runx1^+$ cell numbers compared with the amount of intact $Runx1^+$ mACMs revealed that the Runx1 expression peaked in ACMs at 7dpI, whereas the maximum of the total Runx1 expression was already detectable at 4dpI (Figure 35C). Taken the previous findings into account, a temporary occlusion of the coronary artery followed by 7 days of reperfusion (7dpI/R) turned out as the preferred model and time point to study the cell fate of $Runx1^+$ mACMs in the ischemic heart.

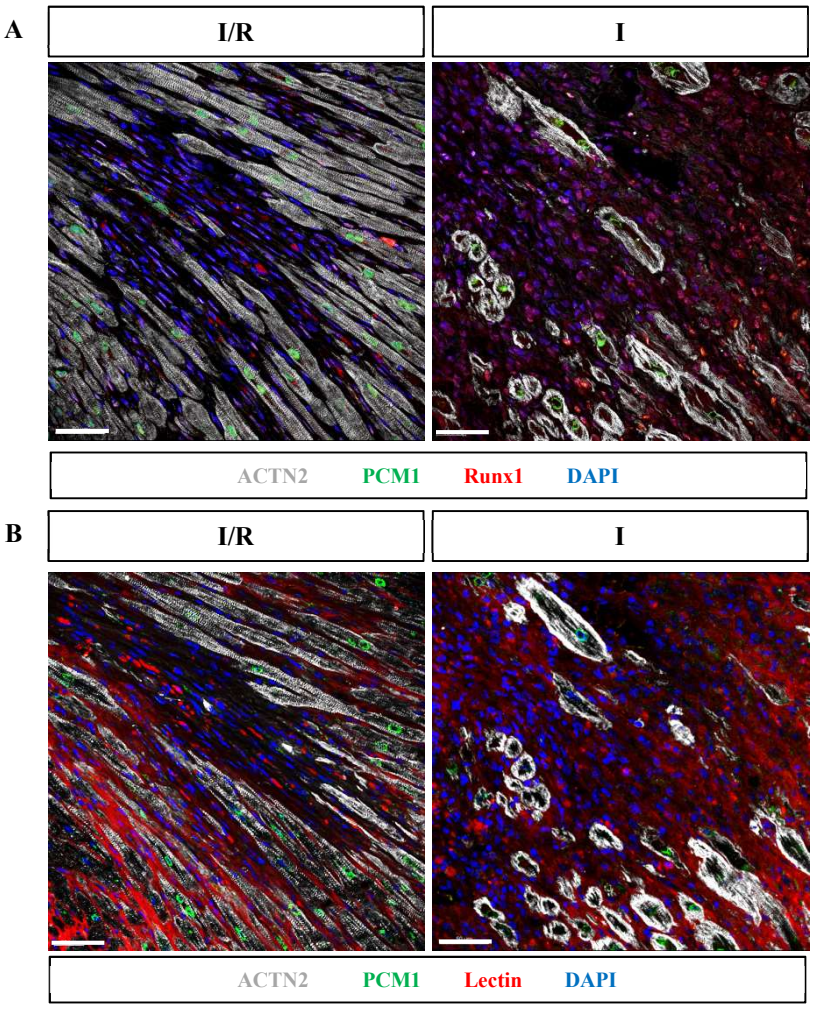

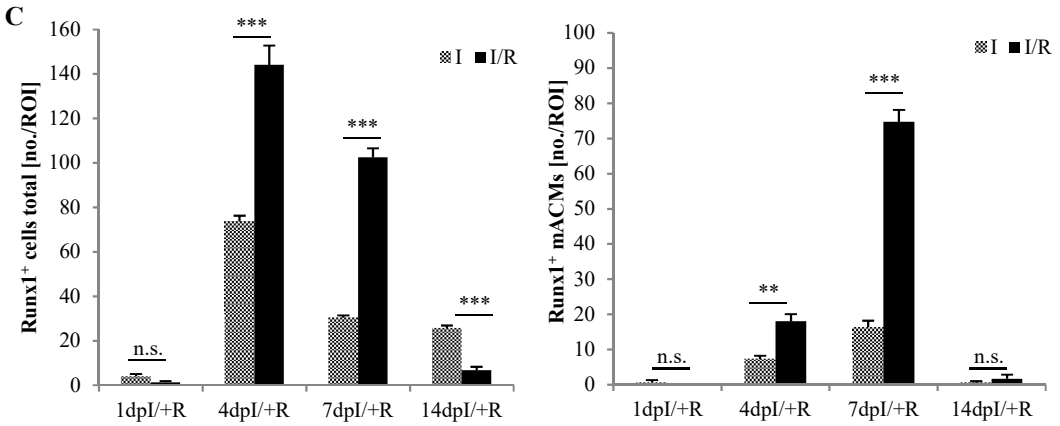

Figure 35: I/R injury increased the amount of Runx1$^+$ mACMs compared to permanent LAD ligation (I). Animals were subjected either to I or to I/R (displayed as I/+R), sacrificed and their hearts were serial cryosectioned. **(A+B)** Representative images of IHC staining at 7dpI/+R are shown. The majority of Runx1$^+$ mACMs (Runx1$^+$/PCM1$^+$/ACTN2$^+$) was identified in both models of experimental MI at 7dpI/+R, with a 5 fold increase in case of I/R compared to the I model. The comparative immunohistological imaging analysis of I/+R was done by visualizing intact (B, Lectin surrounded), surviving ACMs (PCM1$^+$/ACTN2$^+$) and marking Runx1$^+$ mACMs (A, Runx1$^+$/PCM1$^+$/ACTN2$^+$) within the ischemic region, which was taken for quantification (C). **(C)** An image-based quantification of the total amount of Runx1$^+$ cells (C, left) compared to Runx1$^+$ ACMs (C, right) was done for the time course of cardiac remodeling (at 1, 4, 7, 14dpI/+R). Scale bars = 50µm.

4.11. Morphological characteristics and expression of dedifferentiation markers were observed on a microscopic and nanoscopic level in Runx1 Tracer mice at 7dpI/R

Before proceeding with a deep cell-based analysis, I wanted to substantiate the evidence for the existence of cardiomyocyte dedifferentiation in the I/R model. Therefore, I used at first the well-established structural marker Moesin, which has been shown to be present in dedifferentiated cells (Hirao 1996, Alge 2003, Pöling 2012, Miyawaki 2016). I took Runx1 Tracer animals, subjected them to I/R and harvested their hearts at 7dpI/R. Here, Moesin$^+$ mACMs could be identified within the ischemic region, whereas the structural marker was mainly detected at the boundaries and edges of ACMs (Figure 36). Beyond that, Moesin$^+$ mACMs showed a decline of sarcomeres (ACTN2), indicating dedifferentiation processes. A double staining of Moesin and Runx1 was not possible due to the incompatibility of the available antibodies. Nevertheless, these correlative observations confirmed the appearance of mACM dedifferentiation in the I/R model via an additional marker in vivo.

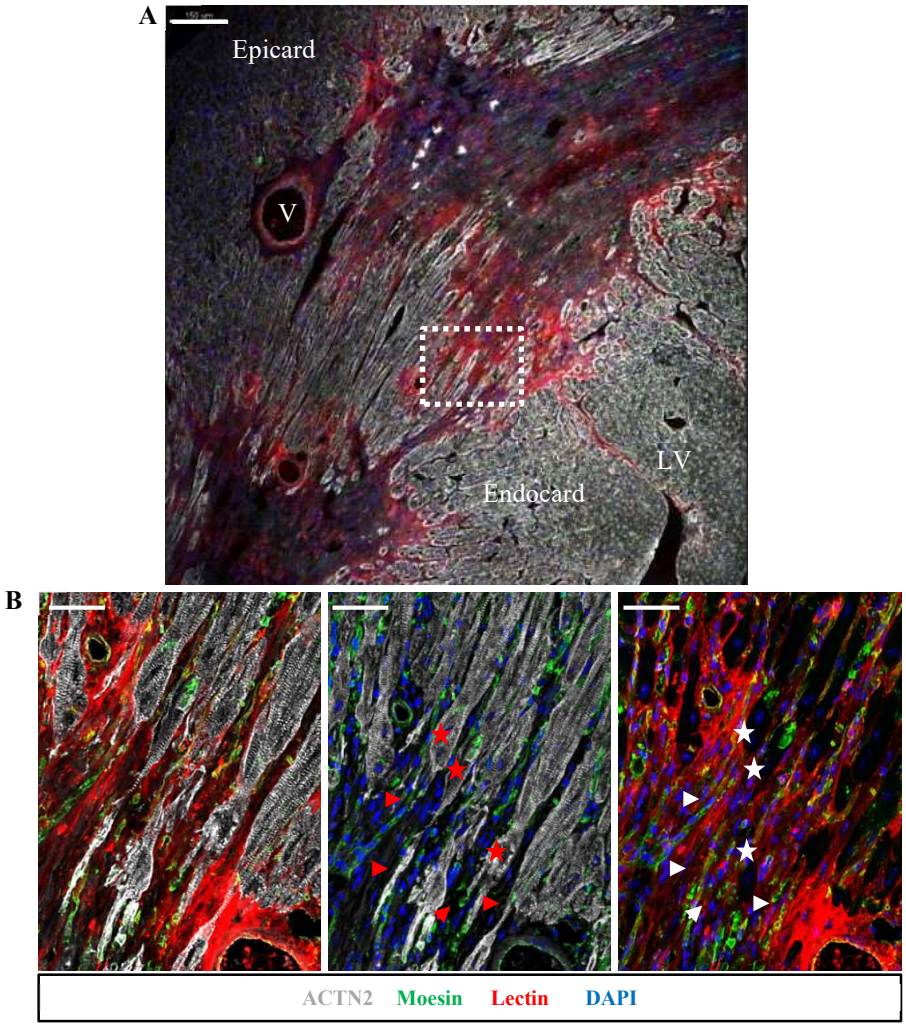

Figure 36: Signs of dedifferentiation were detectable in animals post I/R in vivo. Runx1 Tracer animals were sacrificed at 7dpI/R, representing the time point of maximum Runx1 expression in ischemic mACMs. IHC analysis of the dedifferentiation marker Moesin proved the appearance of Moesin^{+} ACMs together with a drop of sarcomeres (ACTN2) in such CMs. **(A)** A representative overview image of the infarcted region, which revealed surviving myocardium within the infarct zone, is displayed. **(B)** Magnification of the corresponding region of interest (ROI) enhanced the positive correlation of Moesin with a decreased ACTN2 expression as well as the formation of cell protrusions and the presence of elongated mACMs post MI. As a matter of fact, these results confirmed the appearance of mACM dedifferentiation in vivo via an independent and second marker protein. (V) = valvular region, (LV) = left ventricle. Scale bars = 150µm (A), = 40µm (B).

To further validate the extent of dedifferentiation in this animal model, electron microscopy was used to characterize the processes of dedifferentiation on an ultrastructural level. Therefore, transmission electron microscopy (TEM) of the LV from ischemic hearts revealed a damaged and frayed myocardial structure with signs of dedifferentiation at 7dpI/R (Figure 37.1-6). mACMs within the ischemic region appeared with a burst filamentous formation of sarcomeres, accompanied by an inordinate disorganization (Figure 37.1-2&5). These alterations were associated with staggered Z-bands and dilated intercalated discs (Figure 37.3&5). Furthermore, the majority of

mitochondria were leached and showed signs of cristaelysis with less electron density (Figure 37.3-4), though some mitochondria revealed a high electron density with an intact and tight shape (Figure 37.1-3&5). Even on the ultrastructural level, CMs within the LV seemed to be elongated and showed characteristical protrusions with a width of approximately 2µm (Figure 37.6). In contrast, the myocardium of the RV from ischemic hearts, which served as controls, appeared dense and organized (Figure 37.9-11) at 7dpI/R. Most RV mitochondria revealed high electron density material and well-defined cristae (Figure 37.8-11). Here, the intercalated discs showed a normal constitution and most sarcomeres were equally distributed as well as shaped in form of parallel arrangements up to cell boundaries (Figure 37.7&11). These findings clearly indicated processes of CM dedifferentiation in vivo post ischemic injury on a micro- and nanoscopic scale and confirmed my previous conclusions (Figure 20-36). Nevertheless, the cell fate of dedifferentiated mACMs in terms of proliferation and regeneration remained still unclear.

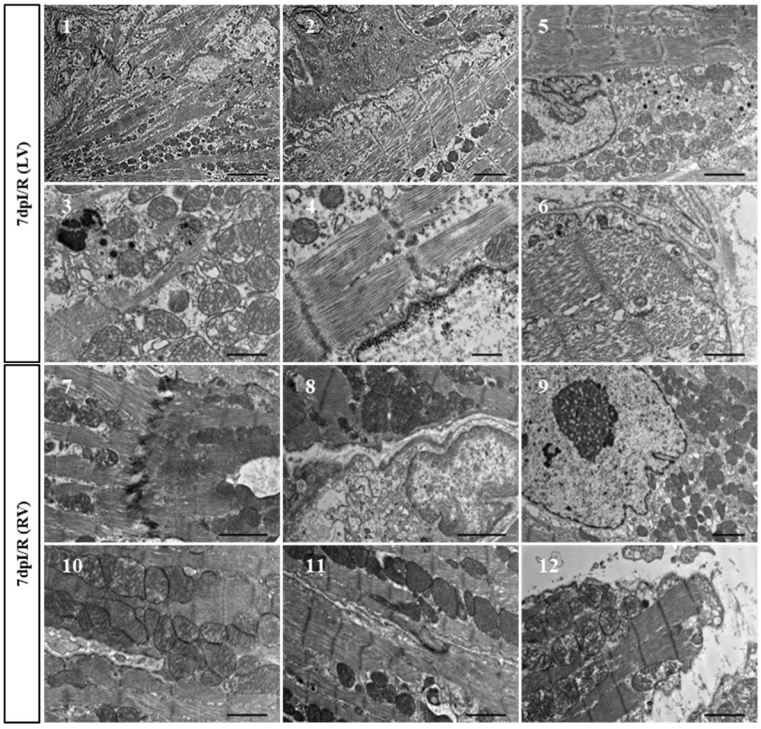

Figure 37: Ultramicrotomy-based TEM revealed signs of dedifferentiation on a nanoscopic level in animals at 7dpI/R. Analysis of the ultrastructure from left (LV) and right (RV) ventricle declared less compact sarcomeres (1, 2, 5) within the ischemic region (LV) and less electron density in mitochondria, indicating critaelysis (3-5). Furthermore, intercalated discs appeared dilated and Z-band staggered (1, 3, 5). Other signs of dedifferentiation were validated by the appearance of characteristical protrusions up to a width of 2µm, going along with elongation of mACMs within the LV (6). In contrast, the myocardium of the RV revealed overall an equally distributed and organized sarcomeric structure (7, 10-12) with high electron density and intact mitochondria (9-11). Surprisingly, heterochromatin appeared regular (3, 9) and only in some cells of the LV parietal and swollen (not shown). Scale bars = 5µm (1), = 2µm (2, 3, 7-9, 11, 12), = 1µm (4, 6, 10), = 500nm (5).

4.12. Isolation and sorting of living Runx1^{+} mACMs post I/R enabled downstream next-generation sequencing (NGS) analysis

For achieving deeper knowledge about the properties of dedifferentiated Runx1^{+} mACMs upon myocardial damage, I isolated surviving CMs from the ischemic area and profiled the cardiac cells via next-generation sequencing (NGS). Therefore, I used a sui generis live-cell sorting approach, which acquired an endogenous fluorescent labeling of living mACMs. By replacing lacZ with red fluorescent protein (RFP) in my Runx1 Tracer animals, I was able to mark and follow a Runx1 expression in mACMs in form of an endogenous RFP labeling. To induce a Runx1-initiated RFP tracing, Tracer animals were subjected to I/R, sacrificed at 7 days post myocardial injury and fluorescent, ischemic mACMs were isolated from the infarcted hearts via Langendorff perfusion (Skrzypiec-Spring 2007). In the next step, Runx1-traced RFP^{+} (Runx1$_{traced}$RFP^{+}) mACMs were fixed and stained for ACTN2 to verify differentiation and DAPI to monitor nuclei. Runx1$_{traced}$lacZ^{+} mACMs were carried along as internal controls to demonstrate an equivalent tracing. By this means, I could demonstrate that lacZ and corresponding RFP expressions were detectable in mACMs post induction of ischemia. Furthermore, Runx1$_{traced}$RFP^{+} mACMs appeared ACTN2^{+} and were identified as mature CMs by the presence of 2 nuclei per cell (Figure 38).

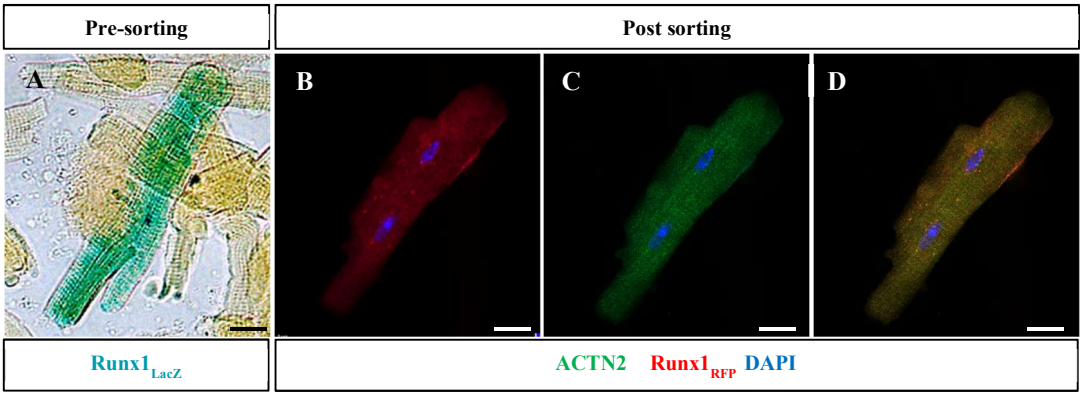

Figure 38: Switching Runx1 tracing label from lacZ to RFP in order to enable single live-cell sorting. Runx1 Tracer animals were subjected to I/R and sacrificed at day 7 post ischemia. **(A-C)** mACMs were isolated from I/R hearts via Langendorff perfusion, fixed and stained for lacZ (A) or RFP (B), respectively. To validate RFP staining in Runx1RFP Tracer animals, mACMs were double stained with ACTN2 (C) to label sarcomeres and DAPI to monitor nuclei. **(D)** Overlay of RFP, ACTN2 and DAPI typically revealed a positive correlation between RFP and ACTN2 as well as 2 nuclei per cells. Scale bars = 10µm.

Proceeding with knowledge of an optimal MI model for tracing and sorting, Runx1$_{RFP}$ Tracer mice were subjected to I/R and sacrificed at different time points post myocardial ischemia. Hereby, I was able to address the cell fate of mACMs by monitoring the RFP

fluorescence at 4, 7 and 14dpI/R. Critical steps of the established isolation and sorting procedure are visualized in Figure 39. As shown, after isolation of mACMs via Langendorff perfusion, heart regions were divided into CM suspensions from the ischemic zone of the LV (IZ^{**}) and from the remote zone mainly of the RV (RZ^{*}). Here, RZ^{*} served as an optimal internal control for sorting and further NGS analyses. Exclusion of doublets and dead mACMs was enabled by an optimized gating strategy (Figure 39 / detailed gating strategy in the methods Figure 19). In addition, autofluorescence of mACM was used to ensure a reliable detection of the RFP signals by gating for GFP/RFP. Sorting of GFP^{-}/RFP^{+} mACMs with a high time of flight (TOF) enabled that only intact, relatively long CMs were taken for down-stream analyses. A comparative analysis of remote and ischemic regions revealed no significant difference in CMs lengths (Figure 39-40) at 7dpI/R. Furthermore, the majority of $Runx1_{traced}RFP^{+}$ mACMs was detectable in IZ^{**} post I/R, as displayed by a significant peak height (PkHt) of the RFP intensity (Figure 39B).

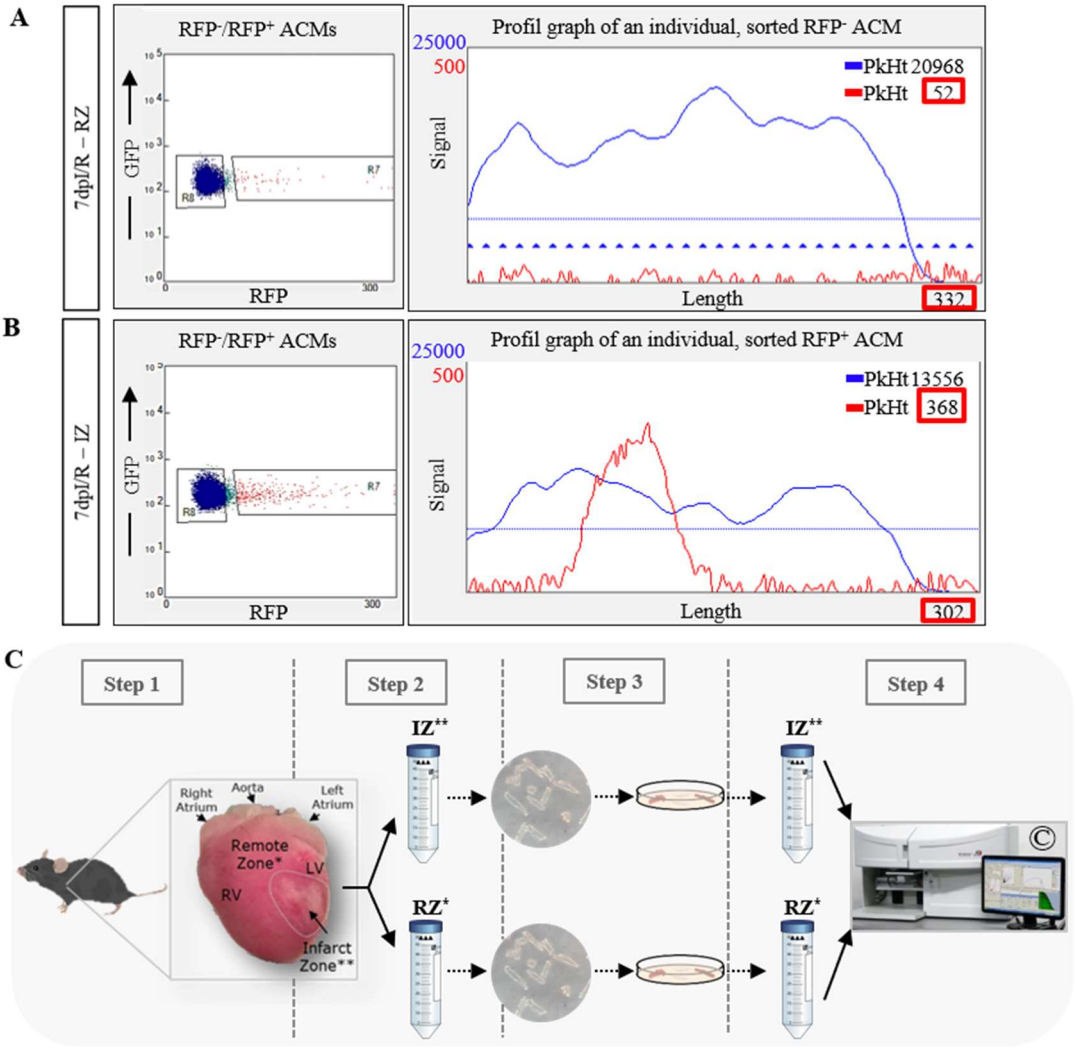

Figure 39: Live-cell sorting of Runx1$_{traced}$RFP^{+} mACMs enabled the isolation and separation of single CMs undergoing dedifferentiation. (A) Representing gates for live-cell sorting of isolated mACMs from infarcted hearts revealed that Runx1$_{traced}$RFP^{+} mACMs were detectable in the whole heart at 7dpI/R. The majority of Runx1$_{traced}$RFP^{+} mACMs were measured inside the ischemic region (IZ**). In addition, a clear maximum with a significant peak height (PkHt) of RFP fluorescence was detected within IZ. Both profile graphs showed a similar mACM shape in RZ* and IZ**, as indicated by the blue line. In addition, no significant differences in CM lengths (time of flight - TOF) were observed between IZ** and RZ*. **(B+C)** The schematic workflow of critical steps for the mACM isolation and sorting procedure is visualized. In step 1, mice were sacrificed and hearts were withdrawn upon MI, according to the approved animal protocol. In step 2, Langendorff perfusion of infarcted hearts was performed for maximal 60 minutes. Afterwards, the ischemic zone from the LV (IZ**) and the remote zone mainly from the RV (RZ*) were separated with followed by post in-solution digestion in 50mL falcons. In step 3, after successful dissociation of the tissue and centrifugation steps, the cell solution was pre-plated for 60 minutes on 37°C to avoid fibroblasts contamination. In step 4, purified ACMs were gently re-transferred into falcons and diluted with perfusion buffer for biosorting. ©Union Biometrica, Inc.: Print and publication permission acquired and given by David Strack, President & CEO of Union Biometrica

Quantification of the biosorting data (Figure 40) delivered a clear separation of Runx1$_{traced}$RFP^{+} mACMs from IZ and Runx1 negative mACMs from RZ (Runx1$_{negative}$) due to significantly different fluorescence intensity levels (represented as RFP peak height). In comparison to 1.26%(±0.44) Runx1$_{traced}$RFP^{+} CMs that could be measured in RZ of the infarcted heart, most of living Runx1$_{traced}$RFP^{+} CMs were detected within the ischemic region (3.11%(±1.80)). The amount of living Runx1$_{negative}$ mACMs kept relatively stable in both regions over time (97-99%). Approximately 1% living Runx1$_{traced}$RFP^{+} mACMs were found within the infarcted area at 4 and still at 14dpI/R, representing survival of once Runx1 expressing mACMs in some ischemic regions. Thereby, living Runx1$_{traced}$RFP^{+} mACMs were barely measured in the remote zone (RZ*) of the same hearts. The percentage of living Runx1$_{negative}$ mACMs dropped down to 96% in IZ** at 7dpI/R, which correlated with the highest amount of living Runx1$_{traced}$RFP^{+} mACMs within the ischemic region (IZ**) at this time point. For further downstream analysis, mRNA was extracted for the profiling of Runx1$_{traced}$RFP^{+} mACMs by NGS.

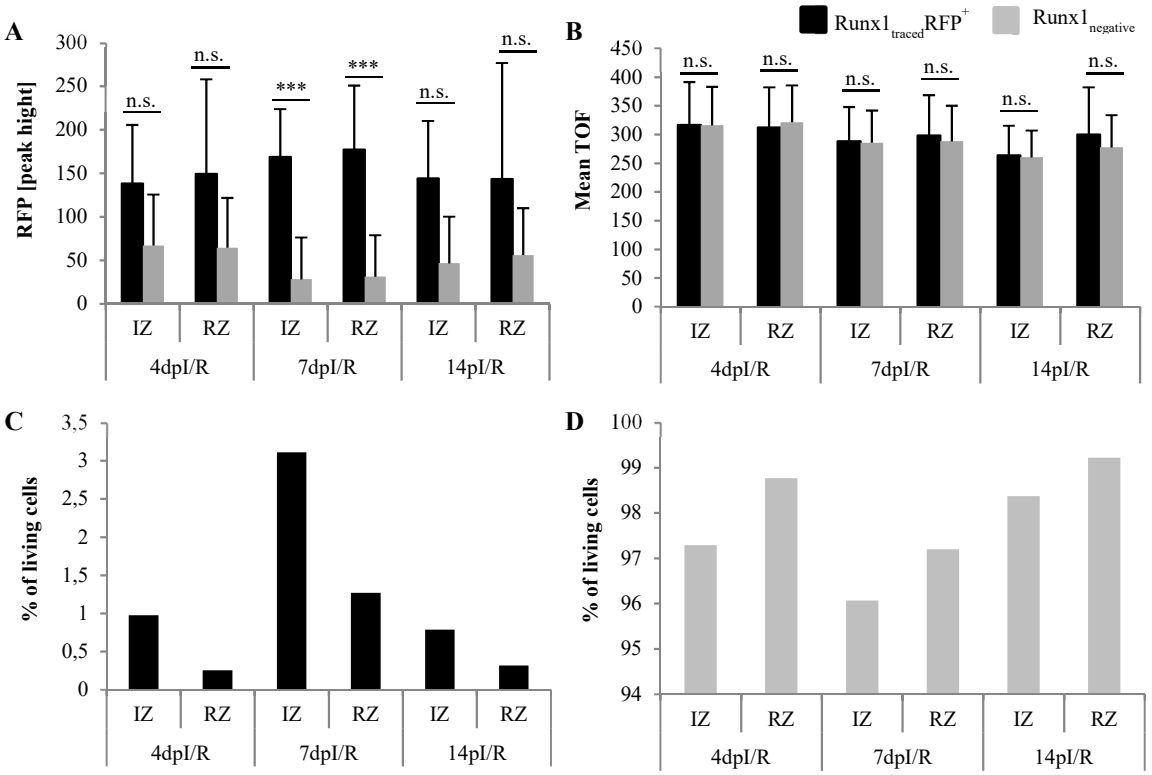

Figure 40: Quantification of biosorting data at different time points post I/R. (A) Intensity of the fluorescent signal was representatively measured by RFP peak height (PkHt). The fluorescent intensity itself of $Runx1_{traced}RFP^{+}$ CMs did not vary over time, representing a strong and detectable RFP expression, which was triggered by Runx1. **(B)** A significant difference between $Runx1_{traced}RFP^{+}$ and $Runx1_{negative}$ ACMs was observed in the peak height, whereas the CM lengths, represented as time of flight (TOF), did not differ from each other. Surviving mACMs of IZ^{**} and RZ^{*} seemed to have an almost equal size, irrespective of their intracellular Runx1 expression. **(C+D)** The majority of $Runx1_{traced}RFP^{+}$ ACMs was measured at 7dpI/R, in line with previous results of this thesis. Nevertheless, $Runx1_{traced}RFP^{+}$ ACMs were already detectable at 4dpI/R and almost 1% seemed to survive within the ischemic region at 14dpI/R. The percentage of $Runx1_{negative}$ ACMs appeared relatively stable in different heart regions at 4dpI/R (n=2) and at 14dpI/R (n=2) but dropped slightly at 7dpI/R (n=5). Mean TOF = average TOF of acquired cells; % of living cells = amount of DAPI negative cells within the subpopulation of $Runx1_{traced}RFP^{+}$ and $Runx1_{negative}$ ACMs. Statistical significances were obtained by a 2-tailed unpaired t-test. ***P<0.001, n.s. P>0.05.

4.13. NGS analysis revealed 2081 differentially expressed genes and clusters of 2 subpopulations with a distinct genetic profile of $Runx1_{traced}$ mACMs post I/R

A cumulative data set for NGS was acquired from 4 biological replicates (n=4), but which were sequenced individually. The associated sorting data set is displayed in Figure 39 and Figure 40. Correlative RNA analyses of significant differentially expressed genes (DEG) identified a strong clustering of each subgroup of IZ^{**} and RZ^{*} populations with spearman coefficients > 0.90 (Figure 41A). Furthermore, a principle component analysis (PCA) identified 2 groups of genes as $Runx1_{negative}$ and $Runx1_{traced}RFP^{+}$, with the largest amount of divergence for both mACM subpopulations (Figure 41B). A high distribution within

the subpopulations suggested differential expression patterns of Runx1$_{traced}$RFP^{+} and Runx1$_{negative}$ ACMs, respectively.

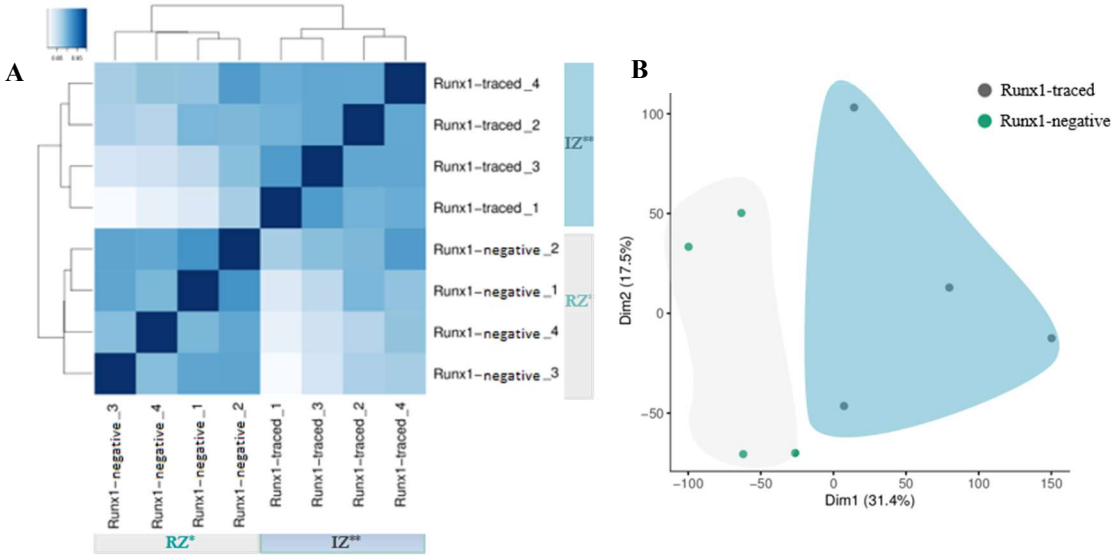

Figure 41: Correlative NGS analysis of isolated and sorted mACMs at 7 days post ischemic heart injury. (A) Spearman correlation of 4 biological replicates (n=4) indicated strong clustering of different subpopulations in IZ** or RZ* (coefficients >0.90), respectively. **(B)** Principal component analysis (PCA) identified 2 gene clusters with the largest amount of divergence, Runx1$_{negative}$ (displayed as Runx1 negative) and Runx1$_{traced}$RFP^{+} (displayed as Runx1-traced) CMs. A clustering was observed in dimension 1 (Dim1), pointing to a strong biological effect within different subpopulations, but revealed a high distribution in dimension 2 (Dim2).

Moreover, 2-dimensional (2D) scatter plots were used to visualize gene expression data sets. This allowed the identification of injury-induced transcriptional responses in Runx1^{+} and Runx1^{-} ACMs within the infarcted heart. Here, genes with similar expression values but without significant differences were marked in grey, whereas upregulated genes could be identified in green for the Runx1$_{traced}$RFP^{+} mACMs or in red for the Runx1$_{negative}$ subpopulation (Figure 42). Overall, NGS analysis identified 2081 significant differentially expressed genes, whereas the majority of those genes could be identified in CMs, which had once expressed Runx1 (Figure 42-43C). Ischemia-triggered transcriptional responses were also detectable in Runx1$_{negative}$ mACMs of the remote region within the infarcted heart.

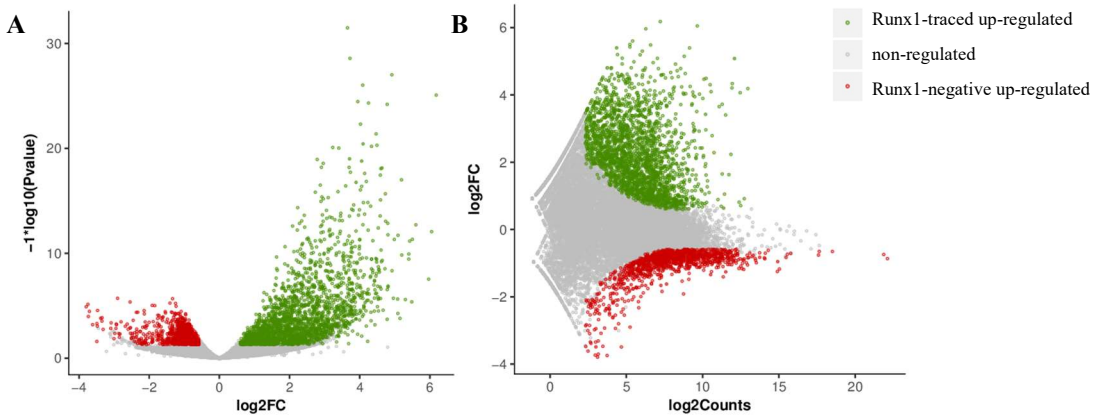

Figure 42: Visualization of gene expression data sets in Runx1$_{traced}$RFP^{+} or Runx1$_{negative}$ mACMs post ischemia via 2D scatter plots. (A) Volcano plot portrayed differentially expressed genes, which displayed both a large-magnitude fold change (log2FC, x-axis) as well as high statistical significance (-log10 p-value, y-axis) in mACMs after the onset of myocardial injury. Especially in the Runx1$_{traced}$RFP^{+} subpopulation (highlighted in green), genes were significantly upregulated to a high content. Differentially expressed genes could also be identified in Runx1$_{negative}$ mACMs from the RZ (highlighted in red). **(B)** MA plot indicated a high density of genes with similar expression levels and no significant differences in both subpopulations. Furthermore, a high intensity-pattern within Runx1$_{traced}$RFP^{+} mACMs is highlighted, indicating an increased amount of transcriptional changes in those cells.

Hierarchical clustering of the TOP50, most significantly regulated and normalized genes are combined and shown in heat maps in Figure 43, whereas genes below the detection level (counts<5) were removed. Acting as quality control, the heat map, displaying the gene candidates with maximal abundance, showed 22 genes, which were mainly or absolutely restricted to the expression in adult heart tissue (Figure 43A). This indicated a high purity of my mACM sorting prior sequencing. However, genes restricted to cardiac muscle were relatively higher expressed in RZ* compared to IZ**, indicating a slight down regulation of structural markers. Furthermore, 14 highly expressed genes could be related to mitochondrial proteins (e.g. mt-Co1) or RNAs (e.g. mt-Tm), which indicated a large number of mitochondria within ACMs. Moreover, 5 identified genes within the TOP50 hits were barely characterized. As an example, Gm26917, a long non-coding RNA, has been only shown to promote proliferation and survival of muscle stem cells (Chen 2018). Another, Malat1, the currently best characterized lncRNA, appeared within the list of highly expressed genes. Malat1 was supposed to be upregulated in tumors and as well correlated with regulatory gene expression and proliferation (Zuo 2017, Amodio 2018). Moreover, Tnf (tumor necrosis factor) was also identified in the data set of the most differentially expressed genes. Tnf was 4.31 fold upregulated in Runx1$_{traced}$RFP^{+} ACMs (Figure 43B-C). Furthermore, all significant differentially expressed genes were sorted by the smallest adjusted p-value (padj) and visualized with their deviation from the mean,

resulting in the Z-score heat map to acknowledge opposing trends (Figure 43C). Hence, strongly upregulated genes were identified within the Runx1$_{traced}$RFP^{+} subpopulation, which belonged to cardiac-related genes. Interestingly, 24 highly and differentially expressed genes (e.g. Adamts2, Emilin1, Mrc2, Piezo2, Serpinb1a, Srpx2) had very low basal expression levels in the healthy adult heart, but have been identified to be strongly upregulated upon myocardial damage (Li 2019).

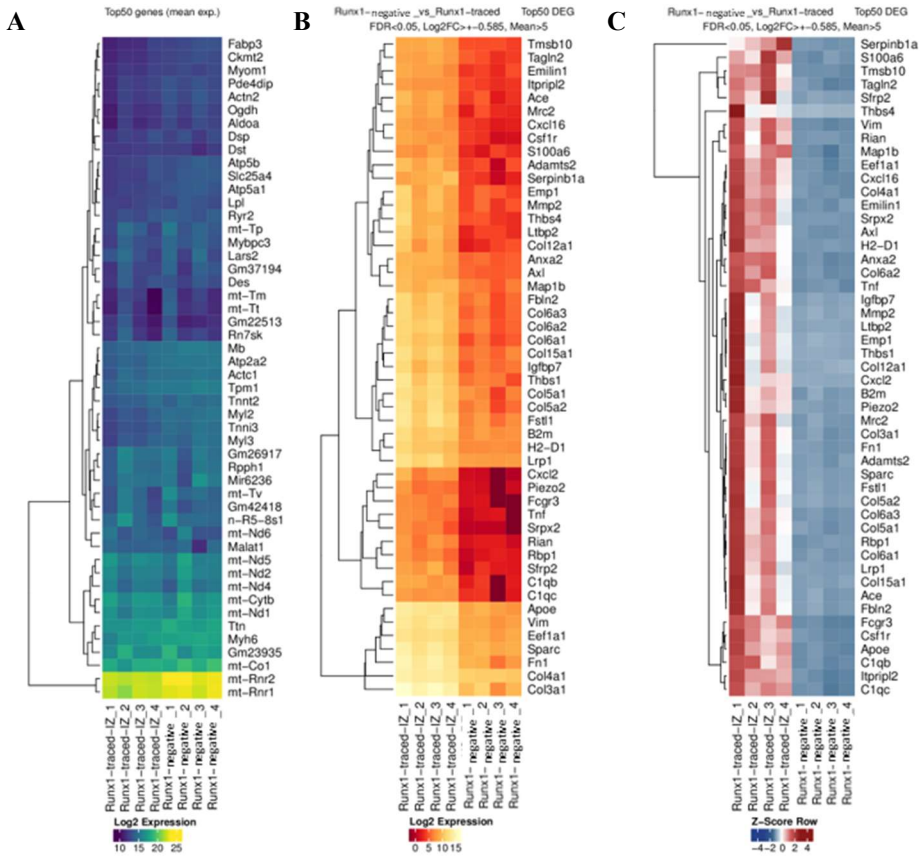

Figure 43: RNA-sequencing analysis of TOP50 differentially expressed genes revealed injury-induced transcriptional responses in Runx1$_{traced}$RFP^{+} ACMs within the ischemic heart. (A) Heat mapping was used to display the maximal, normalized expression of gene candidates over all samples (mean differentially expressed sequences). **(B)** Clustering could be observed between biological replicates of RZ* and the repetitive samples of IZ** subgroups. **(C)** Significantly deregulated genes were sorted by the smallest adjusted p-value (padj), shown with their deviation from the mean to visualize opposing trends between IZ** and RZ*.

Additionally, I used different gene set enrichment analyses, which allowed a more comprehensive and unbiased view of the transcriptional landscape (Young 2010, Krupp 2012). First, gene ontology analysis allowed the identification of distinct regulatory processes in dedifferentiated Runx1^{+} ACMs. Here, cellular and developmental processes appeared as highly gene-enriched with at least 500 genes, whereas processes related to

mitochondria, i.e. oxidation-reduction-processes, were shown to be downregulated (Figure 44A). In addition, the PANTHER analysis revealed a high amount of significantly enriched genes related to Integrin and TGFβ signaling and to angiogenic processes (Figure 44B). Furthermore, KEGG (Kyoto Encyclopedia of Genes and Genomes) ontology groups were calculated to discriminate molecular networks in Runx1$_{traced}$RFP^{+} mACMs. By this means, 10 pathways were identified, which contained significantly downregulated gene groups such as fatty acid degradation, cardiac muscle contraction and oxidative phosphorylation (Figure 44C). Furthermore, the most downregulated genes coherently appeared in metabolic pathways. Moreover, KEGG analysis revealed 10 pathways linked to significantly upregulated genes like PI3K/AKT signaling, focal adhesion signaling, ECM-receptor interactions and pathways involved in cancer disease, pointing again to genes like Tnf and Piezo2.

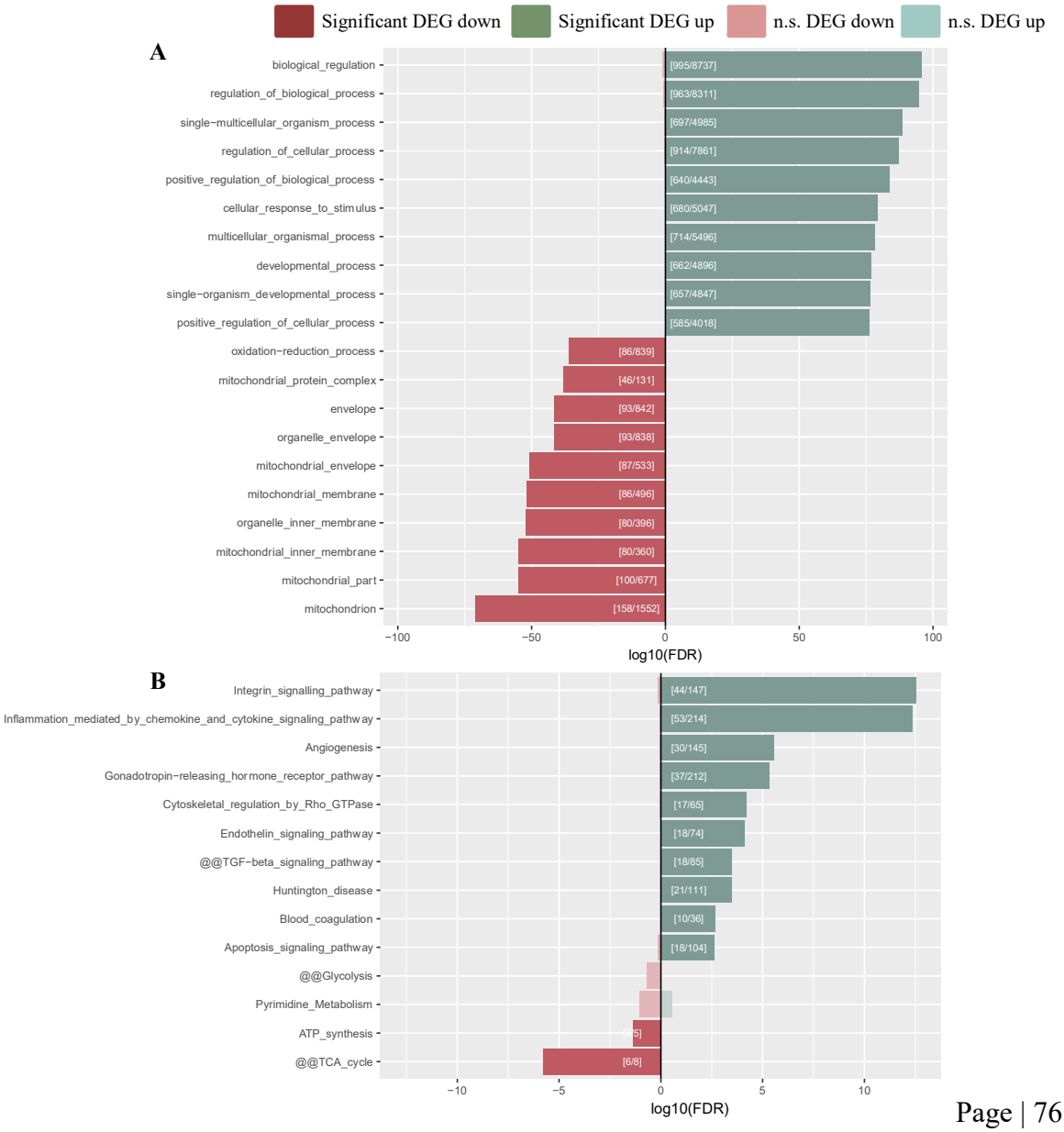

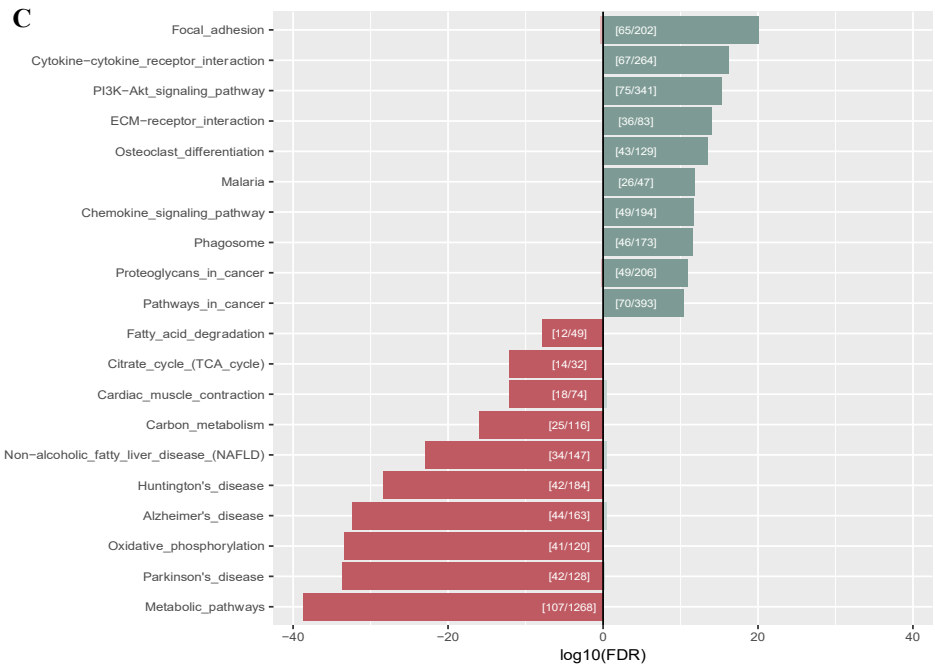

Figure 44: Gene set enrichment analysis related to NGS data of isolated and sorted ischemic mACMs. **(A)** Gene ontology analysis pointed to upregulated cellular and developmental processes, while processes related to mitochondria were downregulated. **(B)** PANTHER analysis revealed a high amount of significantly upregulated genes connected to Integrin and TGFβ signaling as well as 30 genes correlated with angiogenesis. **(C)** KEGG analysis identified fatty acid degradation, cardiac muscle contraction and oxidative phosphorylation as significantly downregulated in $Runx1_{traced}RFP^{+}$ mACMs, whereas PI3K/AKT signaling, focal adhesion, ECM receptor interactions and pathways in cancer appeared as significantly upregulated in ischemic mACMs.

Further extraction hits of the acquired NGS data set are documented in Table 1. Here, differentially expressed and interesting genes with normalized counts are presented as means of different subpopulations each with their calculated SEM, p-value and fold change (FC). For instance, the "cardiokine" Fstl1 as well as genes correlated with angiogenesis (Sfrp2, Piezo2, Srpx2) were identified as significantly upregulated in $Runx1_{traced}RFP^{+}$ mACMs of the ischemic myocardium.

Table 1: Differentially expressed genes connected to significantly enriched pathways in ischemic mACMs (n=4 for each condition). Statistical significances were obtained by a 2-tailed unpaired t-test. Data are presented as mean ± SEM. ***P<0.001; **P<0.01; *P<0.05; n.s. = P>0.05.

Gene	$Runx1_{traced}RFP^{+}$		$Runx1_{negative}$		p-value	FC IZ^{**}/RZ^{*}
Pcm1	733.25	±89.83	607.5	±120.15	n.s.	1.21
Vimentin	4026	±567.61	319.25	±47.63	***	12.61
Fstl1	2837.75	±860.28	165	±43.14	*	17.20
Fibronectin1	7496.25	±1890.97	370.5	±120.20	**	20.23
Tnf	128.25	±23.62	5.5	±2.22	**	23.32

Sfrp2	298.75	±95.91	11.5	±3.93	**	25.98
Piezo2	129.25	±38.96	4.5	±1.55	**	28.72
Srpx2	117.75	±29.65	2.25	±0.75	***	52.33

Furthermore, I was able to point out additional specific genes, which were associated with structural remodeling post ischemia, and thus provided a comprehensive characterization of dedifferentiated $Runx1_{traced}RFP^{+}$ mACMs (Figure 45). Here, differentially expressed genes are shown in relation to PCM1 (cardiac nuclei marker) levels, which did not significantly alter. Established genes involved in processes of cardiomyocyte dedifferentiation (ACTN1, αSMA, Moesin) were upregulated in $Runx1_{traced}RFP^{+}$ mACMs. Thereby, Runx1 itself appeared more than 7.2 fold upregulated, but did not reach a significant level due to the high variances between samples (Figure 41B&45B). Furthermore, the transcriptional profile of ischemic and dedifferentiated CMs was additionally validated by the high abundance of hypoxia-induced genes like ANP (6.2 fold up) or Hif1a (1.35 fold up). Myoglobin transcripts appeared significantly downregulated (Figure 45A), which have been demonstrated to play a beneficial role for re-vascularization of the injured heart (Hazarika 2008). Besides that, structural marker genes characteristically expressed in the myocardial cytoskeleton such as Myosin-Heavy-Chain6 (Myh6), sarcomeric α-actinin (ACTN2, Actn2) and myomesin-2 (Myom2) were significantly downregulated in ischemic $Runx1_{traced}RFP^{+}$ mACMs (Figure 45C). Furthermore, dedifferentiation in $Runx1_{traced}RFP^{+}$ mACMs came along with a significant gene enrichment of proliferation markers like Pcna (2.35 fold), Ki67 (5.7 fold), Dab2 (7.1 fold) and Cyclin D1 (2.1 fold) (Figure 45D). This was accompanied by the increased expression of cardiokines and gene transcripts involved in angiogenesis (Piezo2, Sfrp2, Srpx2) as well as vimentin, fibronectin1, Fstl1 and PDGFRalpha/beta (PDGFRα/β, *9.2 fold/*3.5 fold up). Even more, $Runx1_{traced}RFP^{+}$ ACMs revealed a high expression of chemokines like CCl4 (**112.6 fold up), Cxcl2 (*91.2 fold up), Cxcl16 (**13.5 fold up) and OSM, which were only detectable in ischemic CMs.

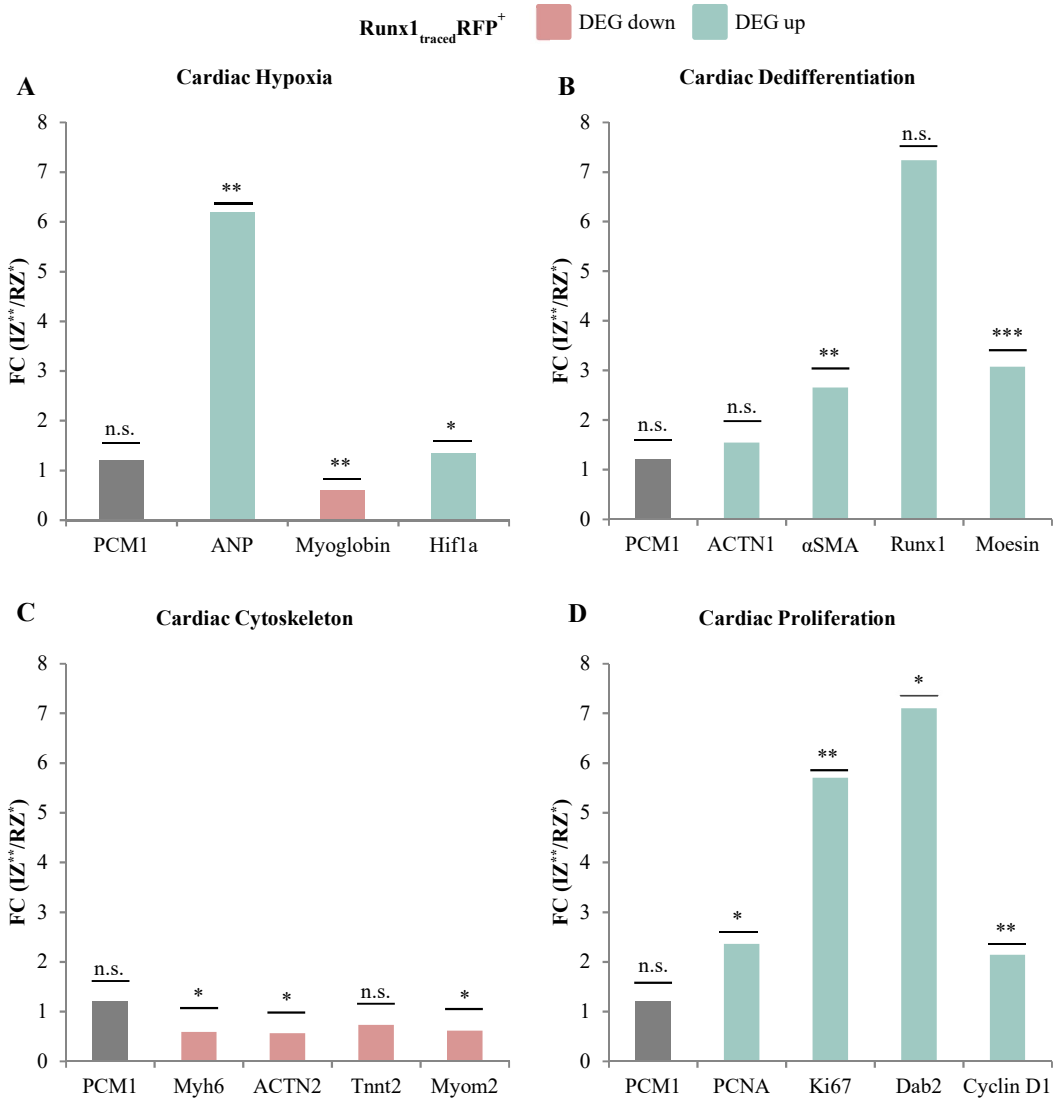

Figure 45: Structural remodeling processes were highly evident in Runx1$_{traced}$RFP^{+} mACMs undergoing dedifferentiation after the onset of MI. Differentially expressed genes involved in structural remodeling processes were displayed in relation to PCM1 (cardiac nuclei marker) levels, which did not alter. **(A)** Genes related to cardiac hypoxia like ANP (6.2 fold) and Hif1a (1.35 fold) were found to be upregulated, whereas myoglobin was significantly downregulated. **(B)** Prominent genes expressed during cardiomyocyte dedifferentiation such as αSMA (2.65 fold), Moesin (3.07 fold), ACTN1 (1.54 fold) and Runx1 (7.23 fold) were highly abundant in Runx1$_{traced}$RFP^{+} mACMs. **(C)** Most genes related to the cardiac cytoskeleton like Myh6, ACTN2, Tnnt2, Myom2 turned up to be downregulated. **(D)** Genes related to cardiac proliferation such as Pcna (2.36 fold), Ki67 (5.7 fold), Dab2 (7.1 fold) and Cyclin D1 (2.14 fold) were highly and significantly upregulated in Runx1$_{traced}$RFP^{+} mACMs post ischemia. Data are presented as fold change and related to expression levels of IZ/RZ (n=4). Statistical significance was determined by a 2-tailed unpaired t-test. ***P<0.001; **P<0.01; *P<0.05; n.s. = P>0.05.

5. Discussion

5.1. Serum conditions effected the OSM-induced Runx1 expression, which triggered signs of dedifferentiation in adult mouse cardiomyocytes in vitro

In the first part of my doctoral studies, I assessed, if the expression of Runx1 was related to the initiation of adult mouse cardiomyocyte (mACMs) dedifferentiation. Here, I was able to show that the mouse OSM-induced Runx1 expression in cultured mACMs clearly correlated with typical morphological signs of dedifferentiation paralleled with the repression/degradation of sarcomeric structures. Surprisingly, a deferred Runx1 expression could also be identified in BSA/CON-stimulated cell cultures, which served as negative controls, in association with phenotypical adaptions intrinsically restricted to dedifferentiation. Several studies demonstrated that serum factors influence cellular growth besides differentiation at different magnitudes and are able to induce dedifferentiation processes (Pivarcsi 2001, Gissel 2006, Zhang 2010). A successful isolation and culturing of cardiac stem cells and progenitor cells as well as the maintenance during long-term cell cultures of primary embryonic rat CMs during long-term cell cultures have been possible under serum-free conditions (Das 2004, Gissel 2006). Moreover, Kessler-Icekson et al. and others demonstrated that a serum-free medium is required to study proliferation activity and cell integrity of neonatal rat CMs (Claycomb 1981, Mohamed 1983, Kessler-Icekson 1984). To evaluate the regenerative behavior of this cell type, the intracellular signaling pathways have been elucidated, although serum was included for an initial period of time (Kessler-Icekson 1984, Louch 2011, Vidyasekar 2015). However, it has been demonstrated that the cultivating of adult CMs in a serum-supplemented medium induces spreading and changes in the ultrastructure (Mitcheson 1998). Therefore, I tried to minimize serum-effects by reducing serum conditions during culturing. Even though delayed in time, BSA/CON-stimulated mACMs displayed spreading and elongation**,** indicating serum-effects on adult CMs in my studies. But studying differentiated and contracting adult mouse CMs, especially mimicking in vivo conditions over time, requires at least low serum containing medium for maintaining survival and viability of these cells (Mitcheson 1998, Nippert 2017, Golan-Lagziel 2018). Because of this technical limitation, further investigations are necessary to improve a successful serum-unbiased method, which could preserve primary adult CMs in their original texture (Li 2014).

5.2. Runx1 deficient mACMs responded to mOSM-activated signaling in vitro, but were masked by fibroblast contamination-mediated signaling and therefore lacked the re-expression of fetal genes as well as the capability to trigger processes of dedifferentiation

To validate the hypothesis of Runx1-mediated dedifferentiation, I used mACM cultures of heart specific Runx1 knock-out animals ($Runx1^{fl/fl}/\alpha MHC^{Cre}$). In 2018, McCarroll et al. postulated a critical role of Runx1 in CMs after myocardial infarction, in which the CM specific Runx1 deficiency ameliorated cardiac function and contractility post induction of myocardial ischemia (McCarroll). Consistent with their in vivo results, I was able to show in vitro that CMs, lacking the capability to express Runx1, lost their competence to dedifferentiate and their acquirement to re-express fetal genes (ANP, ACTN1), what indicated that Runx1 deficient CMs were no longer able to gain a proliferative, progenitor-like phenotype. On the other side, sustained Runx1 expression was achieved due to prolonged OSM stimulation, but kept CMs in a persistent dedifferentiated state, which were also unable to re-acquire a regenerated, contractile phenotype. These findings led me to the assumption that a spatiotemporal Runx1 expression might be critical in terms of potential redifferentiation to retain a fully functional and contractile ACM profile. To minimize serum-related effects during dedifferentiation, I reduced the serum concentration in the medium of the Runx1 deficient CM cultures. This decrease resulted in a high mACMs drop off and therefore low protein concentrations for downstream analyses, with the consequence of poor statistical values (i.e. high SEM, no statistical significance). Here, I failed to demonstrate on a protein level a significant increase of fetal genes and expected marker genes of dedifferentiation in control samples. My insignificant results might also be explained by contamination of fibroblasts, which masked the differential protein expression in the analyzed total lysate. Moreover, a slightly increased expression level of Runx1 was detectable in CMs of $Runx1^{fl/fl}/\alpha MHC^{Cre}$ animals**,** indicating either a less effective Runx1 deletion by homologue flox/Cre recombination or a less pure CM population**,** resulting in contaminations with Runx1 expressing fibroblasts. Mainly 2 basic methods for culturing adult ventricular myocytes have been defined originally by Jacobson and Piper to gain Ca^{2+}-tolerant CMs: A) the redifferentiated model and B) the rapid attachment model (Jacobson 1986, Mitcheson 1998). Hence, Pontén et al. concluded in their report that none of the current methods enable to yield a pure CM isolation (Ponten 2013). But this

assumption was not in line with the findings of cultured CMs from adult C57Bl6/J mice, in which I could not detect proliferating fibroblasts during my observations. In addition, Pugach et al. were able to show that prolonged Cre expression, driven by the alpha-myosin heavy chain (αMHC) promotor, can be cardiotoxic, resulting in enhanced fibrosis, inflammation and DNA damage (Pugach 2015). Their findings suggested a potential overrepresentation of fibroblasts in the Runx1 knock-out hearts prior isolation, which could have led to a contamination with non-CMs during the performed isolation procedures. Moreover, Golan-Lagziel et al. have recently identified the expression of transcription factors such as Tead, Sox9 and Runx1 in cardiac fibroblasts, which play a key role in both healthy and diseased states due to their control of ECM structures as well as their multiple electrical and paracrine interactions with CMs (Lajiness 2014, Lighthouse 2016, Pinto 2016, Golan-Lagziel 2018). Accordingly, fibroblasts have also been demonstrated to respond to OSM with phenotypic alterations comparable to CMs, which even further allows the presumption of existing transcriptional control of CM plasticity and CM transdifferentiation, since unidirectional reprogramming of fibroblasts into CMs has already been shown (Chen 2013, Lighthouse 2016). In addition, Sohara et al. demonstrated that cultured human myofibroblasts revealed an increased Timp1 level upon OSM stimulation (Sohara 2002). These observations might explain that OSM stimulation triggered the expected OSM-related signaling pathways (JAK/Stat3, $ERK_{1/2}$/MAP Kinase, PI3' Kinase) in my cultures, even in Runx1 deficient mACMs**,** which were masked by responding fibroblasts and which consequently expressed Runx1 as well as Timp1. To avoid such masking effects of contamination, mACMs could be isolated directly from adult mice (7-12 weeks old), which have lost their regenerative potential but do not develop molecular signs of cardiac toxicity, since such effects have only been discovered due to prolonged Cre expression in αMHC^{Cre} mice at 3 months of age or older (Pugach 2015). Irrespective of possible fibroblast contaminations, I was able to show that the transcription factor Runx1 is crucial to initiate morphological processes of dedifferentiation as well as to upregulate fetal genes (SMA, ACTN1)**,** displaying Runx1 as a unique and causative marker of CM dedifferentiation.

5.3. Successful tracing of mACMs confirmed the capability to follow processes of dedifferentiation via Runx1 expression

A targeting of the Rosa26 locus combined with an inducible Cre-recombinase and controlled by the Tet-Off system has been favorably applied**,** if a gene of interest in a single cell needed to be labeled within a whole cell population (Gunschmann 2014). By the means of such an approach, I was able to visualize the Runx1 cell lineages in the ischemic heart and analyzed their characteristics in vitro and in vivo. The 2 most common Cre-induced reporters were β-galactosidase (β-gal) and fluorescent proteins (Vorhagen 2015). In my PhD study, cells expressing β-gal (encoded by the lacZ gene) due to a successful Runx1 tracing were sufficiently visualized via staining of the substrate X-gal. Here, β-gal expressing cells appeared X-gal^{+} represented by a dark blue precipitate, as it has already been shown in former studies (Soriano 1999). As expected, Runx1$_{traced}$lacZ^{+} mACMs obtained phenotypical characteristics of dedifferentiation upon OSM stimulation as well as a significant upregulation of Runx1 and Timp1 on protein levels. These results reflected the capability of CMs from Runx1 transgenic mice to respond with the same emergence upon mOSM treatment as wildtype CMs, which was the basis for further in vivo studies.

5.4. Myocardial ischemia model impacted the amount of Runx1^{+} CMs in vivo

To heightening the knowledge about dedifferentiation and its role during cardiac remodeling, I investigated the expression pattern of Runx1 in the ischemic mouse heart upon I/R in comparison to persistent LAD ligation and validated those observations in correlative studies by assessing characteristics of CM dedifferentiation on a micro- and nanoscopic level. Either a permanent or transient occlusion of the left descending coronary artery has been frequently used to elucidate the pathophysiological and molecular mechanisms of cardiac remodeling (Anversa 1998, Soonpaa 1998, Yang 2002, Takagawa 2007, Wohlschlaeger 2010). In both animal models of experimental myocardial injury, it has been shown that the abrogation of oxygen and nutrients induces complex cellular responses in CMs and other cardiovascular cells, including microvascular endothelial cells as well as the activation of the innate immune system, mediating myocardial injury and healing at the same time (Jordan 1999, Zhang 2018) Accordingly, finding the right model and time point to enlarge the number of

dedifferentiating CMs was an important point in my thesis. Even more, taking the optimal model was necessary to proceed with the lineage tracing studies that made it possible to follow the cell fate of once Runx1 expressing mACMs after the onset of myocardial infarction. In comparison to permanently ligated hearts, I/R injury revealed a 2.5 fold smaller infarct size at day 7 post MI and much more important a 4.5 fold increase of $Runx1^+$ ACMs in the ischemic region (IZ + BZ) of the infarcted tissue. Based on the available results, which suggested a higher yield of isolated $Runx1^+$ ACMs and therefore promised a higher success rate for the project, I decided to continue the following studies with the I/R model. Usually absent in adult CMs, recent studies revealed an activated Runx1 expression in the border zone adjacent to the infarct region in both patients and experimental MI animal models (Wang 2012, McCarroll 2018). In my studies, I identified a clear peak of the dedifferentiation marker Runx1 in the ischemic region including the border zone (BZ) at day 7 post myocardial injury, a finding, which was in line with those of McCarrol et al. (McCarroll 2018). Surprisingly, the verification of Runx1 in CMs was masked by the overall Runx1 expression within the ischemic heart, since the Runx1 expression peaked at day 4 post injury and correlated with the high amount of infiltrating immune cells, which have been shown to constitutively express Runx1 (Luo 2016). In addition, maturation of a granulation tissue in both models of experimental MI hindered a valid quantification of $Runx1^+$ CMs, because Runx1 appeared abundant in almost all cells contributing to cardiac repair, including non-CMs such as immune cells and (myo-) fibroblasts, as demonstrated in previous studies (Leri 2015). Even a combination of immunohistochemical and conventional staining (data not shown) did not deliver more insights into the fate of dedifferentiating mACMs. Overall, it was barely possible to distinguish between different cell types, what was a drawback of my tracing approach.

5.5. Loss of sarcomeres and other signs of dedifferentiation were detectable in Runx1 transgenic animals on a microscopic and nanoscopic scale post I/R

To finally validate and visualize signs of dedifferentiation post I/R, I used a conclusive nanoscopic and microscopic histological approach. Here, I explicitly used Runx1 Tracer mice, since this line was also utilized for subsequent downstream analyses. By this means, I found typical morphological changes of reperfusion injury in infarcted Runx1 Tracer mice such as increased sarcolemma fragility, degradation of myofibrillar proteins and loss/disorganization of T-tubules as well as mitochondrial damage, in line with previous

results (Solomon 1996, Portbury 2011, Neri). Apart from these clear degenerative changes, I also detected several well-known structural hallmarks of dedifferentiation like myolysis, glycogen accumulation, dispersion of nuclear chromatin and changes in mitochondrial shape and size (Ausma 1997, Ausma 2002). On a microscopic level, I identified signs of dedifferentiation in the Runx1 transgenic animals post I/R inter alia via immunohistochemical stainings of Moesin, a member of the Ezrin/Radixin/Moesin (ERM) family, as described by Miyawaki et al.(Miyawaki 2016). This cytoskeletal linker protein has been shown to be re-expressed in CMs of patients suffering from dilative cardiomyopathy in order to stabilize the actin membrane barrier in the failing heart by a coordinative recruitment of F-actin and Myosin (McClatchey 2014, Miyawaki 2016). Furthermore, I was able to correlate a decline of sarcomeric α-actinin (ACTN2) with a positive Moesin expression, which was mainly detectable in patches of surviving CMs or in the border zone of the ischemic myocardium**,** accompanied by extraordinary protrusions as visualized via Lectin staining, similar to the findings of Miyawaki et al. (Miyawaki 2016). Interestingly, isolated CMs co-cultured with fibroblasts reflected the same observations compared to I/R-treated animals at the ultrastructural level: (A) cell spreading, (B) Z-line disruption, (C) loss of sarcomeres and mitochondria alignment, but lacked obvious degenerative signs such as mitochondrial swelling, extensive formation of lysosomes and loss of sarcolemma integrity (Dispersyn 2001). Hence, the intercellular connectivity and extracellular communication between CMs and fibroblasts might have a high impact on cardiac remodeling, potentially maintaining dedifferentiation and inhibiting redifferentiation processes in the ischemic heart (Rücker-Martin 2002).

5.6. Isolation and a successful live-cell sorting for downstream analysis was possible due to a stable endogenous tracing of RFP in Runx1$_{traced}$ mACMs

The complex histomorphological findings of I/R injury consequently necessitated the isolation of Runx1$_{traced}$RFP^{+} mACMs from the agglomerated infarct tissue to further characterize dedifferentiated CMs via live-cell sorting followed by a deep sequencing analysis. But profiling a subpopulation of the infarcted adult mouse heart required at first a successful isolation of intact rod-shaped CMs, which was simply a delicate and tedious process. I focused on mouse rod-shaped CMs, which were considerably more fragile than rat ACMs, because it has been shown in other studies that mACMs are more likely to be disrupted during the initial isolation procedure, when compared to rat ACMs due to an

influx of extracellular Ca^{2+} caused by a leaky cell membrane (Smith 2014). Furthermore, the cell sorting of adult ventricular CMs, which have been demonstrated to be highly variable in cell sizes and shapes, is limited by the nozzle size of the cytometer and therefore negatively affected the flow cytometry performance (Larcher 2018). In addition, the scarcity of murine CM material (i.e. low protein, RNA content) further restricted the possibility of subsequent analyzes. Most studies circumvented these technical problems by switching to rat adult, embryonic or neonatal mouse CMs as well as by using (induced) pluripotent stem cells (Ponten 2013, Ban 2017). However, to study the cell fate of adult CMs upon myocardial infarction by an endogenous tracing approach, it was inevitable to use adult mice with all its advantages and disadvantages. For this concept, a separation of the left and right ventricle was a critical issue to increase the amount of $Runx1_{traced}RFP^{+}$ mACMs in order to guarantee a successful sorting procedure. For focusing on lineage-traced cells via tracking an intrinsic fluorescent protein, it was essential to rely on a live-cell sorting method. This enabled me to detect and follow $Runx1_{traced}RFP^{+}$ expressing mACMs during sorting without any need of additional fixation or antibody staining steps, because especially fixation is known to come along with major impairments: (1) fixative-induced autofluorescence and (2) quenched endogenous protein fluorescence, which disturbs the separation and the identification of different emission spectra (Kiernan 2014). Nevertheless, addressing biological investigations directly in living cells and tissues entailed the problem of naturally occurring endogenous fluorescence or autofluorescence, which often compromises an effective discrimination of fluorescent proteins from autofluorescence (Knight 2001, Marcek Chorvatova 2019). In particular, autofluorescent cells were successfully detected in my studies after excitation with visible blue/green light in the GFP channel during acquisition and used to define morphologically intact Runx1 negative subpopulations for sorting, similar to the findings of Larcher et al. and Billinton et al. (Knight 2001, Larcher 2018). Furthermore, it has been shown that CMs contain endogenous fluorophores such as sarcomeric proteins, aromatic amino acids and flavin coenzymes, what permitted their discrimination from non-CMs (Knight 2001, Garcia 2007, Larcher 2018). According to their cellular autofluorescence, detectable in the GFP channel, I was able to confirm the characteristic identity of CMs and moreover to proof the purity of my sorting procedure. In addition, $Runx1_{traced}$ ACMs were unequivocally identified by their endogenous fluorescence of intrinsic RFP expression and utilized for subsequent subpopulation sorting. In conclusion, this method with its uniquely

established workflow enabled the highest possible yield of $Runx1_{traced}RFP^{+}$ mACMs for further downstream analyses via next-generation sequencing.

5.7. Dedifferentiated CMs might act as active modulators of the innate immune response after myocardial injury

I aimed to identify differentially expressed genes in isolated, ischemic mouse CMs undergoing dedifferentiation by using next-generation sequencing (NGS) and bioinformatic approaches. First, a process called unsupervised hierarchical clustering was used, which grouped similar entities together to find coincidences in the data points. Surprisingly, gene ontology analyses of the unsupervised hierarchical clustered RNA-seq samples identified miscellaneous and partial contrary upregulated pathways. Besides the expected and validated CM markers (ACTN2, Mhy6, Myl2), RNA-seq analyses revealed the expression pattern of genes related to macrophages (Ptprc, Mertk) and fibroblasts (Pdgfra, Thy1) as reported before by Quaife-Ryan et al. (Quaife-Ryan 2017). Even more, the identification of chemokinetic genes (CCl4, Cxcl2, Cxcl16) in ischemic CMs from the infarcted myocardium pointed either to partial contamination during the sorting procedure or to interactive modulators of the immune response post MI. In line with Yoshimura et al. and others, several cell types such as fibroblasts, keratinocytes, osteoblasts and epithelial cells have been shown to produce chemoattractant proteins and consequently to play a pivotal role in guiding leukocyte trafficking during inflammatory responses (Marriott 2005, Lai 2012, Yoshimura 2014). In this context, Mylonas et al. increased the expression of Cxcl2 and Cxcl5 in fibroblasts to highlight their impact on neutrophil recruitment to injured hearts post MI (Mylonas 2017). Ferreira et al. demonstrated in cardiomyopathy hearts of Chargas disease a cytokine-related gene expression pattern**,** which is not ordinarily expressed by inflammatory cells (Cunha-Neto 2005, Ferreira 2014). Additionally, it has been shown that *T. cruzi*-infected CMs behaved similarly to dedifferentiated mACMs by reactivating an embryonic gene expression pattern (Cunha-Neto 2009, Pöling 2012, Ferreira 2014). To validate the assumption of ischemic CMs as active modulators of the immune response, additional sorting and sequencing cycles must be performed in future studies. An outline of such an experimental procedure would need to include a non-CM depleting cardiac cell preparation, which might lead to a high loss of mACMs withdrawn from an infarcted heart, as mentioned in former studies (Skelly 2018). To increase the ACM population for

sequencing, cell pooling of different animals could be an alternative option. This would allow the combination of further purification methods to reliably overcome a potential leukocyte contamination, which was not possible in my studies since the amount of dedifferentiated CMs per animal was already below the 2% range. Furthermore, I wanted to stick to non-pooled sample sequencing**,** because pool-sequencing has been demonstrated to create new problems: A) loosing biological individuality of replicates, B) a biased significance of RNA-seq sample clustering and C) the most challenging problem, correctly identifying rare variants with a potential functional role (Nelson 2012, Tennessen 2012, Anand 2016). Another approach could be a specific leukocyte (e.g. F4/80-Cre) tracing combined with inducible fibroblast (e.g. Postn-Cre) tracing mouse lines in association with the established Runx1 tracing strategy, which might enable a contamination-free sorting via double or triple fluorescent labeling (Abram 2014, Kaur 2016). But generating those lines via pronuclear DNA-microinjection is a time consuming, tedious and expensive process and would potentially even generate a spectral overlap of endogenously expressed fluorophores during the sorting procedure (Progatzky 2013, Usmani 2016). Finally, I decided to focus on dedifferentiated CMs by sorting $Runx1_{traced}RFP^{+}$ ACMs in a first step. This has already enabled me to characterize a particular cell type, but raised new questions that need to be answered in the future.

5.8. Highly upregulated genes indicate cell transformation processes and might implicate a regeneration potential of $Runx1_{traced}$ ACMs

According to the results of my deep sequencing analysis, Runx1-traced mACMs showed an upregulation of proliferation and cell cycle markers like Cyclin D1 and of such pathways (e.g. PI3K/Akt), which have been reported to be upregulated in processes of stem cell-derived CM regeneration, predominantly mediated by leukemia inhibitory factor (LIF) (Kanda 2016). LIF has been reported in the self-renewal of neural stem cells, re-myelination and axonal regeneration (Deverman 2012). Interestingly, Qadi et al. demonstrated an association between LIF and Runx1 via its regulatory role of both, the general and the placental LIFR promotors by Runx1 (Qadi 2016). I identified an increased LIF/LIFR expression in isolated CMs from MI hearts, but gene expression levels were slightly and therefore not significantly downregulated in Runx1-traced mACMs. This could be explained by predominantly ischemic conditions in the myocardium, since Johnson et al. have shown that hypoxia reduces LIFR/STAT3 signaling in breast cancer

cells (Johnson 2016). Beyond the potential of well-established stem cell markers to induce proliferation and regeneration, I was able to identify a significant upregulation of the angiogenic factor follistatin-like protein 1 (Fstl1), which has been expressed in proliferative fibroblasts after skeletal muscle injury and has been demonstrated to exert cardioprotective action by mitigating post MI-related cardiac dysfunction (Gorgens 2013, Wei 2015, Maruyama 2016, Xi 2016, Kretzschmar 2018). In addition, Oshima et al. demonstrated that Fstl1 is an Akt-regulated cardioprotective factor, which protected cultured neonatal rat ventricular myocytes from hypoxia/re-oxygenation-induced apoptosis (Oshima 2008). FSLT1-responsive CMs in the experiments of Wei et al. had even less mature sarcomeric and limited electrophysiological properties, which indicated a dedifferentiated state of those cells (Wei 2015). In addition, Wei et al. were able to demonstrate that epicardial delivery of Fstl1 in a preclinical swine model of I/R stimulated a stable recovery of contractile function and limited fibrosis as well as scar size (Wei 2015). Besides its description as a cardiomyogenic factor of epicardial origin, fibroblasts of neonatal and adult hearts robustly express Fstl1 under physiological and pathophysiological conditions (Kretzschmar 2018). I was able to identify a significant**,** 17 fold upregulation of Fstl1 in Runx1-traced ischemic mACMs. In line with the studies of Wei et al., my findings indicate a positive correlation of Fstl1and Runx1, which might even further support the Fstl1-mediated possibility of dedifferentiated CMs to regenerate by regaining the ability to re-enter the cell cycle (Wei 2015). Furthermore, the increased Fstl1 expression in ischemic Runx1-traced CMs post MI could also be related to an endogenous capacity for the secretion of CM-derived peptides in order to regulate cardiovascular homeostasis, systemic metabolism and even inflammation (Oshima 2008, Chiba 2018). Conclusively, these findings suggested an active participation of dedifferentiated CMs in the remodeling process of the heart upon myocardial injury. Interestingly, my deep sequencing profiling of ischemic Runx1-traced mACMs revealed a dramatic upregulation (52 fold) of the Sushi repeat-containing protein X-linked 2 (Srpx2), which has been recently described as a novel mediator of angiogenesis (Miljkovic-Licina 2009, Gao 2015). Miljkovic-Licina et al. identified Srpx2 to regulate endothelial cell migration and tube formation for modulating angiogenesis (Miljkovic-Licina 2009). They concluded that upon appropriate stimuli, such as angiogenic and proteolytic enzymes, vascular-specific cell adhesion molecules, secreted growth factors and their signaling receptors, quiescent endothelial cells started to proliferate and generated blood vessels from de novo through angiogenesis (Goh 2007, Miljkovic-Licina

2009). Besides that, Srpx2 has been demonstrated by Gäbel et al. to be part of a molecular fingerprint for terminal abdominal aortic aneurysm disease (Gäbel 2017). Here, Srpx2 was localized in pericytes and adipocytes of microvessels in the medial-adventitial border zone and Srpx2 expression was positively associated with ruptured AAA (abdominal aortic aneurysm) (Gäbel 2017). Other groups illustrated Srpx2/uPAR ligand/receptor interaction, whereas uPAR signaling was also associated with patho-/physiological processes such as fibrinolysis, enhanced immune response, inflammation, angiogenesis, cell growth and cancer metastasis (Royer-Zemmour 2008). But the role of the Srpx2/uPAR ligand/receptor system in the heart remains unknown to date and therefore Srpx2 might be an interesting candidate for further cardiovascular research.

5.9. A temporally and spatially limited expression of Runx1 ensures the survival of adult cardiomyocytes post MI

The Runx1-mediated dedifferentiation of cardiomyocytes appears to have various implications, depending on the pathophysiological context. McCarrol et al. demonstated that a partial inactivation of the Runx1 gene and thus a reduction of Runx1 levels in CMs preserves cardiac contractility after MI (McCarroll 2018). This result was indirectly supported by my in vitro experiments, since the Runx1^{+} CMs, which continued to dedifferentiate over time, no longer exhibited any contractile, sarcomeric structures. Otherwise, my cell tracing and live-cell sorting analyses also indicated that a temporary Runx1 expression ensured the survival of at least some ischemic CMs, although I have not provided any direct evidence by the means functional in vitro studies. Furthermore, Koth et al. showed in their recently published study that the ablation of Runx1 in a subpopulation of hematopoietic stem cells led to an increase of CM proliferation within cryo-damaged myocardium and thus to an improved regeneration of the zebrafish heart (Koth and Bonkhofer 2019). The authors´ findings supported my NGS data, from which an immunomodulatory effect of Runx1 could be deduced. Thus, the question of the role of Runx1^{+} immune cells for ischemia-induced cardiac remodeling arises, but which can only be answered in a separate study. In addition, the importance of Runx1-mediated dedifferentiation as a possibility for increased cardiomyocyte proliferation has already been discussed by Wang et al. (Wang 2017). The researchers were able to demonstrate that the path to renewed proliferation of CMs is only possible via the step of dedifferentiation and that dedifferentiated CMs with the potential for proliferation, shown

via the expression of various proliferation markers, are Runx1 positive (Wang 2017). From all these findings can be concluded that a temporarily and regionally limited as well as restricted Runx1 expression ensures the survival and proliferation of ischemic CMs and thereby reduces cardiac damage post myocardial infarction.

5.10. Conclusions and outlook

My unique combinatory analysis**,** starting with experimental myocardial infarction of transgenic animals followed by a live-cell-sorting approach and finally analyzed via NGS**,** enabled me to elucidate the cell fate of dedifferentiated CMs in the ischemic myocardium. Here, the transcriptional landscape delivered a strong downregulation of typically metabolic pathways (e.g. oxidative phosphorylation) in healthy CMs**,** indicating reduced energy levels**,** but exhibited the induction of survival mechanisms as pointed out by a strong upregulation of proliferative genes like PCNA, Ki67, Dab2 and Cyclin D1 in $Runx_{traced}RFP^{+}$ mACMs. Furthermore, my results implied a decisive role of Runx1 expressing CMs undergoing dedifferentiation upon oxygen abrogation in the infarcted heart. This presumption is based on the fact that dedifferentiated mACMs seemed to actively contribute to the modulation of the immune response post MI by expressing and potentially secreting chemoactive cytokines like CCl4, Cxcl2 and Cxcl16 (Sokol 2015). Furthermore, dedifferentiating CMs enhanced fibroblast activation during cardiac remodeling via release of Fibronectin, Vimentin and PDGFRα/β (Chintalgattu 2010, Lighthouse 2016, Maruyama 2016, Zhou 2017) . By this means, $Runx1^{+}$ mACMs seemed to play a conductive role during myocardial remodeling. On top of my findings**,** a potential stimulation of neovascularization was indicated as shown by a dramatic upregulation of pro-angiogenetic factors like Fstl1, Srfp2, Piezo2 and Srpx2 in ischemic CMs, which opens up the possibility of generating novel therapeutic strategies for restoring tissue functions by regaining probably the structural integrity of the myocardium. A re-capitulatory scheme of the cell fate of a once Runx1 expressing CM after the onset of myocardial infarction is shown in Figure 46 as an illustration of the summarized results, which are presented in this thesis.

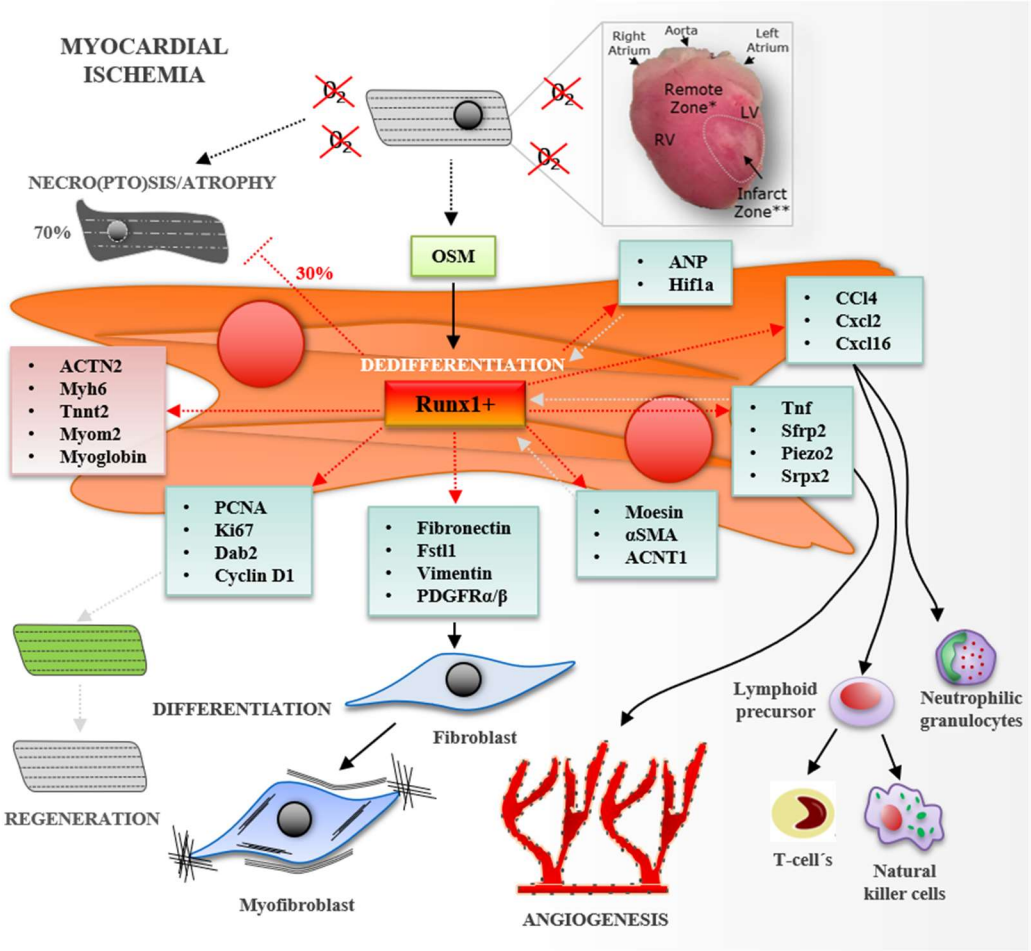

Figure 46: Profile and cell fate of once Runx1 expressing adult CMs after the onset of myocardial infarction. OSM-stimulated Runx1^{+} mACMs demonstrated typical signs of CMs dedifferentiation like elongation, sprouting and flattening along with a loss of sarcomeric structures and a dismantled contractile apparatus. These in vitro observations were validated in vivo via transcriptional profiling of isolated and sorted living Runx1-traced mACMs upon myocardial injury. Acute ischemic conditions led to a drop out of the majority of mACMs within the hypoxic region and to an induction of Runx1 expression in surviving CMs, which correlated with a dramatic increase of dedifferentiation markers like actinin-1 (ACTN1), smooth-muscle actin (SMA) and Moesin, and indicated the capability to regenerate the injured heart. Deep sequencing analyses confirmed signs of dedifferentiation by the downregulation of cytoskeletal marker genes (ACTN2, Myh6, Tnnt2, Myom2 and Myoglobin) as well as the upregulation of atrial natriuretic peptide (ANP) and hypoxia-inducible factor-1(Hif1a) in mACMs. Moreover, Runx1-traced mACMs gained the ability to proliferate, as shown by the upregulation of PCNA, Ki67, Dab2 and Cyclin D1. In addition, Runx1 expressing mACMs were associated with Follistatin-like 1 (Fstl1) expression, which is known to promote fibroblast activation, as well as Susi repeat protein X-linked 2 (Srpx2) expression representing a novel mediator of angiogenesis (Miljkovic-Licina 2009). The increased expression of vimentin and fibronectin indicated that dedifferentiated mACMs contribute to ECM processes, what might prevent heart rupture and support survival (Burnier 2011, Bonnans 2014).

The development of new therapeutic approaches for treating patients with ischemic heart disease is still an ultimate goal of cardiac regeneration studies (Behfar 2014, Hashimoto 2018). Promising, so-called first-generation cell-based therapies are therefore pursuing the concept of regenerative cell repair in the damaged tissue (Beltrami 2003, Meyer 2006, Behfar 2014). Several clinical trials and different studies from Meyer et al. and others

have elucidated 3 to 7 days post MI as critical time points for such interventions (Assmus 2002, Meyer 2006, Schächinger 2006, Wernly 2019). Here, a temporally and locally limited enhanced expression of Runx1, which I have shown to peak in ischemic CMs at day 7 post MI, could improve the outcome of these clinical studies. In line with my findings, Kohli et al. and others have also identified transcription factors, i.e. the GATA family as well as Myocardin and myocyte enhancer factor-2 (MEF-2), as key targets for promising therapeutic interventions (Kohli 2011, Kinnunen 2018). In my analysis, one of the most clearly Runx1-regulated genes in dedifferentiated CMs was Srpx2, a novel chondroitin sulfate proteoglycan, which has been shown to promote proliferation, migration, adhesion and invasion of cells and to stimulate angiogenesis - all properties known to promote potential re-vascularization by endothelial cell remodeling in the infarcted heart (Miljkovic-Licina 2009, Zhang 2018). To increase Runx1 expression within the ischemic heart, the recently identified Runx1 mutants K83R and H179K could be used as protein-based Runx1 activators and potentially applied via hydrogel combined intracardial injections post MI. Such a Runx1 overexpression might lead to an enhancement of pro-angiogenetic factors like Srpx2 and also Fstl1 in order to increase the neovascularization and consequently the number of newly formed or regenerated CMs (Figure 47, Strategy 1). In addition, a specific inhibition of the Runx1-triggered secretion of cytokines (CCl4, CxCl2, Cxcl16) would be mandatory with the purpose of reducing the number of infiltrating leukocytes and therefore diminishing the degree of degradation processes within the infarcted myocardium (Frangogiannis 2014, Saxena 2016). Therefore, shortening the duration of Runx1 expression would automatically reduce the amount of infiltrating and destructive leukocytes (Figure 47, Strategy 2). This therapeutic strategy could be enhanced by a triggered stimulation of Fstl1 to increase the re-vascularization of the ischemic region**,** either in combination with enhanced or diminished triggering of Srpx2, in dependence of the pathophysiological context of Srpx2 upon MI. On the other site a temporal Runx1 expression could reduce the progression of CM dedifferentiation, which then might promote Runx1-initiated proliferative processes in order to facilitate the regeneration of already existing, ischemic CMs. In 2016, Illendula et al. explored the small molecule inhibitor of CBFβ-Runx1 binding, 2-pyridyl benzimidazole AI-4-57, which significantly affected Runx1-mediated proliferation and re-vascularization activity (Illendula 2016). This molecule could be used as an effective tool to probe the utility of targeting Runx1 in a distinct spatial/temporal manner and therefore to create a regulatory feedback loop for cardiomyocyte de- and redifferentiation

after the onset of MI (Ben-Ami 2009, Illendula 2016). Recently, Kinnunen et al. published an efficient way to specifically deliver compounds like potent inhibitors of transcription factors in an experimental model of hypertension or myocardial infarction (Kinnunen 2018). Here, they used micro- and nanoparticles loaded with the appropriate compound and injected it either intramyocardially or intravenously by this means. These tools could be used to selectively trigger Runx1 activation (Li 2007, Kinnunen 2018), which consequently might induce early dedifferentiation (when applied in the first hours post MI) or even differentiation processes (when applied up to 7dpMI) and thus could potentially increase the amount of surviving CMs within the ischemic region of the infarcted myocardium without the negative effects of leucocyte infiltration and immune cell-initiated OSM signaling (Li 2007, Kubin 2011, Richards 2013).

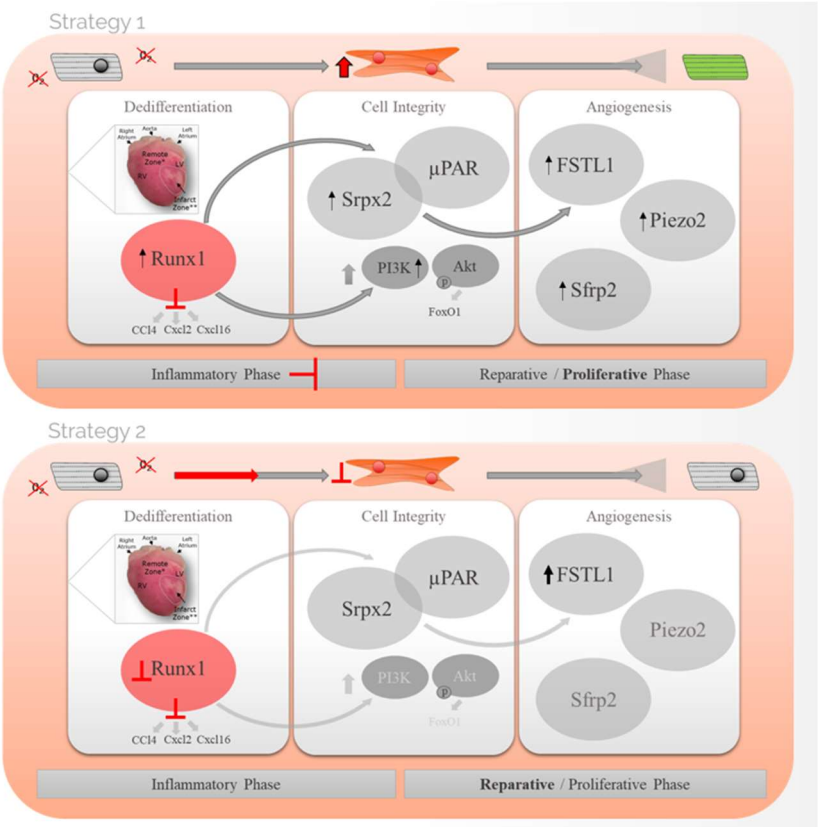

Figure 47: Therapeutic strategies to enhance Runx1-mediated cardioprotective effects of regeneration and neovascularization. Strategy 1 is targeting a protein-based Runx1 overexpression approach via hydrogel-combined intracardial applications of the Runx1 mutants K83R and H179K post MI in order to enhance the effects of pro-angiogenetic factors like Srpx2 and Fstl1. This might lead to an activation of neovascularization paralleled by an increased number of newly formed or regenerated CMs, possibly in combination with the inhibition of Runx1-triggered cytokine release in order to prevent an enhanced or prolonged immune cell-mediated remodeling of the infarcted myocardium. Strategy 2 is mainly focusing on a temporally controlled Runx1 expression and therefore on controlled dedifferentiation processes, which might support proliferation of the ischemic mACMs. This potentially facilitates the regenerative capacity by replacing already damaged CMs along with Fstl1-initiated processes of neovascularization.

6. Summary

Myocardial infarction (MI) is based on the lack of blood supply in the heart muscle with the possible consequence of irreversible structural changes, known as cardiac remodeling. These ischemia-related adaption mechanisms include the dedifferentiation of cardiomyocytes (CMs). Despite intensive research, the dynamic pattern of dedifferentiated CMs, their cell fate and molecular characteristics during cardiac remodeling are still insufficiently described. I assumed in my doctoral thesis that the Runt-related transcription factor 1 (Runx1) is the central inductor and regulator of CM dedifferentiation and therefore used Runx1 as the primary target gene for further characterization of this process in the context of experimental myocardial infarction. First, I was able to demonstrate that Runx1 deficient adult mouse cardiomyocytes (mACMs) originated from a heart-specific Runx1 knock-out strain lacked the ability to sprout, elongate and decline sarcomeric proteins as typical signs of dedifferentiation. In contrast, OSM signaling, which constituted a central modulator pathway for the induction of CM dedifferentiation, was not impaired, indicating an OSM-initiated but Runx1-triggered dedifferentiation. In the second part of my study, I established a reproducible Runx1 tracing approach. There, I used different transgenic reporter mouse strains and applied them to models of MI in order to characterize ischemic and dedifferentiated $Runx1^{+}$ CMs more in depth. Here, a strong induction of Runx1 expression was noted adjacent to the infarcted region. The number of $Runx1^{+}$ ACMs, which also demonstrated a dedifferentiated phenotype at this time, increased within the first 7 days post MI and declined thereafter. Furthermore, living once Runx1 expressing ACMs were found throughout the entire remodeling process, what indicated that Runx1 is directly associated with the survival of ischemic CMs. Last, profiling of Runx1-traced CMs by a unique live-cell sorting approach in combination with next-generation sequencing revealed an active pro-angiogenic, proliferative and immunomodulative character with the ability of those cells to contribute to regenerative processes of the infarcted heart. Overall, I could show that the time-limited and regional Runx1-mediated dedifferentiation of CMs is neither an artificial occurrence generated in the petri dish nor a meaningless adaptation mechanism, but instead dynamically shapes cardiac remodeling processes of the ischemic heart to prevent further organ damage and resulting functional restrictions in an auto- and paracrine way of intercellular communication.

7. Zusammenfassung

Der Myokardinfarkt (MI) beruht auf der mangelnden Blutversorgung des Herzmuskels mit der möglichen Folge irreversibler struktureller Veränderungen, bekannt als kardiales Remodelling. Zu den Ischämie-bedingten Anpassungsmechanismen gehört die Dedifferenzierung von Kardiomyozyten (CMs). Trotz intensiver Forschung sind das dynamische Muster dedifferenzierter Herzmuskelzellen, ihr zelluläres Schicksal sowie die molekularen Eigenschaften während des Remodelling-Prozesses noch unzureichend beschrieben. In meiner Doktorarbeit ging ich davon aus, dass der Runt-verwandte Transkriptionsfaktor 1 (Runx1) der zentrale Induktor und Regulator der Dedifferenzierung in CMs ist und verwendete daher Runx1 als primäres Targetgen für eine weitere Charakterisierung dieses Prozesses im Kontext eines experimentellen Myokardinfarktes. Zunächst konnte ich nachweisen, dass Runx1-defiziente adulte Mauskardiomyozyten (mACMs), die von herzspezifischen Runx1-Knock-out-Mäusen stammten, nicht die Fähigkeit besaßen, typische Charakteristika der Dedifferenzierung, wie ein vermehrtes Längenwachstum und der Verlust sarkomerer Strukturen, aufzuzeigen. Im Gegensatz dazu war der OSM-Signalweg, der einen zentralen Modulator für die Induktion einer kardiomyozytären Dedifferenzierung darstellte, nicht beeinträchtigt, was zwar auf eine OSM-initiierte aber durch Runx1-ausgelöste Dedifferenzierung hinwies. Im zweiten Teil meiner Studie etablierte ich einen reproduzierbaren Runx1-Tracing-Ansatz. Hierzu nutzte ich verschiedene transgene Reportermausstämme und wandte bei diesen MI-Modelle an, um ischämische und dedifferenzierte Runx1^{+}-ACMs eingehender zu charakterisieren. Dabei wurde eine starke Induktion der Runx1-Expression in der Nähe der infarzierten Region festgestellt. Die Anzahl der Runx1^{+}-ACMs, die zu diesem Zeitpunkt ebenfalls einen dedifferenzierten Phänotyp aufwiesen, stieg innerhalb der ersten 7 Tage nach dem MI an und nahm danach ab. Darüber hinaus wurden während des gesamten Remodelling-Prozesses lebende, einmal Runx1-exprimierende ACMs gefunden, was darauf hindeutete, dass Runx1 mit dem Überleben von ischämischen CMs direkt assoziiert ist. Schließlich ergab das Profiling von Runx1-markierten CMs, in einem einzigartigen Ansatz zur Sortierung lebender Zellen und in Kombination mit einer Next-Generation-Sequenzierung, aktiv pro-angiogene, proliferative und immunmodulative Eigenschaften und damit verbunden die Fähigkeit dieser Zellen, zur Regeneration des infarzierten Herzens beizutragen. Insgesamt konnte ich zeigen, dass die Runx1-vermittelte Dedifferenzierung von CMs

weder ein künstliches, also in der Petrischale erzeugtes Ereignis noch ein bedeutungsloser Anpassungsmechanismus ist, sondern stattdessen die kardialen Remodelling-Prozesse des ischämischen Herzens dynamisch beeinflusst, um so den weiteren Organschaden und daraus resultierende Funktionseinschränkungen durch einen auto- und parakrinen Weg sowie durch interzelluläre Kommunikation zu verhindern.

8. List of abbreviations

Abbreviation	Meaning
Actin	Pan-actin
ACTN1	Alpha-actinin
Akt	RAC-alpha serine/threonine-protein kinase (gene)
ALY	Always early (gene)
AML	Acute myeloid leukemia
ANP	Atrial natriuretic peptide
ATG	Translation initiation codon
bp	Base pairs
BSA (CON)	Bovin serum albumin (control)
BZ	Border zone
C/EBP	CCAAT/Enhancer-binding-protein
C57Bl6/J	most frequently used wildtype inbred mouse substrain purchased from Jackson laboratory
CAG	CMV enhancer, chicken beta-actin promoter
CBFα/β	Core-binding factor-alpha/-beta
CBP	CREB-Binding Protein
CCL	C-C motif ligands
Chr	Chromosome
c-Kit	Stem cell factor receptor
CLIC	Chloride intracellular channel protein
CM(s)	Cardiomyocyte(s)
Cre/LoxP	Cre/LoxP recombinase system
Cxcl	C–X–C motif ligand
Dab2	Disabled homolog 2
DAPI	4′,6-Diamidin-2-phenylindol
DNA	Deoxyribonucleic acid
dNTPs	Desoxynucleosidtriphosphate
dpI	Days post infarction
dps	Days post stimulation
DTT	Dithiothreitol
E	Embryonic day
Ear2	Eosinophil-associated, ribonuclease A family, member 2
ECM	Extracellular matrix
EXT	Optical density
F-actin	Filamentous actin
FC	Fold change
FCS	Fetal calf serum
FLP	Flippase recombinase
FOCA	Fluidics and optics core assemblies
FRT	FLP recognition target sites
Fstl1	Follistatin-related protein 1
gp130	Interleukin-6-transducer-chain
H	Human
H&E	Hematoxylin–eosin
HBSS	Hank's Balanced Salt Solution
I	Permanent occlusion of the LAD
I/R	Ischemia/reperfusion, i.e. temporary occlusion of the LAD
IL-6	Interleukin-6
intein	Interventing protein splicing domain

IS	Infarct size
IZ	Infarct zone
IZ**	CMs isolated from the ischemic zone of the left ventricle
JAK	Januskinasen
Kb	Kilo bases
kDa	Kilo dalton
KEGG	Kyoto Encyclopedia of Genes and Genomes
KLF4	Krüppel-like factor 4
KM	Ketamine/xylazine in ml/mg
KO	Knock-out
lacZ	Beta-galactosidas
LAD	Left descending coronary artery
$LC1^{Cre}$	Luciferase-Cre
lncRNA	Long non-coding RNA
LV	Left ventricle
mACM(s)	Adult mouse cardiomyocyte(s)
MAP/MAPK	Mitogen-activated protein/ Kinase
Mef2c	Myocyte-specific enhancer factor 2C
MI	Myocardial infarction
miRNA	MicroRNA
MMP-1	Matrix metalloproteinase-1
mRNA	Messenger RNA
Myb	Myeloblastosis oncogene
NF-κB	Nuclear factor 'kappa-light-chain-enhancer' of activated B-cells
NGN3	Neurogenin 3
NGS	Next-generation sequencing
Nkx2.5	Cardiac-specific homeobox 1
OCT4	Octamer binding transcription factor 4
OECD	Organization for economic co-operation and development
OSM	Oncostatin M
OSM/con	Oncostatin M divided by control
OSMR	Oncostatin M receptor
P1	Promotor 1 (distal)
P2	Promotor 2 (proximal)
PBS	Phoshate buffer saline
PCA	Principle component analysis
PCM1	Pericentriolar material 1
PCR	Polymerase chain reaction
Pdgfra	Platelet-derived growth factor receptor alpha (in gene set)
PDGFRα/β	Platelet-derived growth factor receptor alpha/beta
PDX1	Duodenum homeobox 1
PFA	Paraformaldehyde
PI3	Phosphoinositid-3
PI3K	Phosphoinositid-3 kinase
PKC	Protein kinase C
PKCδ	PKC delta
PkHt	Peak height
PSCI-M	Perfusion Systems for Cell Isolation
rACM(s)	Adult rat cardiomyocyte(s)
RD	Repression domain
RHD	Runt DNA-binding domain
RFP	Red fluorescent protein

RHD	Runt DNA-binding domain
RNA	Ribonucleic acid
$Rosa26^{stopfloxlacZ}$	Trangenic lacZ expressing mouse line upon induction with Cre recombination
rpm	Revolutions per minute
RT	Room temperature
RT-PCR	Reverse transcription polymerase chain reaction
Runx	Runt-related transcription factor (protein)
RUNX	Runt-related transcription factor (gene)
Runx1 Tracer	$Runx1^{tTA}/LC1^{Cre}/Rosa26^{stopfloxlacZ}$
Runx1 Viewer	$Runx1^{tTA}/Tg^{GFPtetO7lacZ}$
$Runx1^{fl2}$	Runx1-flox-flox
$Runx1^{fl2}/\alpha MHC^{Cre}$	Runx1 deficient CMs from heart specific Runx1 knock-out animals
$Runx1_{negative}$	Runx1 negative
$Runx1_{traced}$	Runx1 traced ($lacZ^{+}$ or RFP^{+})
$Runx1^{tTA}$	Runx1-t2A-tTA-t2A
RV	Right ventricle
RZ	Remote zone
RZ*	CMs isolated from the remote zone mainly of the right ventricle
SDS-PAGE	Sodium dodecyl sulfate polyacrylamide gel electrophoresis
SEM	Standard error of the mean
Sfrp2	Secreted frizzled related protein 2
SOX2	Sex determining region Y-box 2
Srpx2	Sushi repeat containing protein X-linked 2
STAT	Signal transducers and activators of transcription
TAD	Transactivation domain
TAE	Tris-Acetat-EDTA
TEM	Transmission electron microscopy
Tet-OFF	Tetracycline-sensitive system
TGFβ	Transforming growth factor beta
$Tg^{GFPtetO7lacZ}$	Trangenic GFP and lacZ expressing mouse line responsive for tTA
Timp1	Tissue inhibitor of metalloproteinases
TLE	Transducin-like enhancer of split
Tnf	Tumor necrosis factor
TOF	Time of flight
TRE o. tetO7	Bi-directional tetracycline-responsive element
tTA	Transcriptional activator
U/µL	Units per µL
UTR	Untranslated regions
UV	Ultraviolet
V	Valvular region
X-gal	5-Brom-4-chlor-3-indoxyl-β-D-galactopyranosid
YAP	Yes-associated protein
αCA	Alpha-cardiac actin
αMHC	Alpha-myosin heavy chain
αMHC^{Cre}	Cre expressing mouse line controlled by the αMHC promotor
αSKA/αSA/ACTN2/Sarc actinin	Sarcomeric alpha-actinin, alpha-sarcomeric actin
αSMA/α SM actinin/Acta2/SM actin	Alpha-smooth-muscle actin, alpha smooth muscle actinin
βgal	Beta-galactosidase

9. List of figures

Figure 1: Main causes of mortality across OECD countries in 2017, adapted from OECD (2019). 1

Figure 2: Cross-sectional view post myocardial infarction (MI), adapted from Awada et al. (Awada 2016).. 1

Figure 3: Histological analysis of 3 distinct morphological zones within the infarcted myocardium, adapted from Sparta et al. (Spata 2013). 2

Figure 4: Repair and regeneration mechanisms of the infarcted myocardium driven by delivery of proteins that address distinctive MI pathologies, adapted from Awada et al. (Awada 2016). 4

Figure 5: Reprogramming, transdifferentiation and dedifferentiation, adapted from Jopling et al. (Jopling 2011). 5

Figure 6: The different properties of dedifferentiated (left) and mature (right) CMs, adapted from Bloomekatz et al. (Bloomekatz 2016). 6

Figure 7: Morphological characteristics of purified CMs, adapted from Zhang et al. (Zhang 2010). 6

Figure 8: Dedifferentiation of pre-existing CMs, adapted from Leri et al. (Leri 2015). 7

Figure 9: Affymetrix DNA microarray analysis from embryonic stem cells subjected to CM differentiation (CB/EB) in comparison to Oncostatin M (OSM)-treated CMs (OSM/con), adapted from Kubin et al. (Kubin 2011). 8

Figure 10: OSM receptor (OSMR) signaling, adapted from Richards and modified from Fritz (Fritz 2010, Richards 2013). 9

Figure 11: The mammalian RUNX genes: structure and mode of function, adapted from Levanon et al. (Levanon 2003, Levanon 2004). 10

Figure 12: The structure of the RUNX1 gene and Runx1 protein, adapted from Tang et al. (Tang 2018).. 11

Figure 13: Runx1 activity in skeletal and soft tissues of neonatal mice, adapted from Lian et al. and Levanon et al. (Levanon 2001, Lian 2003).. 12

Figure 14: Genetic lineage tracing strategies, adapted from Chong et al. (Chong 2014). 13

Figure 15: Illustration of an unbiased experimental omics approach by using transcriptomic profiling, adapted from Perrino et al. (Perrino 2017). 14

Figure 16: Genetic Runx1-t2A-tTA-t2A construct of the $Runx1^{tTA}$ knock-in model. 25

Figure 17: Schematic illustration of the genetic lineage tracing approach. 26

Figure 18: Schematic illustration of the genetic labeling approach. 27

Figure 19: A 3-step gating strategy for live-cell sorting of ischemic $Runx1_{traced}$ mACMs. 41

Figure 20: Phenotypical changes of mouse Oncostatin M (OSM)-stimulated cultures of mouse adult cardiomyocytes (mACMs). 45

Figure 21: Visualized Runx1 expression in OSM-stimulated cultures of mACMs. 46

Figure 22: Expression patterns of Runx1 and Timp1 in OSM-treated mACMs. 48

Figure 23: In vitro study of mACMs from $Runx1^{fl2}$ and Runx1 deficient ($Runx1^{fl2}/\alpha MHC^{Cre}$) mice upon OSM treatment. 49

Figure 24: Immunofluorescence and phase contrast imaging of isolated CMs from $Runx1^{fl2}$ and $Runx1^{fl2}/\alpha MHC^{Cre}$ mice (heart specific knock out) subjected to OSM treatment. 50

Figure 25: Dynamic expression pattern of different dedifferentiation and ACM markers of isolated CMs from adult $Runx1^{fl2}$ and $Runx1^{fl2}/\alpha MHC^{Cre}$ mice (heart specific knock out) subjected to OSM application to induce dedifferentiation in vitro. 52

Figure 26: OSM stimulation of transgenic mACMs revealed the same Runx1 responsivity as wildtype mACMs. 53

Figure 27: Runx1 and Timp1 expression of cultivated and stimulated Runx1 Tracer mACMs. 55

Figure 28: Runx1 expression upon experimental myocardial ischemia. 56

Figure 29: Kinetic pattern of Runx1 expression in wildtype animals after myocardial infarction. 58

Figure 30: Runx1 expression of heart specific deficient mice, which were subjected to permanent LAD ligation. 59

Figure 31: Monitoring of the current Runx1 expression in correlation with lacZ expression in Runx1 Viewer animals upon myocardial ischemia. 60

Figure 32: Tracking the cell fate of $Runx1_{traced}$lacZ expression in Runx1 Tracer animals upon myocardial ischemia. 61

Figure 33: Myocardial damage and remodeling in Runx1 Tracer animals upon I/R injury. 63

Figure 34: Comparative analysis of the infarct size in different experimental MI animal models. 64

Figure 35: I/R injury increased the amount of $Runx1^{+}$ mACMs compared to permanent LAD ligation (I). 66

Figure 36: Signs of dedifferentiation were detectable in animals post I/R in vivo. 67

Figure 37: Ultramicrotomy-based TEM revealed signs of dedifferentiation on a nanoscopic level in animals at 7dpI/R. 68

Figure 38: Switching Runx1 tracing label from lacZ to RFP in order to enable single live-cell sorting. 69

Figure 39: Live-cell sorting of $Runx1_{traced}RFP^{+}$ mACMs enabled the isolation and separation of single CMs undergoing dedifferentiation. 71

Figure 40: Quantification of biosorting data at different time points post I/R. 72

Figure 41: Correlative NGS analysis of isolated and sorted mACMs at 7 days post ischemic heart injury. 73

Figure 42: Visualization of gene expression data sets in $Runx1_{traced}RFP^{+}$ or $Runx1_{negative}$ mACMs post ischemia via 2D scatter plots..... 74

Figure 43: RNA-sequencing analysis of TOP50 differentially expressed genes revealed injury-induced transcriptional responses in $Runx1_{traced}RFP^{+}$ ACMs within the ischemic heart. 75

Figure 44: Gene set enrichment analysis related to NGS data of isolated and sorted ischemic mACMs. . 77

Figure 45: Structural remodeling processes were highly evident in $Runx1_{traced}RFP^{+}$ mACMs undergoing dedifferentiation after the onset of MI. 79

Figure 46: Profile and cell fate of once Runx1 expressing adult CMs after the onset of myocardial infarction. 92

Figure 47: Therapeutic strategies to enhance Runx1-mediated cardioprotective effects of regeneration and neovascularization..... 94

10. Bibliography

Abe, N.; Kohu, K.; Ohmori, H.; Hayashi, K.; Watanabe, T.; Hozumi, K.; Sato, T., Habu, S.; Satake, M., "Reduction of Runx1 Transcription Factor Activity Up-Regulates Fas and Bim Expression and Enhances the Apoptotic Sensitivity of Double Positive Thymocytes," The Journal of Immunology, vol. 175, no. 7, pp. 4475-4482, 2005.

Abram, C.L.; Roberge, G.L.; Hu, Y.; Lowell, C.A., "Comparative analysis of the efficiency and specificity of myeloid-Cre deleting strains using ROSA-EYFP reporter mice," J Immunol Methods, vol. 408, pp. 89-100, Jun, 2014.

Adrian-Segarra, J.M.; Sreenivasan, K.; Gajawada, P.; Lörchner, H.; Braun, T.; Pöling, J., "The AB loop of oncostatin M (OSM) determines species-specific signaling in humans and mice," J Biol Chem, vol. 293, no. 52, pp. 20181-20199, Dec 28, 2018.

Agah, R.; Frenkel, P.A.; French, B.A.; Michael, L.H.; Overbeek, P.A.; Schneider, M.D., "Gene Recombination in Postmitotic Cells - Targeted Expression of Cre Recombinase Provokes Cardiac-restricted, Site-specific Rearrangement in Adult Ventricular Muscle In Vivo," J. Clin. Invest., no. 1, pp. 169-179, 1997.

Alge, C.S.; Suppmann, S.; Priglinger, S.G.; Neubauer, A.S.; May, C.A.; Hauck, S.; Welge-Lussen, U.; Ueffing, M.; Kampik, A., "Comparative Proteome Analysis of Native Differentiated and Cultured Dedifferentiated Human RPE Cells," Investigative Opthalmology & Visual Science, vol. 44, no. 8, pp. 3629, 2003.

Amodio, N.; Raimondi, L.; Juli, G.; Stamato, M.A.; Caracciolo, D.; Tagliaferri, P.; Tassone, P., "MALAT1: a druggable long non-coding RNA for targeted anti-cancer approaches," J Hematol Oncol, vol. 11, no. 1, pp. 63, May 8, 2018.

Anand, S.; Mangano, E.; Barizzone, N.; Bordoni, R.; Sorosina, M.; Clarelli, F.; Corrado, L.; Martinelli Boneschi, F.; D'Alfonso, S.; De Bellis, G., "Next Generation Sequencing of Pooled Samples: Guideline for Variants' Filtering," Sci Rep, vol. 6, pp. 33735, Sep 27, 2016.

Anversa, P., Kajstura, J., "Ventricular myocytes are not terminally differentiated in the adult mammalian heart," Circ Res, vol. 83, no. 1, pp. 1-14, Jul 13, 1998.

Assmus, B.; Schachinger, V.; Teupe, C.; Britten, M.; Lehmann, R.; Dobert, N.; Grunwald, F.; Aicher, A.; Urbich, C.; Martin, H.; Hoelzer, D.; Dimmeler, S.; Zeiher, A.M., "Transplantation of Progenitor Cells and Regeneration Enhancement in Acute Myocardial Infarction (TOPCARE-AMI)," Circulation, vol. 106, no. 24, pp. 3009-17, Dec 10, 2002.

Ausma, J.; Borgers, M., "Dedifferentiation of atrial cardiomyocytes: from in vivo to in vitro," Cardiovascular Research, vol. 55, pp. 9-12, 2002.

Ausma, J.; Wijffels, M.; Van Eys, G.; Koide, M.; Ramaekers, F.; Allessie, M.; Borgers, M., "Dedifferentiation of Atrial Cardiomyocytes as a Result of Chronic Atrial Fibrillation," AJP, vol. 151, no. 4, pp. 985-997, 1997.

Awada, H.K.; Hwang, M.P.; Wang, Y., "Towards comprehensive cardiac repair and regeneration after myocardial infarction: Aspects to consider and proteins to deliver," Biomaterials, vol. 82, pp. 94-112, Mar, 2016.

Ban, K.; Bae, S.; Yoon, Y.S., "Current Strategies and Challenges for Purification of Cardiomyocytes Derived from Human Pluripotent Stem Cells," Theranostics, vol. 7, no. 7, pp. 2067-2077, 2017.

Behfar, A.; Crespo-Diaz, R.; Terzic, A.; Gersh, B.J., "Cell therapy for cardiac repair—lessons from clinical trials," Nature Reviews Cardiology, vol. 11, pp. 232, 03/04/online, 2014.

Beltrami, A.P.; Barlucchi, L.; Torella, D.; Baker, M.; Limana, F.; Chimenti, S.; Kasahara, H.; Rota, M.; Musso, E.; Urbanek, K.; Leri, A.; Kajstura, J.; Nadal-Ginard, B.; Anversa, P., "Adult Cardiac Stem Cells Are Multipotentand Support Myocardial Regeneration," Cell, vol. 114, pp. 763–776, 2003.

Ben-Ami, O.; Pencovich, N.; Lotem, J.; Levanon, D.; Groner, Y., "A regulatory interplay between miR-27a and Runx1 during megakaryopoiesis," vol. 106, no. 1, pp. 238-243, 2009.

Bergmann, O.; Zdunek, S.; Alkass, K.; Druid, H.; Bernard, S.; Frisen, J., "Identification of cardiomyocyte nuclei and assessment of ploidy for the analysis of cell turnover," Exp Cell Res, vol. 317, no. 2, pp. 188-94, Jan 15, 2011.

Bergmann, O.; Zdunek, S.; Felker, A.; Salehpour, M.; Alkass, K.; Bernard, S.; Sjostrom, S.L.; Szewczykowska, M.; Jackowska, T.; Dos Remedios, C.; Malm, T.; Andra, M.; Jashari, R.; Nyengaard, J.R.; Possnert, G.; Jovinge, S.; Druid, H.; Frisen, J., "Dynamics of Cell Generation and Turnover in the Human Heart," Cell, vol. 161, no. 7, pp. 1566-75, Jun 18, 2015.

Bersell, K.; Arab, S.; Haring, B.; Kuhn, B., "Neuregulin1/ErbB4 signaling induces cardiomyocyte proliferation and repair of heart injury," Cell, vol. 138, no. 2, pp. 257-70, Jul 23, 2009.

Bloomekatz, J.; Galvez-Santisteban, M.; Chi, N.C., "Myocardial plasticity: cardiac development, regeneration and disease," Current Opinion in Genetics & Development, vol. 40, pp. 120-130, 2016/10/01, 2016.

Blyth, K.; Cameron, E.R.; Neil, J.C., "The RUNX genes: gain or loss of function in cancer," Nat Rev Cancer, vol. 5, no. 5, pp. 376-87, May, 2005.

Boettger, T.; Beetz, N.; Kostin, S.; Schneider, J.; Kruger, M.; Hein, L.; Braun, T., "Acquisition of the contractile phenotype by murine arterial smooth muscle cells depends on the Mir143/145 gene cluster," J Clin Invest, vol. 119, no. 9, pp. 2634-47, Sep, 2009.

Bonnans, C.; Chou, J.; Werb, Z., “Remodelling the extracellular matrix in development and disease,” Nat Rev Mol Cell Biol, vol. 15, no. 12, pp. 786-801, Dec, 2014.

Bundesministeriums der Justiz und für Verbraucherschutz, "Tierschutzgesetz in der Fassung der Bekanntmachung vom 18. Mai 2006 (BGBl. I S. 1206, 1313), das zuletzt durch Artikel 101 des Gesetzes vom 20. November 2019 (BGBl. I S. 1626) geändert worden ist," 1972.

Burnette, W.N., ““Western Blotting”: Electrophoretic transfer of proteins from sodium dodecyl sulfate-polyacrylamide gels to unmodified nitrocellulose and radiographic detection with antibody and radioiodinated protein A,” Analytical Biochemistry, vol. 112, no. 2, pp. 195-203, 1981/04/01/, 1981.

Burnier, J.V.; Wang, N.; Michel, R.P.; Hassanain, M.; Li, S.; Lu, Y.; Metrakos, P.; Antecka, E.; Burnier, M.N.; Ponton, A.; Gallinger, S.; Brodt, P., “Type IV collagen-initiated signals provide survival and growth cues required for liver metastasis,” Oncogene, vol. 30, no. 35, pp. 3766-83, Sep 1, 2011.

Cai, S.; Fu, X.; Sheng, Z., “Dedifferentiation: A New Approach in Stem Cell Research,” BioScience, vol. 57, no. 8, pp. 655-662, September 2007, 2007.

Califf, R.M.; Phillips, H.R.; Hindman, M.C.; Mark, D.B.; Lee, K.L.; Behar, V.S.; Johnson, R.A.; Pryor, D.B.; Rosati, R.A.; Wagner, G.S.; Harrell Jr., F.E., “Prognostic Value of a Coronary Artery Jeopardy Score,” J Am Coll CardioI, vol. 5, no. 5, pp. 1055-63, 1985.

Challen, G.A.; Goodell, M.A., “Runx1 isoforms show differential expression patterns during hematopoietic development but have similar functional effects in adult hematopoietic stem cells,” Exp Hematol, vol. 38, no. 5, pp. 403-16, May, 2010.

Chen, W.; Frangogiannis, N.G., “Fibroblasts in post-infarction inflammation and cardiac repair,” Biochim Biophys Acta, vol. 1833, no. 4, pp. 945-53, Apr, 2013.

Chen, Z.; Bu, N.; Qiao, X.; Zuo, Z.; Shu, Y.; Liu, Z.; Qian, Z.; Chen, J.; Hou, Y., “Forkhead Box M1 Transcriptionally Regulates the Expression of Long Noncoding RNAs Snhg8 and Gm26917 to Promote Proliferation and Survival of Muscle Satellite Cells,” Stem Cells, vol. 36, no. 7, pp. 1097-1108, Jul, 2018.

Cherry, A.B.; Daley, G.Q., “Reprogramming cellular identity for regenerative medicine,” Cell, vol. 148, no. 6, pp. 1110-22, Mar 16, 2012.

Cherry, S.R.; Sorenson, J.A.; Phelps, M.E., "chapter 9 - Nuclear Counting Statistics," Physics in Nuclear Medicine (Fourth Edition), S. R. Cherry, J. A. Sorenson and M. E. Phelps, eds., pp. 125-140, Philadelphia: W.B. Saunders, 2012.

Chiba, A.; Watanabe-Takano, H.; Miyazaki, T.; Mochizuki, N., “Cardiomyokines from the heart,” Cell Mol Life Sci, vol. 75, no. 8, pp. 1349-1362, Apr, 2018.

Chintalgattu, V.; Ai, D.; Langley, R.R.; Zhang, J.; Bankson, J.A.; Shih, T.L.; Reddy, A.K.; Coombes, K.R.; Daher, I.N.; Pati, S.; Patel, S.S.; Pocius, J.S.; Taffet, G.E.; Buja, L.M.; Entman, M.L.; Khakoo, A.Y., "Cardiomyocyte PDGFR-beta signaling is an essential component of the mouse cardiac response to load-induced stress," J Clin Invest, vol. 120, no. 2, pp. 472-84, Feb, 2010.

Chong, J.J.; Forte, E.; Harvey, R.P., "Developmental origins and lineage descendants of endogenous adult cardiac progenitor cells," Stem Cell Res, vol. 13, no. 3 Pt B, pp. 592-614, Nov, 2014.

Chorvatova, A.M.; Kirchnerova, J.; Cagalinec, M.; Mateasik, A.; Chorvat, D., Jr., "Spectrally and spatially resolved laser-induced photobleaching of endogenous flavin fluorescence in cardiac myocytes," Cytometry A, vol. 95, no. 1, pp. 13-23, Jan, 2019.

Chuang, L.S.H.; Ito, K.; Ito, Y., "RUNX family: Regulation and diversification of roles through interacting proteins," International Journal of Cancer, vol. 132, no. 6, pp. 1260-1271, 2013.

Claycomb, W.C., "Culture of cardiac muscle cells in serum-free media," Experimental Cell Research, vol. 131, no. 1, pp. 231-236, Jan, 1981.

Coirault, C.; Guellich, A.; Barbry, T.; Samuel, J.L.; Riou, B.; Lecarpentier, Y. (2007). "Oxidative stress of myosin contributes to skeletal muscle dysfunction in rats with chronic heart failure," Am J Physiol Heart Circ Physiol, vol. 292, no. 2, pp. 1009-1017, Feb, 2007

Couse, J.F.; Davis, V.L.; Tally, W.C.; Korach, K.S., "An improved method of genomic DNA extraction for screening transgenic mice," Biotechniques, vol. 17, no. 6, pp. 1030-2, Dec, 1994.

Cunha-Neto, E.; Drigo, SA; Nogueira, LG; Teixeira; PC; Goldberg, AC; Fonseca, SG; Bilate, AM; Ramasawmy, R.; Kalil, J., "Immunological and non-immunological effects of cytokines and chemokines in the pathogenesis of chronic Chagas disease cardiomyopathy," Mem Inst Oswaldo Cruz, vol. 104, pp. 252-258, 2009.

Cunha-Neto, E.; Dzau, V.J.; Allen, P.D.; Stamatiou, D.; Benvenutti, L.; Higuchi, M.L.; Koyama, N.S.; Silva, J.S.; Kalil, J.; Liew, C.-C., "Cardiac Gene Expression Profiling Provides Evidence for Cytokinopathy as a Molecular Mechanism in Chagas' Disease Cardiomyopathy," The American Journal of Pathology, vol. 167, no. 2, pp. 305-313, 2005.

Das, M.; Molnar, P.; Gregory, C.; Riedel, L.; Jamshidi, A.; Hickman, J.J., "Long-term culture of embryonic rat cardiomyocytes on an organosilane surface in a serum-free medium," Biomaterials, vol. 25, no. 25, pp. 5643-7, Nov, 2004.

Davidson, S.M.; Ferdinandy, P.; Andreadou, I.; Botker, H.E.; Heusch, G.; Ibanez, B.; Ovize, M.; Schulz, R.; Yellon, D.M.; Hausenloy, D.J.; Garcia-Dorado, D., "Multitarget Strategies to Reduce Myocardial Ischemia/Reperfusion Injury: JACC Review Topic of the Week," J Am Coll Cardiol, vol. 73, no. 1, pp. 89-99, Jan 8, 2019.

Davis, M.P.A.; van Dongen, S.; Abreu-Goodger, C.; Bartonicek, N.; Enright, A.J., “Kraken: A set of tools for quality control and analysis of high-throughput sequence data,” Methods, vol. 63, no. 1, pp. 41-49, 2013/09/01/, 2013.

De Bruijn, M.; Dzierzak, E., “Runx transcription factors in the development and function of the definitive hematopoietic system,” Blood, vol. 129, no. 15, pp. 2061-2069, Apr 13, 2017.

Deverman, B.E.; Patterson, P.H., “Exogenous leukemia inhibitory factor stimulates oligodendrocyte progenitor cell proliferation and enhances hippocampal remyelination,” J Neurosci, vol. 32, no. 6, pp. 2100-9, Feb 8, 2012.

DeVries, H.; Fritsma, G.A., "2 - Quality assurance in hematology and hemostasis testing," Rodak's Hematology (Sixth Edition), E. M. Keohane, C. N. Otto and J. M. Walenga, eds., pp. 8-30, St. Louis (MO): Content Repository Only!, 2020.

Dispersyn, G.D.; Geuens, E.; Ver Donck, L.; Ramaekers, F.C.S.; Borgers, M., “Adult rabbit cardiomyocytes undergo hibernation-like dedifferentiation when co-cultured with cardiac fibroblasts,” Cardiovascular Research, vol. 51, pp. 230-240, 2001.

Drechsler, J.; Grötzinger, J.; Hermanns, H.M., “Characterization of the Rat Oncostatin M Receptor Complex Which Resembles the Human, but Differs from the Murine Cytokine Receptor,” PLOS ONE, vol. 7, no. 8, pp. e43155, 2012.

Driesen, R.B.; Verheyen, F.K.; Debie, W.; Blaauw, E.; Babiker, F.A.; Cornelussen, R.N.; Ausma, J.; Lenders, M.H.; Borgers, M.; Chaponnier, C.; Ramaekers, F.C., “Re-expression of alpha skeletal actin as a marker for dedifferentiation in cardiac pathologies,” J Cell Mol Med, vol. 13, no. 5, pp. 896-908, May, 2009.

Driesen, R.B.; Verheyen, F.K.; Dijkstra, P.; Thoné, F.; Cleutjens, J.P.; Lenders, M.-H.; Ramaekers, F.C.S.; Borgers, M., “Structural remodelling of cardiomyocytes in the border zone of infarcted rabbit heart,” Molecular and Cellular Biochemistry, vol. 302, no. 1, pp. 225-232, August 01, 2007.

Dumbreck, S.; Flynn, A.; Nairn, M.; Wilson, M.; Treweek, S.; Mercer, S.W.; Alderson, P.; Thompson, A.; Payne, K.; Guthrie, B., “Drug-disease and drug-drug interactions: systematic examination of recommendations in 12 UK national clinical guidelines,” BMJ, vol. 350, pp. h949, Mar 11, 2015.

Emde, B.; Heinen, A.; Godecke, A.; Bottermann, K., “Wheat germ agglutinin staining as a suitable method for detection and quantification of fibrosis in cardiac tissue after myocardial infarction,” Eur J Histochem, vol. 58, no. 4, pp. 2448, Dec 17, 2014.

Eppenberger-Eberhardt, M.; Flamme, I.; Kurer, V.; Eppenberger, H.M., “Reexpression of α-smooth muscle actin isoform in cultured adult rat cardiomyocytes,” Developmental Biology, vol. 139, no. 2, pp. 269-278, 1990/06/01/, 1990.

European Parliament and the Council of the European Union, "Directive 2010/63/EU of the European Parliament and of the Council of 22 September 2010 on the protection of animals used for scientific purposes," Official Journal of the European Union, European Parliament and the Council of the European Union, 2010, pp. 33-79.

Feldman, A.T.; Wolfe, D., "Tissue processing and hematoxylin and eosin staining," Methods Mol Biol, vol. 1180, pp. 31-43, 2014.

Ferdinandy, P.; Hausenloy, D.J.; Heusch, G.; Baxter, G.F.; Schulz, R., "Interaction of risk factors, comorbidities, and comedications with ischemia/reperfusion injury and cardioprotection by preconditioning, postconditioning, and remote conditioning," Pharmacol Rev, vol. 66, no. 4, pp. 1142-74, Oct, 2014.

Ferreira, L.R.; Frade, A.F.; Baron, M.A.; Navarro, I.C.; Kalil, J.; Chevillard, C.; Cunha-Neto, E., "Interferon-gamma and other inflammatory mediators in cardiomyocyte signaling during Chagas disease cardiomyopathy," World J Cardiol, vol. 6, no. 8, pp. 782-90, Aug 26, 2014.

Fischer, A.H.; Jacobson, K.A.; Rose, J.; Zeller, R., "Cryosectioning tissues," CSH Protoc, vol. 2008, pp. pdb prot4991, Aug 1, 2008.

Foglia, M.J.; Poss, K.D., "Building and re-building the heart by cardiomyocyte proliferation," Development, vol. 143, no. 5, pp. 729-40, Mar 1, 2016.

Foot, N.C., "The Masson Trichrome Staining Methods in Routine Laboratory Use," Stain Technology, vol. 8, no. 3, pp. 101-110, 1933/01/01, 1933.

Frangogiannis, N.G., "Regulation of the inflammatory response in cardiac repair," Circ Res, vol. 110, no. 1, pp. 159-73, Jan 6, 2012.

Frangogiannis, N.G., "The inflammatory response in myocardial injury, repair, and remodelling," Nat Rev Cardiol, vol. 11, no. 5, pp. 255-65, May, 2014.

Fritz, D.K., "The role of the oncostatin M—STAT6 axis in pulmonary eosinophilia, goblet cell hyperplasia, airway hyperresponsiveness and pulmonary fibrosis.," ETD Collection For McMaster University., 2010.

Gäbel, G.; Northoff, B.H.; Weinzierl, I.; Ludwig, S.; Hinterseher, I.; Wilfert, W.; Teupser, D.; Doderer, S.A.; Bergert, H.; Schonleben, F.; Lindeman, J.H.N.; Holdt, L.M., "Molecular Fingerprint for Terminal Abdominal Aortic Aneurysm Disease," J Am Heart Assoc, vol. 6, no. 12, Nov 30, 2017.

Gao, X.-M.; White, D.A.; Dart, A.M.; Du, X.-J., "Post-infarct cardiac rupture: Recent insights on pathogenesis and therapeutic interventions," Pharmacology & Therapeutics, vol. 134, no. 2, pp. 156-179, May, 2012.

Gao, Z.; Zhang, J.; Bi, M.; Han, X.; Han, Z.; Wang, H.; Ou, Y., “SRPX2 promotes cell migration and invasion via FAK dependent pathway in pancreatic cancer,” Int J Clin Exp Pathol vol. 8, no. 5, pp. 4791-4798, 2015.

Garcia, D.I.; Lanigan, P.; Webb, M.; West, T.G.; Requejo-Isidro, J.; Auksorius, E.; Dunsby, C.; Neil, M.; French, P.; Ferenczi, M.A., “Fluorescence lifetime imaging to detect actomyosin states in mammalian muscle sarcomeres,” Biophys J, vol. 93, no. 6, pp. 2091-101, Sep 15, 2007.

Gauthier, T.D.; Hawley, M.E.; "CHAPTER 5 - STATISTICAL METHODS," Introduction to Environmental Forensics (Second Edition), B. L. Murphy and R. D. Morrison, eds., pp. 129-183, Burlington: Academic Press, 2007.

Gauvrit, S.; Villasenor, A.; Strilic, B.; Kitchen, P.; Collins, M.M.; Marin-Juez, R.; Guenther, S.; Maischein, H.M.; Fukuda, N.; Canham, M.A.; Brickman, J.M.; Bogue, C.W.; Jayaraman, P.S.; Stainier, D.Y.R. (2018). "HHEX is a transcriptional regulator of the VEGFC/FLT4/PROX1 signaling axis during vascular development." Nat Commun, vol. 9, no. 1, pp. 2704-2718, 2018.

Girbardt, M. “G. SCHIMMEL und W. VOGELL (Herausgeber), Methodensammlung der Elektronenmikroskopie, Fascicle 1-5. VIII - 784 S., 131 Abb., Lit.-zitate: 1396 - Loseblatt-System - 2 Ringhefter. Stuttgart 1973: Wissenschaftliche Verlagsgesellschaft. DM 374.00,” vol. 14, no. 2, pp. 173-174, 1974.

Gissel, C.; Doss, M.X.; Hippler-Altenburg, R.; Hescheler, J.; Sachinidis, A., "Generation and Characterization of Cardiomyocytes Under Serum-Free Conditions," Embryonic Stem Cell Protocols: Volume 2: Differentiation Models, K. Turksen, ed., pp. 191-219, Totowa, NJ: Humana Press, 2006.

Goh, P.P; Sze, D.M.; Roufogalis, B.D., “Molecular and Cellular Regulators of Cancer Angiogenesis,” Current Cancer Drug Targets, vol. 7, pp. 743-758, 2007.

Golan-Lagziel, T.; Lewis, Y.E.; Shkedi, O.; Douvdevany, G.; Caspi, L.H.; Kehat, I., “Analysis of rat cardiac myocytes and fibroblasts identifies combinatorial enhancer organization and transcription factor families,” J Mol Cell Cardiol, vol. 116, pp. 91-105, Mar, 2018.

Gonatas, N.K.; Avrameas, S., “Detection of plasma membrane carbohydrates with lectin peroxidase conjugates,” J Cell Biol, vol. 59, no. 2 Pt 1, pp. 436-43, Nov, 1973.

Gorgens, S.W.; Raschke, S.; Holven, K.B.; Jensen, J.; Eckardt, K.; Eckel, J., “Regulation of follistatin-like protein 1 expression and secretion in primary human skeletal muscle cells,” Arch Physiol Biochem, vol. 119, no. 2, pp. 75-80, May, 2013.

Gossen, M.; Bujard, H., “Tight control of gene expression in mammalian cells by tetracycline-responsive promoters,” Proceedings of the National Academy of Sciences of the United States of America, vol. 89, no. 12, pp. 5547-5551, 1992.

Grafi, G., “The complexity of cellular dedifferentiation: implications for regenerative medicine,” Trends Biotechnol, vol. 27, no. 6, pp. 329-32, Jun, 2009.

Graham, M.M.; Faris, P.D.; Ghali, W.A.; Galbraith, P.D.; Norris, C.M.; Badry, J.T.; Mitchell, L.B.; Curtis, M.J.; Knudtson, M.L., “Validation of three myocardial jeopardy scores in a population-based cardiac catheterization cohort,” Am Heart J, vol. 142, no. 2, pp. 254-61, Aug, 2001.

Grant S.L.; Begley C.G., “The oncostatin M signalling pathway: reversing the neoplastic phenotype?,” MOLECULAR MEDICINE TODAY, vol. 5, 1999.

Growney, J.D.; Shigematsu, H.; Li, Z.; Lee, B.H.; Adelsperger, J.; Rowan, R.; Curley, D.P.; Kutok, J.L.; Akashi, K.; Williams, I.R.; Speck, N.A.; Gilliland, D.G., “Loss of Runx1 perturbs adult hematopoiesis and is associated with a myeloproliferative phenotype,” Blood, vol. 106, no. 2, pp. 494-504, Jul 15, 2005.

Gunschmann, C.; Chiticariu, E.; Garg, B.; Hiz, M.M.; Mostmans, Y.; Wehner, M.; Scharfenberger, L., “Transgenic mouse technology in skin biology: inducible gene knockout in mice,” J Invest Dermatol, vol. 134, no. 7, pp. 1-4, Jul, 2014.

Hall, B.; Limaye, A.; Kulkarni, A.B., “Overview: generation of gene knockout mice,” Curr Protoc Cell Biol, vol. Chapter 19, pp. Unit 19 12 19 12 1-17, Sep, 2009.

Hamacher-Brady, A.; Brady, N.R.; Logue, S.E.; Sayen, M.R.; Jinno, M.; Kirshenbaum, L.A.; Gottlieb, R.A.; Gustafsson, A.B., “Response to myocardial ischemia/reperfusion injury involves Bnip3 and autophagy,” Cell Death Differ, vol. 14, no. 1, pp. 146-57, Jan, 2007.

Hashimoto, H.; Olson, E.N.; Bassel-Duby, R., “Therapeutic approaches for cardiac regeneration and repair,” Nat Rev Cardiol, vol. 15, no. 10, pp. 585-600, Oct, 2018.

Hashmi, S.; Ahmad, H.R., “Molecular switch model for cardiomyocyte proliferation,” Cell Regen (Lond), vol. 8, no. 1, pp. 12-20, Jun, 2019.

Hausenloy, D.J.; Garcia-Dorado, D.; Botker, H.E.; Davidson, S.M.; Engel, F.B.; Jennings, R.; Lecour, S.; Leor, J.; Madonna, R.; Ovize, M.; Perrino, C.; Prunier, F.; Schulz, R.; Sluijter, J.P.G.; Van Laake, L.W.; Vinten-Johansen, J.; Yellon, D.M.; Ytrehus, K.; Heusch, G.; Ferdinandy, P., “Novel targets and future strategies for acute cardioprotection: Position Paper of the European Society of Cardiology Working Group on Cellular Biology of the Heart,” Cardiovasc Res, vol. 113, no. 6, pp. 564-585, May 1, 2017.

Hausenloy, D.J.; Yellon, D.M., “Myocardial ischemia-reperfusion injury: a neglected therapeutic target,” J Clin Invest, vol. 123, no. 1, pp. 92-100, Jan, 2013.

Hazarika, S.; Angelo, M.; Li, Y.; Aldrich, A.J.; Odronic, S.I.; Yan, Z.; Stamler, J.S.; Annex, B.H., “Myocyte Specific Overexpression of Myoglobin Impairs Angiogenesis After Hind-Limb Ischemia,” Arterioscler Thromb Vasc Biol., vol. 28, no. 12 pp. 2144–2150, Dec, 2008

Heinrich, P.C.; Behrmann, I.; Mueller-Newen, G.; Scharper, F.; Graeve, L., “Interleukin-6-type cytokine signalling through the gp130/Jak/STAT pathway,” Biochem. J., vol. 334; pp. 297-314, 1998, 1998.

Heusch, G.; Gersh, B.J., “The pathophysiology of acute myocardial infarction and strategies of protection beyond reperfusion: a continual challenge,” Eur Heart J, vol. 38, no. 11, pp. 774-784, Mar 14, 2017.

Hirao, H., “Regulation mechanism of ERM (ezrin/radixin/moesin) protein/plasma membrane association: possible involvement of phosphatidylinositol turnover and Rho-dependent signaling pathway,” The Journal of Cell Biology, vol. 135, no. 1, pp. 37-51, 1996.

Hofstetter, J.R.; Zhang, A.; Mayeda, A.R.; Guscar, T.; Nurnberger, J.I.; Lahiri, D.K., “Genomic DNA from Mice: A Comparison of Recovery Methods and Tissue Sources,” Biochemical and Molecular Medicine, vol. 62, no. 2, pp. 197-202, 1997/12/01/, 1997.

Hohensinner, P.J.; Kaun, C.; Rychli, K.; Niessner, A.; Pfaffenberger, S.; Rega, G.; Furnkranz, A.; Uhrin, P.; Zaujec, J.; Afonyushkin, T.; Bochkov, V.N.; Maurer, G.; Huber, K.; Wojta, J., “The inflammatory mediator oncostatin M induces stromal derived factor-1 in human adult cardiac cells,” The FASEB Journal, vol. 23, no. 3, pp. 774-782, 2009/03/01, 2008.

Horne, A.D, "Statistics, Use in Immunology," Encyclopedia of Immunology (Second Edition), P. J. Delves, ed., pp. 2211-2215, Oxford: Elsevier, 1998.

Hsu, Y.C., “Theory and Practice of Lineage Tracing,” Stem Cells, vol. 33, no. 11, pp. 3197-204, Nov, 2015.

https://www.jax.org/strain/010673. "MOUSE STRAIN DATASHEET - JAX Stock No 010673." B6;129-Runx1tm3.1Spe/J.

https://www.jax.org/strain/018913. "MOUSE STRAIN DATASHEET - JAX Stock No 018913." B6N.Cg-Tg(tetO-GFP,-lacZ)G3Rsp/J.

Hübner, K.; Cabochette, P.; Dieguez-Hurtado, R.; Wiesner, C.; Wakayama, Y.; Grassme, K.S.; Hubert, M.; Guenther, S.; Belting, H.G.; Affolter, M.; Adams, R.H.; Vanhollebeke, B.; Herzog, W. (2018). "Wnt/beta-catenin signaling regulates VE-cadherin-mediated anastomosis of brain capillaries by counteracting S1pr1 signaling." Nat Commun, vol. 9, no. 1, pp. 4860-4877, 2018.

Ibanez, B.; Macaya, C.; Sanchez-Brunete, V.; Pizarro, G.; Fernandez-Friera, L.; Mateos, A.; Fernandez-Ortiz, A.; Garcia-Ruiz, J.M.; Garcia-Alvarez, A.; Iniguez, A.; Jimenez-Borreguero, J.; Lopez-Romero, P.; Fernandez-Jimenez, R.; Goicolea, J.; Ruiz-Mateos, B.; Bastante, T.; Arias, M.; Iglesias-Vazquez, J. A.; Rodriguez, M. D.; Escalera, N.; Acebal, C.; Cabrera, J. A.; Valenciano, J.; Perez de Prado, A.; Fernandez-Campos, M. J.; Casado, I.; Garcia-Rubira, J. C.; Garcia-Prieto, J.; Sanz-Rosa, D.; Cuellas, C.; Hernandez-Antolin, R.; Albarran, A.; Fernandez-Vazquez, F.; de la Torre-Hernandez, J. M.; Pocock, S.; Sanz, G.; Fuster, V., “Effect of early metoprolol on infarct size in ST-segment-elevation myocardial infarction patients undergoing primary percutaneous coronary intervention: the Effect of Metoprolol in Cardioprotection During an Acute Myocardial Infarction (METOCARD-CNIC) trial,” Circulation, vol. 128, no. 14, pp. 1495-503, Oct 1, 2013.

Illendula, A.; Gilmour, J.; Grembecka, J.; Tirumala, V.S.S.; Boulton, A.; Kuntimaddi, A.; Schmidt, C.; Wang, L.; Pulikkan, J.A.; Zong, H.; Parlak, M.; Kuscu, C.; Pickin, A.; Zhou, Y.; Gao, Y.; Mishra, L.; Adli, M.; Castilla, L. H.; Rajewski, R. A.; Janes, K. A.; Guzman, M. L.; Bonifer, C.; Bushweller, J. H., "Small Molecule Inhibitor of CBFbeta-RUNX Binding for RUNX Transcription Factor Driven Cancers," EBioMedicine, vol. 8, pp. 117-131, Jun, 2016.

Institute of Medicine (US), Cardiovascular Disability: Updating the Social Security Listings.: Washington (DC): National Academies Press (US) 2010.

Ito, Y.; Bae, S.C.; Chuang, L.S., "The RUNX family: developmental regulators in cancer," Nat Rev Cancer, vol. 15, no. 2, pp. 81-95, Feb, 2015.

Jacobson, S.L.; Piper, H.M., "Cell Cultures of Adult Cardiomyocytes as Models of the Myocardium," J MoI Cell Cardiol vol. 18, pp. 661-678, 24 January 1986, 1986.

Jaisser, F., "Inducible gene expression and gene modification in transgenic mice," J Am Soc Nephrol, vol. 11 Suppl 16, pp. S95-s100, Nov, 2000.

Johnson, R.W.; Finger, E.C.; Olcina, M.M.; Vilalta, M.; Aguilera, T.; Miao, Y.; Merkel, A.R.; Johnson, J.R.; Sterling, J.A.; Wu, J.Y.; Giaccia, A.J., "Induction of LIFR confers a dormancy phenotype in breast cancer cells disseminated to the bone marrow," Nat Cell Biol, vol. 18, no. 10, pp. 1078-1089, Sep 19, 2016.

Jones, S.P.; Girod, W.G.; Palazzo, A.J.; Granger, D.N.; Grisham, M.B.; Jourd'Heuil, D.; Huang, P.L.; Lefer, D.J., "Myocardial ischemia-reperfusion injury is exacerbated in absence of endothelial cell nitric oxide synthase," Am J Physiol, vol. 276, no. 5, pp. H1567-73, May, 1999.

Jopling, C.; Boue, S.; Izpisua Belmonte, J.C., "Dedifferentiation, transdifferentiation and reprogramming: three routes to regeneration," Nat Rev Mol Cell Biol, vol. 12, no. 2, pp. 79-89, Feb, 2011.

Jordan, J.E.; Zhao, Z.-Q.; Vinten-Johansen, J., "The role of neutrophils in myocardial ischemia–reperfusion injury," Cardiovascular Research vol. 43, pp. 860–878, 1999.

Kanda, M.; Nagai, T.; Takahashi, T.; Liu, M.L.; Kondou, N.; Naito, A. T.; Akazawa, H.; Sashida, G.; Iwama, A.; Komuro, I.; Kobayashi, Y., "Leukemia Inhibitory Factor Enhances Endogenous Cardiomyocyte Regeneration after Myocardial Infarction," PLoS One, vol. 11, no. 5, pp. e0156562, 2016.

Kaur, H.; Takefuji, M.; Ngai, C.Y.; Carvalho, J.; Bayer, J.; Wietelmann, A.; Poetsch, A.; Hoelper, S.; Conway, S.J.; Mollmann, H.; Looso, M.; Troidl, C.; Offermanns, S.; Wettschureck, N., "Targeted Ablation of Periostin-Expressing Activated Fibroblasts Prevents Adverse Cardiac Remodeling in Mice," Circ Res, vol. 118, no. 12, pp. 1906-17, Jun 10, 2016.

Kessler-Icekson, G.; Sperling,O.; Rotem, C.; Wasserman, L., “Cardiomyocytes Cultured in Serum-free Medium - Growth and Creatine Kinase Activity,” Experimental Cell Research, vol. 155 pp. 113-120, 1984.

Kiernan, J.A.; Wessendorf, M.,"Autofluorescence: Causes and Cures ", Wright Cell Imaging Facility, Toronto Western Reserach Institute, University Health Network, 2014.

Kilbey, A.; Terry, A.; Jenkins, A.; Borland, G.; Zhang, Q.; Wakelam, M.J.; Cameron, E.R.; Neil, J.C., “Runx regulation of sphingolipid metabolism and survival signaling,” Cancer Res, vol. 70, no. 14, pp. 5860-9, Jul 15, 2010.

Kinnunen, S.M.; Tolli, M.; Valimaki, M.J.; Gao, E.; Szabo, Z.; Rysa, J.; Ferreira, M.P.A.; Ohukainen, P.; Serpi, R.; Correia, A.; Makila, E.; Salonen, J.; Hirvonen, J.; Santos, H.A.; Ruskoaho, H., “Cardiac Actions of a Small Molecule Inhibitor Targeting GATA4-NKX2-5 Interaction,” Sci Rep, vol. 8, no. 1, pp. 4611, Mar 15, 2018.

Kloner, R.A.; Przyklenk, K.; Whittaker, P., “Deleterious Effects of Oxygen Radicals in Ischemia/Reperfusion - Resolved and Unresolved Issues,” Circulation, vol. 80, no. 5, pp. 1115-1127, November 1989, 1989.

Knight, A.W.; Billinton, N., “Distinguishing GFP from Cellular Autofluorescence,” Biophotonics International, vol. 8, no. 42, 2001.

Kohli, S.; Ahuja, S.; Rani, V., “Transcription Factors in Heart: Promising Therapeutic Targets in Cardiac Hypertrophy,” Current Cardiology Reviews, vol. 7, pp. 262-271, 2011.

Koth, J.; Wang, X.; Killen, A.C.; Stockdale, W.T.; Potts, H.G.; Jefferson, A.; Bonkhofer, F.; Riley, P.R.; Patient, R.; Göttgens, B.; Mommersteeg, M.T.M., "Runx1 promotes scar deposition and inhibits myocardial proliferation and survival during zebrafish heart regeneration," bioRxi,pp. 1-24, Oct, 2019.

Krestel, H.E.; Mayford, M.R.; Seeburg, P.H.; Sprengel, R., “A GFP-equipped bidirectional expression module well suited formonitoring tetracycline-regulated gene expression in mouse,” Nucleic Acids Research, vol. 29, no. 7e39, 2001.

Kretzschmar, K.; Post, Y.; Bannier-Helaouet, M.; Mattiotti, A.; Drost, J.; Basak, O.; Li, V.S.W.; van den Born, M.; Gunst, Q.D.; Versteeg, D.; Kooijman, L.; van der Elst, S.; van Es, J.H.; van Rooij, E.; van den Hoff, M.J.B.; Clevers, H., “Profiling proliferative cells and their progeny in damaged murine hearts,” Proc Natl Acad Sci U S A, vol. 115, no. 52, pp. E12245-E12254, Dec 26, 2018.

Krupp, M.; Marquardt, J.U.; Sahin, U.; Galle, P.R.; Castle, J.; Teufel, A., “RNA-Seq Atlas—a reference database for gene expression profiling in normal tissue by next-generation sequencing,” Bioinformatics, vol. 28, no. 8, pp. 1184-1185, 2012.

Kubin, T.; Pöling, J.; Kostin, S.; Gajawada, P.; Hein, S.; Rees, W.; Wietelmann, A.; Tanaka, M.; Lörchner, H.; Schimanski, S.; Szibor, M.; Warnecke, H.; Braun, T., "Oncostatin M is a major mediator of cardiomyocyte dedifferentiation and remodeling," Cell Stem Cell, vol. 9, no. 5, pp. 420-32, Nov 04, 2011.

Kuenne, C.; Günther, S.; Looso, M.; Zhang, T.; Krueger, M.; Zhou, Y.; Braun, T.; Kim, J., "RNA-Seq analysis of isolated satellite cells in Prmt5 deficient mice," Genom Data, vol. 5, pp. 122-5, Sep, 2015.

Lai, Y.; Li, D.; Li, C.; Muehleisen, B.; Radek, K.A.; Park, H.J.; Jiang, Z.; Li, Z.; Lei, H.; Quan, Y.; Zhang, T.; Wu, Y.; Kotol, P.; Morizane, S.; Hata, T.R.; Iwatsuki, K.; Tang, C.; Gallo, R. L., "The antimicrobial protein REG3A regulates keratinocyte proliferation and differentiation after skin injury," Immunity, vol. 37, no. 1, pp. 74-84, Jul 27, 2012.

Lajiness, J.D.; Conway, S.J., "Origin, development, and differentiation of cardiac fibroblasts," J Mol Cell Cardiol, vol. 70, pp. 2-8, May, 2014.

Larcher, V.; Kunderfranco, P.; Vacchiano, M.; Carullo, P.; Erreni, M.; Salamon, I.; Colombo, F.S.; Lugli, E.; Mazzola, M.; Anselmo, A.; Condorelli, G., "An autofluorescence-based method for the isolation of highly purified ventricular cardiomyocytes," Cardiovasc Res, vol. 114, no. 3, pp. 409-416, Mar 1, 2018.

Laue, M., "Electron microscopy of viruses," Methods Cell Biol, vol. 96, pp. 1-20, 2010.

Lee, P.Y.; Costumbrado, J.; Hsu, C.Y.; Kim, Y.H., "Agarose gel electrophoresis for the separation of DNA fragments," J Vis Exp, no. 62, Apr 20, 2012.

Leri, A.; Rota, M.; Pasqualini, F.S.; Goichberg, P.; Anversa, P., "Origin of cardiomyocytes in the adult heart," Circ Res, vol. 116, no. 1, pp. 150-66, Jan 2, 2015.

Levanon, D.; Brenner, O.; Negreanu, V.; Bettoun, D.; Woolf, E.; Eilam, R.; Lotem, J.; Gat, U.; Otto, F.; Speck, N.; Groner, Y., "Spatial and temporal expression pattern of Runx3 (Aml2) and Runx1 (Aml1) indicates non-redundant functions during mouse embryogenesis," Mechanisms of Development, vol. 109, no. 2, pp. 413-417, 2001/12/01/, 2001.

Levanon, D.; Brenner, O.; Otto, F.; Groner, Y., "Runx3 knockouts and stomach cancer," EMBO Rep, vol. 4, no. 6, pp. 560-4, Jun, 2003.

Levanon, D.; Groner, Y., "Structure and regulated expression of mammalian RUNX genes," Oncogene, vol. 23, no. 24, pp. 4211-9, May 24, 2004.

Li, D.; Sinha, K.K.; Hay, M.A.; Rinaldi, C.R.; Sauntharajah, Y.; Nucifora, G., "RUNX1-RUNX1 homodimerization modulates RUNX1 activity and function," J Biol Chem, vol. 282, no. 18, pp. 13542-51, May 4, 2007.

Li, D.; Wu, J.; Bai, Y.; Zhao, X.; Liu, L., “Isolation and culture of adult mouse cardiomyocytes for cell signaling and in vitro cardiac hypertrophy,” J Vis Exp, no. 87, May 21, 2014.

Li, R.K.; Tumiati, L.C.; Weisel, R.D.; Mickle, D.A.G., “Isolation of cardiomyocytes from human myocardium for primary cell culturing,” Journal of tissue culture methods, vol. 15, no. 3, pp. 147-154, 1993/09/01, 1993.

Li, Z.; Solomonidis, E.G.; Meloni, M.; Taylor, R.S.; Duffin, R.; Dobie, R.; Magalhaes, M.S.; Henderson, B.E.P.; Louwe, P.A.; D'Amico, G.; Hodivala-Dilke, K.M.; Shah, A.M.; Mills, N.L.; Simons, B.D.; Gray, G.A.; Henderson, N.C.; Baker, A.H.; Brittan, M., “Single-cell transcriptome analyses reveal novel targets modulating cardiac neovascularization by resident endothelial cells following myocardial infarction,” Eur Heart J, Jun 4, 2019.

Li, Z.; Song, W.J.; Gilliland, G.; Speck, N., "A new floxed allele of Runx1 " Z. S. Li, W.J.; Gilliland, G.; Speck, N., ed., MGI Direct Data Submission, 2004.

Lian, J.B.; Balint, E.; Javed, A.; Drissi, H.; Vitti, R.; Quinlan, E.J.; Zhang, L.; Van Wijnen, A.J.; Stein, J.L.; Speck, N.; Stein, G.S., “Runx1/AML1 hematopoietic transcription factor contributes to skeletal development in vivo,” J Cell Physiol, vol. 196, no. 2, pp. 301-11, Aug, 2003.

Lian, J.B.; Javed, A.; Zaidi, S.K.; Lengner, C.; Montecino, M.; van Wijnen, A.J.; Stein, J.L.; Stein, G.S. (2004). "Regulatory controls for osteoblast growth and differentiation: role of Runx/Cbfa/AML factors." Crit Rev Eukaryot Gene Expr 14(1-2): 1-41.

Liao, Y.; Smyth, G.K.; Shi, W., “featureCounts: an efficient general purpose program for assigning sequence reads to genomic features,” Bioinformatics, vol. 30, no. 7, pp. 923-30, Apr 1, 2014.

Lighthouse, J.K.; Small, E.M., “Transcriptional control of cardiac fibroblast plasticity,” J Mol Cell Cardiol, vol. 91, pp. 52-60, Feb, 2016.

Lörchner, H.; Pöling, J.; Gajawada, P.; Hou, Y.; Polyakova, V.; Kostin, S.; Adrian-Segarra, J. M.; Boettger, T.; Wietelmann, A.; Warnecke, H.; Richter, M.; Kubin, T.; Braun, T., “Myocardial healing requires Reg3beta-dependent accumulation of macrophages in the ischemic heart,” Nat Med, vol. 21, no. 4, pp. 353-62, Apr, 2015.

Louch, W.E.; Sheehan, K.A.; Wolska, B.M., “Methods in cardiomyocyte isolation, culture, and gene transfer,” J Mol Cell Cardiol, vol. 51, no. 3, pp. 288-98, Sep, 2011.

Lowry, O.H.; Rosebrough, N.J.; Farr, A.L.; Randall, R.J., “Protein measurement with the Folin phenol reagent,” J Biol Chem, vol. 193, no. 1, pp. 265-75, Nov, 1951.

Luche, H.; Weber, O.;Nageswara Rao, T.; Blum, C.; Fehling, H.J., “Faithful activation of an extra-bright red fluorescent protein in "knock-in" Cre-reporter mice ideally suited for lineage tracing studies,” Eur J Immunol, vol. 37, no. 1, pp. 43-53, Jan, 2007.

Lukacs, E.; Magyari, B.; Toth, L.; Petrasi, Z.; Repa, I.; Koller, A.; Horvath, I., "Overview of large animal myocardial infarction models (review)," Acta Physiol Hung, vol. 99, no. 4, pp. 365-81, Dec, 2012.

Luo, M.C.; Zhou, S.Y.; Feng, D.Y.; Xiao, J.; Li, W.Y.; Xu, C.D.; Wang, H.Y.; Zhou, T., "Runt-related Transcription Factor 1 (RUNX1) Binds to p50 in Macrophages and Enhances TLR4-triggered Inflammation and Septic Shock," J Biol Chem, vol. 291, no. 42, pp. 22011-22020, Oct 14, 2016.

Lutgens, E.; Daemen, M.J.; de Muinck, E.D.; Debets, J.; Leenders, P.; Smits, J.F., "Chronic myocardial infarction in the mouse: cardiac structural and functional changes," Cardiovasc Res, vol. 41, no. 3, pp. 586-93, Mar, 1999.

Mann, D.L.; Felker, G.M., "Heart Failure: A Companion to Braunwald's Heart Disease, 3rd Edition," pp. 784, 10 Feb 2015, 2016.

Marriott, I.; Gray, D.L.; Rati, D.M.; Fowler, V.G., Jr.; Stryjewski, M.E.; Levin, L.S.; Hudson, M.C.; Bost, K.L., "Osteoblasts produce monocyte chemoattractant protein-1 in a murine model of Staphylococcus aureus osteomyelitis and infected human bone tissue," Bone, vol. 37, no. 4, pp. 504-12, Oct, 2005.

Maruyama, S.; Nakamura, K.; Papanicolaou, K.N.; Sano, S.; Shimizu, I.; Asaumi, Y.; van den Hoff, M.J.; Ouchi, N.; Recchia, F.A.; Walsh, K., "Follistatin-like 1 promotes cardiac fibroblast activation and protects the heart from rupture," EMBO Mol Med, vol. 8, no. 8, pp. 949-66, Aug, 2016.

Mateti, U.; Rajakannan, T.; Nekkanti, H.; Rajesh, V.; Mallaysamy, S.; Ramachandran, P., "Drug-drug interactions in hospitalized cardiac patients," J Young Pharm, vol. 3, no. 4, pp. 329-33, Oct, 2011.

Mbogo, G.W.; Nedeva, C.; Puthalakath, H., "Isolation of Cardiomyocytes and Cardiofibroblasts for Ex Vivo Analysis," Programmed Cell Death: Methods and Protocols, H. Puthalakath and C. J. Hawkins, eds., pp. 117-129, New York, NY: Springer New York, 2016.

McCarroll, C.S.; He, W.; Foote, K.; Bradley, A.; McGlynn, K.; Vidler, F.; Nixon, C.; Nather, K.; Fattah, C.; Riddell, A.; Bowman, P.; Elliott, E.B.; Bell, M.; Hawksby, C.; MacKenzie, S.M.; Morrison, L.J.; Terry, A.; Blyth, K.; Smith, G.L.; McBride, M.W.; Kubin, T.; Braun, T.; Nicklin, S.A.; Cameron, E.R.; Loughrey, C.M., "Runx1 Deficiency Protects Against Adverse Cardiac Remodeling After Myocardial Infarction," Circulation, vol. 137, no. 1, pp. 57-70, Jan 2, 2018.

McCarroll, C.S.; He, W.; Foote, K.K.; Nather, K.; Fattah, C.; Elliott, E.B.A.; Cochrane, A.; Bowman, P.; Bell, M.; Kubin, T.; Braun, T.; Nicklin, S.A.; Cameron, E.R.; Loughrey, C.M., "Runx1 Deficiency Protects against Adverse Cardiac Remodelling Following Myocardial Infarction," Heart, vol. 101, no. Suppl 6, pp. A3-A3, Nov, 2015.

McClatchey, A. I., "ERM proteins at a glance," J Cell Sci, vol. 127, no. Pt 15, pp. 3199-204, Aug 1, 2014.

Mevel, R.; Draper, J.E.; Lie, A. Ling M.; Kouskoff, V.; Lacaud, G., "RUNX transcription factors: orchestrators of development," Development, vol. 146, no. 17, Sep 5, 2019.

Meyer, G.P.; Wollert, K.C.; Lotz, J.; Steffens, J.; Lippolt, P.; Fichtner, S.; Hecker, H.; Schaefer, A.; Arseniev, L.; Hertenstein, B.; Ganser, A.; Drexler, H., "Intracoronary bone marrow cell transfer after myocardial infarction: eighteen months' follow-up data from the randomized, controlled BOOST (BOne marrOw transfer to enhance ST-elevation infarct regeneration) trial," Circulation, vol. 113, no. 10, pp. 1287-94, Mar 14, 2006.

Michel, G.; Yu, Y.; Chang, T.; Yee, J.K., "Site-specific gene insertion mediated by a Cre-loxP-carrying lentiviral vector," Mol Ther, vol. 18, no. 10, pp. 1814-21, Oct, 2010.

Miljkovic-Licina, M.; Hammel, P.; Garrido-Urbani, S.; Bradfield, P.F.; Szepetowski, P.; Imhof, B.A., "Sushi repeat protein X-linked 2, a novel mediator of angiogenesis," The FASEB Journal, vol. 23, no. 12, pp. 4105-4116, 2009.

Mitcheson, J.S.; Hancox, J.C.; Levi, A.J., "Cultured adult cardiac myocytes: Future applications, culture methods, morphological and electrophysiological properties," Cardiovascular Research, vol. 39 pp. 280–300, 1998.

Miyawaki, A.; Mitsuhara, Y.; Orimoto, A.; Nakayasu, Y.; Tsunoda, S.; Obana, M.; Maeda, M.; Nakayama, H.; Yoshioka, Y.; Tsutsumi, Y.; Fujio, Y., "Moesin is activated in cardiomyocytes in experimental autoimmune myocarditis and mediates cytoskeletal reorganization with protrusion formation," Am J Physiol Heart Circ Physiol, vol. 311, no. 2, pp. H476-86, Aug 1, 2016.

Mohamed, S.N.W.; Holmes, R.; Hartzell, C.R., "A serum-free, chemically-defined medium for function and growth of primary neonatal rat heart cell cultures," J In Vitro, vol. 19, no. 6, pp. 471-478, June 01, 1983.

Murphy, E.; Steenbergen, C., "Mechanisms underlying acute protection from cardiac ischemia-reperfusion injury," Physiol Rev, vol. 88, no. 2, pp. 581-609, Apr, 2008.

Murry, C.E.; Jennings, R.B.; Reimer, K.A., "Preconditioning with ischemia: a delay of lethal cell injury in ischemic myocardium," Circulation, vol. 74 no. 5, pp. 1124-1136, November 1986, 1986.

Myers, R.W.; Pearlman, A.S.; Hyman, R.M.; Goldstein, R.A.; Kent, K.M.; Goldstein, R.E.; Epstein, S.E., "Beneficial Effects of Vagal Stimulation and Bradyeardia During Experimental Acute Myocardial Ischemia," Circulation, vol. XLIX, pp. 943-947, May 1974, 1974.

Mylonas, K.J.; Turner, N.A.; Bageghni, S.A.; Kenyon, C.J.; White, C.I.; McGregor, K.; Kimmitt, R.A.; Sulston, R.; Kelly, V.; Walker, B.R.; Porter, K.E.; Chapman, K.E.; Gray, G.A., "11beta-HSD1 suppresses cardiac fibroblast CXCL2, CXCL5 and neutrophil recruitment to the heart post MI," J Endocrinol, vol. 233, no. 3, pp. 315-327, Jun, 2017.

Nagahama, K.Y.; Togo, S.; Holz, O.; Magnussen, H.; Liu, X.; Seyama, K.; Takahashi, K.; Rennard, S.I., "Oncostatin M modulates fibroblast function via signal transducers and activators of transcription proteins-3," Am J Respir Cell Mol Biol, vol. 49, no. 4, pp. 582-91, Oct, 2013.

Nahrendorf, M.; Pittet, M.J.; Swirski, F.K., “Monocytes: protagonists of infarct inflammation and repair after myocardial infarction,” Circulation, vol. 121, no. 22, pp. 2437-45, Jun 8, 2010.

Nakagawa, M.; Takemura, G.; Kanamori, H.; Goto, K.; Maruyama, R.; Tsujimoto, A.; Ohno, T.; Okada, H.; Ogino, A.; Esaki, M.; Miyata, S.; Li, L.; Ushikoshi, H.; Aoyama, T.; Kawasaki, M.; Nagashima, K.; Fujiwara, T.; Minatoguchi, S.; Fujiwara, H., “Mechanisms by which late coronary reperfusion mitigates postinfarction cardiac remodeling,” Circ Res, vol. 103, no. 1, pp. 98-106, Jul 3, 2008.

Nelson, M.R.; Wegmann, D.; Ehm, M.G.; Kessner, D.; Jean, P.St.; Verzilli, C.; Shen, J.; Tang, Z.; Bacanu, S.-A.; Fraser, D.; Warren, L.; Aponte, J.; Zawistowski, M.; Liu, X.; Zhang, H.; Zhang, Y.; Li, J.; Li, Y.; Li, L.; Woollard, P.; Topp, S.; Hall, M.D.; Nangle, K.; Wang, J.; Abecasis, G.; Cardon, L.R.; Zöllner, S.; Whittaker, J.C.; Chissoe, S.L.; Novembre, J.; Mooser, V., “An abundance of rare functional variants in 202 drug target genes sequenced in 14.002 people. ,” Science, vol. 337, pp. 100-104, 2012.

Neri, M.; Riezzo, I.; Pascale, N.; Pomara, C.; Turillazzi, E., “Ischemia/Reperfusion Injury following Acute Myocardial Infarction: A Critical Issue for Clinicians and Forensic Pathologists,” Mediators Inflamm, vol. 2017, pp. 7018393, 2017.

Nippert, F.; Schreckenberg, R.; Schluter, K.D., “Isolation and Cultivation of Adult Rat Cardiomyocytes,” J Vis Exp, no. 128, Oct 19, 2017.

Nolan, P.E., Jr.; Marcus, F.I., “Cardiovascular Drug Use in the Elderly,” Am J Geriatr Cardiol, vol. 9, no. 3, pp. 127-129, May, 2000.

O’Connell, T.D.; Rodrigo, M.C.; Simpson, P.C., "Isolation and Culture of Adult Mouse Cardiac Myocytes," Cardiovascular Proteomics: Methods and Protocols, F. Vivanco, ed., pp. 271-296, Totowa, NJ: Humana Press, 2007.

OECD, “Health at a Glance 2019: OECD indicators,” OECD Publishing, Paris, https://doi.org/10.1787/4dd50c09-en, 2019.

Oh-McGinnis, R.; Jones, M.J.; Lefebvre, L., “Applications of the site-specific recombinase Cre to the study of genomic imprinting,” Brief Funct Genomics, vol. 9, no. 4, pp. 281-93, Jul, 2010.

Okada, H.; Watanabe, T.; Niki, M.; Takano, H.; Chiba, N.; Yanai, N.; Tani, K.; Hibino, H.; Asano, S.; Mucenski, M. L.; Ito, Y.; Noda, T.; Satake, M., “AML1(-/-) embryos do not express certain hematopoiesis-related gene transcripts including those of the PU.1 gene,” Oncogene, vol. 17, no. 18, pp. 2287-93, Nov 5, 1998.

Okuda, T.; v. Deursen, J.; Hiebert, S.W.; Grosveld, G.; Downing, J.R., “AML1, the Target of Multiple Chromosomal Translocations in Human Leukemia, Is Essential for Normal Fetal Liver Hematopoiesis,” Cell, vol. 84, pp. 321–330, 1996.

Olivetti, G.; Capasso, J.M.; Sonnenblick, E.H.; Anversa, P., "Side-to-side slippage of myocytes participates in ventricular wall remodeling acutely after myocardial infarction in rats," Circ Res, vol. 67, no. 1, pp. 23-34, Jul, 1990.

Oshima, Y.; Ouchi, N.; Sato, K.; Izumiya, Y.; Pimentel, D.R.; Walsh, K., "Follistatin-like 1 is an Akt-regulated cardioprotective factor that is secreted by the heart," Circulation, vol. 117, no. 24, pp. 3099-108, Jun 17, 2008.

Pell, V.R.; Chouchani, E.T.; Frezza, C.; Murphy, M.P.; Krieg, T., "Succinate metabolism: a new therapeutic target for myocardial reperfusion injury," Cardiovasc Res, vol. 111, no. 2, pp. 134-41, Jul 15, 2016.

Perrino, C.; Barabasi, A.L.; Condorelli, G.; Davidson, S.M.; De Windt, L.; Dimmeler, S.; Engel, F.B.; Hausenloy, D.J.; Hill, J.A.; Van Laake, L.W.; Lecour, S.; Leor, J.; Madonna, R.; Mayr, M.; Prunier, F.; Sluijter, J.P.G.; Schulz, R.; Thum, T.; Ytrehus, K.; Ferdinandy, P., "Epigenomic and transcriptomic approaches in the post-genomic era: path to novel targets for diagnosis and therapy of the ischaemic heart? Position Paper of the European Society of Cardiology Working Group on Cellular Biology of the Heart," Cardiovasc Res, vol. 113, no. 7, pp. 725-736, Jun 1, 2017.

Perrino, C.; Naga Prasad, S.V.; Mao, L.; Noma, T.; Yan, Z.; Kim, H.S.; Smithies, O.; Rockman, H.A., "Intermittent pressure overload triggers hypertrophy-independent cardiac dysfunction and vascular rarefaction," J Clin Invest, vol. 116, no. 6, pp. 1547-60, Jun, 2006.

Peters, S.R., "The Art of Embedding Tissue for Frozen Section. Part I: A System for Precision Face Down Cryoembedding of Tissues Using Freezing Temperature-Embedding Wells," Journal of Histotechnology, vol. 26, no. 1, pp. 11-19, 2003/03/01, 2003.

Peters, S.R., "The Art of Embedding Tissue for Frozen Section. Part II: Frozen Block Cryoembedding," Journal of Histotechnology, vol. 26, no. 1, pp. 23-28, 2003/03/01, 2003.

Pinto, A.R.; Ilinykh, A.; Ivey, M.J.; Kuwabara, J.T.; D'Antoni, M.L.; Debuque, R.; Chandran, A.; Wang, L.; Arora, K.; Rosenthal, N.A.; Tallquist, M.D., "Revisiting Cardiac Cellular Composition," Circ Res, vol. 118, no. 3, pp. 400-9, Feb 5, 2016.

Piper, H.M.; Garcña-Dorado, D.; Ovize, M., "A fresh look at reperfusion injury1," Cardiovascular Research, vol. 38, no. 2, pp. 291-300, 1998.

Pivarcsi, A.; Szell, M.; Kemeny, L.; Dobozy, A.; Bata-Csorgo, Z., "Serum factors regulate the expression of the proliferation-related genes alpha5 integrin and keratin 1, but not keratin 10, in HaCaT keratinocytes," Arch Dermatol Res, vol. 293, no. 4, pp. 206-13, Apr, 2001.

Pöling, J.; Gajawada, P.; Lörchner, H.; Polyakova, V.; Szibor, M.; Böttger, T.; Warnecke, H.; Kubin, T.; Braun, T., "The Janus face of OSM-mediated cardiomyocyte dedifferentiation during cardiac repair and disease," Cell Cycle, vol. 11, no. 3, pp. 439-45, Feb 01, 2012.

Ponten, A.; Walsh, S.; Malan, D.; Xian, X.; Scheele, S.; Tarnawski, L.; Fleischmann, B.K.; Jovinge, S., "FACS-based isolation, propagation and characterization of mouse embryonic cardiomyocytes based on VCAM-1 surface marker expression," PLoS One, vol. 8, no. 12, pp. e82403, 2013.

Portbury, A.L.; Willis, M.S.; Patterson, C., "Tearin' up my heart: proteolysis in the cardiac sarcomere," J Biol Chem, vol. 286, no. 12, pp. 9929-34, Mar 25, 2011.

Poss, K.D., "Advances in understanding tissue regenerative capacity and mechanisms in animals," Nat Rev Genet, vol. 11, no. 10, pp. 710-22, Oct, 2010.

Prabhu, S.D.; Frangogiannis, N.G., "The Biological Basis for Cardiac Repair After Myocardial Infarction: From Inflammation to Fibrosis," Circ Res, vol. 119, no. 1, pp. 91-112, Jun 24, 2016.

Progatzky, F.; Dallman, M.J.; Lo Celso, C., "From seeing to believing: labelling strategies for in vivo cell-tracking experiments," Interface Focus, vol. 3, no. 3, pp. 20130001, Jun 6, 2013.

Pugach, E.K.; Richmond, P.A.; Azofeifa, J.G.; Dowell, R.D.; Leinwand, L.A., "Prolonged Cre expression driven by the alpha-myosin heavy chain promoter can be cardiotoxic," J Mol Cell Cardiol, vol. 86, pp. 54-61, Sep, 2015.

Puri, S.; Folias, A.E.; Hebrok, M., "Plasticity and dedifferentiation within the pancreas: development, homeostasis, and disease," Cell Stem Cell, vol. 16, no. 1, pp. 18-31, Jan 8, 2015.

Qadi, A.A.; Taberlay, P.C.; Phillips, J.L.; Young, A.; West, A.C.; Brettingham-Moore, K.H.; Dickinson, J.L.; Holloway, A.F., "The Leukemia Inhibitory Factor Receptor Gene Is a Direct Target of RUNX1," J Cell Biochem, vol. 117, no. 1, pp. 49-58, Jan, 2016.

QIAGEN, miRNeasy Micro Handbook: QIAGEN, 2012.

Quaife-Ryan, G.A.; Sim, C.B.; Ziemann, M.; Kaspi, A.; Rafehi, H.; Ramialison, M.; El-Osta, A.; Hudson, J.E.; Porrello, E.R., "Multicellular Transcriptional Analysis of Mammalian Heart Regeneration," Circulation, vol. 136, no. 12, pp. 1123-1139, Sep 19, 2017.

Redfors, B.; Shao, Y.; Omerovic, E., "Myocardial infarct size and area at risk assessment in mice," Exp Clin Cardiol, vol. 17, no. 4, pp. 268-272, 2012.

Reimer, L., "Ultramikrotomie," Elektronenmikroskopische Untersuchungs- und Präparationsmethoden, pp. 260-275, Berlin, Heidelberg: Springer Berlin Heidelberg, 1959.

Richards, C.D., "The enigmatic cytokine oncostatin m and roles in disease," ISRN Inflamm, vol. 2013, pp. 512103, 29 September 2013, 2013.

Richards, C.D.; Shoyab, M.; Brown, T.J.; Gauldie, J., "Selective regulation of metalloproteinase inhibitor (TIMP-1) by oncostatin M in fibroblasts in culture," The Journal of Immunology, vol. 150, no. 12, pp. 5596, 1993.

Rodriguez, C.I.; Buchholz, F.; Galloway, J.; Sequerra, R.; Kasper, J.; Ayala, R.; Stewart, A.F.; Dymecki, S.M., "High-efficiency deleter mice show that FLPe is an alternative to Cre-loxP," Nat Genet, vol. 25, no. 2, pp. 139-40, Jun, 2000.

Royer-Zemmour, B.; Ponsole-Lenfant, M.; Gara, H.; Roll, P.; Leveque, C.; Massacrier, A.; Ferracci, G.; Cillario, J.; Robaglia-Schlupp, A.; Vincentelli, R.; Cau, P.; Szepetowski, P., "Epileptic and developmental disorders of the speech cortex: ligand/receptor interaction of wild-type and mutant SRPX2 with the plasminogen activator receptor uPAR," Hum Mol Genet, vol. 17, no. 23, pp. 3617-30, Dec 1, 2008.

Rücker-Martin, C.; Pecker, F.; Godreau, D.; Hatem, S.N., "Dedifferentiation of atrial myocytes during atrial fibrillation: role of fibroblast proliferation in vitro," Cardiovascular Research, vol. 55, pp. 38-52, 2002.

Ruiz-Meana, M.; Garcia-Dorado, D.;Pina, P.; Inserte, J.; Agullo, L.; Soler-Soler, J., "Cariporide preserves mitochondrial proton gradient and delays ATP depletion in cardiomyocytes during ischemic conditions," Am J Physiol Heart Circ Physiol, vol. 285, no. 3, pp. H999-1006, Sep, 2003.

Ruzicka, D.L.; Schwartz, R.J., "Sequential activation of alpha-actin genes during avian cardiogenesis: vascular smooth muscle alpha-actin gene transcripts mark the onset of cardiomyocyte differentiation," J Cell Biol, vol. 107, no. 6 Pt 2, pp. 2575-2586, 1988.

Saiki, R.K.; Gelfand, D.H.; Stoffel, S.; Scharf, S.J.; Higuchi, R.; Horn, G.T.; Mullis, K.B.; Erlich, H.A., "Primer-directed enzymatic amplification of DNA with a thermostable DNA polymerase," vol. 239, no. 4839, pp. 487-491, 1988.

Salwig, I.; Spitznagel, B.; Vazquez-Armendariz, A. I.; Khalooghi, K.; Guenther, S.; Herold, S.; Szibor, M.; Braun, T., "Bronchioalveolar stem cells are a main source for regeneration of distal lung epithelia in vivo," EMBO J, vol. 38, no. 12, Jun 17, 2019.

Sanchez-Iranzo, H.; Galardi-Castilla, M.; Minguillon, C.; Sanz-Morejon, A.; Gonzalez-Rosa, J.M.; Felker, A.; Ernst, A.; Guzman-Martinez, G.; Mosimann, C.; Mercader, N., "Tbx5a lineage tracing shows cardiomyocyte plasticity during zebrafish heart regeneration," Nat Commun, vol. 9, no. 1, pp. 428, Jan 30, 2018.

Saxena, A.; Russo, I.; Frangogiannis, N.G., "Inflammation as a therapeutic target in myocardial infarction: learning from past failures to meet future challenges," Transl Res, vol. 167, no. 1, pp. 152-66, Jan, 2016.

Scaffidi, A.K.; Mutsaers, S.E.; Moodley, Y.P.; McAnulty, R.J.; Laurent, G.J.; Thompson, P.J.; Knight, D.A., "Oncostatin M stimulates proliferation, induces collagen production and inhibits apoptosis of human lung fibroblasts," British Journal of Pharmacology, vol. 136, 2002.

Schächinger, V.; Erbs, S.; Elsässer, A.; Haberbosch, W.; Hambrecht, R.; Hölschermann, H.; Yu, J.; Corti, R.; Mathey, D.G.; Hamm, C.W.; Süselbeck, T.; Assmus, B.; Tonn, T.; Dimmeler, S.; Zeiher, A.M.,

"Intracoronary Bone Marrow–Derived Progenitor Cells in Acute Myocardial Infarction " N Engl J Med, vol. 355, pp. 1210-21, 2006.

Schägger, H.; von Jagow, G., "Tricine-sodium dodecyl sulfate-polyacrylamide gel electrophoresis for the separation of proteins in the range from 1 to 100 kDa," Analytical Biochemistry, vol. 166, no. 2, pp. 368-379, 1987/11/01/, 1987.

Schönig, K.; Schwenk, F.; Rajewsky, K.; Bujard, H., "Stringent doxycycline dependent control of CRE recombinase in vivo," Nucleic Acids Research, vol. 30, no. 23e134, 2002.

Sitte, H., Ultramikrotomie - Häufige Probleme und Fehler, Universität des Saarlandes, Medizinische Fakultät, 1982.

Skelly, D.A.; Squiers, G.T.; McLellan, M.A.; Bolisetty, M.T.; Robson, P.; Rosenthal, N.A.; Pinto, A.R., "Single-Cell Transcriptional Profiling Reveals Cellular Diversity and Intercommunication in the Mouse Heart," Cell Rep, vol. 22, no. 3, pp. 600-610, Jan 16, 2018.

Skrzypiec-Spring, M.; Grotthus, B.; Szelag, A.; Schulz, R., "Isolated heart perfusion according to Langendorff---still viable in the new millennium," J Pharmacol Toxicol Methods, vol. 55, no. 2, pp. 113-26, Mar-Apr, 2007.

Slack, J.M.W., "Metaplasia and somatic cell reprogramming," The Journal of Pathology, vol. 217, no. 2, pp. 161-168, 2009.

Slack, J.M.W., "Origin of Stem Cells in Organogenesis," Science, vol. 322, no. 5907, pp. 1498-1501, Dec 5, 2008.

Slack, J.M.W.; Tosh, D., "Transdifferentiation and metaplasia — switching cell types," Current Opinion in Genetics & Development vol. 11, pp. 581–586, 2001.

Smith, A.J.; Lewis, F.C.; Aquila, I.; Waring, C.D.; Nocera, A.; Agosti, V.; Nadal-Ginard, B.; Torella, D.; Ellison, G.M., "Isolation and characterization of resident endogenous c-Kit+ cardiac stem cells from the adult mouse and rat heart," Nat Protoc, vol. 9, no. 7, pp. 1662-81, Jul, 2014.

Sohara, N.; Trojanowska, M; Reuben, A., "Oncostatin M stimulates tissue inhibitor of metalloproteinase-1 via a MEK-sensitive mechanism in human myofibroblast," Journal of Hepatology vol. 36 pp. 191-199, 2002.

Sokol, C.L.; Luster, A.D., "The chemokine system in innate immunity," Cold Spring Harb Perspect Biol, vol. 7, no. 5, Jan 29, 2015.

Solomon, V.; Goldberg, A.L., "Importance of the ATP-Ubiquitin-Proteasome Pathway in the Degradation of Soluble and Myofibrillar Proteins in Rabbit Muscle Extracts*," J. Biol. Chem., vol. 271, no. October, pp. 26690–26697, 1996.

Song, H.Y.; Kim, M.R.; Lee, M.J.; Jeon, E.S.; Bae, Y.C.; Jung, J.S.; Kim, J.H., "Oncostatin M decreases adiponectin expression and induces dedifferentiation of adipocytes by JAK3- and MEK-dependent pathways," The International Journal of Biochemistry & Cell Biology, vol. 39, no. 2, pp. 439-449, 2007/01/01/, 2007.

Soonpaa, M.H.; Field, L.J., "Survey of studies examining mammalian cardiomyocyte DNA synthesis," Circ Res, vol. 83, no. 1, pp. 15-26, Jul 13, 1998.

Soriano, P., "Generalized lacZ expression with the ROSA26 Cre reporter strain," Nat Genet, vol. 21, no. 1, pp. 70-71, Jan, 1999.

Spata, T.; Bobek, D.; Whitson, B.A.; Parthasarathy, S.; Mohler, P.J.; Higgins, R.S.; Kilic, A., "A nonthoracotomy myocardial infarction model in an ovine using autologous platelets," Biomed Res Int, vol. 2013, pp. 938047, 2013

Staudt, A.; Eichler, P.; Trimpert, C.; Felix, S.B.; Greinacher, A., "Fc(gamma) receptors IIa on cardiomyocytes and their potential functional relevance in dilated cardiomyopathy," J Am Coll Cardiol, vol. 49, no. 16, pp. 1684-92, Apr 24, 2007.

Sukhacheva, T.V.; Chudinovskikh, Y.A.; Eremeeva, M.V.; Serov, R.A.; Bockeria, L.A., "Proliferative Potential of Cardiomyocytes in Hypertrophic Cardiomyopathy: Correlation with Myocardial Remodeling," Bull Exp Biol Med, vol. 162, no. 1, pp. 160-169, Nov, 2016.

Szibor, M., Pöling, J.; Warnecke, H.; Kubin, T.; Braun, T., "Remodeling and dedifferentiation of adult cardiomyocytes during disease and regeneration," Cell Mol Life Sci, vol. 71, no. 10, pp. 1907-16, May, 2014.

Takagawa, J.; Zhang, Y.; Wong, M.L.; Sievers, R.E.; Kapasi, N.K.; Wang, Y.; Yeghiazarians, Y.; Lee, R.J.; Grossman, W.; Springer, M.L., "Myocardial infarct size measurement in the mouse chronic infarction model: comparison of area- and length-based approaches," J Appl Physiol (1985), vol. 102, no. 6, pp. 2104-11, Jun, 2007.

Takemura, G.; Nakagawa, M.; Kanamori, H.; Minatoguchi, S.; Fujiwara, H., "Benefits of reperfusion beyond infarct size limitation," Cardiovasc Res, vol. 83, no. 2, pp. 269-76, Jul 15, 2009.

Tang, X.; Sun, L.; Wang, G.; Chen, B.; Luo, F., "RUNX1: A Regulator of NF-kB Signaling in Pulmonary Diseases," Curr Protein Pept Sci, vol. 19, no. 2, pp. 172-178, 2018.

Taqueti, V.R.; Di Carli, M.F., "Coronary Microvascular Disease Pathogenic Mechanisms and Therapeutic Options: JACC State-of-the-Art Review," J Am Coll Cardiol, vol. 72, no. 21, pp. 2625-2641, Nov 27, 2018.

Tennessen, J.A.; Bigham, A.W.; O'Connor,T.D.; Fu, W.; Kenny, E.E.; Gravel, S.; McGee, S.; Do, R.; Liu, X.; Jun, G.; Kang, H.M.; Jordan, D.; Leal, S.M.; Gabriel, S.; Rieder, M.J.; Abecasis, G.; Altshuler, D.; Nickerson, D.A.; Boerwinkle, E.; Sunyaev, S.; Bustamante, C.D.; Bamshad, M.J.; Akey, J.M.,

"Evolution and Functional Impact of Rare Coding Variation from Deep Sequencing of Human Exomes," SCIENCE, vol. 337, no. 6090, pp. 64-69, 2012.

Thomas, S.M.; Moreno, R.F.; Tilzer, L.L., "DNA extraction with organic solvents in gel barrier tubes," Nucleic acids research, vol. 17, no. 13, pp. 5411-5411, 1989.

Toma, C.; Pittenger, M.F.; Cahill, K.S.; Byrne, B.J., Kessler, P.D., "Human Mesenchymal Stem Cells Differentiate to a Cardiomyocyte Phenotype in the Adult Murine Heart," vol. 105, no. 1, pp. 93-98, 2002.

Tosh, D.; Slack, J.M., "How cells change their phenotype," Nat Rev Mol Cell Biol, vol. 3, no. 3, pp. 187-94, Mar, 2002.

Tsang, A.; Hausenloy, D.J.; Mocanu, M.M.; Carr, R.D.; Yellon, D.M., "Preconditioning the diabetic heart: the importance of Akt phosphorylation," Diabetes, vol. 54, no. 8, pp. 2360-4, Aug, 2005.

Turan, R.D.; Aslan, G.S.; Yucel, D.; Doger, R.; Kocabas, F., "Evolving approaches to heart regeneration by therapeutic stimulation of resident cardiomyocyte cell cycle," Anatol J Cardiol, vol. 16, no. 11, pp. 881-886, Nov, 2016.

Usmani, A.; Ganguli, N.; Jain, S.K.; Ganguli, N.; Sarkar, R.K.; Choubey, M.; Shukla, M.; Sarkar, H.; Majumdar, S.S., "Robust generation of transgenic mice by simple hypotonic solution mediated delivery of transgene in testicular germ cells," Mol Ther Methods Clin Dev, vol. 3, pp. 16076, 2016.

Vidyasekar, P.; Shyamsunder, P.; Santhakumar, R.; Arun, R.; Verma, R.S., "A simplified protocol for the isolation and culture of cardiomyocytes and progenitor cells from neonatal mouse ventricles," Eur J Cell Biol, vol. 94, no. 10, pp. 444-52, Oct, 2015.

Vorhagen, S.; Jackow, J.; Mohor, S.G.; Tanghe, G.; Tanrikulu, L.; Skazik-Vogt, C.; Tellkamp, F., "Lineage tracing mediated by cre-recombinase activity," J Invest Dermatol, vol. 135, no. 1, pp. 1-4, Jan, 2015.

Wang, C.Q.; Jacob, B.; Nah, G.S.S.; Osato, M., "Runx family genes, niche, and stem cell quiescence," Blood Cells, Molecules, and Diseases, vol. 44, no. 4, pp. 275-286, 2010.

Wang, F.; Flanagan, J.; Su, N.; Wang, L.C.; Bui, S.; Nielson, A.; Wu, X.; Vo, H.T.; Ma, X.J.; Luo, Y., "RNAscope: a novel in situ RNA analysis platform for formalin-fixed, paraffin-embedded tissues," J Mol Diagn, vol. 14, no. 1, pp. 22-9, Jan, 2012.

Wang, Q.; Stacy, T.; Binder, M.; Marin-Padilla, M.; Sharpe, A.H.; Speck, N.A., "Disruption of the Cbfa2 gene causes necrosis and hemorrhaging in the central nervous system and blocks definitive hematopoiesis," Proc Natl Acad Sci U S A, vol. 93, no. 8, pp. 3444-9, Apr 16, 1996.

Wang, W.E.; Li, L.; Xia, X.; Fu, W.; Liao, Q.; Lan, C.; Yang, D.; Chen, H.; Yue, R.; Zeng, C.; Zhou, L.; Zhou, B.; Duan, D.D.; Chen, X.; Houser, S.R.; Zeng, C.;, "Dedifferentiation, Proliferation, and

Redifferentiation of Adult Mammalian Cardiomyocytes After Ischemic Injury," Circulation, vol. 136, no. 9, pp. 834-848, Aug 29, 2017.

Wei, K.; Serpooshan, V.; Hurtado, C.; Diez-Cunado, M.; Zhao, M.; Maruyama, S.; Zhu, W.; Fajardo, G.; Noseda, M.; Nakamura, K.; Tian, X.; Liu, Q.; Wang, A.; Matsuura, Y.; Bushway, P.; Cai, W.; Savchenko, A.; Mahmoudi, M.; Schneider, M. D.; van den Hoff, M. J.; Butte, M. J.; Yang, P. C.; Walsh, K.; Zhou, B.; Bernstein, D.; Mercola, M.; Ruiz-Lozano, P., "Epicardial FSTL1 reconstitution regenerates the adult mammalian heart," Nature, vol. 525, no. 7570, pp. 479-85, Sep 24, 2015.

Weiss, T.W.; Kvakan, H.; Kaun, C.; Zorn, G.; Speidl, W. S.; Pfaffenberger, S.; Maurer, G.; Huber, K.; Wojta, J., "The gp130 ligand oncostatin M regulates tissue inhibitor of metalloproteinases-1 through ERK1/2 and p38 in human adult cardiac myocytes and in human adult cardiac fibroblasts: a possible role for the gp130/gp130 ligand system in the modulation of extracellular matrix degradation in the human heart," J Mol Cell Cardiol, vol. 39, no. 3, pp. 545-51, Sep, 2005.

Wernly, B.; Mirna, M.; Rezar, R.; Prodinger, C.; Jung, C.; Podesser, B. K.; Kiss, A.; Hoppe, U.C; Lichtenauer, M., "Regenerative Cardiovascular Therapies: Stem Cells and Beyond," Int J Mol Sci, vol. 20, no. 6, Mar 21, 2019.

Wohlschlaeger, J.; Levkau, B.; Brockhoff, G.; Schmitz, K.J.; von Winterfeld, M.; Takeda, A.; Takeda, N.; Stypmann, J.; Vahlhaus, C.; Schmid, C.; Pomjanski, N.; Bocking, A.; Baba, H.A., "Hemodynamic support by left ventricular assist devices reduces cardiomyocyte DNA content in the failing human heart," Circulation, vol. 121, no. 8, pp. 989-96, Mar 2, 2010.

Xi, Y.; Gong, D.W.; Tian, Z., "FSTL1 as a Potential Mediator of Exercise-Induced Cardioprotection in Post-Myocardial Infarction Rats," Sci Rep, vol. 6, pp. 32424, Aug 26, 2016.

Xu, X.; Colecraft, H.M., "Primary Culture of Adult Rat Heart Myocytes," JoVE, no. 28, pp. e1308, 2009/06/16/, 2009.

Xu, Z.; McElhanon, K.E.; Beck, E.X.; Weisleder, N., "A Murine Model of Myocardial Ischemia–Reperfusion Injury," Traumatic and Ischemic Injury: Methods and Protocols, B. Tharakan, ed., pp. 145-153, New York, NY: Springer New York, 2018.

Xue, R.; Lei, S.; Xia, Z. Y.; Wu, Y.; Meng, Q.; Zhan, L.; Su, W.; Liu, H.; Xu, J.; Liu, Z.; Zhou, B.; Xia, Z., "Selective inhibition of PTEN preserves ischaemic post-conditioning cardioprotection in STZ-induced Type 1 diabetic rats: role of the PI3K/Akt and JAK2/STAT3 pathways," Clin Sci (Lond), vol. 130, no. 5, pp. 377-92, Mar, 2016.

Yan, J.; Liu, Y.; Lukasik, S.M.; Speck, N.A.; Bushweller, J.H., "CBFbeta allosterically regulates the Runx1 Runt domain via a dynamic conformational equilibrium," Nat Struct Mol Biol, vol. 11, no. 9, pp. 901-6, Sep, 2004.

Yang, F.; Liu, Y.-H.; Yang, X.-P.; Xu, J.; Kapke, A.; Carretero, O.A., "Myocardial infarction and cardiac remodelling in mice," Experimental Physiology, vol. 87, pp. 547-555, 2002.

Yellon, D.M.; Hausenloy, D.J., “Myocardial Reperfusion Injury,” vol. 357, no. 11, pp. 1121-1135, 2007.

Yoshimura, T.; Galligan, C.; Takahashi, M.; Chen, K.; Liu, M.; Tessarollo, L.; Wang, J.M., “Non-Myeloid Cells are Major Contributors to Innate Immune Responses via Production of Monocyte Chemoattractant Protein-1/CCL2,” Front Immunol, vol. 4, pp. 482, Jan 7, 2014.

Young, M.D.; Wakefield, M.J.; Smyth, G.K.; Oshlack, A., “Gene ontology analysis for RNA-seq: accounting for selection bias,” Genome Biology vol. 11, no. R14, pp. 1-12, 2010.

Zhao, J. M., N.; Williams, L.; Libs, L.; Avivi, Y.; Grafi, G. (2001), "Two phases of chromatin decondensation during dedifferentiation of plant cells: distinction between competence for cell fate switch and a commitment for S phase." J Biol Chem 276(25): 22772-22778.

Zhang, C.; Fu, X.; Chen, P.; Bao, X.; Li, F.; Sun, X.; Lei, Y.; Cai, S.; Sun, T.; Sheng, Z., “Dedifferentiation derived cells exhibit phenotypic and functional characteristics of epidermal stem cells,” J Cell Mol Med, vol. 14, no. 5, pp. 1135-45, May, 2010.

Zhang, M.; Li, X.; Fan, Z.; Zhao, J.; Liu, S.; Zhang, M.; Li, H.; Goscinski, M.A.; Fan, H.; Suo, Z., “High SRPX2 protein expression predicts unfavorable clinical outcome in patients with prostate cancer,” Onco Targets Ther, vol. 11, pp. 3149-3157, 2018.

Zhang, W.; Chen, C.; Liu, L.; He, Y.; Chen, Q., “Mitophagy in Cardiomyocytes and in Platelets: A Major Mechanism of Cardioprotection Against Ischemia/Reperfusion Injury,” Physiology (Bethesda), vol. 33, no. 2, pp. 86-98, Mar 1, 2018.

Zhang, Y.; Gago-Lopez, N.; Li, N.; Zhang, Z.; Alver, N.; Liu, Y.; Martinson, A.M.; Mehri, A.; MacLellan, W.R., “Single-cell imaging and transcriptomic analyses of endogenous cardiomyocyte dedifferentiation and cycling,” Cell Discov, vol. 5, pp. 30, 2019.

Zhang, Y.; Li, T.S.; Lee, S.T.; Wawrowsky, K.A.; Cheng, K.; Galang, G.; Malliaras, K.; Abraham, M.R.; Wang, C.; Marban, E., “Dedifferentiation and proliferation of mammalian cardiomyocytes,” PLoS One, vol. 5, no. 9, pp. e12559, Sep 3, 2010.

Zhou, T.; Luo, M.; Cai, W.; Zhou, S.; Feng, D.; Xu, C.; Wang, H.; , “Runt-Related Transcription Factor 1 (RUNX1) Promotes TGF-β-Induced Renal Tubular Epithelial-to-Mesenchymal Transition (EMT) and Renal Fibrosis through the PI3K Subunit p110δ,” EBioMedicine, vol. 31, pp. 217-225, 2018/05/01/, 2018.

Zhou, Y.; Richards, A.M.; Wang, P., “Characterization and Standardization of Cultured Cardiac Fibroblasts for Ex Vivo Models of Heart Fibrosis and Heart Ischemia,” Tissue Eng Part C Methods, vol. 23, no. 7, pp. 422-433, Jul, 2017.

Zuo, Y.; Li, Y.; Zhou, Z.; Ma, M.; Fu, K., “Long non-coding RNA MALAT1 promotes proliferation and invasion via targeting miR-129-5p in triple-negative breast cancer,” Biomed Pharmacother, vol. 95, pp. 922-928, Nov, 2017.

11. Attachments

The NGS data set shown here was selected according to the following criteria: counts>5, FC>5, with significant p-values (>0.05).

Gene name	Mean IZ**	Mean RZ*	FC IZ**/RZ*	p-value
Mdk	43	0	170	0.018062267
Ccl4	85	1	112.6666667	0.017355299
Trem2	53	1	105.5	1.93519E-05
Saa3	25	0	100	0.037771969
Frzb	75	1	99.66666667	0.049897149
Col8a2	75	1	99.33333333	0.045691295
Cxcl2	297	3	91.23076923	0.049911334
Gli2	22	0	88	0.012905469
Cilp	1584	23	68.86956522	0.011753545
Evpl	17	0	67	0.036340914
Lpxn	17	0	67	0.000592135
Hist1h2ai	33	1	65	0.020639112
Slc2a13	16	0	63	0.028349296
Clec4n	15	0	61	0.021197205
Foxs1	15	0	61	0.006622666
Psrc1	15	0	60	0.00083807
Pla2g4a	44	1	58.33333333	0.026305716
Osm	29	1	57.5	2.95738E-05
Kcp	14	0	57	0.024394473
Cemip	42	1	56	0.005814894
Srpx2	118	2	52.33333333	0.008039809
Slc11a1	51	1	50.5	0.00642337
Adgrg2	25	1	50.5	0.001113938
Gdf6	13	0	50	0.036284683
Fcgr4	25	1	50	0.000119418
Nfatc4	25	1	49.5	0.004369622
Grhl1	12	0	49	0.011397229
Ly9	25	1	49	0.008856914
Cdh3	37	1	49	0.008646368
Has2	12	0	48	9.16174E-06
Crlf1	45	1	45.25	0.040150613
Kcne4	44	1	44.25	0.030396268
AC153143.1	11	0	44	0.020096445
Gm9869	11	0	44	0.002827375
Ccl21a	33	1	43.66666667	0.000732211
Pde1a	54	1	43.2	0.011792115
Gli3	65	2	43.16666667	0.031318404
Pou2f2	11	0	42	0.038111118

Ptn	256	7	39.42307692	0.006323407
Apobec1	78	2	39.125	0.014836261
Mtmr11	29	1	39	0.045922446
Olfml1	19	1	38.5	0.029851277
Cd300c2	19	1	38.5	0.018396576
Cthrc1	211	6	36.73913043	0.024723346
Ccl3	55	2	36.33333333	0.017030118
Tnfaip6	72	2	35.875	0.031165691
Thbs3	62	2	35.42857143	0.003304763
Fcgr1	35	1	35.25	0.013440773
Mmp19	18	1	35	0.045837106
Capn6	26	1	35	0.010618893
Slfn10-ps	18	1	35	0.006767649
Tnfrsf11b	18	1	35	0.00486784
Sh3bp2	35	1	35	0.001775389
Ifi44	70	2	34.75	0.039324651
Hpgd	17	1	34.5	0.008848097
Pgf	26	1	34	0.001463423
Postn	8453	249	33.98090452	0.031903745
Ccl2	142	4	33.47058824	0.022370735
Ms4a6d	33	1	33.25	0.007092037
Fcrls	66	2	33.125	0.040670296
Fcgr3	132	4	32.9375	9.35511E-05
Gpr132	24	1	32.33333333	0.013982366
Rbm47	32	1	32.25	0.01894037
Serpinb1a	579	18	32.16666667	0.006358998
Il2rg	40	1	31.8	0.000186796
Pawr	23	1	30.66666667	0.003820112
Hck	23	1	30.66666667	0.00034755
Cercam	61	2	30.625	0.015223562
Fcna	15	1	30.5	0.042423031
Sfrp1	266	9	30.42857143	0.031809391
Pla1a	60	2	30	0.022112225
Il1b	97	3	29.92307692	0.003376147
Cd84	66	2	29.33333333	0.023871089
Stk26	22	1	29	0.009023238
Piezo2	129	5	28.72222222	0.018617296
Ltbp2	728	26	28.53921569	0.036205679
Tlr13	36	1	28.4	0.008581154
Mmp23	71	3	28.2	0.000368548
Ssc5d	127	5	28.16666667	0.003224299
Cd40	28	1	27.75	0.008837492
Clec4a3	21	1	27.66666667	0.006151493
Chtf18	14	1	27.5	0.039323907
Aspn	621	23	27.27472527	0.01800425

1500015O10Rik	20	1	27	0.047545314
Mfap4	463	17	26.82608696	0.030247861
Arhgef26	27	1	26.75	0.005048981
Sema3d	27	1	26.75	0.004614967
Adamts4	80	3	26.58333333	0.022500715
AB124611	13	1	26.5	0.033715263
Fmod	184	7	26.28571429	0.049944307
Lair1	39	2	26	0.002986466
Sfrp2	299	12	25.97826087	0.024238769
C1qb	331	13	25.94117647	0.001028736
Mfap5	308	12	25.6875	0.025775809
Cx3cr1	32	1	25.6	0.002656801
Hhipl1	26	1	25.5	0.020092176
Cdca2	13	1	25.5	0.002778342
Pak3	19	1	25.33333333	0.005125689
Ptpro	32	1	25.2	0.016388357
Wfdc17	31	1	25	0.025631818
Srpx	31	1	25	0.002617696
Ptafr	31	1	24.6	0.001517984
Reps2	24	1	24.25	0.005867945
Fndc1	489	20	24.16049383	0.010177131
Fap	42	2	24.14285714	0.000877788
Mcub	12	1	24	2.01965E-05
Il1r1	168	7	23.96428571	0.031424231
Cxcl1	365	15	23.90163934	0.044933282
Ncf4	24	1	23.5	0.005330373
Tnf	128	6	23.31818182	0.002066046
Eya2	12	1	23	0.034560351
Pyroxd2	12	1	23	0.00629356
Col5a2	2295	101	22.77419355	0.030935146
Igfbp6	80	4	22.71428571	0.01684081
Mlph	11	1	22.5	0.04790398
Gatm	23	1	22.5	0.041740482
Acan	17	1	22.33333333	0.024030893
Slco2a1	28	1	22.2	0.017273887
Cd55	61	3	22	0.024437892
Slc7a2	60	3	21.90909091	0.039414163
Tyrobp	66	3	21.83333333	0.000554385
Tmem45a	43	2	21.625	0.018201141
Aldh3b1	11	1	21	0.016348858
Cd52	37	2	20.85714286	0.007703974
Ctla2a	52	3	20.6	0.003399244
Lilra5	10	1	20.5	0.049661863
Tlr8	31	2	20.5	0.033925567
Ackr2	10	1	20.5	0.024375734

C77080	31	2	20.5	0.003273746
Slc35d2	10	1	20.5	3.69571E-05
Tpst1	56	3	20.45454545	0.004951254
Adamtsl3	97	5	20.42105263	0.036639708
Fn1	7496	371	20.23279352	0.009390593
Egfr	137	7	20.22222222	0.007730946
Basp1	71	4	20.21428571	0.003489594
Tsku	25	1	20.2	0.014575998
Clec7a	30	2	20.16666667	0.046664613
Cks2	20	1	20	0.02484949
Bgn	2740	138	19.88747731	0.033826547
Il3ra	20	1	19.75	0.003067273
Ect2	20	1	19.5	0.024895836
Col14a1	752	39	19.40645161	0.025539332
Adcy7	150	8	19.38709677	0.004305877
Rian	179	9	19.32432432	0.005455787
Igsf10	101	5	19.28571429	0.023938257
Col6a1	1104	57	19.27947598	0.008667444
Abcc3	43	2	19.11111111	0.001064386
Slc41a2	38	2	19	0.000649272
Gpnmb	104	6	18.95454545	0.011619367
Ctss	513	27	18.82568807	0.006683915
Tnfsf9	24	1	18.8	0.000133221
Ifi27l2a	102	6	18.59090909	0.009541516
Col1a2	7370	398	18.5169598	0.018710062
Serpinf1	328	18	18.45070423	0.015875237
Cybb	221	12	18.4375	0.002788978
Bcat1	23	1	18.4	0.005560525
Fam171a2	14	1	18.33333333	0.047261526
Col3a1	15154	830	18.26913803	0.008632267
Slc15a3	41	2	18.22222222	0.042782485
Ccl9	68	4	18.2	0.010349546
Tmem119	46	3	18.2	0.009888003
Nupr1	82	5	18.11111111	0.049029598
Pak1	36	2	17.875	0.037901625
Adamts2	521	29	17.82051282	0.012571775
Csf1r	280	16	17.77777778	0.001255936
Cacng7	13	1	17.66666667	0.024717821
Serpinb8	13	1	17.66666667	0.003782116
Adamts12	106	6	17.58333333	0.012975269
Alcam	31	2	17.42857143	0.010495541
Angptl7	22	1	17.4	0.028711272
Adgre1	174	10	17.4	0.00132961
Trerf1	44	3	17.4	0.001298008
Lrrc25	13	1	17.33333333	0.015477465

Col6a3	1240	72	17.27526132	0.006601241
Itih5	155	9	17.25	0.013711115
Pik3ap1	103	6	17.20833333	0.007301995
Cd72	65	4	17.2	0.005681397
Fstl1	2838	165	17.19848485	0.021037112
Naalad2	133	8	17.16129032	0.049338675
Sec16b	34	2	17.125	0.042533809
Itga11	73	4	17.05882353	0.019677223
Svep1	213	13	17.04	0.026768661
Orai2	13	1	17	0.041741614
Cd300ld	34	2	17	0.013566486
C1qc	233	14	16.90909091	6.71972E-05
Mmp14	427	25	16.9009901	0.017203615
Mmp2	802	48	16.88421053	0.046430497
Anxa1	483	29	16.8	0.010676369
Col1a1	10645	635	16.77698976	0.014481375
Tubb4a	17	1	16.75	0.002975195
Efs	25	2	16.66666667	0.0420182
Mxra7	146	9	16.65714286	0.027258299
Slamf7	54	3	16.53846154	0.000831544
Gja4	25	2	16.5	0.000876545
Ckap2l	29	2	16.42857143	0.036617753
Col15a1	1675	102	16.37652812	0.02441184
Ephb2	25	2	16.33333333	0.02714181
Abi3bp	142	9	16.2	0.036592666
Gxylt2	109	7	16.18518519	0.028732255
Pdgfrl	69	4	16.11764706	0.032070749
Csf2rb2	36	2	16.11111111	0.027775402
Mmrn1	89	6	16.09090909	0.02153402
Lyz2	1256	78	16.04472843	0.001547183
Atp1a3	16	1	15.75	0.049373285
Rcn3	213	14	15.74074074	0.005173727
Spp1	169	11	15.69767442	0.013062667
Rbp1	141	9	15.63888889	0.007443965
Ms4a14	35	2	15.55555556	0.029049921
Loxl3	156	10	15.55	0.045142142
Col6a2	1348	87	15.53602305	0.002516258
Dsel	66	4	15.52941176	0.049310898
Sall2	23	2	15.5	0.038143941
Rbms3	93	6	15.5	0.034853351
Dpt	356	23	15.48913043	0.034130951
Usp35	35	2	15.44444444	0.023520245
P2ry6	35	2	15.44444444	0.00083624
Plaur	35	2	15.33333333	0.011641531
Hpgds	31	2	15.25	0.015216395

Cbr2	15	1	15.25	0.000604521
Lum	486	32	15.171875	0.042015761
Cd14	121	8	15.09375	0.007758065
F2rl3	15	1	15	0.037441868
Ccl5	11	1	15	0.015314146
Col5a1	1939	129	15	0.008026329
Trim30a	109	7	14.96551724	0.004739755
Capg	105	7	14.96428571	0.001474509
Mrc2	344	23	14.94565217	0.012138918
H2-Q5	19	1	14.8	0.006039294
C1qtnf6	110	8	14.66666667	0.006957867
B3galt1	11	1	14.66666667	0.004506713
Eln	270	19	14.59459459	0.027423931
Reck	29	2	14.5	0.035150653
Tlr2	101	7	14.42857143	0.019423182
Cpxm1	76	5	14.42857143	0.01235164
Antxr1	211	15	14.3220339	0.010639542
Lgals3	150	11	14.28571429	0.024338472
Arg1	35	3	14.1	0.000148823
Mpeg1	291	21	14.03614458	0.011089929
Ace	427	31	14.00819672	0.018128842
Prrt2	11	1	14	0.008164598
Vcam1	294	21	13.97619048	0.041985788
Prss23	70	5	13.95	3.57592E-06
Cxcr4	73	5	13.9047619	0.006546798
Cep295nl	21	2	13.83333333	0.045674697
Slfn2	104	8	13.83333333	0.008474489
Apcdd1	14	1	13.75	0.001654505
C1qa	226	17	13.6969697	0.00047922
Myof	250	18	13.68493151	0.010918317
Tmem108	10	1	13.66666667	0.045721157
Col6a6	21	2	13.66666667	0.00299993
Creb3l1	85	6	13.64	0.012268188
Casp1	17	1	13.6	0.027743805
Pld4	61	5	13.55555556	0.023536485
Cxcl16	251	19	13.55405405	0.001455286
C3ar1	98	7	13.51724138	6.67483E-05
Fbln2	1185	88	13.46022727	0.017613123
Fads2	30	2	13.44444444	0.001622957
Dhcr24	24	2	13.42857143	0.003102158
Rai14	191	14	13.40350877	0.042608387
Tnc	705	53	13.35545024	0.003290469
Timp1	167	13	13.34	0.016761295
Slc25a45	20	2	13.33333333	0.019919313
Diaph3	40	3	13.33333333	4.13376E-05

Arrdc1	13	1	13.25	0.001001826
Apoe	4629	350	13.23445318	0.000744526
Sprr1a	367	28	13.21621622	0.026034482
Nckap1l	122	9	13.18918919	0.001647099
Sulf1	376	29	13.1754386	0.023923327
Igfbp7	1163	89	13.14124294	0.029748646
Sfxn3	59	5	13.11111111	0.011751132
Ms4a7	101	8	13.03225806	0.000661
H2-Q7	42	3	13	0.003517607
Cmklr1	55	4	12.94117647	0.012953703
Col11a1	139	11	12.90697674	0.037176053
Plek	277	22	12.89534884	0.048770164
Dzip1	23	2	12.85714286	0.018242978
Rbl1	39	3	12.83333333	0.007081488
Tgif1	106	8	12.81818182	0.039641223
Spi1	32	3	12.8	0.010035676
Cmtm3	48	4	12.8	0.001331469
Fgd2	16	1	12.8	0.000262815
Pf4	38	3	12.75	0.023560666
Sphk1	32	3	12.7	0.022038262
Vim	4026	319	12.61080658	0.000627275
Efemp2	57	5	12.55555556	0.021085765
S100a6	242	19	12.54545455	0.003118484
Olfml3	131	11	12.47619048	0.019523666
Fcer1g	62	5	12.35	3.64567E-05
Myo1f	56	5	12.33333333	0.01233823
Cplx2	22	2	12.28571429	0.036341316
Islr	163	13	12.28301887	0.024391491
Laptm5	172	14	12.25	0.001114607
Dbn1	171	14	12.21428571	0.010004443
Hs6st2	18	2	12.16666667	0.03255312
Aplp1	30	3	12.1	0.006573085
Nlrp3	73	6	12.08333333	0.039606406
P3h3	111	9	12.02702703	0.021931922
Dok1	15	1	12	0.027907651
Fosl1	18	2	12	0.013063219
Tmem255b	21	2	12	0.009150037
Pid1	78	7	11.96153846	0.000785996
Cenpe	78	7	11.92307692	0.002188698
Kirrel	104	9	11.88571429	0.013796558
Ctsk	53	5	11.83333333	0.034821927
Capn5	15	1	11.8	0.021470697
Phf11b	12	1	11.75	0.023009382
Ptgis	118	10	11.75	0.018055444
Pltp	82	7	11.75	0.000171649

Cd248	170	15	11.72413793	0.003843319
Spata6	64	6	11.68181818	0.005133988
Dse	91	8	11.67741935	0.034042411
Meox1	236	20	11.64197531	0.013919855
Fcgr2b	110	10	11.57894737	0.006201495
Mcm3	98	9	11.55882353	5.98433E-05
Ddr2	182	16	11.53968254	0.023200612
Has3	12	1	11.5	0.009270081
Dcn	1444	126	11.46031746	0.020247857
Ebf1	160	14	11.44642857	0.03527944
Agmo	14	1	11.4	0.041967076
Csf2rb	48	4	11.35294118	0.011765458
Tnfrsf14	17	2	11.33333333	0.021816424
Sp140	20	2	11.28571429	0.023954424
Slc1a5	70	6	11.24	0.009094794
Cd83	250	22	11.23595506	0.021013783
Papss2	73	7	11.23076923	0.007416694
Bmf	28	3	11.2	0.028634514
Lonrf3	25	2	11.11111111	0.001659136
Slc1a4	33	3	11.08333333	0.010834577
Dlg2	44	4	11.0625	0.041178506
Thbs2	555	50	11.04477612	0.014113872
Tnfrsf1b	126	12	10.95652174	0.022713068
Homer3	41	4	10.93333333	0.044897871
Tuba1a	139	13	10.90196078	0.007601677
Mxra8	243	22	10.8988764	0.01557072
B3galnt1	19	2	10.85714286	0.010944475
Icosl	35	3	10.84615385	0.034514778
Tril	46	4	10.82352941	0.000782679
Sox17	73	7	10.77777778	0.011723022
Fbn1	2140	199	10.76855346	0.037745324
Galnt6	11	1	10.75	0.034870685
Gpr161	16	2	10.66666667	0.002966867
H2-Q4	141	13	10.66037736	0.013492666
Emilin1	306	29	10.65217391	0.003991413
Sparc	5327	503	10.60149254	0.016708884
Ccnb2	26	3	10.5	0.00952795
Cd180	21	2	10.5	0.00467759
Col24a1	18	2	10.42857143	0.006444423
Slamf9	29	3	10.36363636	0.017017131
Nfam1	23	2	10.33333333	0.0183611
Bok	18	2	10.28571429	0.02278613
Anln	51	5	10.25	0.028058446
Socs1	13	1	10.2	0.000822734
Tbc1d9	41	4	10.1875	0.041412386

Col18a1	272	27	10.1682243	0.007160046
Map3k7cl	15	2	10.16666667	0.002520096
C1ra	79	8	10.16129032	0.004058768
Sept5	53	5	10.14285714	0.025774847
C1s1	104	10	10.09756098	0.04832608
Pdpn	60	6	10.04166667	0.001932763
S100a11	148	15	10.03389831	0.006634892
Cd9	93	9	10.02702703	0.048621192
Btk	13	1	10	0.0416381
Ighm	48	5	10	0.023267961
Racgap1	45	5	10	0.018304637
Cd68	100	10	9.975	0.000356001
H2-Q6	167	17	9.970149254	0.007145297
Loxl1	538	54	9.958333333	0.009296418
Cfp	27	3	9.909090909	0.004787964
Mmp3	22	2	9.888888889	5.62157E-05
Rab7b	61	6	9.8	0.033867517
Ston1	51	5	9.666666667	0.037152844
Xaf1	56	6	9.652173913	0.038896521
Ndn	27	3	9.636363636	0.012786795
Runx3	19	2	9.625	0.046174511
Tgfbi	224	23	9.623655914	0.003976624
Tmsb10	390	41	9.617283951	0.001436945
Rasa4	63	7	9.615384615	0.012385182
Gbp3	163	17	9.573529412	0.022264287
Arrb2	81	9	9.558823529	0.002987954
Pdlim2	22	2	9.555555556	0.015219165
Endod1	117	12	9.551020408	0.024513867
Sh3tc1	60	6	9.52	0.02402049
Arhgap22	14	2	9.5	0.017286214
AA467197	14	2	9.5	0.009666205
Dusp2	29	3	9.5	0.000248192
Tubb2b	26	3	9.454545455	0.025702498
Trim47	116	12	9.448979592	0.000287857
Atp8b1	128	14	9.444444444	0.006632712
Serping1	425	45	9.392265193	0.02033724
Myo1d	174	19	9.378378378	0.025263858
Alox5ap	19	2	9.375	0.006245745
Gpx7	45	5	9.368421053	0.012127642
Sncg	33	4	9.357142857	0.001782618
Irf7	236	25	9.346534653	0.009802758
Foxc1	28	3	9.333333333	0.0201374
Sertad4	51	6	9.318181818	0.024224994
Stmn2	30	3	9.307692308	0.016668852
Igf1	216	23	9.290322581	0.00703095

Pdgfra	259	28	9.25	0.049907576
Csgalnact1	49	5	9.238095238	0.019946912
Fxyd5	161	18	9.214285714	0.000889753
Aff3	30	3	9.153846154	0.035329301
H19	215	24	9.138297872	0.035518093
Clec12a	57	6	9.12	0.010001683
Asns	27	3	9.083333333	0.025363193
Pirb	52	6	9.043478261	0.000640163
Bst2	61	7	9.037037037	0.002774293
Wisp1	102	11	9.022222222	0.025049223
Matn2	142	16	9.015873016	0.037703056
Cdt1	18	2	9	0.026871448
Kcnab2	16	2	9	0.007623351
Oaf	126	14	8.982142857	0.026071886
Susd2	36	4	8.9375	0.0230689
Plat	170	19	8.934210526	0.014132661
Sema3f	89	10	8.925	0.005302536
Fosb	1191	134	8.917602996	0.039395131
Tcaf2	27	3	8.916666667	0.031256481
Serpini1	25	3	8.909090909	0.028625921
Pde5a	47	5	8.904761905	0.011042264
Ecm1	227	26	8.901960784	0.016071416
Ncf1	78	9	8.885714286	0.00186101
Nfkbiz	673	76	8.848684211	0.039716062
Spon2	73	8	8.818181818	0.000505166
Ptpn22	11	1	8.8	0.04320007
Prcp	92	11	8.785714286	0.016875386
Samd9l	158	18	8.777777778	0.049575919
Tagln2	338	39	8.772727273	0.000966534
Knstrn	18	2	8.75	0.016441249
E2f7	18	2	8.75	7.12073E-05
Mrc1	287	33	8.748091603	0.005633228
Dusp6	423	49	8.716494845	0.038221423
Unc93b1	198	23	8.692307692	0.00139083
Birc5	26	3	8.666666667	0.012086987
Ifi30	58	7	8.62962963	0.001711047
Pnp	101	12	8.595744681	0.000334414
2610020C07Rik	15	2	8.571428571	0.01294884
Adrb2	19	2	8.555555556	0.011914083
Aebp1	360	42	8.526627219	0.028007002
Bmper	38	5	8.5	0.036627402
Apbb1ip	49	6	8.47826087	0.030543921
Kctd17	68	8	8.46875	0.01168891
Lxn	34	4	8.4375	0.003093833
Loxl2	255	30	8.421487603	0.015186986

Ccl6	109	13	8.384615385	0.000141264
Ccdc80	1222	147	8.337883959	0.029247537
Cd302	46	6	8.318181818	0.011427033
Arhgap30	54	7	8.307692308	0.003786494
Agpat4	35	4	8.294117647	0.004104253
Cd109	64	8	8.290322581	0.013393305
Nuak2	29	4	8.285714286	0.006832771
Cmip	110	13	8.264150943	0.011804951
Lhfpl2	99	12	8.25	0.015138118
Ly6a	187	23	8.230769231	0.004873733
Emp3	58	7	8.214285714	0.000312992
Sytl2	10	1	8.2	0.004002148
Rhoj	184	23	8.177777778	0.01478392
Ncf2	47	6	8.173913043	0.033173924
Crispld2	186	23	8.164835165	0.031606785
H2-Aa	128	16	8.142857143	0.003338213
Scube1	16	2	8.125	0.043891673
Tspan15	35	4	8.117647059	0.007732048
AW112010	45	6	8.090909091	0.016286566
Zfp423	67	8	8.090909091	0.011527828
Tppp3	87	11	8.069767442	0.012487475
Il21r	30	4	8.066666667	0.043463914
Grrp1	40	5	8.05	0.005994671
Map6	48	6	8.041666667	0.000880525
Wnt4	12	2	8	0.047765034
Hspa1b	116	15	7.982758621	0.047516375
Sh3pxd2b	180	23	7.977777778	0.014952605
Mest	58	7	7.965517241	0.013015861
Plekho2	169	21	7.941176471	0.000318171
Clip3	69	9	7.914285714	0.017871234
Tgfb3	192	24	7.907216495	0.000354982
Tnfsf12	18	2	7.888888889	0.045544082
Gm13456	18	2	7.888888889	0.009152933
Itgb4	18	2	7.888888889	0.001605738
H2-Eb1	156	20	7.886075949	0.01117153
Itgb3	34	4	7.882352941	0.006721797
Anxa2	531	68	7.862962963	0.000970071
Nav3	122	16	7.85483871	0.010039917
C1qtnf1	39	5	7.85	0.012299364
Ednrb	96	12	7.836734694	0.003830164
Ppic	261	33	7.834586466	0.014529652
Dnah6	12	2	7.833333333	0.026592198
Dnm1	59	8	7.833333333	0.025288015
Atp10a	47	6	7.833333333	0.021534462
Pcsk5	33	4	7.823529412	0.029842999

Lrp1	2102	269	7.820465116	0.019450025
Nid1	1288	165	7.814871017	0.02458316
Gas7	119	15	7.786885246	0.000894305
Inpp5d	142	18	7.780821918	0.004700225
Gpsm3	18	2	7.777777778	0.003162483
Sp110	33	4	7.764705882	0.002097883
Clec9a	16	2	7.75	0.040986931
Spc25	23	3	7.75	0.020041273
Ahnak2	81	11	7.738095238	0.003250827
Srgn	174	23	7.722222222	0.021084024
Cntln	112	15	7.689655172	0.000975598
Renbp	31	4	7.6875	0.004598249
Scarf2	62	8	7.6875	0.004537107
Ncoa7	92	12	7.666666667	0.024219076
Anpep	132	17	7.666666667	0.000136592
Sh3bgrl2	44	6	7.652173913	0.017222256
Itpripl2	214	28	7.651785714	0.000210529
Lfng	27	4	7.642857143	0.01897344
Il4ra	200	26	7.619047619	0.0028543
B2m	1541	202	7.616810878	0.013581936
Ebf2	38	5	7.6	0.038141702
Igfbp4	393	52	7.599033816	0.004390187
Dram1	55	7	7.586206897	0.017197544
Ldlrad3	49	7	7.576923077	0.013527212
Slc16a2	57	8	7.566666667	0.005059071
H2-D1	1205	160	7.554858934	0.00872905
Tpm4	538	71	7.547368421	0.01118952
Crmp1	11	2	7.5	0.0130108
Themis2	23	3	7.5	0.000615718
Pip4k2a	69	9	7.486486486	0.028374268
Id2	365	49	7.482051282	0.039005323
Nckap5l	51	7	7.481481481	0.023530136
Adgrd1	75	10	7.475	0.001490657
Clec4a1	32	4	7.470588235	0.015851219
Axl	478	64	7.46484375	0.003749041
Prrg3	78	11	7.452380952	0.024371018
Apobec3	41	6	7.409090909	2.66445E-05
Cxcl14	46	6	7.4	0.049605228
Brip1	19	3	7.4	0.044372702
Numbl	35	5	7.368421053	0.031251993
Synm	61	8	7.363636364	0.003021063
Skil	696	95	7.340369393	0.027266285
Nfkbid	18	3	7.3	0.044466239
Cox4i2	26	4	7.285714286	0.039906392
Knl1	33	5	7.277777778	0.000869656

Aspm	47	7	7.269230769	0.009580059
Slc12a9	22	3	7.25	0.040511656
Cyth4	60	8	7.242424242	0.008234741
Egr3	24	3	7.230769231	0.031540398
Mertk	101	14	7.214285714	0.012147083
Spns2	43	6	7.208333333	0.00151707
Specc1	70	10	7.205128205	0.033893143
Gbp2	180	25	7.2	0.025293336
Plac8	18	3	7.2	0.004870701
Irf5	40	6	7.181818182	0.028359644
C4b	140	20	7.166666667	0.007655337
P2rx7	38	5	7.142857143	0.030724804
Lbp	25	4	7.142857143	0.004895044
Hpcal1	63	9	7.142857143	0.002061159
Dab2	293	41	7.096969697	0.014738733
Pqlc3	43	6	7.083333333	0.01951597
Ifi211	23	3	7.076923077	0.010667101
Enpp3	34	5	7.052631579	0.024756764
Soat1	107	15	7.032786885	0.001240854
Map1a	244	35	7.014388489	0.000398808
Ly86	25	4	7	0.036642367
Ror2	19	3	7	0.012704385
Ptprc	136	20	6.974358974	0.014846785
Myl9	129	19	6.972972973	0.007720422
Elmo1	101	15	6.965517241	0.002825822
Sh3bgrl3	96	14	6.963636364	0.015596253
Il33	45	7	6.961538462	0.007286612
S100a10	247	36	6.943661972	0.000748117
Pi16	192	28	6.927927928	0.02882394
Ncam1	116	17	6.925373134	0.001631636
Eef1a1	2756	398	6.925251256	0.001391126
Phf11d	64	9	6.918918919	0.02135905
Frk	21	3	6.916666667	0.029097748
Cotl1	138	20	6.9125	0.004224049
Ahr	45	7	6.884615385	0.021871361
Vav1	41	6	6.875	0.00099264
Id3	438	64	6.84375	0.036972326
Scd1	98	14	6.842105263	0.020825425
Rap2b	21	3	6.833333333	0.014219523
Mcm6	87	13	6.823529412	0.001986142
Aif1	32	5	6.789473684	0.017645987
Litaf	202	30	6.781512605	0.034493012
Col5a3	219	32	6.775193798	0.037503832
Map1b	674	100	6.7375	0.000345052
Nid2	150	22	6.730337079	0.002747942

Scn7a	146	22	6.724137931	0.042210637
Heph	24	4	6.714285714	0.039659783
Fam124b	12	2	6.714285714	0.03514614
Sp100	154	23	6.695652174	0.04464567
Cald1	678	101	6.691358025	0.005000066
Oasl2	74	11	6.681818182	0.031202859
Ptpn6	75	11	6.666666667	7.36851E-05
Nusap1	28	4	6.647058824	0.002012426
Spry1	116	18	6.642857143	0.021512117
Rassf2	70	11	6.619047619	0.007314319
Pgm1	55	8	6.606060606	0.046887689
Flrt2	58	9	6.6	0.047547021
Cacnb3	48	7	6.586206897	0.028782584
Fam114a1	131	20	6.5625	0.036348828
Bicc1	251	39	6.512987013	0.016835323
Nbl1	64	10	6.512820513	0.011948152
Ripk3	20	3	6.5	0.049901363
Lrrc32	141	22	6.471264368	0.026945216
Epsti1	24	4	6.466666667	0.049923866
Dhx58	32	5	6.45	0.015530042
Anxa3	168	26	6.442307692	0.008199551
Shisa5	114	18	6.394366197	0.007174986
Galnt16	62	10	6.384615385	0.000988807
Lcp1	195	31	6.37704918	0.000824293
Kdelr3	40	6	6.36	0.004819495
Il10ra	80	13	6.36	0.002223956
Angpt2	60	10	6.342105263	0.003192201
Lhx6	19	3	6.333333333	0.014754409
Ptger4	43	7	6.296296296	0.045627734
Ildr2	27	4	6.294117647	0.035282384
Sntb2	227	36	6.291666667	0.00974375
St8sia4	93	15	6.288135593	0.016294096
Tcirg1	97	16	6.274193548	0.016095053
Aim2	17	3	6.272727273	0.045714697
Tmsb4x	1217	194	6.270618557	0.00462718
Egr2	66	11	6.238095238	0.007755129
Vat1	187	30	6.233333333	0.012430962
Slc9a9	50	8	6.21875	0.006268734
Cd74	433	70	6.204301075	0.001196736
Sdc3	397	64	6.203125	0.002318698
Kifl1	47	8	6.2	0.033204171
Nppa	1083	175	6.195994278	0.008643261
Evc	50	8	6.1875	0.01380981
Jag1	139	23	6.177777778	0.038036838
Plxnc1	39	6	6.16	0.041412402

Cygb	193	31	6.16	0.008881099
Cd33	34	6	6.136363636	0.035676563
Arpc1b	155	25	6.128712871	0.019499314
Nod2	14	2	6.111111111	0.043319223
Fam198b	429	70	6.110320285	0.003090079
Isg15	31	5	6.1	0.046561007
Fbxw9	15	3	6.1	0.010918068
Cebpa	63	10	6.097560976	0.003264682
Tpx2	52	9	6.088235294	0.027503056
Ikbke	18	3	6.083333333	0.029367028
Nptxr	38	6	6.08	0.014158718
Nes	589	97	6.074742268	0.001256022
H2-Ab1	187	31	6.06504065	0.001394445
Cnn1	26	4	6.058823529	0.025774383
Prickle2	59	10	6.051282051	0.014003477
Pcdhb14	32	5	6.047619048	0.018261321
Plvap	100	17	6.03030303	0.005295785
Stab1	257	43	6.01754386	0.020960012
Nsg1	12	2	6	0.037682468
Tead2	17	3	6	0.016313484
Wdr62	23	4	6	0.011687481
Kif4	29	5	6	0.007613573
Ceacam1	29	5	6	0.005016948
Adamts17	21	4	6	0.001436507
Nfkbia	859	143	5.998254799	0.029297654
Fat4	206	35	5.971014493	0.016711702
Casp8	75	13	5.96	0.00172376
Gucy1a3	130	22	5.954022989	0.017600424
Adgra2	80	14	5.925925926	0.008741289
Ifitm3	377	64	5.917647059	0.002492109
Dll1	18	3	5.916666667	0.000657671
Gsdmd	44	8	5.9	0.013635617
Flnb	552	94	5.890666667	0.009011607
Dlgap5	25	4	5.882352941	0.005499703
Map3k15	12	2	5.875	0.028526329
Mcam	259	44	5.875	0.00033079
Scara3	43	7	5.862068966	0.009380065
S1pr2	29	5	5.85	0.002730106
2200002D01Rik	38	7	5.846153846	0.006621929
Cdk14	137	24	5.808510638	0.030377101
Arhgap25	38	7	5.807692308	0.005555422
Sgce	58	10	5.8	0.020409001
Pcolce	252	44	5.793103448	0.003678119
Acvrl1	177	31	5.786885246	0.0074812
Cd163	64	11	5.772727273	0.006412726

Gpc3	25	4	5.764705882	0.009025071
Arhgap28	23	4	5.75	0.045042947
Tcaf1	112	20	5.743589744	0.015834035
Nr2f2	72	13	5.74	0.028357775
Cd44	340	60	5.714285714	0.001317388
Siglec1	44	8	5.709677419	0.006089901
Hells	39	7	5.703703704	0.013844002
Sptlc2	168	30	5.703389831	0.002896588
Mki67	382	67	5.701492537	0.002104147
Pfkfb3	115	20	5.691358025	0.000340239
Evi2a	23	4	5.6875	0.041650792
Arhgap6	44	8	5.677419355	0.015915329
Maml2	89	16	5.650793651	0.005205204
Ptma	440	78	5.626198083	0.011983886
AU021092	23	4	5.625	0.042946635
Ifitm2	45	8	5.625	0.042828632
Prkar1b	14	3	5.6	0.005838959
Neurl3	88	16	5.587301587	0.000264873
Marcksl1	68	12	5.571428571	0.002140173
Prkcb	32	6	5.565217391	0.021034878
Ccdc112	13	2	5.555555556	0.012517982
Zbp1	21	4	5.533333333	0.018029862
Lyve1	48	9	5.514285714	0.010346259
Samsn1	19	4	5.5	0.028184856
Rem1	11	2	5.5	0.019028171
Mcf2l	177	32	5.488372093	0.040278969
Sema3g	48	9	5.485714286	0.021052465
Sowahc	36	7	5.461538462	0.028374032
Unc5b	130	24	5.452631579	0.036688632
Cpne2	27	5	5.45	0.020884847
Usp49	12	2	5.444444444	0.011078188
Plcb1	99	18	5.438356164	0.027156746
Cd34	529	97	5.437017995	0.002317711
Sipa1	144	27	5.433962264	0.006365186
H2-K1	897	165	5.433333333	0.009966868
Itgb2	107	20	5.430379747	0.015941789
Gm38120	16	3	5.416666667	0.047386233
B4galnt1	16	3	5.416666667	0.027384981
Dtx4	50	9	5.405405405	0.031641553
Flna	1236	229	5.395196507	0.008788515
Nkd2	31	6	5.391304348	0.009769699
Ikzf1	28	5	5.380952381	0.024813988
Sparcl1	1684	313	5.37669593	0.022513633
Megf6	26	5	5.368421053	0.042287279
App	1554	290	5.36701209	0.004672456

Stk17b	121	23	5.366666667	0.003746692
Snhg18	44	8	5.363636364	0.014409671
Nav1	343	64	5.33463035	0.032733195
Fmnl3	226	43	5.323529412	0.022670854
Npdc1	80	15	5.316666667	0.013118403
Rab3il1	50	10	5.289473684	0.003323279
Myo5a	200	38	5.284768212	0.035224777
Mlkl	33	6	5.28	0.026916803
Fscn1	213	40	5.279503106	0.000122273
Arhgdib	88	17	5.268656716	0.000106897
Fndc3a	207	39	5.267515924	0.011403874
Sntb1	20	4	5.266666667	0.04365934
Eva1b	55	11	5.261904762	0.005112058
Uchl1	147	28	5.258928571	0.034159142
Rtp4	51	10	5.256410256	0.049320456
Parvg	21	4	5.25	0.016571655
Epb41l2	416	79	5.242902208	0.017500789
Ppp1r18	176	34	5.23880597	0.009235008
Glis3	29	6	5.227272727	0.039936961
Dpysl3	452	87	5.225433526	8.06778E-05
1600002H07Rik	12	2	5.222222222	0.023687014
Cd200	144	28	5.218181818	0.047389876
Gpr153	123	24	5.212765957	0.012456148
Aoc3	68	13	5.211538462	0.006570582
Ltbp4	783	150	5.209650582	0.044492149
Tap1	112	22	5.197674419	0.00350262
Dpysl2	360	69	5.194945848	0.010027768
Map3k8	61	12	5.191489362	0.00482659
Adap2	48	9	5.189189189	0.006673101
Comtd1	14	3	5.181818182	0.044546228
Blnk	23	5	5.166666667	0.020619289
Nrp2	471	92	5.144808743	0.007932095
Rasip1	126	25	5.132653061	0.021754708
Smad7	387	76	5.125827815	0.046635986
Timp2	718	140	5.125	0.001556182
Kit	42	8	5.121212121	0.02158125
Clic1	211	41	5.121212121	0.006285792
Fgd3	24	5	5.105263158	0.049280915
Crip1	179	35	5.078014184	0.001193932
Marcks	326	64	5.073929961	0.037648344
Selplg	36	7	5.071428571	0.001803293
Prex1	125	25	5.060606061	0.016741883
Rassf5	22	4	5.058823529	0.012293404
Cd53	43	9	5.058823529	0.010813159
Calhm2	24	5	5.052631579	0.02276432

Tbxas1	24	5	5.052631579	0.002346511
Myo1b	202	40	5.05	0.037969215
Tm4sf1	273	54	5.046296296	0.002900118
Kif15	30	6	5.041666667	0.002292586
Tmem106a	49	10	5.025641026	0.023572002
Tmod3	310	62	5.024291498	0.008589153
Lsp1	315	63	5.023904382	0.004741573
Enc1	73	15	5.017241379	0.023656298
Nr4a2	93	19	5.013513514	0.034319317
8430429K09Rik	15	3	5	0.041881157
Brca1	15	3	5	0.031057529
Gmip	50	10	5	0.00477031
Ephx1	173	35	5	0.001470692

12. List of publications

(2013-2018) Poster and presentations; Internal meetings, MPI-HLR Bad Nauheim, Germany

(2016) Poster and presentation; Retreat International Max Planck Research School, Schloss Tegernsee, Germany

(2017) Poster; Retreat DZHK; Frankfurt, Germany

(2017) Poster; Symposium Seeing is believing; EMBL EMBO Heidelberg, Germany

13. Erklärung zur Dissertation

„Hiermit erkläre ich, dass ich die vorliegende Arbeit selbständig und ohne unzulässige Hilfe oder Benutzung anderer als der angegebenen Hilfsmittel angefertigt habe. Alle Textstellen, die wörtlich oder sinngemäß aus veröffentlichten oder nichtveröffentlichten Schriften entnommen sind, und alle Angaben, die auf mündlichen Auskünften beruhen, sind als solche kenntlich gemacht. Bei den von mir durchgeführten und in der Dissertation erwähnten Untersuchungen habe ich die Grundsätze guter wissenschaftlicher Praxis, wie sie in der „Satzung der Justus-Liebig-Universität Gießen zur Sicherung guter wissenschaftlicher Praxis“ niedergelegt sind, eingehalten sowie ethische, datenschutzrechtliche und tierschutzrechtliche Grundsätze befolgt. Ich versichere, dass Dritte von mir weder unmittelbar noch mittelbar geldwerte Leistungen für Arbeiten erhalten haben, die im Zusammenhang mit dem Inhalt der vorgelegten Dissertation stehen, oder habe diese nachstehend spezifiziert. Die vorgelegte Arbeit wurde weder im Inland noch im Ausland in gleicher oder ähnlicher Form einer anderen Prüfungsbehörde zum Zweck einer Promotion oder eines anderen Prüfungsverfahrens vorgelegt. Alles aus anderen Quellen und von anderen Personen übernommene Material, das in der Arbeit verwendet wurde oder auf das direkt Bezug genommen wird, wurde als solches kenntlich gemacht. Insbesondere wurden alle Personen genannt, die direkt und indirekt an der Entstehung der vorliegenden Arbeit beteiligt waren. Mit der Überprüfung meiner Arbeit durch eine Plagiatserkennungssoftware bzw. ein internetbasiertes Softwareprogramm erkläre ich mich einverstanden.“

_____ _____

Ort, Datum Unterschrift

14. Acknowledgment

„Strive not be a success, but rather to be of value.“ – Albert Einstein

First, I would like to thank Professor Dr. Dr. Thomas Braun and PD Dr. Jochen Pöling, who took the risk to engage a young mother of a 15 months old son and dedicate her to such a complex and challenging project. During all those years I felt supported, trusted, challenged and sometimes just pushed in the right direction. Thomas, you gave me a true opportunity to grow, to follow my own path and to take responsibility for my own project. I am deeply thankful for all the trust and your time, whenever I needed it the most. Jochen and also Dr. Holger Lörchner, I am deeply thankful for being a part of the Poeling group. I would like to thank you both for giving me the possibility to join your group for my PhD time and for all the support and resources, you offered me for this project. Jochen, I am grateful for all those discussions we had, for your intensive support, feedback and constructive criticism to finally get the thesis done.

I have to thank so many people at the MPI, who made this journey special and unforgettable, so that I simply do it in a chronological order: Marcus, Soraya, Silvia, Sriram, Henrick, Ellen, Aaron and Sharif – the former mass spec group and my first little “home” at the MPI, Dr. Stefan Günther – master of the NGS data, Peter, Frank, Hosro, Mario, Carsten, Franz, Nina, Daniel – the IT and bioinformatic department and our knights in shining amour, Marita – the good soul of the house – miss u guys!

And I am thankful for those people who just crossed my life path during this PhD journey but nevertheless left a footprint in my mind: PD Dr. Michael Potente, Xuejun, Birgit, Isabelle, Keynoosh, Pumaree, Angelina, Kerstin W., Krishnan, Moni, Katja, Susanne K. and of course the people of the animal facility, which did so many things behind the scenes and intensively supported my research, with their work they did for my animals!!! A big *Thank YOU* to Nouha, Jennifer, Annika and Sina!

I am still grateful for those special and incredibly talented people I met, without those I would not have managed to pass this challenge: Brigitte Matzke (you’ll stay in my heart) and Boris Strilic, who both introduced me to immunohistochemistry and confocal microscopy and therefore kindled this passion for imaging in me, Dr. Marten Szibor for the cloning of mice constructs, what enabled me to start this project in the first place, Dr. Yunlong Hou and Marion Wiesnet for the enormous amount of operations and help with

the cardio isolations, Janett Piesker for her friendship and the support with the EM data set, Dr. Juan Adrian Segarra for his engaging effort to bring statistical analysis into my brain and for simply sitting by my side at the lab bench - I didn't want to have someone else next to me. And I would like to highlight especially Ann Atzberger and Kerstin Richter, who spent hours and hours with me at the BioSorter to get this challenging approach done! I have to say: you both are amazing! Thank you for staying by my side, for all those tears and laughter, for being upset together and simply for getting it done! I would not have made it without you!

The most I have to thank my boys at home: Meinem liebevollen und geduldigen Ehemann Stefan (tack sa mycket min älkling - jag älskar dig verkligen mycket), meinem Papa, der oftmals die Kinder übernommen und in schwierigen Zeiten immer an mich geglaubt hat, und meinen beiden Chaoten, die oft auf ihre Mama verzichten mussten. Ich hoffe, Ihr seid stolz auf mich!

Der Lebenslauf wurde aus der elektronischen Version der Arbeit entfernt.

The curriculum vitae was removed from the electronic version of the paper.